University of Southampton

Faculty of Medicine

School of Cancer Sciences

Identification of novel CD8+ T cell epitopes in the CT26 tumour model through a peptide filter relation algorithm

by

Eliuth David Arcia Anaya

ORCID ID 0000-0002-9902-5819

Thesis for the degree of PhD in Cancer Sciences

March 2022

University of Southampton

Abstract

Faculty of Medicine

School of Cancer Sciences

Doctor of Philosophy

Identification of novel CD8+ T cell epitopes in the CT26 tumour model through a peptide filter relation algorithm

by

Eliuth David Arcia Anaya

Cancer represents one of the deadliest diseases in humans, and current approved therapeutic strategies fail to eliminate tumours from patients whilst correlating with the development of numerous side effects. Over the last few years, cancer immunotherapy approaches have proven their utility for the treatment of this disease, showing complete remission in some treated patients. Some components of the immune system, specifically CD8+ T cells, are considered the main effectors of these anti-cancer therapies as these cells can recognize and eliminate cancer cells through a myriad of cytotoxic mechanisms. However, the majority of the most common immunotherapeutic approaches do not take into consideration the epitopes recognised by CD8+ T cells involved in the immune control of tumours. Moreover, different strategies have shown that vaccination with tumour-specific epitopes are able to induce strong and long-lasting CD8+ T cell responses that are associated with tumour regression. Despite this, the identification of these epitopes in the clinical setting is challenging whilst studies regarding the importance of peptide abundance and affinity in the immunogenicity and therapeutic benefit of such peptides are inconclusive.

In order to improve our understanding on the immunodominance patterns of tumour epitopes and their role in the development of anti-tumour responses, we aimed to identify novel CD8+ T cell epitopes and their role in tumour rejection in the widely-tested CT26 colorectal carcinoma model. For this, and using publicly available immune-transcriptomic data, we used a peptide filter relation model that incorporates the cellular abundance of the source protein alongside their predicted MHC-I affinity, in order to rank the candidate peptides in terms of likelihood of being presented at the cell surface of tumour cells. Using this approach, we identified three novel epitopes, which showed a preferential targeting in mice with regressing tumours upon depletion of regulatory T cells, indicating a potential prediction of clinically-relevant epitopes using the peptide filter relation model compared to classical predictions of MHC-I binding affinities. Dextramer assays confirmed the presence of CD8+ T cells specific for these epitopes, which showed similar activation, memory, and exhaustion phenotypes to CD8+ T cells specific for the other two known CT26 epitopes, GSW11 and AH1. Thus, our study highlights the importance of incorporating abundance and affinity parameters for the selection of cancer-derived peptides, which could significantly improve the design of more specific immunotherapy approaches.

Table of Contents

Table of Tables

Table of Figures

Research Thesis: Declaration of Authorship

Print name: Eliuth David Arcia Anaya

Title of thesis: Identification of novel CD8+ T cell epitopes in the CT26 tumour model through a peptide filter relation algorithm

I declare that this thesis and the work presented in it are my own and has been generated by me as the result of my own original research.

I confirm that:

1. This work was done wholly or mainly while in candidature for a research degree at this University;
2. Where any part of this thesis has previously been submitted for a degree or any other qualification at this University or any other institution, this has been clearly stated;
3. Where I have consulted the published work of others, this is always clearly attributed;
4. Where I have quoted from the work of others, the source is always given. With the exception of such quotations, this thesis is entirely my own work;
5. I have acknowledged all main sources of help;
6. Where the thesis is based on work done by myself jointly with others, I have made clear exactly what was done by others and what I have contributed myself;
7. None of this work has been published before submission

Signature: Eliuth David Arcia Anaya..... Date: 4th March 2022

Acknowledgements

This four-years journey wouldn't have been possible with the tremendous amount of help and support from different people and organisations.

I would like to thank Colciencias (Departamento Administrativo de Ciencia, Tecnología e Innovación) and the Colombian Ministry of Science, Technology, and Innovation, for the generous scholarship that allowed me to fulfil my studies, as well as Colfuturo for their impeccable management of the funds.

To professor David Wilson, whose incredible help and support during my recruitment and admission processes made it so much easier for me to find my place in the United Kingdom. Without his help, I would probably never have had this amazing experience, and I will be forever grateful for this.

To professors Tim Elliott and Edd James, for giving me the opportunity to complete my doctoral studies in a fascinating environment and research group, which led me to develop further both academically and personally. For all the help and support in times where I felt like I was going in circles, and for trusting and believing in my scientific potential.

To the Elliott/James lab members, past and present: Gessa, Rachel, Andy, Emma, Luke, Joe, Hope, Louise, Denise, Michaela, Elisa, and Nasia, for always being friendly and helpful with all the silly questions that a relatively-inexperienced postgraduate student can have in the early months (perhaps years). Special mentions to Gessa, for training me in animal work and tutoring me during my first experiments in the lab. To Denise, for being an incredible support in times where I felt the project was hitting some walls, for working in the development of the PFR algorithm and helping me mining the CT26 database that ultimately allowed us to obtain amazing data, and for being an amazing friend and a good companion for morning coffees. To Louise, for being a great friend to have weird conversations about cats, the movie "The Room", as well as serious life topic. To Elisa, for always cheering me up at any time, teaching me great Italian cooking tips, and for the unforgettable gossip afternoons drinking espresso after lunch. To Michaela, for being an incredible person with a kind a passionate heart, for laughing with me at dumb mistakes we often did, but most importantly for her invaluable friendship. And to Nas, one of the most unique and amazing persons that I met in the UK, thanks for teaching me a lot, not just lab-wise, but also about life. For always introducing me to some weird but amazing music genre, for presenting me the amazing addiction that is Dim-Sum, and for being one of the best friends I made while living abroad.

Acknowledgements

To Patrick and Leon from the Protein Core Facility, for always taking their time to walk me through all the different troubleshooting regarding cloning and protein expression and purification.

To the PCU staff (Nick, Sam, Lisa, and Vikki), for always taking care of our mice, and being so helpful during my training and experimental procedures. On this same note, I want to recognise the 314 BALB/c mice that were sacrificed during my training and experiments. Hopefully the results from this study will help us develop better cancer immunotherapies, so their death are not in vain.

To the CCI management group, for taking care of the installations and being so supportive and helpful to all the users of the building.

To my housemates in 13 Blackberry Terrace: Diego, Preeti, Cata, Diana and Eva, for being my second family away from home, for all those Wednesday evenings of 10p chicken wings and cheap beer, and for all the laughs and good times we had in these two years we lived together. Special mention to my parcero Diego, who was the first person to open the doors of their house to a complete stranger, for giving me invaluable tips for living in the UK, and for always being a supportive and amazing friend.

To all the friends and amazing people from all over the world that I met: Horacio, Viktor, Yustina, Nico, Chucho, Joel, Eric, Monse, Marilu, Charys, Lara, Aminu, Vineeth, Sudha, Juan, Gerardo, Gabi, Cecilia, Iain, F-M, Enah, and so many more. Thanks for all the cycling trips, squash sessions, international food nights, world-cup and pints afternoons, and the infamous Mexican parties.

To the Colombian gang in Southampton: Santiago, Yurany, Leidy, Lina, Andres, Diana, Vivi, Nubia, Carolina, and Luis. For those afternoons/evenings where we would meet and laugh and eat, which made it much easier (for all of us) to overcome homesickness.

To my beloved wife Yurany. For being the most loyal and loving companion I could have ever dreamt of; for supporting me through all the downs that a PhD student has (especially during these times of pandemic); for partially leaving behind her family, friends, and career to join me to the unknown in the UK; but more importantly for her unconditional love and support. I wouldn't have managed to finish this chapter of my life without her.

Last, but more importantly, to my Mom and Dad. For always believing in me and my education, for their continuous emotional support, for being the best example of resilience and honesty, but especially for their unpaired love, often putting myself above them in times of

scarcity. All their sacrifices and efforts have shaped the person I am, and this life will not be enough to repay them all they have done for me. This PhD thesis is dedicated to them.

Abbreviations

In alphabetical order:

ADCP ..... Antibody-dependent cell phagocytosis
ANOVA ..... Analysis of variance
AMP..... Adenosine monophosphate
AP-1..... Activating protein-1
Apaf-1..... Apoptotic protease activating factor 1
APC..... Allophycocyanin
APCs ..... Antigen presenting cells
APP ..... Antigen presentation pathway
ATP ..... Adenosine triphosphate
Bak..... Bcl-2 homologous antagonist killer
Batf3..... Basic Leucine Zipper ATF-Like Transcription Factor 3
Bax ..... Bcl-2-associated X protein
Bcl-2 ..... B-cell lymphoma 2
Bcl-xL..... B-cell lymphoma-extra-large
BFA ..... Brefeldin-A
BHL ..... β2M-heavy chain linker
BSA ..... Bovine serum albumin
BV421..... Brilliant violet 421
BV510..... Brilliant violet 510
BV785..... Brilliant violet 785
CAR-T..... Chimeric antigen receptor T cells
CCR2 ..... C-C Motif Chemokine Receptor 2
CCR7 ..... C-C Motif Chemokine Receptor 7
ccRCC..... Clear-cell renal cell carcinoma
CD..... Cluster of differentiation
cDC1s..... Conventional DCs type 1
cDC2s..... Conventional DCs type 2
CDKN2A..... Cyclin-dependent kinase inhibitor 2A
CFSE..... Carboxyfluorescein succinimidyl ester
CLEC9A ..... C-Type Lectin Domain Containing 9A
CNN ..... Convolutional neural network
ConA..... Concanavalin A

CPRG ..... Chlorophenol red-β-D-galactopyranoside
CREB..... Cyclic-AMP-responsive-element-binding protein
CREBBP ..... CREB-binding protein
CT26..... Colon Tumour 26
CTLA-4..... Cytotoxic T-lymphocyte associated protein-4
CX3CL1 ..... C-X3-C motif ligand 1
CXCL9 ..... C-X-C motif chemokine ligand 9
CXCL10 ..... C-X-C motif chemokine ligand 10
CXCL11 ..... C-X-C motif chemokine ligand 11
CXCR3..... C-X-C motif chemokine receptor 3
CXCR5..... C-X-C motif chemokine receptor 5
cyt C ..... Cytochrome C
DAI ..... Differential agretopicity index
DAMPs ..... Damage-associated molecular patterns
DAVID..... Database for annotation, visualization and integrated discovery
DCs..... Dendritic cells
DEN ..... Diethylnitrosamine
DMSO..... Dimethyl sulfoxide
dNTPs..... Deoxynucleotide triphosphates
EDTA ..... Ethylenediaminetetraacetic acid
ELISPOT..... Enzyme-Linked ImmunoSpot
EMS..... Ethyl methane sulphonate
EOMES ..... Eomesodermin
ER ..... Endoplasmic reticulum
ERAP..... ER aminopeptidase
ERAAP ..... ER aminopeptidase associated with antigen processing
FACS..... Fluorescent activated cell sorting
FADD ..... Fas-associated death domain
FasL..... Fas ligand
FBS ..... Foetal bovine serum
FITC ..... Fluorescein isothiocyanate
FOXP3 ..... Forkhead box P3
GAPDH ..... Glyceraldehyde-3-phosphate dehydrogenase
GAS ..... IFNγ-activated sites
GAS7 ..... Growth arrest-specific gene 7
GATA3..... GATA binding protein 3

GM-CSF..... Granulocyte-macrophage colony-stimulating factor
GO ..... Gene ontology
Gy ..... Gray
HAT..... Hypoxanthine-aminopterin-thymidine
HAUS6 ..... HAUS augmin-like complex subunit 6
HEPES ..... 4-(2-hydroxyethyl)-1-piperazineethanesulfonic acid
HER2..... Human epidermal growth factor receptor 2
HERV..... Human endogenous retroviruses
HIV-1 ..... Human immunodeficiency virus type 1
HNSCC ..... Head and neck squamous cell carcinoma
HPLC..... High performance liquid chromatography
HPV..... Human papilloma virus
HRP..... Horseradish peroxidase
HT..... Hypoxanthine-thymidine
i.p. ..... Intra-peritoneal
IBs..... Inclusion bodies
ICOS..... Inducible T-cell costimulatory
ICS ..... IFNγ Intracellular cytokine staining
IFNGR1 ..... Interferon gamma receptor 1
IFNGR2 ..... Interferon gamma receptor 2
IFNγ ..... Interferon gamma
IL-1β ..... Interleukin 1 beta
IL-2..... Interleukin 2
IL-2Rβ ..... IL-2 receptor β chain
IL-4..... Interleukin 4
IL-4Rα ..... IL-4 receptor α chain
IL-6..... Interleukin 6
IL-10 ..... Interleukin 10
IL-12 ..... Interleukin 12
IL-13 ..... Interleukin 13
IL-15Rα ..... IL-15 receptor α chain
IL-18 ..... Interleukin 18
iNKT..... Invariant natural killer T cell
iNOS ..... Inducible nitric oxide synthase
IPTG..... Isopropyl β-D-1-thiogalactopyranoside
IRAEs ..... Immune-related adverse effects

IRF1 ..... Interferon regulatory factor 1
IRF9 ..... Interferon regulatory factor 9
IRG ..... Interferon responsive genes
ITAM ..... Immunoreceptor tyrosine-based activation motifs
ITIM ..... Immunoreceptor tyrosine-based inhibitory motifs
JAK ..... Janus kinases
KIR ..... Killer immunoglobulin-like receptors
KRAS ..... Kirsten rat sarcoma virus
LAG-3 ..... Lymphocyte Activating 3
LB ..... Lysogeny broth
LC-MS ..... Liquid chromatography-mass spectrometry
LCMV ..... Lymphocytic choriomeningitis virus
LPS ..... Lipopolysaccharide
MAE ..... Mild acid elution
MAGE ..... Melanoma antigen gene
MAGE-A3 ..... MAGE family member A3
MAGE-C2 ..... MAGE family member C2
MART-1 ..... Melanoma-associated antigen recognized by T cells 1
MCA ..... Methylcholanthrene
Mcl-1 ..... Myeloid cell leukemia-1
MCM5 ..... Minichromosome maintenance deficient 5
MDA5 ..... Melanoma differentiation-associated protein 5
MDSCs ..... Myeloid-derived suppressor cells
MeP_i ..... Equilibrium cell surface abundance of a given peptide bound to MHC at the cell surface
MFI ..... Mean fluorescence intensity
MHC-I ..... Major histocompatibility class-I
MICA ..... MHC class I polypeptide-related sequence A
MICB ..... MHC class I polypeptide-related sequence B
MLKL ..... Mixed lineage kinase domain-like protein
MoDCs ..... Monocyte-derived DCs
MuLV ..... Murine leukaemia virus
NBR1 ..... Neighbour of BRCA1 gene 1
NFAT ..... Nuclear factor of activated T-cells
NF-κB ..... Nuclear factor-kappa B
NK ..... Natural killer

NMU ..... N-nitroso-N-methylurethane

NOD/SCID ..... Non-obese diabetic/Severe combined Immunodeficiency

NP40 ..... Nonyl phenoxypolyethoxylethanol

Nrp1 ..... Neuropilin-1

NSCLC ..... Non-small cell lung cancer

NY-ESO-1 ..... New York esophageal squamous cell carcinoma-1

O.D ..... Optical density

OVA ..... Ovalbumin

PBL ..... Peptide-β2M linker

PBS ..... Phosphate-buffered saline

PCR ..... Polymerase chain reaction

PD-1 ..... Programmed death 1

PD-L1 ..... Programmed death-ligand 1

PD-L2 ..... Programmed death-ligand 2

pDCs ..... Plasmacytoid DCs

PE ..... Phycoerythrin

PE-Cy7 ..... PE-Cyanine7

PEG ..... Polyethylene glycol

PerCP ..... Peridinin-Chlorophyll-Protein

PFA ..... Paraformaldehyde

PFR ..... Peptide Filter Relation

PLC ..... Peptide-loading complex

PMA ..... Phorbol 12-myristate 13-acetate

p/MHC-I ..... Peptide/MHC-I complex

Poly-ICLC ..... Polyinosinic-Polycytidylic Acid Stabilized with Polylysine and Carboxymethylcellulose

PRAME ..... Preferentially Expressed Antigen In Melanoma

PRF1 ..... Perforin 1

PRRs ..... Pattern recognition receptors

PSA ..... Prostate-specific antigen

pTregs ..... Peripherally-derived Tregs

RAG-2 ..... Recombination activating 2

RIP1 ..... Receptor interacting protein 1

RIP3 ..... Receptor interacting protein 3

RNA-Seq ..... RNA-Sequencing

RPKM ..... Reads mapped per kilobase of transcript length per million mapped

reads

s.c. ..... Subcutaneous

Sca-1 ..... Stem cell antigen 1

SCT ..... Single chain trimer

SDM ..... Site directed mutagenesis

SDS-PAGE ..... Sodium dodecyl sulphate – polyacrylamide gel electrophoresis

SEB ..... Staphylococcal enterotoxin B

SH2 ..... SRC homology 2

SNV ..... Single nucleotide mutations

SOC ..... Super optimal broth

SOCS1 ..... Suppressor of cytokine signalling 1

STAT1 ..... Signal transducer and activator of transcription 1

STING ..... Stimulator of interferon genes

$t_{1/2}$ ..... Half-life

TAAs ..... Tumour-associated antigens

TAMs ..... Tumour-associated macrophages

TAP ..... Transporter associated with antigen processing

TAPBPR ..... TAP-binding protein related

T-bet ..... T-box expressed in T cells

tBid ..... Truncated Bid

TCF1 ..... T cell factor 1

TCGA ..... The Cancer Genome Atlas

T_{CM} ..... Central-memory T cells

TCR ..... T cell receptor

tdLNs ..... Tumour-draining lymph nodes

TE ..... Tris-EDTA

T_{EFF} ..... Effector T cells

T_{EM} ..... Effector memory T cells

TGF-β ..... Transforming growth factor β

TIGIT ..... T cell immunoreceptor with Ig and ITIM domains

TILs ..... Tumour-infiltrating lymphocytes

TIM-3 ..... T cell immunoglobulin and mucin-domain containing-3

TLR ..... Toll-like receptor

TLSs ..... Tertiary lymphoid structures

TME ..... Tumour microenvironment

TNFα ..... Tumour necrosis factor α

TRAIL ..... TNF-related apoptosis-inducing ligand

Tregs..... CD4+ regulatory T cells

T_{RM} ..... Resident memory T cells

TRP-2 ..... Tyrosinase-related protein-2

TSAs..... Tumour-specific antigens

T_{SCM} ..... Stem cell memory T cells

tTregs ..... Thymus-derived Tregs

UBASH3A..... Ubiquitin-associated (UBA) and Src homology 3 (SH3) domain containing A

WB..... Western blots

WES ..... Whole-exome sequencing

WT..... Wild-type

XCR1 ..... X-C motif chemokine receptor 1

β2M..... β2-microglobulin

Chapter 1 Introduction

One of the biggest challenges of modern medicine has been finding an effective treatment for cancer. Since the first use of nitrogen mustard for the treatment of Non-Hodgkin's lymphoma in 1942, several chemotherapeutic approaches have been developed for different types of cancer (Chabner and Roberts 2005). However, none of these drugs can eradicate cancer cells in all patients, they are nonspecific, and are associated with a wide array of side effects, which has led to an exhaustive search for more specific and safer therapeutic strategies. In this regard cancer immunotherapy has become one of the most promising approaches, as these therapies target different components of the immune system with the purpose to stimulate anti-cancer immune responses that can ultimately lead to tumour control. The promising results observed thus far in clinical trials have led this approach to be declared as breakthrough of the year 2013 (Couzin-Frankel 2013), as well as being recognised with The Nobel Prize in Physiology or Medicine in 2018 given to James Allison and Tasuku Honjo *"for their discovery of cancer therapy by inhibition of negative immune regulation"* (The_Nobel_Prize 2018). Cancer immunotherapy can be divided into "passive" or "active" immunotherapy, depending on the mechanisms employed to induce an anti-tumour immune response. "Passive" immunotherapy strategies rely on the administration of molecules or cells with intrinsic anti-tumour activities, such as anti-tumour antibodies, adoptive transfer of cytotoxic cells, or oncolytic viruses. On the other hand, the goal of "active" immunotherapy is to induce the expansion and migration of cancer-specific immune cells to the tumour, using anti-cancer vaccines, checkpoint inhibitors, pattern recognition receptors (PRRs) agonists, pro-inflammatory cytokines, tissue remodelling inhibitors, among others (Galluzzi, Vacchelli et al. 2014, Palucka and Coussens 2016). One of the main targets of active immunotherapy strategies are CD8+ T cells, as these cells can eliminate cancer cells by cell-mediated cytotoxicity (Appay, Douek et al. 2008) through the recognition of cancer-derived epitopes presented on the cell surface by major histocompatibility class-I (MHC-I) molecules (Sharma and Allison 2015). Besides the recognition of cancer peptides through MHC-I molecules, CD8+ T cells require costimulatory signals provided by dendritic cells (DCs) as well as an appropriate pro-inflammatory environment to sustain an anti-tumour activity, adding extra layers of complexity for the activation of this cell population that must be addressed in the development of new therapeutic approaches (Palucka and Coussens 2016). In addition, several immune regulatory mechanisms in the tumour microenvironment (TME) can impede the correct activation of CD8+ T cells, such as a skewed pro-tumour inflammatory environment that promotes T cell anergy as well as high expression of co-inhibitory molecules like cytotoxic T-lymphocyte associated protein-4 (CTLA-4) and programmed death 1 (PD-1) (Waldman, Fritz et al. 2020).

Moreover, the presence of immunosuppressive populations of cells (including regulatory T and B cells, as well as myeloid-derived suppressor cells (MDSCs)) (Tcyganov, Mastio et al. 2018), and barriers that prevent infiltration of T cells (Peng, Chen et al. 2016, Zhang, Guan et al. 2020), can also decrease the anti-tumour activity of this cell population. Although different active immunotherapeutic strategies aimed at boosting anti-tumour CD8+ T cell responses have been approved for use in humans, not all patients benefit and cases of resistance to immunotherapy have been widely described (Dersh, Holly et al. 2021). Furthermore, the majority of immunotherapy strategies follow a blind approach regarding the epitopes recognised by CD8+ T cells in patients and deciphering how to generate robust anti-tumour CD8+ T cell responses bypassing the regulatory mechanisms while targeting highly immunogenic epitopes represents a crucial step for the development of therapeutic strategies that can eliminate cancer cells in patients.

1.1 CD8+ T cells in cancer immunotherapy

Although developments regarding immune-related therapies have been described relatively recently, the idea that immune cells were able to detect and eradicate cancer cells was first raised in 1970, in a term coined as cancer immunosurveillance (Burnet 1970). More than 10 years later, Thomas hypothesised that the cancer immunosurveillance hypothesis could explain why a vast majority of transplanted patients with continuous immunosuppressive therapies developed a wide array of cancers, attributing this phenomenon to a defective control of neoplastic cells by immune cells (Thomas 1982). It was only in 1994 that Dighe *et al.* proved the role of the immune system in the elimination of cancer cells, as treatment with a neutralizing antibody against IFNγ abrogated the lipopolysaccharide (LPS)-mediated protection of the methylcholanthrene (MCA)-induced Meth-A sarcoma in BALB/c mice (Dighe, Richards et al. 1994). Further experiments in mouse models showed that endogenous IFNγ protected from the development of spontaneous tumours and that anti-IFNγ treatment led to an increased susceptibility to develop both spontaneous and transplantable tumours (Kaplan, Shankaran et al. 1998). The role of lymphocytes in immune control of cancer was later demonstrated in Recombination Activating 2 (RAG-2)-knockout mice, which lack the capability to undergo the recombination event which forms antigen receptors and therefore have a deficiency in both T and B cells, as these animals developed MCA-induced sarcomas more rapidly and aggressively than wild-type (WT) mice. Moreover, among the T cell populations, CD8+ T cells were considered the main effector cells targeting neoplastic cells, as the adoptive transfer of cancer-specific CD8+ T cells led to the elimination of established tumours in mice (Hanson, Donermeyer et al. 2000). In addition, the presence of CD8+ tumour-infiltrating lymphocytes (TILs) has been correlated with good prognosis

in a wide array of human cancers, including colorectal (Hu, Sun et al. 2019), ovarian (Webb, Milne et al. 2014), oesophageal (Schumacher, Haensch et al. 2001), and lung carcinomas (Ganesan, Clarke et al. 2017). These studies shed lights on the importance of the immune system in the recognition and elimination of cancer and the steps that occur during the anti-cancer immune response, events which have been described as the cancer-immunity cycle (**Figure 1.1**). This cycle initiates when immature DCs (or other professional antigen-presenting cell) capture cancer antigens from the developing tumour, which together with activation signals mediated by damage-associated molecular patterns (DAMPs), leads to the maturation and migration of these cells to lymph nodes, where they can prime and activate naïve CD8+ T cells. Activated T cells then traffic and infiltrates the developing tumour, where they can recognize cancer-specific antigens that lead to the elimination of tumour cells (Chen and Mellman 2013). This cycle concludes with the eradication of neoplastic cells when the immune response is strong enough. However, when the immune response is unable to eliminate neoplastic cells, the developing tumour enters an equilibrium state where low immunogenic cells are selected by the pressure of the immune system, which ultimately leads to the proliferation of poorly recognized cancer cells in a process known as cancer immunoediting (Dunn, Bruce et al. 2002). A crucial step during the first phases of the cancer-immunity cycle involves the antigen presentation of immunogenic epitopes, which must be intracellularly processed and presented by MHC-I molecules to DCs and CD8+ T cells, leading to the elimination of tumour cells through a myriad of mechanisms.

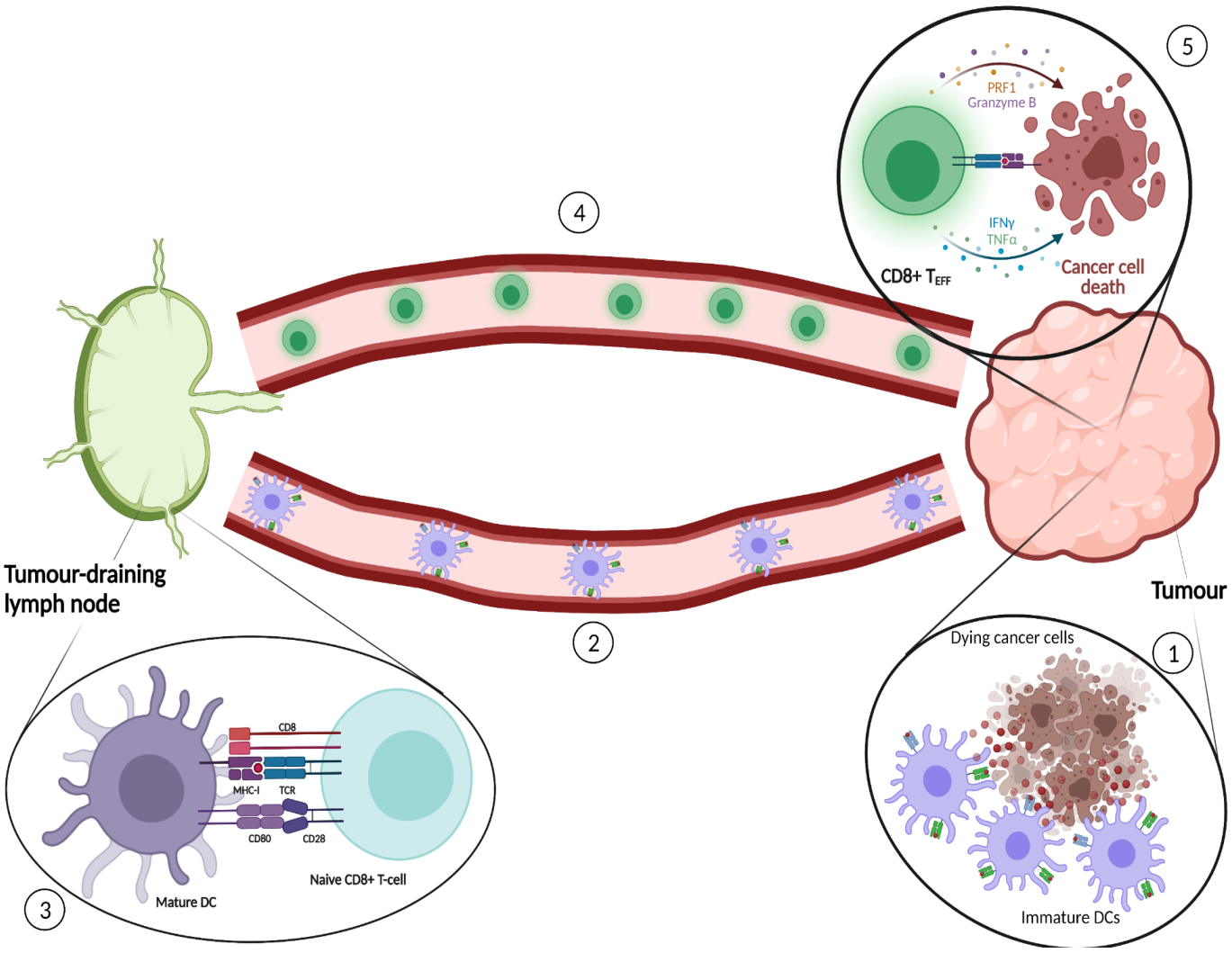

Figure 1.1 The cancer immunity cycle. The generation of effective anti-tumour CD8+ T cell responses follow a series of steps that start with the acquisition of tumour antigens by immature dendritic cells in the TME (1), maturation and migration of these cells towards secondary lymphoid organs (2), priming of naïve CD8+ T cells (3), infiltration of effector T cells (T_{EFF}) to the tumour bed (4), and elimination of cancer cells (5). Although the classic cancer immunity cycle involves the migration of antigen-loaded DCs to secondary lymphoid organs, T cell priming can also be performed within the tumour bed in tertiary lymphoid structures (Not depicted). Created with BioRender.com.

1.1.1 The importance of the MHC-I antigen presentation pathway in cancer

A proper understanding of antigen presentation through MHC-I is crucial for the success of immunotherapies aimed at boosting CD8+ T cell responses. As mentioned earlier, there are two critical steps that must occur in the successful antigen presentation: i) Uptake of tumour antigens by professional Ag-presenting cells and MHC-I cross-presentation to naïve CD8+ T cells for priming, and ii) Presentation of the cancer antigen by MHC-I molecules on the cell surface of tumour cells for the interaction with TCR of CD8+ T cells. The MHC-I antigen presentation pathway (APP) initiates with the calnexin-mediated folding and assembly of the MHC-I heavy chain in the endoplasmic reticulum (ER), which then associates with β2-microglobulin (β2M) in the absence of peptide, resulting in a highly unstable complex. Subsequently, the core of the peptide-loading complex (PLC), composed of the chaperone tapasin associated with ERp57 and calreticulin, binds and stabilizes the initial MHC-I complex through TAP (transporter associated with antigen processing). Intracellular proteins destined towards MHC-I antigen presentation undergo initial proteolysis in the cytoplasm either by the proteasome and/or by cellular proteases, resulting in the generation of peptide fragments that are transported to the ER through TAP. Once in the ER, these peptides are further processed by the aminopeptidase ERAAP (ER aminopeptidase associated with antigen processing in mice; ERAP – Endoplasmic reticulum aminopeptidase in humans), which performs N-terminal trimming of incoming peptides in order to generate peptides with optimal MHC-I binding length (between 8 – 10 amino acids). Tapasin proofreads peptides for stable binding in the groove formed by the α1 and α2 domains of the MHC-I heavy chain. Binding of optimal peptides to the corresponding MHC-I molecule induces the detachment of the peptide-MHC-I (p/MHC-I) complex from the PLC, which is then transported to the cell surface for antigen presentation (Rock, Farfan-Arribas et al. 2014, Jhunjhunwala, Hammer et al. 2021) (**Figure 1.2**). Although this MHC-I APP was initially described for the presentation of intracellular peptides, this pathway can also participate in the antigen presentation of exogenous peptides through MHC-I to CD8+ T cells, in a phenomenon known as cross-presentation, characterised by the intracellular processing of ingested or phagocyted antigens in endosomes, leading to the generation of peptides able to bind MHC-I molecules (Muntjewerff, Meesters et al. 2020).

Given that MHC-I antigen presentation is crucial for triggering anti-tumour CD8+ T cell responses, several mechanisms of immune evasion targeting the APP have been described in cancer. Tumours can "deplete" their antigenic repertoire in order to escape the immune system through copy number losses at the genomic level, via epigenetic modifications that impair RNA transcription, and by post-translational mechanisms in tumour-associated antigens (TAAs) and Neoantigens, as often these proteins can be dispensable for the tumour and are just a by-product

of oncogenesis (Jhunjhunwala, Hammer et al. 2021)(Section 1.3.1). Furthermore, tumours can also mutate MHC-I and β2M genes, leading to an impaired production of these molecules (Dhatchinamoorthy, Colbert et al. 2021). Such mutations have been detected in 3.3 - 4% of human cancers for MHC-I, and in 0.86% for β2M, especially in tumours with T-cell enrichment (Rooney, Shukla et al. 2015, Shukla, Rooney et al. 2015). Overall, cancers with a high neoantigen burden, such as microsatellite instability-high cancers, exhibit a higher frequency of loss-of-function mutations in MHC-I and β2M genes (Castro, Ozturk et al. 2019). Importantly, as these manifestations are observed at the genomic level, the decrease in the expression and/or function of MHC-I and β2M molecules can be irreversible. Nevertheless, this MHC-I downregulation is not a complete escape mechanism, as downregulation of MHC-I can trigger the "missing-self" elimination of tumour cells by natural killer (NK) cells, resulting in a loss of inhibitory signals in NK cells normally mediated by the interaction between MHC-I molecules and killer immunoglobulin-like receptors (KIRs), and the subsequent activation of these cells through the interaction of NK cell activator receptors (such as NKG2D) with their ligands (including MHC class I polypeptide-related sequence A (MICA) and MICB) (Myers and Miller 2021). On the other hand, some tumours can induce reversible changes in the levels of expression of APP components, mostly at the transcriptional and post-translational level, including hypermethylation of promoter genes of different APP genes (Ye, Shen et al. 2010, Qifeng, Bo et al. 2011), overexpression of the transcription factor DUX2 that inhibits IFNγ signalling (Chew, Campbell et al. 2019), and the redirection of MHC-I molecules towards the macroautophagy pathway in NBR1-rich vesicles (Yamamoto, Venida et al. 2020), among others.

Following the intracellular processing of antigens into epitopes presented by MHC-I molecules, optimal activation of CD8+ T cells requires the presentation of antigens by antigen presenting cells (APCs). Although several professional APCs have been described in health and disease, the most important players in antigen presentation for the generation of anti-tumour immune responses are DCs and tumour-associated macrophages (TAMs). DCs are considered professional APCs, as they can internalize, process and present antigens in both MHC-I and MHC-II molecules to CD8+ or CD4+ T cells, respectively. Moreover, the three signals required for T cell activation can be mediated by DCs, i.e., the interaction between p/MHC-I and TCR, co-stimulatory signals such as the ones resulting from the interaction of CD80/CD86 in DCs with CD28 in T cells, and cytokines like IL-12 and IFNγ (Wang, Xiang et al. 2020). DCs usually reside in peripheral tissues in an immature state, characterised by a high efficiency in antigen uptake, low expression of MHC-I and -II molecules, as well as low expression of co-stimulatory molecules. In tumours, DCs maturation is mainly mediated by the recognition of damage-associated molecular patterns (DAMPs) by Toll-like receptors (TLRs) (Gardner and Ruffell 2016), and upon antigen uptake, DCs acquire high

motility while migrating towards secondary lymphoid organs for antigen presentation to naïve T cells, in addition to a reduced ability to uptake and process antigens but a higher expression of co-stimulatory, MHC-I and -II molecules, and an increased production of cytokines (Wang, Xiang et al. 2020). This T-cell/DC interaction also favours the maturation of DCs through the cross-linking of CD40L on T cells with CD40 on DCs, which leads to an increase in IL-12, CD80 and CD86 expression in DCs, creating a positive feedback loop that favours T cell activation (Tay, Lee et al. 2017).

Although DCs are highly diverse, studies in mice have roughly classified these cells into four populations: conventional DCs type 1 (cDC1s), cDC2s, plasmacytoid DCs (pDCs), and monocyte-derived DCs (MoDCs). Both types of cDCs arise from a common DC precursor from bone marrow but trigger different immunological responses. In mice, cDC1s are characterised by the expression of either CD8α (resident) or CD103 (migratory), as well as XCR1 (X-C Motif Chemokine Receptor 1), CLEC9A (C-Type Lectin Domain Containing 9A), and CD205 (Wculek, Cueto et al. 2020). They are categorised as the most efficient cross-presenting cells, able to internalize extracellular antigens and cross-presenting them to CD8+ T cells (Chiang, Tullett et al. 2016). cDC1s are also high producers of IL-12 and play an important role in the development of CD4+ Th1 responses. On the other hand, cDC2s represent a more heterogeneous population in both human and mice, but can be distinguished by the expression of CD11b, along with CD172a and CD11c (Wculek, Cueto et al. 2020), and are strong inducers of Th2 responses in tumour settings (Williams, Tjota et al. 2013, Binnewies, Mujal et al. 2019). pDCs, characterised by the expression of B220 in mice, derive from both common DC precursors and lymphoid progenitors. These cells are not considered good at cross presentation and have low expression levels of MHC molecules but are considered the main producers of IFN type I, playing an important role in clearance of viral infections (Mitchell, Chintala et al. 2018). Lastly, MoDCs are differentiated in inflamed tissues upon CCR2-mediated trafficking. These cells represent a highly heterogeneous population, and their activity is dependent on the inflammatory context, as they can drive Th1, Th2, and Th17 responses alike (Wculek, Cueto et al. 2020).

Among these subsets, cDC1s are considered the most important drivers of anti-tumour CD8+ T cell responses, as evidenced by the role of both Batf3+ CD8α+ cDC1s in the rejection of the highly immunogenic H31m1 fibrosarcoma model (Hildner, Edelson et al. 2008), as well as in the loss of protective function of the combined anti-CD137/anti-PD-1 immunotherapy against the B16 melanoma model in *Batf3*$^{-/-}$ mice (Sanchez-Paulete, Cueto et al. 2016). Moreover, cDC1s are necessary for the reactivation of central-memory T cells (T_{CM}) and conversion of these into resident memory T cells (T_{RM}) (Enamorado, Iborra et al. 2017), for the recruitment of CD8+ T cells via CXCL9 (C-X-C Motif Chemokine Ligand 9) and CXCL10 via activation of the stimulator of interferon genes (STING) pathway (Spranger, Dai et al. 2017), and for the production of IL-12

triggered by T-cell-released IFNγ, which augments T cell function (Ruffell, Chang-Strachan et al. 2014, Garris, Arlauckas et al. 2018). Although theoretically DCs from both the TME and tumour-draining lymph nodes (tdLNs) can prime CD8+ T cell responses, the relevance of the location of these cells for the adequate T cell priming is still unknown. Nonetheless, abundance of cDC1s in the TME is associated with better prognosis and T cells infiltration (Mayoux, Roller et al. 2020), suggesting that cDC1s can directly cross-present antigens to tumour specific T cells in the TME. The role of TAMs in antigen presentation is still debatable. Macrophages have been classically defined as M1 and M2, where IFNγ-polarized M1 macrophages display a pro-inflammatory phenotype producing IL-6, IL-1β and inducible nitric oxide synthase (iNOS), whereas IL-4 or IL-13-polarized M2 macrophages are important in tissue repairment after inflammation and homeostasis through the production and expression of arginase 1, CD206 and IL-4Rα (Muntjewerff, Meesters et al. 2020). This classical dichotomic classification of macrophages does not translate entirely to TAMs, as evidenced in studies from human and mice tumours showing the concomitant expression of both M1 and M2 signature genes in TAM populations (Azizi, Carr et al. 2018, Singhal, Stadanlick et al. 2019, Zhang, Li et al. 2020). Despite these results, the current consensus considers TAMs as an M2-like population within the TME that helps establishing an immunosuppressive microenvironment inhibiting T cell functions and promoting tumour growth (Sica, Schioppa et al. 2006). However, studies have shown that TAMs can cross-present antigens to CD8+ T cells, inducing an IFNγ response in the latter (Muraoka, Seo et al. 2019). Nonetheless, TAMs are considered less efficient at cross presentation than DCs, possibly due to a reduced migratory potential, enhanced proteolytic activities within endosomes leading to peptide destruction, and reduced expression of co-stimulatory molecules and/or production of cytokines like IL-12 (Stopforth and Ward 2020).

Although the classical paradigm of T cell priming and activation involves antigen capture by DCs in the tumour and subsequent trafficking to tdLNs, this priming could also be performed within the tumour bed. In this regard, tertiary lymphoid structures (TLSs) have been described as an important site for the generation of anti-tumour T cell responses. These structures represent discrete functional regions within the tumour enriched in immune cells such as T cells, DCs, and B cells, which originate in peripheral tissues upon chronic antigen stimulation (Verneau, Sautes-Fridman et al. 2020). In tumours, TLSs resemble a B-cell germinal centre characterised by a CD20+ B cell zone with plasma cells and follicular DCs that favour antibody production against tumour cells, surrounded by a CD3+ T cell zone containing CD4+ and CD8+ T cells, as well as mature DCs, thus representing a potential important location for T cell priming and activation (Sautes-Fridman, Petitprez et al. 2019). Indeed, enrichment of mature DCs in TLSs in patients with non-small cell lung cancer (NSCLC) is associated with strong infiltration of effector-memory T cells, Th1-polarised

CD4+ T cells, and CD8+ T cells (Goc, Germain et al. 2014). Furthermore, in samples from metastatic melanoma patients, co-localization of CD8+ T cells and CD20+ B cells was associated with high infiltration of memory T cells (Cabrita, Lauss et al. 2020). Moreover, several studies have shown that a high density of TLSs within tumour represents a good prognostic marker in different solid malignancies, including but not limited to NSCLC (Germain, Gnjatic et al. 2014, Goc, Germain et al. 2014), colorectal cancer (Di Caro, Bergomas et al. 2014), pancreatic cancer (Hiraoka, Ino et al. 2015), and invasive breast cancer (Lee, Kim et al. 2015). This evidence highlights the potential of TLSs for inducing strong anti-tumour immune responses *in situ*, and novel therapies aiming to promote the formation of such structures could represent a fascinating strategy that might improve the success of conventional immunotherapy regimes.

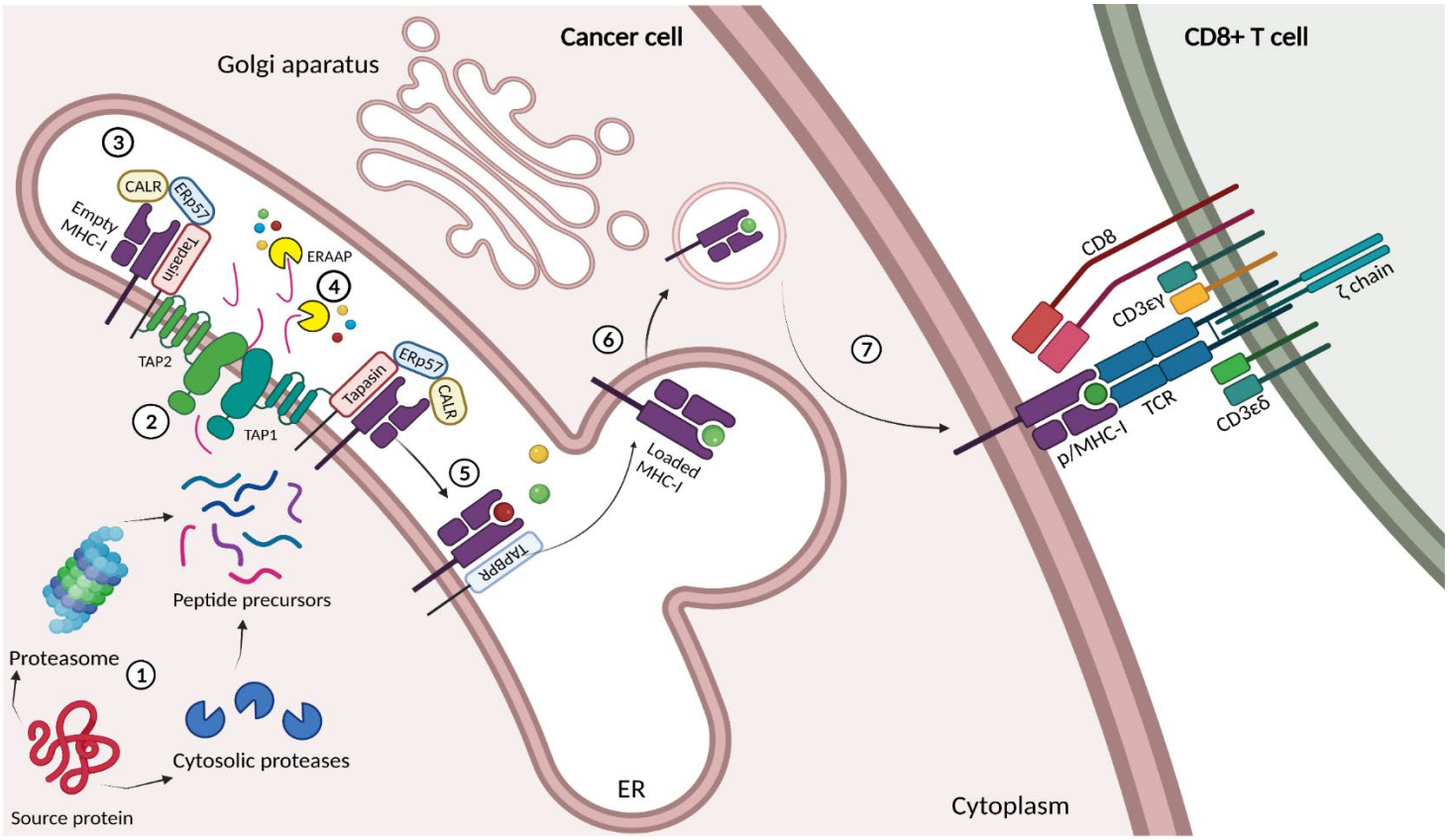

Figure 1.2 **MHC-I antigen presentation.** Peptides presented by MHC-I molecules at the cell surface are first intracellularly processed by the proteasome and/or cytosolic proteases (1), resulting in long peptides that are transported to the ER via TAP (2). In the ER, TAP associates with tapasin and empty MHC-I molecules through ERp57 and calreticulin (CALR), which together form the PLC (3). Once long peptides are transported to the ER, these are further trimmed by ERAAP (in mice) or ERAP (in humans), resulting in short peptide fragments of the adequate length for MHC-I biding (8 to 10 amino acids) (4). As a result of the proofreading function of tapasin, MHC-I molecules loaded with high-affinity peptides disassociate from the PLC. However, if the peptide bound to MHC-I does not induce a stable conformation, a second peptide editing step can be carried out by TAPBPR (TAP- binding protein related) (5). When a stable p/MHC-I complex is formed, it gets transported to the cell surface through the Golgi complex (6), for the activation of CD8+ T cells (7). Created with BioRender.com

1.1.2 Cytotoxic and phenotypic traits of anti-tumour CD8+ T cells

1.1.2.1 Induction of apoptosis through granzymes and death ligands

The previous evidence highlights the importance of the APP to induce anti-tumour CD8+ T cell responses. Once a primed CD8+ T cell recognises the p/MHC-I complex at the cell surface of tumour cells through its TCR, it can exert its cytotoxic functions using different mechanisms. TCR stimulation triggers cytotoxic mechanisms such as expression of death ligands like FasL (Fas ligand) and TRAIL (TNF-related apoptosis-inducing ligand), and production and release of cytotoxic granules through the granule exocytosis pathway. These granules mainly contain perforin 1 (PRF1) and several types of granzymes (being the most studied Granzymes A and B), which are mobilized towards the cell surface of CD8+ T cells at the immunological synapse (de Saint Basile, Menasche et al. 2010). The initial consensus about the mechanism of action of PRF1 was that this molecule could pierce the plasma membrane of target cells so that granzymes could enter the cytoplasm (Lopez, Susanto et al. 2013). However, novel studies have suggested that granzymes can enter the cells independently of PRF1 through clathrin-mediated endocytosis (Chang, Bzeih et al. 2016), and that the pores formed by PFR1 can directly kill target cells through osmotic cell lysis (Metkar, Wang et al. 2011). Regardless on the mechanism by which granzymes enter the cytoplasm of target cells, they exert their cytotoxic function through the induction of apoptosis using several pathways. Granzyme B can directly induce apoptosis through the cleavage and activation of the effector caspase-3 and -7. This granzyme can also cleave the proapoptotic Bcl-2 family protein Bid, generating truncated Bid (tBid), which activates Bak/Bax oligomerization on the mitochondrial outer membrane, allowing the release of cytochrome C (cyt C) from mitochondria. Once in the cytoplasm, cyt C form a complex called apoptosome along with Apaf-1 and procaspase-9, resulting in the activation of caspase-9. Lastly, granzyme B can also activate the mitochondrial pathway by disassociating the complex formed by the proapoptotic Bcl-2 family protein Bim with the antiapoptotic proteins Mcl-1 and Bcl-xL, resulting in the translocation of Bim into the mitochondria. Granzyme A regulates the production of proinflammatory cytokines (IL-1β) by a mechanism dependent on caspase-1 and the inflammasome (Martinez-Lostao, Anel et al. 2015). Although the only granzyme with a confirmed direct apoptotic activity is granzyme B, the cytotoxic activity of this granzyme is not always apoptotic, as observed by the killing activity of cytotoxic T cells mediated by PRF1 and granzyme B in targets where the mitochondrial apoptotic pathway and caspases are blocked (Pardo, Wallich et al. 2008).

CD8+ T cells can also drive apoptosis of target cells by the engagement of death ligands with their respective receptors, being FasL and TRAIL the most widely studied. Binding of these ligands to their death receptors (Fas for FasL, and TRAIL-R1/2 for TRAIL) induces receptor oligomerization at

the plasma membrane, which in turn leads to the recruitment of the adaptor protein FADD (Fas-associated death domain) through homotypic interaction between their death domains. This results in the activation of procaspase-8 via the death effector domain of FADD, triggering two different apoptotic pathways. The first pathway involves the activation of procaspase-3, which degrades different cellular substrates that result in apoptosis, whereas the second pathway initiates with the cleavage of the BH3-only proapoptotic protein Bid, generating tBid, which activates the previously described mitochondrial apoptotic pathway. In certain cases where caspase-8 is inactive, TRAIL receptors can recruit receptor interacting protein (RIP)1 and RIP3, forming a complex called necrosome, which phosphorylates MLKL, promoting its oligomerization and subsequent insertion into the plasma membrane, leading to increased cell permeabilization and ultimately necrotic cell death (Annibaldi and Walczak 2020).

Among these mechanisms, the most critical players in cancer immunosurveillance are PRF1 and granzymes. Several studies in PRF1-KO mice have shown that these mice have an increased susceptibility to develop spontaneous tumours, mostly of haematological origin (Smyth, Thia et al. 2000), and a faster growth kinetics in transplanted tumour models such as MC57G fibrosarcoma, and EL-4 and MBL-2 lymphomas (van den Broek, Kagi et al. 1996). In addition, loss-of-function mutations in the *PFR1* gene in humans have been associated with predisposition to develop lymphoma and leukaemia (Trapani, Thia et al. 2013). Knock-out of granzyme A and B in mice have shown contrasting data, as some studies have demonstrated that these mice are able to control tumour just as well as WT mice (Davis, Smyth et al. 2001, Smyth, Street et al. 2003), whereas others have published an increased susceptibility to tumour development (Revell, Grossman et al. 2005), although these results could be explained by a compensatory mechanism of other non-A non-B granzymes. Regarding TRAIL and TRAIL-R, mice knocked-out for either of these molecules tend to display a higher predisposition to death from transplanted tumour models such as the A20 B cell lymphoma (Sedger, Glaccum et al. 2002), as well as an increased susceptibility to develop MCA-induced fibrosarcomas (Cretney, Takeda et al. 2002) and diethylnitrosamine (DEN)-induced hepatocarcinomas (Finnberg, Klein-Szanto et al. 2008). Despite these results, no mutations in TRAIL or TRAIL-R have been associated with cancer development and/or susceptibility in humans (Martinez-Lostao, Anel et al. 2015).

1.1.2.2 The relevance of IFNγ in anti-cancer immune responses

As previously mentioned, IFNγ was the first immunological factor associated with cancer immunosurveillance in mouse models and is one of the most important cytokines involved in the anti-cancer activities of CD8+ T cells. Early studies not only showed that blocking IFNγ with monoclonal antibodies abrogated the LPS-induced clearance of MCA-induced fibrosarcomas, but

also demonstrated that tumours arising from IFNγ-blocked hosts showed different patterns of immunogenicity, as rechallenging WT mice who initially cleared the tumour with IFNγ-insensitive fibrosarcoma cell lines resulted in fast tumour growth, in sharp contrast with rechallenge using WT cell lines that did not show signs of tumour development in immune mice (Dighe, Richards et al. 1994). Importantly, this behaviour was also observed in Interferon Gamma Receptor 1 (IFNGR1) or Signal Transducer and Activator of Transcription 1 (STAT1) knock-out mice (Kaplan, Shankaran et al. 1998), which are critical components of the IFNγ signalling pathway (described below). Further pieces of evidence regarding the role of IFNγ in the control of cancer development were published a few years later, as studies showed that PRF1-KO IFNγ-KO double mutated animals displayed a significantly faster rate of metastasis in the DA3 model of mammary carcinoma (Street, Cretney et al. 2001), and that C57BL/6 IFNγ-KO mice developed spontaneous lymphomas more frequently than their WT counterparts (Street, Trapani et al. 2002). In humans, an elegant immunogenomic analysis of 33 different cancer types from The Cancer Genome Atlas (TCGA) showed that highly mutated breast invasive carcinoma, gastric cancer, ovarian cancer, head and neck squamous cell carcinoma (HNSCC), and cervical tumors, showed an IFNγ-dominant gene signature, characterised by a high M1/M2 macrophage polarisation, strong CD8 signals, high TCR diversity, high proliferation rate, and high TIL fractions (Thorsson, Gibbs et al. 2018). In addition, IFNγ gene signatures comprising genes involved in antigen presentation, cytotoxicity, proliferation, and chemokine expression, have been associated with clinical benefit to anti-PD-1 checkpoint blockade therapy in patients with melanoma (Grasso, Tsoi et al. 2020), gastric cancer, and HNSCC (Ayers, Lunceford et al. 2017).

Transcription of the *IFNG* gene can be triggered by several stimuli, including TCR signalling; soluble factors like IL-2, leukotrienes, and hydrogen peroxidase; and transcription factors such as AP-1, T-bet, Eomes, NFAT, and NF-κB. Two cytokines (IL-12 and IL-18) can also induce IFNγ production, as IL-18 acts as a cofactor together with NF-κB and AP-1, whereas IL-12 promotes expression of the IL-18 receptor, thus creating a feedback loop. IL-12 and IL-18 can also induce the expression of the protein kinase p38, which binds to the AU-rich element in the 3' untranslated region in the IFNG mRNA, stabilizing it and promoting transcription (Gocher, Workman et al. 2021). The main producers of IFNγ are CD4+ Th1 cells, CD8+ T cells, NK cells, iNKT cells, and γδ T cells, whereas the IFNγ receptors (IFNGR1 and IFNGR2) are ubiquitously expressed on all nucleated cells (Dunn, Koebel et al. 2006). Upon binding to its receptor, IFNγ mediates its biological activities through a signalling pathway involving Janus Kinases (JAK) and STAT proteins. Briefly, binding of IFNγ to the IFNGR1/IFNGR2 complex induces oligomerization of these receptors that lead to autophosphorylation, transphosphorylation and activation of JAK1 and JAK2, which are constitutively associated with each subunits of the receptor. This results in the uncovering of a

docking site for STAT1 within the cytoplasmatic domain of IFNGR1, leading to the phosphorylation of this signal transducer at Tyr701 by JAK1 and/or JAK2, which ultimately induces the disassociation of STAT1 from the receptor and the subsequent homodimerization through SRC homology 2 (SH2)-domain-phosphotyrosine interactions. These activated homodimers are then translocated to the nucleus inducing transcription of IFNγ-activated sites (GAS), in conjunction with co-activators such as CREBBP (cyclic-AMP-responsive-element-binding protein (CREB)-binding protein), p300 and MCM5 (minichromosome maintenance deficient 5). One of the most critical genes being transcribed in response to IFNγ are interferon regulatory factor 1 (IRF1) and IRF9, which further induces transcription of several Interferon responsive genes (IRG) (Platanias 2005).

Given the wide expression of IFNGR1 and IFNGR2 in all nucleated cells, IFNγ have pleiotropic functions depending on the tissue and microenvironment in which it is secreted. Specifically, within the TME IFNγ potentiates the cytotoxic activities of CD8+ T cells directly and indirectly. These effects range from the promotion of T cell infiltration via upregulation of CXCL9, CXCL10 and CXCL11 by the tumour stroma, and their cognate receptor CXCR3 on CD8+ T cells (Colvin, Campanella et al. 2004); increasing tumour antigenicity by upregulating molecules from the MHC-I APP (Mojic, Takeda et al. 2017); inducing the expression of pro-apoptotic factors in immune and tumour cells such as FasL and Fas, respectively (Bhat, Solanki et al. 2018); as well as by the modulation of the pool of memory T cells within the TME (Gocher, Workman et al. 2021). Notwithstanding, IFNγ also modulates other important immune cell populations that are required for the control of tumour growth, such as NK cells, as IFNγ drives NK infiltration via upregulation of CXCR3 (Wendel, Galani et al. 2008), as well as inducing maturation and cytotoxic signals in NK cells via TRAIL (Park, Seol et al. 2004). IFNγ can also suppress the polarization of CD4+ T cells towards a Th2 phenotype via the suppression of SOCS1 (Suppressor of Cytokine Signalling 1)and T-bet, which inhibit IL-4 signalling and GATA3, respectively (Hwang, Szabo et al. 2005). In addition, IFNγ promotes antigen presentation through up-regulation of MHC-I and -II molecules by tumour cells, DCs, B cells and macrophages (Zhou 2009). In DCs, IFNγ promotes differentiation into cDC1s producers of IL-1β and IL-12, which activates Th1 and CD8+ T cells and generates a positive feedback loop (Pan, Zhang et al. 2004). The relevance of IFNγ and its pathway for the induction of strong anti-tumour immune responses has also been evidenced in immunotherapy strategies, as observed in melanoma patients resistant to anti-CTLA-4 therapy harbouring mutations in *IFNG, STAT1, CXCL9, CXCL10, PRF1, GZMA* and *HLA-DRA* (Gao, Shi et al. 2016). Such mutations associated with resistance to immunotherapy have also been observed in melanoma patients unresponsive to anti-PD-1 therapy harbouring mutations in *JAK1* and *JAK2* (Zaretsky, Garcia-Diaz et al. 2016). Taken together, these observations about the autocrine and paracrine activity of IFNγ

produced by CD8+ T cells in the TME highlights the pivotal role this cytokine has in cancer immunosurveillance as well as in the efficacy of checkpoint blockade therapies.

1.1.2.3 Phenotypic traits of effective anti-cancer CD8+ T cells

The phenotype of CD8+ T cell populations play a pivotal role in the immune response against cancer, and therapeutic strategies aimed to stimulate specific phenotypes should theoretically result in an improved control of tumor growth. Upon antigen presentation via APCs in secondary lymphoid organs, naïve T cells differentiate into effector T cells (T_{EFF}), characterised by expression of activation and cytotoxic markers, such as CD25, CD69, Fas, PRF1, and granzymes; as well as by producing cytokines like IFNγ, IL-2 and TNFα (Reiser and Banerjee 2016). Studies have shown that adoptive T cell transfer of CD8+ T_{EFF} in the mouse melanoma model B16 lead to a high frequency of tumour-free survival ranging from 30% to 93% (Perret and Ronchese 2008), as well as a high tumour infiltration, cytotoxic activities and IFNγ production by transferred cells (Palmer, Balasubramaniam et al. 2004). Moreover, adoptive transfer of autologous T_{EFF} derived TILs in melanoma patients after lymphodepleting chemotherapy led to objective clinical responses in 51.4% of the patients (Rosenberg and Dudley 2004). Nonetheless, Gattinoni *et al.* showed that adoptive transfer of T_{EFF} with enhanced *in vitro* activity were less effective in tumour control in the B16 model (Gattinoni, Klebanoff et al. 2005). These results suggest that focusing on T_{EFF} for immunotherapeutic strategies is not always the most efficacious approach, as these cells might have reduced homing potential and are prone to apoptosis-induced clonal contraction (Han, Khatwani et al. 2020). This clonal contraction normally occurs once the immune system has cleared the pathogen and is characterised by a marked decreased in the frequency of T_{EFF}, and by the conversion of a small subset of these cells into memory T cells. Such memory T cells can be further subdivided into effector memory (T_{EM}) or T_{CM} cells. T_{EM} have a more similar phenotype to T_{EFF}, with no expression of CCR7 and low or no expression of CD62L. In humans, T_{EM} are characterised as CD45RA- CD45RO+ CCR7- CD62L-, whereas in mice CD44 is used instead of CD45RO as a marker of antigenic experience (Samji and Khanna 2017). In addition, T_{EM} are high producers of IFNγ and PRF1 upon TCR engagement, are normally circulating in the periphery or localized in inflamed tissues and can quickly differentiate into T_{EFF} (Han, Khatwani et al. 2020). On the contrary, T_{CM} have high expression of the homing markers CCR7 and CD62L, thus locating primarily in secondary lymphoid organs (Reiser and Banerjee 2016). Characterised in humans as CD45RA- CD45RO+ CCR7+ CD62L+, T_{CM} are great producers of IL-2 and have a higher proliferative capacity compared to T_{EM} (Han, Khatwani et al. 2020).

Memory subsets have also been associated with good clinical outcomes in adoptive transfer experiments. In a model of breast cancer in NOD/SCID mice, transferred T_{EM} and T_{CM} were able to migrate to the tumour bed while producing PRF1, whereas naïve T cells did not show this

behaviour (Beckhove, Feuerer et al. 2004). Despite these results, further investigations suggested that T_{CM} had stronger anti-tumour activities *in vivo*. *In vitro*-generated T_{CM}, but not T_{EM}, showed an increased anti-tumour effect upon adoptive cell transfer in the B16 melanoma model, whereas T_{EM} showed marginal therapeutic benefits (Hinrichs, Spolski et al. 2008). Moreover, T_{CM} overexpressed markers associated with homing to lymphoid tissues (as expected), such as CD62L, CCR7, CD103 and CXCR3, in comparison with T_{EM}, and had a 14-fold enrichment in blood and spleen compared to T_{EM} (Klebanoff, Gattinoni et al. 2005). In humans, TCR-transgenic T_{CM} from peripheral blood showed higher anti-tumour activities compared to T_{EM} (Wu, Zhang et al. 2013). In addition, melanoma and NSCLC patients exhibiting a higher T_{CM}/T_{EFF} ratio showed a more inflammatory phenotype in tumours, as well as a higher progression-free survival in patients treated with anti-PD-1 (Manjarrez-Orduno, Menard et al. 2018). Nonetheless, the fact that T_{CM} showed stronger anti-tumour activities in these models does not imply that T_{EM} are not efficient in controlling tumours, as evidenced by the ability of *in vitro*-generated T_{EM} to eliminate large established B16 tumours in an IFNγ-dependent fashion (Klebanoff, Yu et al. 2009), as well as by several studies showing the anti-tumour potential of vaccine-generated T_{EM} in different mouse tumour models (Roider, Jellbauer et al. 2011, van Duikeren, Fransen et al. 2012). Furthermore, studies in metastatic melanoma patients treated with anti-CTLA-4 have shown that high frequencies of T_{EM} in peripheral blood are associated with better prognosis (Wistuba-Hamprecht, Martens et al. 2017, Fairfax, Taylor et al. 2020).

As immunological characterisation of subpopulations becomes more complex aided by the use of high-throughput methodologies, novel populations of immune cells become evident. Beyond the classical dogma of T_{CM} and T_{EM}, two novel memory populations have been described, namely stem cell memory T cells (T_{SCM}) and T_{RM}. T_{SCM} is a circulating population that expresses a naïve-like phenotype while being antigen experienced. In mice they are characterised as $CD44^{-/low}$ CD62L+ Bcl2+ IL-2Rβ/IL-15Rα+ and Sca-1+, whereas in humans they are CD45RA+ CD45RO- CCR7+ CD62L+ CD27+ CD28+ IL-7Rα+ CD95+ IL-2Rβ+ TCF1+. These cells have a high self-renewal rate and can easily differentiate into T_{EFF}, T_{CM} and T_{EM} (Han, Khatwani et al. 2020). Moreover, T_{SCM} have been associated with regression of B16 tumours upon adoptive transfer (Gattinoni, Zhong et al. 2009) and are being currently targeted as an ideal population to develop chimeric antigen receptor (CAR) T cells (Kondo, Ando et al. 2020). This population has also been detected in lung cancer and melanoma patients, where these cells are associated with better clinical outcome to checkpoint blockade therapy (Brummelman, Mazza et al. 2018, Sade-Feldman, Yizhak et al. 2018), thus highlighting the potential to exploit these cells for future immunotherapy advances. T_{RM} cells are localized entirely in tissues, lack expression of lymphoid homing markers like CD62L and CCR7, and express CD49a, CD103 and CD69. These cells represent the largest memory compartment in human adults and have been identified in several epithelial and mucosal tissues (Han, Khatwani et

al. 2020). The importance of this population in cancer has been described in the B16 melanoma model, in which these cells were required for the long-term immunity induced by CD4+ regulatory T cells (Tregs) depletion coupled with surgical incision of the tumour (Malik, Byrne et al. 2017). Indeed, it has been shown in mouse melanoma models that T_{RM} CD8+ T cells expressing CD69 and CD103 are the main effectors in the anti-tumour response (Enamorado, Iborra et al. 2017). Furthermore, CD103+ TILs display a higher cytotoxic activity against E-cadherin+ target cells than CD103- TILs (Le Floc'h, Jalil et al. 2007) and the interaction of these two molecules is crucial for the maturation of the immunological synapse and the degranulation of cytotoxic mediators (Franciszkiewicz, Le Floc'h et al. 2013). Likewise, T_{RM} have also been characterised in a wide array of human tumours, including high grade serous ovarian cancer, paediatric glial tumours, NSCLC, and mesothelioma (Han, Khatwani et al. 2020). Remarkably, in all these cancer types, T_{RM} showed high expression of inhibitory molecules such as PD-1, CTLA-4, TIM-3 (T cell immunoglobulin and mucin-domain containing-3) and TIGIT (Savas, Virassamy et al. 2018, Clarke, Panwar et al. 2019), suggesting an activation/dysfunctional phenotype. Furthermore, high infiltration of T_{RM} in tumours has been associated with improved prognosis in urothelial (Wang, Wu et al. 2015), breast (Wang, Milne et al. 2016), endometrial (Workel, Komdeur et al. 2016), and lung cancers (Djenidi, Adam et al. 2015). A general overview of the phenotypic traits of the aforementioned T cell phenotypes associated with good prognosis in cancer is summarised in **Figure 1.3**. Altogether, the aforementioned data underscores the relevance of studying the different CD8+ T cell populations found within the TME, as this can lead to the development of novel immunotherapeutic strategies aimed towards strong and durable anti-cancer immune responses in patients.

1.2 Overcoming T cell dysfunction: checkpoint blockade in cancer immunotherapy

Despite the numerous reports of promising therapeutic interventions targeting CD8+ T cells, none of them has proven to eliminate cancer cells in all treated patients nor animals. Preclinical studies have shown that CD8+ TILs enter a state of terminal dysfunction (often referred as exhaustion) that can be reversible. CD8+ TILs isolated from vaccinated mice with lymphoma show a significantly impaired ability to kill cancer cells, but a strong anti-tumour response was observed when these cells were isolated from vaccinated mouse without tumours, suggesting that these cells lose their effector functions during the development of the disease (Huang, Obholzer et al. 2005). This inhibition of the CD8+ T cell effector function can be perpetrated by the TME in different ways. Neoplastic cells can counteract the action of the anti-cancer immune response directly or indirectly, by either producing or inducing the production of immunosuppressive

cytokines such as IL-10 and TGF-β (transforming growth factor-β) (Motz and Coukos 2013), or inducing the recruitment of immunoregulatory populations, such as Tregs (Facciabene, Motz et al. 2012). Most importantly, the pro-inflammatory TME together with constant antigen stimulation lead to the expression of co-inhibitory molecules on T cells, such as CTLA-4, PD-1, LAG-3 (Lymphocyte Activating 3), TIM-3, CD244, and CD200, which render these cells incapable of proliferating and/or producing effector cytokines upon stimuli, thus significantly impairing the anti-tumour activity of T cells (van der Leun, Thommen et al. 2020). The dysfunctional state of these cells is not dichotomic, as they mostly represent a pool of cells that undergo several stages of differentiation along the dysfunctional spectrum. This has been evidenced by the differential expression levels of PD-1, CTLA-4 and TIM-3 in T cell populations from mouse and human tumours (Fehlings, Simoni et al. 2017, Thommen, Koelzer et al. 2018), leading the definition of a "pre-dysfunctional" state, in which activated cells express higher levels of inhibitory molecules than naïve T cells, but lower levels and terminally exhausted cells (van der Leun, Thommen et al. 2020). The transition from a pre-dysfunctional T cell phenotype towards a terminally dysfunctional state is not drastic, but rather these cells acquire and lose certain characteristics along the dysfunctional axis. One of such characteristics is proliferation, as surprisingly T cells entering an "early dysfunctional" state acquire high proliferative capacities compared to the remaining CD8+ T cell subtypes within the TME (Li, van der Leun et al. 2019). In addition, these cells express lower levels of inhibitory receptors compared to their non-proliferative counterparts, but higher levels compared to pre-dysfunctional cells. Once these cells progress towards a “late dysfunctional” state, they lose the ability to produce IL-2, IFNγ, TNFα, PRF1 and granzyme B (van der Leun, Thommen et al. 2020) (**Figure 1.3**). Overcoming these dysfunctional states of T cells has been one of the principal goals of immunotherapy, and the two most successful strategies adopted so far involve the use of monoclonal antibodies against inhibitory receptors, such as CTLA-4 and PD-1.

1.2.1 Anti-CTLA-4 therapies

T cells express CTLA-4 in their plasma membrane upon activation, where it downregulates T cell activation by outcompeting the CD28 co-stimulator ligands CD80/CD86, increasing the activation threshold for T cell priming and inducing cell cycle arrest in these cells (Lizee, Overwijk et al. 2013, Postow, Callahan et al. 2015). The inhibitory signalling mediated by CTLA-4 participates in the contraction of T cells after activation and plays a significant role in maintaining tolerance to self-antigens (Walker and Sansom 2011). CTLA-4 was first cloned from mouse T cells in 1987 (Brunet, Denizot et al. 1987) and its role in the control of T cell activation was published eight years later, where mice deficient for this protein showed an increased infiltration of activated lymphocytes in liver, heart, lung and pancreas, leading to autoimmune-related death (Waterhouse, Penninger et

al. 1995). Its relevance as a target for anti-cancer checkpoint blockade came out one year later, when Leach *et al.* demonstrated that treatment with an anti-CTLA-4 antibody lead to tumour regression in a mouse model of colon carcinoma (Leach, Krummel et al. 1996). Since then, CTLA-4 blockade therapy with monoclonal antibodies has shown positive results in different mice tumour models, such as melanoma (Peggs, Quezada et al. 2009) and neuroblastoma (Williams, Dunn et al. 2013). The main targets of anti-CTLA-4 antibodies are activated CD4+ and CD8+ T cells, as the continuous pro-inflammatory status in the TME induces the expression of CTLA-4 in these cells (Hanahan and Weinberg 2011). In addition, anti-CTLA-4 treatment can lead to the mobilization of CD8+ T cells into the tumour stroma, which has been associated with immune control in mouse models of melanoma, pancreatic cancer, and mammary carcinoma (Rashidian, Ingram et al. 2017). Although anti-CTLA-4 treatment is mainly focused on releasing CD4+ and CD8+ T cells from a dysfunctional state, CTLA-4 is also constitutively expressed on CD4+ CD25+ FOXP3+ Tregs (Campbell and Koch 2011), and CTLA-4 blockade in Tregs as well as in CD4+ and CD8+ T cells is necessary for the observed clinical benefit of this therapeutic approach (Peggs, Quezada et al. 2009). These preclinical results showed a potential therapeutic benefit for CTLA-4 blockade in cancer, leading to the development of several clinical trials in humans. Most of these trials have employed ipilimumab, a fully humanised anti-CTLA-4 blocking IgG1 monoclonal antibody, in patients with metastatic melanoma. Treatment with ipilimumab results in objective clinical responses in one fifth of treated patients (Prieto, Yang et al. 2012), and significantly increases the overall survival in such patients (Rozeman, Hoefsmit et al. 2021), which has led to the approval of ipilimumab as a standard-of-care treatment for late stage melanoma in Europe and the United States (Hargadon, Johnson et al. 2018). Mechanistically, ipilimumab exerts its anti-tumour function in humans mainly by blocking the interaction of CTLA-4 with CD80/86, as evidenced by crystallographic data showing that this antibody binds CTLA-4 at the epitope that interacts with CD80/86 (Ramagopal, Liu et al. 2017), thus enhancing CD28 co-stimulation in CD8+ T cells. Indeed, ipilimumab treatment has a direct effect in CD8+ T cell responses in treated patients, as it induces a broadening of the CD8+ T cell repertoire against cancer-germline antigens like NY-ESO-1 (New York Esophageal Squamous Cell Carcinoma-1) and MAGE-C2 (MAGE Family Member C2) (Kvistborg, Philips et al. 2014, Robert, Tsoi et al. 2014). This effect on T cells has also been evidenced in the expansion of neoantigen-specific CD8+ T cells within the TME upon ipilimumab treatment (Fehlings, Simoni et al. 2017), as well as with the infiltration of Th1-like CD4+ T cells co-expressing PD-1, T-bet and ICOS (Wei, Levine et al. 2017). Furthermore, ipilimumab therapy induces the production of anti-NY-ESO-1 antibodies as well as polyfunctional CD8+ T cells, which has been associated with an improved clinical control of metastatic melanoma (Yuan, Gnjatic et al. 2008, Yuan, Adamow et al. 2011). These results highlight the specificity of ipilimumab-induced responses as the induced CD8+ T cells may have the ability to recognize and eliminate tumour

antigens *in vivo*. Although preclinical models have shown that CTLA-4 blockade in Tregs is also important for the observed clinical benefits of this treatment, the results in humans are not conclusive. A study by Du *et al.* using humanised mice expressing human CTLA-4 showed that tumour regression in melanoma was not due to blockade of CTLA-4-CD80/86 interactions, but rather due to Fc receptor-mediated depletion of Tregs in treated animals (Du, Tang et al. 2018). Moreover, *ex vivo* human studies have shown that ipilimumab induces in antibody-dependent cell cytotoxicity of Tregs by non-classical monocytes (Romano, Kusio-Kobialka et al. 2015). Despite these results, ipilimumab was not designed as a depleting antibody, and no evidence of Treg depletion in human samples has been published so far. Other anti-CTLA-4 monoclonal antibodies have also been developed, such as tremelimumab, a fully humanised anti-CTLA-4 IgG2 antibody, however results in clinical trials have not been fully satisfactory as it only induces partial clinical responses in 6% of treated patients (Kirkwood, Lorigan et al. 2010). These results are not due a lack of CD8+ T cell infiltration, as both clinical responders and progressors displayed similar levels of CD8+ TILs, and these cells expressed the same effector memory markers (CD45RO+ HLA-DR+) in both populations (Huang, Jalil et al. 2011). However, further clinical trials in advanced melanoma patients have shown that tremelimumab treatment shows significantly longer response durations compared to chemotherapy (Ribas, Kefford et al. 2013), and at 5-year follow-up tremelimumab shows a 20% survival rate (Eroglu, Kim et al. 2015).

Although anti-CTLA-4 therapies have proven useful for the treatment of different cancers, it is also associated with a high development of immune-related adverse effects (IRAEs), as ~90% of anti-CTLA-4-treated patients develop grade I or II IRAEs affecting mostly the skin and gut (Michot, Bigenwald et al. 2016)

1.2.2 Anti-PD-1 therapies

Similar to CTLA-4, engagement of PD-1 with its receptor blocks T cell activation interfering directly with the TCR signalling pathway (Sharma and Allison 2015). PD-1 was initially cloned from different mouse hybridomas in 1992, where its expression correlated with induced programmed cell death in such cells (Ishida, Agata et al. 1992). Further studies demonstrated the expression of PD-1 in both T and B cells upon TCR and BCR engagement respectively, leading to cell activation and subsequent apoptosis (Agata, Kawasaki et al. 1996). The role of PD-1 in the control of T cell activation was elucidated by the identification of one of its ligands, PD-L1 (B7-H1), a member of the B7 family of proteins expressed on APCs, fibroblasts and endothelial cells (Zou and Chen 2008). Interaction of PD-1 in activated T cells with PD-L1 in APCs leads to the inhibition of TCR-related proliferation and cytokine production in the former (Freeman, Long et al. 2000). Moreover, the finding that tumour cells can express PD-L1 as an adaptive resistance mechanism

to the host immune response supported the importance of targeting the PD-1/PD-L1 axis in cancer immunotherapy (Dong, Strome et al. 2002). PD-1 can also interact with PD-L2, another member of the B7 family (B7-DC); however, its limited expression in tumour cells and contradictory studies showing a pro-inflammatory rather than an inhibitory activity of this ligand, makes it a non-ideal target for immunotherapeutic approaches (Zou and Chen 2008, Zou, Wolchok et al. 2016). Preclinical models of mice melanoma and colon adenocarcinoma showed that anti-PD-1 treatment induces the infiltration of tumour-specific CD8+ T cells into the tumour, with a high proliferative capacity and phenotypic traits of activation and homing, leading to a decrease in tumour size and an increased survival rate (Iwai, Terawaki et al. 2005, Peng, Liu et al. 2012). In humans, and in contrast with anti-CTLA-4 treatments, blocking the PD-1/PD-L1 axis using monoclonal antibodies has been associated with boosting of pre-existing tumour-specific T cell populations, rather than with a broadening of the immune response (Robert, Harview et al. 2014). This has been exemplified in studies showing a rescue of exhausted T cells by anti-PD-1 antibodies in patients with melanoma, where PD-1 blocking allows for the restoration of proximal TCR signalling that leads to T cell reinvigoration (Tumeh, Harview et al. 2014), as well as with the proliferation and expansion of CD8+ T cells co-expressing CXCR5 and PD-1 (Im, Hashimoto et al. 2016), and boosting of neoantigen-specific CD8+ T cells in patients with NSCLC (Forde, Chaft et al. 2018). Moreover, anti-PD-1 therapies have shown a more targeted action in tumours, and a decreased rate of IRAEs compared to anti-CTLA-4 (Topalian, Drake et al. 2015), as ~70% of patients treated with anti-PD-1 develop mild skin manifestations (Michot, Bigenwald et al. 2016). This has led to the implementation of several clinical trials targeting this molecule in humans, showing positive results both in solid and hematologic neoplasias (Zou, Wolchok et al. 2016). The first antibody targeting PD-1 approved for use in human patients was nivolumab, a fully human IgG4κ monoclonal antibody, that showed objective responses in 31.7% of advanced melanoma patients in a phase 3 clinical trial involving patients that had progressed upon anti-CTLA-4 immunotherapy (Weber, D'Angelo et al. 2015). Since then, nivolumab has been approved as standard of care for different cancer types, including but not limited to NSCLC, renal cell carcinoma, HNSCC, and urothelial carcinoma (Wei, Duffy et al. 2018). Although the main focus of anti-PD-1/PD-L1 therapies is to block the negative signalling directly on CD8+ T cells, Tregs also express both PD-1 and PD-L1 in basal levels that increase upon activation, playing important roles in peripheral tolerance mechanisms (Francisco, Sage et al. 2010). Whether the blocking of PD-1/PD-L1 in Tregs is necessary for the effectivity of cancer immunotherapy approaches is yet to be elucidated. Collectively, these results highlight the importance of targeting checkpoint inhibitors such as CTLA-4 and PD-1, as these proteins are expressed in all individuals, whereas tumour antigens can only be expressed in a subset of patients, thus decreasing the likelihood of selecting tumour escape variants.

1.2.3 Novel cancer immunotherapy approaches for the induction of CD8+ T cell responses

1.2.3.1 Inhibition of Treg function

Although the strategies discussed so far are focussed on a direct activation of CD8+ T cells, these cells can be therapeutically targeted indirectly, either by inactivating immunosuppressive populations that prevent their activation, or by boosting the activity of cells that promote their effector function. Regarding the first subject, immunosuppressive cells in the TME, especially Tregs, can dramatically hamper the activity of CD8+ T cells and can express different co-inhibitory and co-stimulatory molecules employed in cancer immunotherapy strategies (CTLA-4, PD-1, PD-L1, TIM-3, OX-40, among others). Tregs can be divided into two groups according to their site of origin: thymus-derived Tregs (tTregs), which are positively selected in the thymus through MHC-II-dependent TCR interactions resulting in a relatively high-avidity selection; and peripherally-derived Tregs (pTregs), which originate in the periphery from conventional T cells as a result of TCR stimulation in the presence of TGF-β and IL-2 (Rodriguez-Perea, Arcia et al. 2016). Regardless of its origin, Tregs exert their immunoregulatory functions through a wide array of mechanisms. Tregs can overexpress inhibitory receptors (such as CTLA-4, TIM-3, PD-1, and LAG-3) and secrete inhibitory cytokines (such as TGFβ, IL-10, and IL-35), hindering T cell activation. Moreover, Tregs can also modulate DCs activities, by inducing a more tolerogenic phenotype of these cells through CTLA-4 and LAG-3 engagement. Furthermore, Tregs can disrupt T cell metabolism by depleting the availability of IL-2 due to the high expression of CD25 (IL-2Rα), as well as by expressing CD39/CD73 that participates in the generation of adenosine from adenosine triphosphate (ATP), which suppresses T_{EFF} cells via the adenosine receptor 2A (Scott, Gocher et al. 2021). The accumulation of Tregs in the TME has been associated with poor prognosis in human cancers, such as melanoma and cervical, renal and breast carcinomas (Shang, Liu et al. 2015). Furthermore, tumour-infiltrating Tregs in NSCLC showed higher levels of expression of CTLA-4, ICOS and 4-1BB compared to Tregs from normal tissue, suggesting that these cells can play important immunoregulatory roles within the TME (Guo, Zhang et al. 2018) (**Figure 1.3**). Nevertheless, the presence of Tregs in TME is not always a correlation of poor immunological control, as it has been demonstrated that an increased infiltration of Tregs in patients with colorectal cancer is associated with increased survival rates (Salama, Phillips et al. 2009). These contradictory results could be explained by the role of Tregs in controlling the Th17-mediated inflammation triggered by bacterial translocation in the gut mucosa, which can be a strong promoter of tumorigenesis (Ladoire, Martin et al. 2011). Regardless of these dissimilar results, most of the therapeutic strategies involving Tregs are focused on the depletion or inhibition of this cell population, with the premise of decreasing inhibitory signals that may render CD8+ T cells dysfunctional (Chao and Savage 2018). Several studies have reported that transient depletion of Tregs prior to tumour

challenge induces a robust CD8+ T cell response able to eliminate the tumour (Onizuka, Tawara et al. 1999, Shimizu, Yamazaki et al. 1999). Further studies have shown that antigen-specific CD8+ T cell populations associated with tumour control are inhibited in Treg-sufficient mice (Golgher, Jones et al. 2002, James, Yeh et al. 2010). Moreover, *in vitro* depletion of Tregs from peripheral blood mononuclear cells of patients with hepatocellular carcinoma improved the cytotoxic activity of CD8+ T cells when stimulated with NY-ESO-1 peptides (Zhang, Mei et al. 2010), indicating altogether that Tregs may prevent the development of appropriate anti-tumour CD8+ T cell responses. Despite these results, the use of monoclonal antibodies aimed to eliminate Tregs may be challenging in clinical settings, as Treg depletion post tumour-engraftment fails to elicit strong anti-tumour CD8+ T cell responses (Quezada, Peggs et al. 2008), thus limiting the benefit of such strategies to pre-tumour stages. Additionally, Tregs are vital cell populations for the maintenance of peripheral tolerance, and inhibition or depletion of these cells may lead to autoimmune disorders that can be life threatening (Sakaguchi, Yamaguchi et al. 2008). Notwithstanding, Treg targeting in cancer immunotherapy approaches represents an interesting field, and further studies aimed to specifically target Tregs in the TME might yield promising therapeutic benefits to patients.

1.2.3.2 DCs as cancer immunotherapy targets

As previously discussed, DCs play an important role in the development of anti-tumour CD8+ T cell responses by the uptake and processing of tumour-derived antigens and subsequent priming of naïve CD8+ T cells in lymph nodes, thus representing a potential target for the development of immunotherapy strategies. The majority of studies so far have been focused on the *ex vivo* expansion of autologous DCs in the presence of maturation-promoter factors and tumour antigens, so that upon inoculation these loaded mature DCs can prime naïve CD8+ T cells and generate an anti-tumour immune response (Santos and Butterfield 2018). Due the low percentage and high phenotypic variability of the DC population in both humans and mice (Haniffa, Collin et al. 2013), most of the studies so far have relied on the differentiation of peripheral blood CD14+ monocytes into DCs using IL-4 and GM-CSF (granulocyte-macrophage colony-stimulating factor) (Santos and Butterfield 2018). After this process, autologous DCs are then exposed to the respective tumour antigen, either by pulsing with the respective peptide, transfecting mRNAs or expression vectors encoding the antigen, or exposing DCs to bulk lysates from tumour cells (Palucka and Banchereau 2012). In the clinical setting, this strategy has shown contrasting results. Patients with stage III-IV melanoma treated with autologous DCs pulsed with a peptide derived from the differentiation antigen MART-1 (Melanoma-associated antigen recognized by T cells-1) had an increase in the frequency of antigen-specific CD8+ T cells but failed to show an objective clinical response (Butterfield, Ribas et al. 2003). However, in another cohort

of patients with advanced melanoma, patients treated with autologous DCs pulsed with a gp-100-derived peptide displayed a significant increase in the frequency and cytotoxicity of antigen-specific CD8+ T cells, as well as partial clinical responses in 25% of the patients (Linette, Zhang et al. 2005). DCs have also been employed in combination with checkpoint inhibitors. In a mouse model of osteosarcoma, combination of anti-CTLA-4 plus tumour lysate-loaded DCs led to the amplification of CD8+ TILs, which correlated with a reduction in metastatic lesions and increased survival (Kawano, Itonaga et al. 2013). These results highlight the important of a proper activation of DCs in cancer immunotherapy and suggests a potential use of these cells in vaccination strategies.

1.2.3.3 Modulation of the APP: The role of ERAAP/ERAP

To eliminate tumour cells, CD8+ T cells must recognize tumour-specific peptides presented in the context of the MHC-I molecule, as previously discussed. However, the antigen processing and presentation pathway heavily influences the repertoire of peptides presented in the cell surface of transformed cells (Neefjes, Jongsma et al. 2011), thus representing a critical pathway that can be therapeutically targeted. In this sense, ERAAP/ERAP plays a pivotal role in the generation of MHC-I peptides, and it has been reported that modulation in the expression of ERAAP drastically affects the repertoire of antigenic peptides presented in the cell surface in mouse models (Hammer, Gonzalez et al. 2006, Nagarajan, de Verteuil et al. 2016). Moreover, in the context of HIV-1 infection, ERAP activity participates in the immunodominant patterns of specific epitopes, affecting the abundance of the presented peptides in the cell surface and therefore the clonality of CD8+ T cells (Tenzer, Wee et al. 2009). Interestingly, in the CT26 mouse model of colorectal carcinoma, ERAAP inhibition leads to the overexpression of the GSW11 peptide by these cancer cells, which has been associated with strong CD8+ T cell responses and tumour control (discussed below) (James, Yeh et al. 2010). Furthermore, animals inoculated with ERAAP-knocked-out CT26 cells were able to eliminate the tumour, accompanied by an increase in the GSW11-specific CD8+ T cell population (James, Bailey et al. 2013), which suggests that ERAAP may over-trim certain MHC-I peptides required for an adequate immune response, and highlights the potential of targeting this molecule for novel immunotherapeutic approaches.

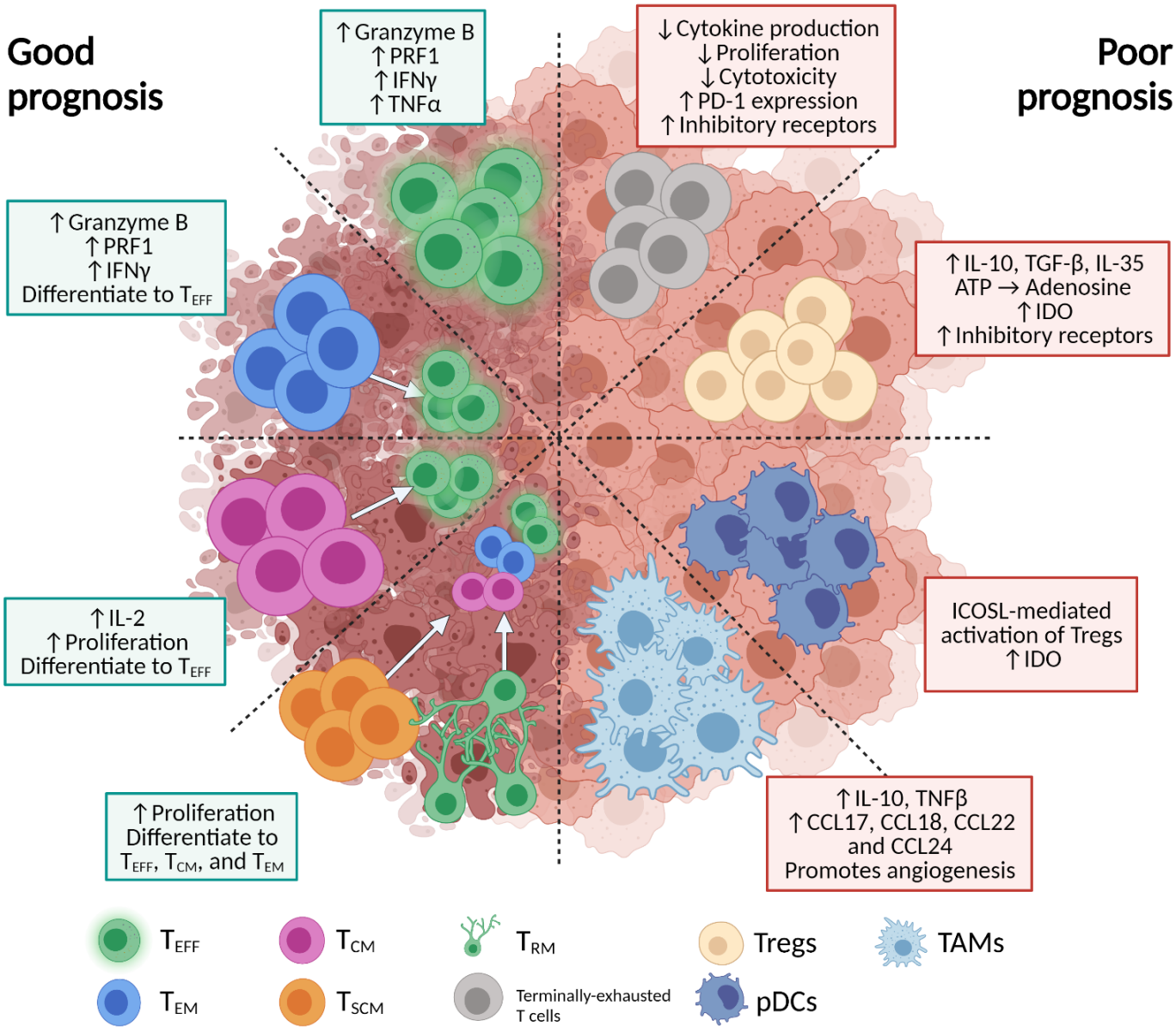

Figure 1.3 **Immune cell populations associated with cancer prognosis.** T cell populations where an association with good cancer prognosis and/or regression in mouse tumour models are shown on the left, alongside their main effector functions involved in the anti-tumour immune response. On the right, cell populations associated with poor cancer prognosis in human cancers and mouse tumour models are shown, as well as the mechanisms involved in the poor immunological control of neoplastic cells mediated by these immune populations. This graph only depicts the cell populations associated with good or bad prognosis mentioned in this thesis and does not include all the immune cell populations where a correlate of prognosis has been made. Created with BioRender.com.

1.3 The antigenic landscape of tumours: tumour-specific antigens, tumour-associated antigens, and immunodominance

1.3.1 Current classification of tumour antigens targeted in immunotherapy

Besides the aforementioned therapeutic strategies aimed at overcoming CD8+ T cell dysfunction, several steps of the cancer-immunity cycle have also been targeted therapeutically with the purpose of inducing effective anti-cancer CD8+ T cell responses. Stages regarding the activation of cancer-specific CD8+ T cells have been mimicked using different vaccination strategies; however, the success of these approaches in clinical trials has been limited (Rosenberg, Yang et al. 2004). These negative results could be explained by the type of antigen used in the vaccination studies, as cancer antigens differ in their pattern of expression and immunogenicity. Broadly, cancer antigens can be categorised in three groups: i) Tumour-associated antigens (TAAs), comprising differentiation antigens, overexpressed antigens, and antigens derived from endogenous retroviruses; ii) Tumour-specific antigens (TSAs), comprised mostly of neoantigens and antigens from oncogenic viruses; and iii) Cancer-germline antigens (Zamora, Crawford et al. 2018). An ideal cancer antigen should be preferentially expressed in cancer cells and not in the healthy tissue and should be able to trigger a strong immune response bypassing central tolerance (Hu, Ott et al. 2018).

Differentiation antigens are expressed by both the tumour and the healthy tissue where the tumour arises. Examples of such antigens are Melan-A/MART, gp100, and tyrosinase-related protein-2 (TRP-2), which are expressed in melanoma cells as well as in melanocytes (Vigneron, Stroobant et al. 2013); mammaglobin-A, which is expressed in breast cancer and in mammary glands (Kim, Goedegebuure et al. 2016); prostate-specific antigen (PSA), expressed in healthy prostate and prostate cancer (Wustemann, Haberkorn et al. 2019); and CD19, observed in normal and malignant B cells from patients with acute lymphoblastic leukaemia, which has been widely targeted in CAR-T cell therapies (Maude, Teachey et al. 2015).

Overexpressed antigens are abundant in certain cancers but are also expressed in different normal tissues, such as antigens derived from PRAME gene (Preferentially Expressed Antigen In Melanoma) in melanoma, and the growth factor HER2/neu (human epidermal growth factor receptor 2) in ovarian and breast carcinomas (Vigneron, Stroobant et al. 2013). The rationale behind the immunogenic nature of overexpressed antigens is associated with the process of negative selection in thymus, as circulating T cells specific for these antigens tend to have low avidity TCRs. Thus, the high expression profile of these antigens is able to prime and activate low-avidity T cells, breaking the barrier of immune tolerance (Thaxton and Li 2014). Nevertheless, the

high similarity between TAAs and self-peptides can severely limit the development of anti-tumour T cell responses due to central tolerance or lower TCR-p/MHC-I binding affinities (Stone, Harris et al. 2015). Indeed, the identification of overexpressed and/or differentiation antigens able to induce strong anti-tumour responses has been challenging and vaccination strategies employing peptides derived from MART-1, gp100 and HER2/neu have failed to show clinical benefit (Rosenberg, Yang et al. 2004).

Although overexpressed or differentiation antigens can be used to induce anti-cancer CD8+ T cell responses in a vast number of patients, they can also show high levels of off-target effects by targeting and destroying normal cells and tissues expressing such antigens. Thus, the hazard of inducing autoimmune responses by activating CD8+ T cells specific against these antigens highlights the importance of targeting antigens more specific to tumour cells. In this last regard, TAAs derived from endogenous retroviruses represent a promising target for the development of immunotherapy strategies, as these sequences tend to be more conserved among the population, they are overexpressed in various cancer types, and can be used as a shared tumour antigen (Dersh, Holly et al. 2021). Indeed, CD8+ T cell epitopes derived from murine endogenous retroviruses have shown to play a key role in the elimination of tumours in vaccination strategies (Takeda, Sato et al. 2000, Rice, Buchan et al. 2002), as well as in immunotherapeutic approaches (James, Yeh et al. 2010, James, Bailey et al. 2013). Regarding human endogenous retroviruses (HERV), the most widely associated type is HERV-K, as transcripts from this HERV have been found in a myriad of cancers, including breast cancer, lymphoma, leukaemia, endometrial and prostate cancers (Vergara Bermejo, Ragonnaud et al. 2020). The cytotoxic potential of CD8+ T cells against tumour cells expressing HERV-K has been demonstrated in ovarian cancer cells, as HERV-K specific CD8+ T cells exhibited high proliferation and IFNγ production in addition to selectively killing cancer cells expressing HERV-K but not normal cells (Rycaj, Plummer et al. 2015). Moreover, CAR-T cells specific against HERV-K *env* prevented tumour metastasis in xenograft breast cancer models in mice (Zhou, Krishnamurthy et al. 2015). Although few reports have used endogenous retroviruses as potential targets for cancer immunotherapy, these data highlight the potential these antigens have to induce strong anti-tumour responses that can be exploited in therapeutic settings.

Targeting more tumour-specific antigens, such as viral antigens, cancer-germline antigens, and neoantigens, can improve the therapeutic efficacy of immunotherapy as they can bypass central tolerance (Coulie, Van den Eynde et al. 2014) making them the ideal therapeutic target for vaccination. Vaccines targeting viral antigens have had promising results in clinical trials, as a quadrivalent vaccine consisting in a mixture of virus-like particles from four human papilloma virus (HPV) types (HPV-6, -11, -16 and -18) showed to significantly prevent the development of

high-grade cervical intraepithelial neoplasia related to HPV-16 and -18 in previously uninfected women (Future II Study Group 2007). Moreover, vaccination of women with HPV-16-positive cervical cancer with overlapping peptides from HPV-16 oncoproteins E6 and E7 induced a broad CD4+ and CD8+ T cell response against HPV-16 (Welters, Kenter et al. 2008).

Cancer-germline antigens are expressed in certain types of cancer, but not in normal tissue (with the exception of male germline cells, foetal ovaries and trophoblastic cells), and includes MAGE and NY-ESO-1 antigens, which are expressed in different cancers, including melanoma, lymphoma, and carcinomas from lung, bladder, colon and breast (Buonaguro, Petrizzo et al. 2011). The differential expression of these antigens in tumours but not in normal tissues makes them an attractive target in immunotherapy approaches. Vaccination strategies employing synthetic peptides derived from these antigens have shown to induce of CD8+ T cells in both mice (Junwei, Xiumin et al. 2016) and humans (Saito, Wada et al. 2014, Baumgaertner, Costa Nunes et al. 2016). Moreover, pilot studies using TCR-engineered T cells against NY-ESO-1 (Robbins, Kassim et al. 2015) and MAGE-A3 (Morgan, Chinnasamy et al. 2013) have shown promising results in patients with melanoma. However, T cells targeting these antigens are not always tumour specific, as fatal cases of brain damage associated with T cell therapies have been reported (Morgan, Chinnasamy et al. 2013).

Lastly, neoantigens can arise from mutated genes when a mutation changes one or more amino acids in the peptide sequence, therefore making the new mutated peptide a cancer-specific target for MHC-I presentation (Vigneron 2015). These type of antigens represent the most ideal targets for vaccination strategies, as they are unique to a specific tumour and bypass the barrier of immune tolerance that can be observed with TAAs, promoting an intra-tumoural immune response in favour of enhanced tumour control (Sahin and Tureci 2018). The first pieces of evidence showing that T cells targeting neoantigens were effective in cancer patients came out in 2005 by two independent groups. Zhou *et al.* demonstrated that T cells isolated from patients with metastatic melanoma showing complete regression after adoptive transfer of expanded autologous TILs were specific against mutated epitopes derived from growth arrest-specific gene 7 (GAS7) and glyceraldehyde-3-phosphate dehydrogenase (GAPDH) gene transcripts (Zhou, Dudley et al. 2005). Moreover, Lennerz *et al.* demonstrated that autologous T cells from a patient from melanoma targeting neoantigens showed higher levels of IFNγ production than T cells targeting epitopes derived from tyrosinase or gp100 (Lennerz, Fatho et al. 2005). This has led to the hypothesis that tumours with a higher mutational burden, i.e. the number of mutations present in a megabase of the genomic region, are more susceptible to checkpoint blockade therapies, which is observed in some patients with melanoma, lung, bladder and head and neck cancers (Yarchoan, Johnson et al. 2017, Chan, Yarchoan et al. 2019). The rationale behind this argument is that a higher frequency of mutations that results from the genomic instability of

tumours ultimately leads to an increase in the generation of neoantigens. Despite this evidence, identifying and targeting neoantigens in cancer immunotherapy can be troublesome. Tetramer-staining assays have shown that as little as 0.5-2% of screened potential neoantigens are able to generate a detectable T cell response in patients with melanoma (Pritchard, Burel et al. 2015), indicating that not all detected mutations are able to generate epitopes that bind MHC-I molecules. In this regard, some studies have shifted towards using the tumour neoantigen burden, i.e. the number of neoantigens per megabase in the genomic region, as a more precise way to predict cancer prognosis (Wang, Chen et al. 2021). In addition, given the high similarity between epitopes derived from neoantigens and epitopes derived from their WT counterpart, it is plausible that T cells able to recognize neoantigens would be underrepresented in the T cell repertoire due to thymic negative selection (Zamora, Crawford et al. 2018). Lastly, neoantigens are mostly patient-specific, and their correct identification is a laborious process that involves the use of high-throughput techniques.

1.3.2 Methodological pipelines for the identification of tumour antigens for immunotherapy

The promising therapeutic results observed in cancer immunotherapy targeting neoantigens has led to the development of high-throughput techniques able to identify such antigens in a wide number of patients. The general pipeline of these strategies involves whole-exome sequencing (WES) and RNA-Sequencing (RNA-Seq) of both tumour and healthy cells, in order to identify somatic mutations that codify for mutated proteins in the tumour (Blass and Ott 2021). This leads to the generation of a personal mutanome, which can serve as a data source to perform predictions about potential neoantigens with MHC-I-binding ability, or as a database to identify epitopes detected by liquid chromatography-mass spectrometry (LC-MS). Once these neoantigens are predicted, they can be synthesised and tested *in vitro* and/or *in vivo* (Hu, Ott et al. 2018). A study using this pipeline in the mouse tumour models MC-38 and TRAMP-C1 identified 1290 and 67 mutations in MC-38 and TRAMP-C1, respectively. From these mutations, and using the NetMHC algorithm, the authors identified 170 neoepitopes for MC-38 and 6 from TRAMP-C1, but data obtained by LC-MS only confirmed seven of such neoantigens of MC-38, and none from TRAMP-C1. Interestingly, these seven neoantigens were derived from highly abundant proteins, and when used as a vaccine prior tumour challenge, led to a complete elimination of tumours in most of the mice (Yadav, Jhunjhunwala et al. 2014). This methodology has also been applied to human tumours with promising results. A study focused on 17 patients with mantle-cell lymphoma showed that most of the neoantigens identified by LC-MS were MHC-II-restricted, with only one of the 13 neoantigens being specific for MHC-I. In addition, sorting a neoantigen-specific

CD4+ T cell clone by tetramer staining showed that, after *in vitro* expansion, cells acquired the ability to produce IL-4 and granzyme and had cytotoxic activities against autologous lymphoma cells (Khodadoust, Olsson et al. 2017). Lastly, a phase I clinical trial was performed in 6 patients with recurrent stage III melanoma using the same methodology to generate personalised vaccines, where each patient was injected with four pools of long peptides (15 – 30-mers) representing up to 20 neoantigens specific for each patient, alongside the TLR3 and MDA5 agonist poly-ICLC. From the six treated patients, four showed no signs of tumour recurrence for up to 32 months after vaccination. Interestingly, the authors found in *in vitro* assays that CD4+ T cells were the main producers of IFNγ when expanded with the correct epitopes (Ott, Hu et al. 2017). The interest for the identification of immunogenic neoantigens from RNA-Seq and WES data have prompted the development of several *in silico* approaches aimed at the identification of such antigens. Just in 2021, three different bioinformatic pipelines based on convolutional neural network (CNN) analysis have been published: DeepImmuno (Li, Iyer et al. 2021), DeepNetBim (Yang, Zhao et al. 2021), and APPM (Hao, Wei et al. 2021).

Although the previously mentioned data shows an incredible potential of personalised neoantigen vaccines in the treatment of cancer, the techniques required to generate the data that helps into the manufacturing of such vaccines have some drawbacks. Even though WES and RNA-Seq approaches have a very low rate of false negatives, i.e., the mutations found in these methodologies are indeed cancer-specific, the mutations *per se* do not account for the generation of a neoantigen. For this, the mutated protein must be processed through the antigen processing machinery, bind an MHC-I molecule, and activate the right T cell that must have the ability to infiltrate the tumour bed (Sahin and Tureci 2018). Moreover, recent studies have demonstrated that neoantigens can also arise from non-canonical translation events such as introns, as well as from genomic rearrangements including gene deletions or gene fusions, which can be often overlooked in conventional analysis of WES and RNA-Seq data (Dersh, Holly et al. 2021). Although the presentation of a given peptide by MHC-I can be detected by LC-MS, this methodology has a high rate of false negatives and is technically laborious to be implemented routinely in the clinical setting. Furthermore, the detection of peptides from immunopeptidomes in traditional LC-MS techniques requires the creation of good datasets for the assignation of the masses of the detected peptides. These databases are often constructed using genomic (WES) and transcriptomic data (RNA-Seq), and considering the point above regarding neoantigens from non-canonical translation events, this can lead to an underrepresentation of presented peptides and can severely impair the detection of neoantigens (Dersh, Holly et al. 2021). This observation has been further confirmed in studies using LC-MS coupled with WES and RNA-Seq data, as only very small portions of the mutations lead to the generation of immunogenic neoantigens, which can be

recognised by both MHC-I and –II. This poses a limitation, as not all tumours behave the same in terms of the generation of somatic mutations, making these strategies useful only for tumours with high mutation burdens (Schumacher and Schreiber 2015). As the access to LC-MS technology can be limited, a great number of researchers have relied on the bioinformatic prediction of the affinity between the neoantigen and MHC-I. Most of these predictions are done with the NetMHCpan algorithm, which uses biochemical data of peptide-MHC interactions and artificial neural networks to predict the affinity of a peptide towards a particular MHC (Jurtz, Paul et al. 2017). However, this methodology does not account for the cellular processing of the peptide and for the protein abundance from where the peptide is derived. Various studies have shown that at high abundance, low-affinity peptides can outcompete low-abundant high-affinity peptides for MHC-I binding (Boulanger, Eccleston et al. 2018), where a 10-fold increase in protein expression could approximately compensate for a 90% decrease in binding potential (Abelin, Keskin et al. 2017). In order to bypass this limitation, novel algorithms coupling antigen-presentation steps into the prediction have been developed, such as Neopepsee (Kim, Kim et al. 2018), MHCflurry 2.0 (O'Donnell, Rubinsteyn et al. 2020), and NAP-CNB (Wert-Carvajal, Sanchez-Garcia et al. 2021). Nonetheless, only Neopepsee considers the abundance of the source protein from a given epitope to calculate the likelihood of antigen presentation (Kim, Kim et al. 2018). Moreover, there are still critical components in the phenomenon of immunodominance that must be addressed in preclinical models in order to design better vaccines targeting neoantigens and to understand the mechanisms involved in tumour control in current immunotherapy strategies.

1.3.3 Ideal features of tumour antigens: affinity, avidity and immunodominance

As discussed before, the identification of tumour antigens able to induce a robust CD8+ T cell response is a critical step for the development of therapeutic vaccines, given the fact that the correct activation of CD8+ T cells ultimately relies on the recognition of a peptide presented by an MHC-I molecule. Two of the most studied characteristics of such antigens is the affinity towards MHC-I, and the functional avidity of the CD8+ T cells. Antigens with high MHC-I binding affinity result in a more stable p/MHC-I complex, which would ultimately lead to an increased likelihood of recognition by the TCR and better anti-tumour CD8+ T cell responses (Fritsch, Rajasagi et al. 2014). However, it has been reported that modified epitopes that increase the interaction times between TCR and the pMHC-I complex can negatively affect T cell activation (Kalergis, Boucheron et al. 2001), and CD8+ T cells against low-affinity epitopes have been associated with immune control in tumour mouse models (Duan, Duitama et al. 2014, Clancy-Thompson, Devlin et al. 2018). Functional avidity, which refers to the sensitivity of a given T cell clone to be activated in different concentrations of the antigen (Stuge, Holmes et al. 2004), may represent a more

plausible indicator of the anti-tumour activity of CD8+ T cells. In mouse melanoma models, it has been established that vaccination with low concentrations of epitopes derived from TRP-2 yields specific CD8+ T cell clones with high functional avidity, i.e., with the ability to recognize and kill target cells pulsed with low concentrations of the peptide. Similar high avidity T cells have also been reported in melanoma patients vaccinated with synthetic peptides, in which vaccination induced an increase of high-avidity CD8+ T cells with anti-tumour activity (Dutoit, Rubio-Godoy et al. 2001, Stuge, Holmes et al. 2004). Furthermore, Speiser *et al.* showed that the high avidity CD8+ T cell population induced by vaccination has a T_{EM} phenotype with high expression levels of granzyme B, IFNγ and PRF1 (Speiser, Baumgaertner et al. 2006). Despite this evidence, focusing exclusively on the activation of high-avidity CD8+ T cells in cancer immunotherapy can be detrimental. Recent studies have shown that NY-ESO-1-specific CD8+ T cells harbouring TCRs with supraphysiologically high avidity are functionally impaired, failing to show phosphorylation of ERK1/2 upon TCR engagement, as well as a transient and reversible phosphorylation of LCK and CD3ζ (Presotto, Erdes et al. 2017). Furthermore, results obtained in our group have shown that CT26-challenged mice that achieve tumour regression after anti-PD-1 therapy display a preferential expansion of low-avidity T cells (Sugiyarto, Unpublished data).

An additional limitation for the development of tumour-specific high-avidity T cells relies on the phenomenon of immunodominance. By definition, pathogen specific CD8+ T cells will only respond towards a small fraction of the potential peptidome generated by any given pathogen, being the immunodominant responses directed towards the epitopes that yield the maximum magnitude of CD8+ T cell responses. These responses are influenced by the abundance of peptide-MHC-I complexes on APCs and the numbers of naïve T cells with specific TCRs able to recognize these complexes (Yewdell 2006). In viral infections, these immunodominant responses are mainly driven by T cells harbouring high-avidity TCRs (Cukalac, Chadderton et al. 2014, Lissina, Chakrabarti et al. 2016), however, the process of negative selection in thymus can impair the development of such high-avidity immunodominant responses in cancer, as T cells harbouring high-avidity TCRs against self-peptides are deleted during T cell ontogeny (Thaxton and Li 2014). Moreover, cancer immunoediting can also shape the frequency of immunodominant epitopes expressed by a tumour, by destroying highly immunogenic tumour cells in the elimination phase, or by promoting epigenetic silencing of immunogenic tumour genes during the early stages of cancer development, thus driving a heterogeneous antigenic landscape in tumours (Matsushita, Vesely et al. 2012, Schumacher and Schreiber 2015). Collectively, these results emphasise the importance of studying the immunodominance patterns of tumour-derived peptides and the functional avidity of CD8+ T cells towards these responses, as fine-tuning these parameters in current immunotherapeutic strategies will likely increase the levels of clinical success.

Regarding the frequency of tumour-specific T cells, there has been a notion that pre-existing CD8+ TILs are necessary for the success of cancer immunotherapy, but this marker alone does not guarantee a beneficial clinical outcome. A preclinical study using the B16 melanoma model showed that up to 20% of the infiltrating lymphocytes were virus-specific, but in contrast with tumour-specific cells, showed no signs of dysfunction and exhaustion (Erkes, Smith et al. 2017). A study using combinatorial tetramer staining to detect the specificities of TILs in samples from patients with lung or colorectal cancer showed that 37.5% of lung cancer patients and 50% of colorectal cancer patients had infiltration of non-cancer-specific TILs, with most being specific for viral antigens (Simoni, Becht et al. 2018). Moreover, a study where the TCRα/β chains of CD8+ TILs was deep-sequenced and then transduced into naïve T cells for functional assays showed striking results. Despite the fact that all the tumours evaluated had a broad TCR repertoire, most of the TCRs obtained from TILs derived from patients with melanoma were reactive against autologous tumour samples, whereas none of the TCRs from ovarian cancer patients responded against autologous tumour cells (Scheper, Kelderman et al. 2019). Altogether, these data help to discriminate two types of cancers according with the degree of infiltration of tumour-specific lymphocytes as well as immunosuppressive cells: tumours with a high infiltration of cancer-specific T cells, known as “hot” tumours, and tumours where the majority of infiltrating lymphocytes are bystander cells, referred as “cold” tumours (Scheper, Kelderman et al. 2019).

The data mentioned previously indicates that for a cancer antigen to be a successful target for the vaccine design, it must fulfil certain requirements. First, it must be preferentially expressed (or ideally uniquely) in tumour cells, with a uniform pattern of expression across the tumour. Moreover, it should bind with a relative high affinity towards the MHC-I molecule, although low-affinity epitopes have also shown to participate in the priming and activation of tumour-specific CD8+ T cells (Sugiyarto, Prossor et al. 2021). Lastly, the TCR of CD8+ TILs must recognise these antigens to generate an immune response. Several strategies have been implemented to address all these criteria, being most of them focused on the identification of neoantigens, as the pool of neoantigen-specific CD8+ T cells are not affected by immune tolerance (Stahl, Sacher et al. 2009). Consequently, the identification of tumour antigens sharing these characteristics represents the ‘holy grail’ of cancer immunotherapy, and ongoing efforts aimed at better understanding the immunodominance patterns of these cancer antigens will greatly improve the likelihood of detecting highly immunogenic and tumour-specific antigens that could be exploited in therapeutic settings.

1.4 Animal models for the evaluation of immunotherapy strategies: the relevance of CT26

A key step in the development and validation of new immunotherapy strategies against cancer involves the pre-clinical evaluation and validation of the anti-cancer effect of a given molecule or compound in mouse tumour models. Such models also represent one of the first insights into the biology of a specific cancer, and the molecular mechanisms that can explain its pathogenesis (Yee, Ignatenko et al. 2015). One of the most studied preclinical tumour models used in research and development of immunotherapy is CT26 (Colon Tumour 26), which is a colorectal carcinoma model developed by Griswold and Corbett in 1975 by intra-rectal exposure of N-nitroso-N-methylurethane (NMU) in BALB/c mice, leading to a fast-growing grade IV carcinoma that can be easily cultured and transplanted (Griswold and Corbett 1975). Genomic and transcriptomic analysis has shown that CT26 tumour cells harbour a homozygotic mutation in the *kras* proto-oncogene, as well as a deletion in the tumour suppressor gene *cdkn2a* (cyclin-dependent kinase inhibitor 2A), showing a genetic phenotype similar to aggressive, undifferentiated, refractory human colorectal carcinoma cells (Castle, Loewer et al. 2014). Interestingly, the highest expressed gene in these cells corresponds to an endogenous retrovirus sequence encoding the envelope glycoprotein (gp70) of an ecotropic murine leukaemia virus (MuLV) (Castle, Loewer et al. 2014), and an H-2L^{d}-restricted epitope derived from this protein (AH-1 – SPSYVYHQF) has been described as the immunodominant CD8+ T cell epitope in naïve mice (Huang, Gulden et al. 1996). Despite these results, vaccination strategies aimed to boost AH1-specific CD8+ T cell responses have failed to eliminate established CT26 tumours (Slansky, Rattis et al. 2000, Jordan, McMahan et al. 2010), highlighting the necessity to identify epitopes that induce stronger CD8+ T cell responses. Recent studies have revealed that upon Treg depletion, CT26 tumours are eliminated in 73% of the animals (Golgher, Jones et al. 2002), and that CD8+ T cells recognizing an H-2D^{d}-restricted epitope from the same MuLV gp70 gene (GSW11 – GGPESFYCASW) are associated with this phenomenon (James, Yeh et al. 2010). Interestingly, GSW11 binds with a significantly lower affinity to H-2D^{d}, compared to AH1 affinity for H-2L^{d}, and in normal conditions, this epitope is overtrimmed by ERAAP (James, Bailey et al. 2013). Altogether, these results demonstrate the role of GSW11 in the development of effective anti-tumour CD8+ T cell responses against CT26 and highlights the requirement for the exploration of novel antigens in both mice and humans with potential therapeutic benefit.

CT26 is one of the most widely used pre-clinical models for the testing of immunotherapeutic approaches, and the anti-tumour activity of different immunotherapeutic strategies has been confirmed in this model, including anti-CTLA-4 (Higashikawa, Yagi et al. 2014), anti-PD-1/PD-L1

(Maute, Gordon et al. 2015), DC-based therapies (Yasuda, Kamigaki et al. 2007) and combinatorial schemes (Duraiswamy, Kaluza et al. 2013). Several other strategies have been tested in CT26, showing promising results. Two studies targeting TIGIT (T cell immunoreceptor with Ig and ITIM Domains) have highlighted the potential therapeutic effect of blocking this molecule in cancer. TIGIT is expressed in activated T cells and NK cells, and engagement of this molecule with any of its ligands (CD112 or CD155) leads to an inhibition of T cell responses (Manieri, Chiang et al. 2017). In addition, upregulation of TIGIT in Tregs leads to an increase in their activity, and the TIGIT-mediated immunosuppression in the CT26 TME is likely to act through a Treg-mediated suppression of CD8+ T cells (Kurtulus, Sakuishi et al. 2015). Not surprisingly, combination of anti-TIGIT and anti-PD-L1 leads to the elimination of tumours in mice (Johnston, Comps-Agrar et al. 2014), suggesting that TIGIT blockade may release CD8+ T cells from Treg-mediated immunosuppression. Some characteristics of the CT26 TME have been studied, as different components of this microenvironment can hamper the development of an anti-tumour immune responses. The production of IL-6 by tumour cells negatively affect the CD8+ T cell response, as IL-$6^{-/-}$ mice exhibit a significant decrease in tumour growth compared to WT mice, which was correlated by an accumulation of both CD4+ and CD8+ T cells, as well as mature DCs in the TME (Ohno, Toyoshima et al. 2017). Altogether, these results show the plasticity of the CT26 model to evaluate different types of immunotherapeutic approaches, and the importance of this model to validate novel strategies to be employed in clinical trials.

1.5 Conclusions

The advent of cancer therapies targeting the immune system instead of cancer cells have proven its utility in clinical settings, as results in clinical trials have shown complete remission employing different strategies, representing a substantial improvement compared to traditional chemo and radiotherapy approaches. However, although some immunotherapy drugs, such as ipilimumab, have already been approved for the treatment of cancer, several aspects should be considered to maximize the efficacy of these drugs. A comprehensive study of tumour antigens in different cancers is crucial, as this would lead to the development of more targeted strategies. Using TSAs for vaccination allows the development of ‘universal’ vaccines, which can be used to immunize a large population of patients, although their clinical efficacy can be limited. Targeting neoantigens can drastically improve the clinical benefit of vaccination strategies, but their unique expression pattern among patients makes them nearly impossible to administer in large cohort of patients, requiring a personalization of the vaccine in order to induce significant clinical responses. The main disadvantage of this strategy is the high costs it entails for patients, and the technical difficulties inherent to the process of the correct identification of such personal neoantigens.

Moreover, although the TME represents an immunosuppressive microenvironment that blocks the development of anti-tumour CD8+ T cell responses, not all cancers share the same immunoregulatory mechanisms in the TME, and an immunological characterization of such mechanisms in human cancers is essential to improve the success of the therapies. Finally, the use of animal models has been of pivotal importance to understand the biology of cancer; however, these results cannot be fully translated into human cancers in some cases, for which the data obtained in these models should be interpreted with cautiousness. Notwithstanding, immunotherapy is perhaps one of the most promising fields for the treatment of cancer and addressing the abovementioned issues in the rational development of new drugs should bring significant clinical benefits to patients.

1.6 Study proposal

The results obtained by our group highlight the relevance of tumour-specific CD8+ T cells in the elimination of CT26 tumours in Treg depleted mice and in mice treated with anti-PD-1 (Golgher, Jones et al. 2002). Of particular relevance, the only two immunogenic epitopes described so far in this tumour model (AH1 and GSW11) derive from the most abundant protein in CT26 and the binding affinity of these epitopes is relatively low compared to immunodominant epitopes from other tumour models (James, Yeh et al. 2010). However, there is a lack of knowledge about other CD8+ T cell epitopes in the CT26 model, and the identification of these will improve our understanding of the immune mechanisms participating in the control of CT26 and represent a crucial analysis for the validation of the relationship between immunodominance and peptide abundance. Therefore, the purpose of this study was to identify novel CD8+ T cell epitopes in the CT26 tumour model by integrating the peptide predicted affinity towards MHC-I molecules. and the abundance of the source protein, to improve the likelihood of detection of immunogenic epitopes. Furthermore, the relationship of such novel epitopes with therapeutic responses, specifically with Treg depletion therapy, was be evaluated. Finally, the immunophenotype of CD8+ T cells specific against these novel epitopes in relevant tissues was also addressed.

1.7 Aims

In order to address the questions raised previously, we aimed to:

- Integrate the predicted peptide affinity with the abundance of the source protein from immune-transcriptomic data in an *in-house* Peptide Filter Relation (PFR) formula to increase the probability of detecting novel immunogenic epitopes.

- Investigate, via intracellular cytokine staining and proliferation assays of CD8+ T cells from naïve and Treg depleted mice, the potential therapeutic relevance of the computationally predicted novel epitopes, and the relationship between affinity and abundance in therapeutically-relevant epitopes.

- Explore the phenotypic traits of antigen-specific CD8+ T cells in tumours and tdLNs and correlate these markers with the therapeutic benefit observed in treated animals.

Chapter 2 Materials and Methods

2.1 Data filtering and sorting for the prediction of novel epitopes

For the identification of novel CD8+ T cell epitopes from the CT26 tumour model, publicly available genomic (WES) and transcriptomic (RNA-Seq) data was used (Castle, Loewer et al. 2014). From these data single nucleotide mutations (SNV) were mined and analysed by NetMHC4.0 (Jurtz, Paul et al. 2017), in order to predict the best epitope harbouring the mutation, the MHC-I restriction, and the affinity towards MHC-I in IC_{50} nanomolar (nM) values. Furthermore, the relative abundance of each mutated peptide was matched based on the gene expression levels of the source protein expressed in RPKM units (reads mapped per kilobase of transcript length per million mapped reads). Once these mutated peptides were sorted based on their MHC-I restriction, transcript abundance and MHC-I affinity, they were ranked using solely the predicted affinity, or using the *in house* PFR that incorporates abundance and affinity using the following simplified formula:

$$[MeP_i] \approx {}^{g_i}/_{u_i^{\alpha}}$$

Where:

- **MeP_i:** equilibrium cell surface abundance of a given peptide bound to MHC at the cell surface
- **g_i:** supply of the peptide via TAP (abundance)
- **u_i:** rate of dissociation of the peptide from MHC-I
- **α:** peptide dependency of tapasin. For this study, we assumed an α value of 2 indicating tapasin dependence for all peptides

In addition to mutated peptides, this analysis was also performed in WT peptides derived from MuLV gp70, considering that this protein is the most abundant in the CT26 proteome, and that the two known CD8+ T cell epitopes in CT26 (AH1 and GSW11) derive from this protein.
In this model, the higher the MeP_i value the higher the likelihood of that peptide being presented at the cell surface, whereas in NetMHC, the lower the IC_{50} the higher the predicted affinity towards the MHC-I molecule. These values were then sorted from higher to lower (for PFR) or lower to higher (for NetMHC) and given a rank based on the relationship between affinity and abundance, or on affinity alone. The schematic representation of this analysis is detailed in **Figure 2.1**. The source genes from the selected peptides were further analysed via Gene Ontology (GO) annotations using the DAVID platform (database for annotation, visualization and integrated discovery) (Huang da, Sherman et al. 2009).

Considering the limitation imposed by using a immuno-transcriptomic profile of CT26 cells from a potentially different batch, we used a new lot of ATCC CT26 cells, which were kept at low passage numbers (7 – 10), in order to better mimic the conditions where the immuno-transcriptomic analyses were performed.

Figure 2.1 Schematical representation of data analysis and sorting for the prediction of novel epitopes

2.2 Mice and immunization strategy

BALB/c mice (6 – 8 weeks old) were bred locally under specific pathogen-free conditions. Animals were housed in individually ventilated cages during all experimental procedures at the Preclinical Unit of the University of Southampton Centre for Cancer Immunology. For Treg depletion, animals were injected intra-peritoneally (i.p.) with 200µg of PC61, an IgG1 anti-mouse CD25 raised in rat, at days -3 and -1 of tumour challenge. Two different PC61 antibodies were used: an in-house PC61 and a commercial version (Bio X Cell, West Lebanon, NH). Bleeding was performed by

drawing 70µl blood from lateral tail vein into 7µl 1mM EDTA. For tumour challenge, mice were injected subcutaneously (s.c.) with 10^5 CT26 cells resuspended in 100µl of sterile endotoxin-free PBS (Sigma-Aldrich, Darmstadt, Germany). Tumour growth was monitored daily from day 6 post tumour challenge, and tumour size was calculated considering the measurements of length and width. Animals were culled when tumour size reached 225mm^2 by Schedule 1 procedures. All animal experiments were carried out under the personal license (PIL) I2D847F47, and the project license (PPL) P1FBFBA35.

2.3 Cell lines

CT26 cells (ATCC® CRL2638™) have been described previously in this manuscript (Griswold and Corbett 1975). Cells were kept *in vitro* at a low passage number and injected into BALB/c mice at passages 6 to 12. P815 cells (ATCC® TIB-64™) are derived from murine mastocytoma, and served as APCs in peptide stimulation assays due to their high expression of classical H-2^d molecules (**Figure 2.2**) (Ralph, Moore et al. 1976). BWZ.36/CD8α cells derive from the thymoma cell line BW5147, where these cells were stably transfected with an NFAT-LacZ construct along with CD8α (Sanderson and Shastri 1994), and were cultured as fusion partners for the development of T cell hybridomas. HeLa cells (ATCC® CRM-CCL-2™) were used as targets for transfection experiments. Lastly, the LacZ-inducible GSW11-specific T cell hybridoma CCD2Z was previously generated by fusing a CT26-specific CD8+ T cell clone with the BWZ.36/CD8α fusion partner (James, Yeh et al. 2010), and served as control cells for Chlorophenol red-β-D-galactopyranoside (CPRG) experiments. RMA-S cells derive from the Rauscher virus-induced H-2^b lymphoma RBL-5 by exposure to the mutagen ethyl methane sulphonate (EMS) and repeated rounds of treatment with antisera against MHC-I molecules and complement (Ljunggren and Karre 1985). Under normal incubation conditions, RMA-S cells have a 20-fold decrease in the cell surface expression of classical MHC-I molecules, owing to a deficiency in TAP (Townsend, Ohlen et al. 1989). Three different RMA-S cells were used: RMA-S Kd, RMA-S Dd and RMA-S Ld, each of them stably transfected with the respective MHC-I molecule. All cell lines and hybridomas used in this study were maintained in R10 media, consisting in RPMI 1640 (Lonza, Basel, Switzerland) supplemented with 10% foetal bovine serum (FBS; GE Healthcare, Chicago, IL), 2mM L-glutamine (Sigma-Aldrich, Darmstadt, Germany), 10% penicillin/streptomycin (Sigma-Aldrich, Darmstadt, Germany), 0.05mM 2-mercaptoethanol (Sigma-Aldrich, Darmstadt, Germany), 1mM sodium pyruvate (Life Technologies-BRL, Rockville, MD), and 1mM HEPES (Lonza, Basel, Switzerland). BWZ.36/CD8α were cultured in R10 with the addition of 0.25mg/ml Hygromycin B (InvivoGen, San Diego, CA) and 1mg/ml G418 (Thermo-Fisher Scientific, Waltham, MA). All cells were cultured at 37°C and 5% CO_2 concentration in a humidified incubator.

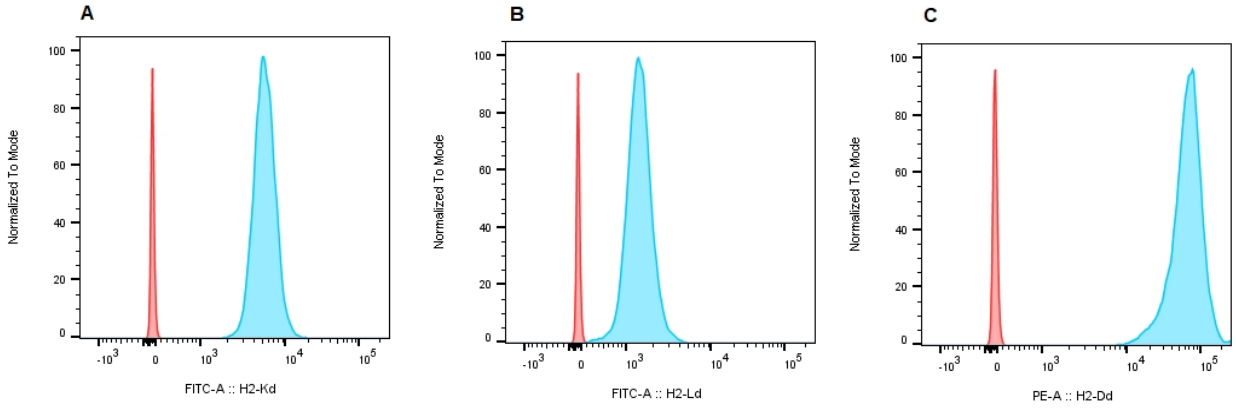

Figure 2.2 P815 cells express high levels of H-2^d molecules. P815 cells were stained with fluorescent-labelled monoclonal antibodies anti-H-2K^d (A), -H-2L^d (B), and –H-2D^d (C). Red histograms represent the background levels in unstained cells, whereas blue histograms depict stained cells with each respective antibody. All histograms represent the staining intensity normalized to mode.

2.4 BFA decay assays

For *in vitro* measuring of peptide affinity towards MHC-I molecules, Brefeldin-A (BFA) decay assays were performed using RMA-S K^d, D^d or L^d cell lines. For each peptide, 90 x 10^5 cells were cultured in R10 at a concentration of 1 x 10^6 cells/ml and pulsed with peptides at a final concentration of 10µM. Pulsed cells were then incubated at 26°C overnight to induce overexpression of MHC-I molecules. For the kinetic measurement of MHC-I decay, 5 x 10^5 pulsed cells were incubated at eight different time points (6h, 5h, 4h, 3h, 2h, 1h, 30 minutes, and time 0) at 37°C, after being washed twice with fresh R10, and resuspended in R10 supplemented with 1:1000 BD GolgiPlug™ (containing BFA, BD Biosciences, Franklin Lakes, NJ). Once all the time points were completed, cells were harvested, washed twice PBS containing 0.5% heat-inactivated FBS and 0.5% EDTA 0.5M (FACS Buffer), and stained with fluorescently-labelled monoclonal antibodies against H-2K^d, H-2D^d, or H-2L^d (Table 2.1) as described in section 2.7.2. Negative controls for this experiment included un-pulsed RMA-S cells kept at 26°C or 37°C, and un-pulsed cells analysed after incubating at the eight time points at 37°C. In order to obtain robust data, three replicate experiments were performed for each peptide. From flow cytometry data, the mean fluorescence intensity (MFI) values from un-pulsed RMA-S cells at the 6h time point was considered the background level of MHC-I expression for each replicate, and this value was subtracted from the MFI from each time point of peptide-pulsed cells. These normalised values were plotted as a one-phase exponential decay, allowing for the calculation of IC_{50} values using the following formulas:

$$Y = (Y_0 - Plateau) \times e^{(-Kx)} + Plateau$$

Where:

- **Plateau:** represents the Y value at infinite times (Constrained to 0 given the correction applied to the data).
- ***K:*** the rate constant, expressed in reciprocal of the X axis time units.

The half-life ($t_{1/2}$) is further calculated as follows:

$$t_{1/2} = {\ln 2}/{K}$$

which allows for the calculation of the IC_{50}:

$$IC_{50} = {\ln 2}/{1000 \times t_{1/2}}$$

2.5 Verification of peptide immunogenicity

The detection of immunogenic responses from the novel peptides was performed using intracellular IFNγ cytokine staining (ICS) assays from mice splenocytes and tdLNs. Briefly, single-cell suspensions were created via mechanical dissociation of the tissues into a 70µm cell strainer (BD Biosciences, Franklin Lakes, NJ). Cells were then resuspended in R10 at a concentration of 10^6 cells/well and seeded into U-bottom 96-well plates. Then, splenocytes were pulsed with CT26-derived peptides in the presence of 0.2µl of BD GolgiPlug™ (BD Biosciences, Franklin Lakes, NJ) to prevent the release of IFNγ into the supernatant and incubated for 4 hours at 37°C and 5% CO_2. Supernatants were removed by centrifuging at 1200min^{-1} for 5 minutes, and cells were stained using the ICS protocol as in section 2.7.3. As positive controls of this technique, different concentrations of Staphylococcal Enterotoxin B (SEB, Sigma-Aldrich, Darmstadt, Germany), Concanavalin A (ConA, Sigma-Aldrich, Darmstadt, Germany), and Phorbol 12-myristate 13-acetate (PMA) plus Ionomycin (Sigma-Aldrich, Darmstadt, Germany) were tested for the same period of time in BALB/c splenocytes. As negative control, the same volume of Dimethyl Sulfoxide (DMSO, Sigma-Aldrich, Darmstadt, Germany) used for peptide stimulation was added to each specimen and incubated for the same amount of time prior ICS. All the peptides used in this study were synthesised by Synpeptide (Shanghai, China) and used at a final concentration of 10µM.

2.6 Proliferation assays

Proliferation of splenocytes stimulated with the tested peptides was performed using carboxyfluorescein succinimidyl ester (CFSE) as an additional test to verify immunogenicity, according to manufacturer instructions. Briefly, spleens from untreated or Treg-depleted mice were harvested at day 11 post-tumour challenge. After obtaining a single-cell suspension, splenocytes were washed twice and resuspended at a concentration of 1 x 10^6 cells/ml with PBS. In parallel, the CellTrace CFSE staining solution (Invitrogen, Carlsbad, CA) was resuspended in 18µL DMSO, which was then added to 20mL pre-warmed PBS to obtain a 5µM staining solution. Subsequently, splenocytes were centrifuged at 1200min^{-1} for 5 minutes and supernatants discarded. The cell pellets were then resuspended in 10 mL of 5µM CellTrace CFSE staining solution and incubated at 37°C for 20 minutes. After incubation, the staining reaction was stopped using pre-warmed R10 and incubating for 5 minutes at 37°C. Cells were washed to eliminate excess CFSE, transferred to flat-bottom 96-well plates, and stimulated with each of the novel peptides at a final concentration of 10µM for 72 hours. As positive control, ConA (Sigma-Aldrich, Darmstadt, Germany) at a final concentration of 5µg/ml was used, whereas the same amount of DMSO was added as negative control for each specimen. Following the 72 hours incubation, cells were harvested, washed twice with FACS buffer, and stained with a viability dye and cell-surface markers as described in section 2.7.4. After data acquisition, proliferation was analysed using the Proliferation, Expansion, and Replication indexes from the Live CD8+ CFSE+ lymphocyte region, using the FlowJo™ Software (BD Biosciences, Franklin Lakes, NJ).

2.7 Flow cytometry assays

All flow cytometry assays performed in this study were carried out using a BD LSRFortessa™ X-20 flow cytometer (BD Biosciences, Franklin Lakes, NJ).

2.7.1 Antibodies

All the monoclonal antibodies used in immunophenotyping, BFA decay, proliferation, and blocking assays are listed in Table 2.1. Antibodies against classical MHC-I molecules were used for blocking assays as well as for staining P815 and CT26 cells. A PE-Cy7-conjugated Rat IgG1 κ (Invitrogen, Carlsbad, CA) was used as isotype control for the PE-Cy7-conjugated anti-mouse IFNγ monoclonal antibody.

Table 2.1 List of monoclonal antibodies and tetramer/dextramers used in flow cytometry assays

Antibody	Fluorochrome	Clone	Host/Isotype	Company
Anti-CD3	APC	17A2	Rat/IgG2b, κ	BioLegend
Anti-CD8α	PE	53-6.7	Rat/IgG2a, κ	Invitrogen
	V450	53-6.7	Rat/IgG2a, κ	BD Biosciences
Anti-IFNγ	PE-Cy7	XMG1.2	Rat IgG1, κ	BD Biosciences
Anti-CD4	PE	GK1.5	Rat/IgG2b, κ	BD Biosciences
Anti-CD4	BV510	RM4-5	Rat/IgG2a, κ	BioLegend
Anti-CD25	FITC	7D4	Rat/IgM, κ	BD Biosciences
Anti-FOXP3	APC	FJK-16s	Rat/IgG2a, κ	Invitrogen
Anti-TCRβ chain	APC	H57-597	Armenian Hamster/IgG	BioLegend
Anti-H-2D^{d}	PE	34-5-8S	Mouse/IgG2a	Invitrogen
Anti-H-2K^{d}	FITC	SF1-1.1	Mouse/IgG2a, κ	BD Biosciences
	BV421	SF1-1.1	Mouse/IgG2a, κ	BioLegend
Anti-H-2L^{d}	FITC	30-5-7S	Mouse/IgG2a, κ	Invitrogen
Anti-CD44	PerCP	IM7	Rat/IgG2b, κ	BioLegend
Anti-CD197 (CCR7)	AlexaFluor 700	4B12	Rat/IgG2a, κ	Invitrogen
Anti-CD62L	APC/Cy7	MEL-14	Rat/IgG2a, κ	BioLegend
Anti-CD279 (PD-1)	BV785	29F.1A12	Rat/IgG2a, κ	BioLegend
Anti-CD366 (TIM-3)	AlexaFluor 647	B8.2C12	Rat/IgG1, κ	BioLegend
Anti-CD223 (LAG-3)	FITC	eBioC9B7W	Rat/IgG1, κ	Invitrogen
GSW11 Tetramer	PE	Single-chain trimer	-	In house development
H-2Ld/ SPSYVYHQF (AH1) Pentamer	PE	Pentamer	-	ProImmune
H-2Kd/DYITVSNNL (Kd34) Dextramer	PE	Dextramer	-	Immudex
H-2Kd/YYLAAPTGT (Kd37) Dextramer	PE	Dextramer	-	Immudex

Antibody	Fluorochrome	Clone	Host/Isotype	Company
Anti-CD16/CD32	Purified	2.4G2	Rat/IgG2b, κ	BD Biosciences

2.7.2 Staining with cell-surface markers

Staining of cells with fluorescent-labelled monoclonal antibodies was performed in U-bottom 96-wells plates, in a final staining volume of 50µl of FACS buffer. For staining conditions including only cell-surface markers, cells were resuspended in R10 at a concentration of 10^6 cells/well. Then, plates were centrifuged at 1500min^{-1} for 2 minutes at room temperature and supernatants discarded. Afterwards, Fc receptors were blocked using an anti CD16/CD32 blocking antibody at a concentration of 0.7µg/µl and incubated for 30 minutes on ice in the dark. After two washing steps using FACS buffer, cells were resuspended with 100µL PBS and 0.1µL LIVE/DEAD™ Fixable Red or Green Dead Cell Stain, where appropriate (Invitrogen, Carlsbad, CA), and incubated for 30 minutes at room temperature protected from light. Cells were then washed twice with FACS buffer, resuspended with 50µL FACS buffer and stained with the respective amounts of cell-surface monoclonal antibodies for 30 minutes on ice in the dark. Subsequently, stained cells were washed twice with FACS buffer, and incubated with 100µL of 1% paraformaldehyde (PFA) for 20 minutes at room temperature in the dark to fix the cells. After fixing, cells were washed twice with FACS buffer, and resuspended in 200µL of this same buffer for subsequent data acquisition.

2.7.3 IFNγ cytokine staining

After the 4h peptide stimulation, cells were resuspended in R10 at a concentration of 10^6 cells/well. Plates were centrifuged at 1500min^{-1} for 2 minutes at room temperature and supernatants discarded. Cells were then washed twice with PBS and incubated with Zombie Green™ Fixable viability dye (BioLegend, San Diego, CA) for 15 minutes at room temperature protected from light. Cells were washed prior to blocking Fc-receptors with CD16/CD32 blocking antibody for 30 minutes on ice in the dark. After this blocking step, cells were washed twice with FACS buffer as mentioned before, resuspended in 50µl of buffer and stained with anti-CD3 and anti-CD8 antibodies. After a 30-minute incubation on ice in the dark, stained cells were washed twice with FACS buffer and incubated with 100µl Fixation/Permeabilization solution (BD Biosciences, Franklin Lakes, NJ) for 20 minutes at 4°C in the dark. Then, cells were washed twice with 1:10 Perm/Wash™ buffer (BD Biosciences, Franklin Lakes, NJ), resuspended in 50µl of this same buffer, and incubated with anti-IFNγ antibody for 30 minutes on ice in the dark. After staining, cells were washed twice with 1:10 Perm/Wash™ buffer and resuspended in 200µl of 1% PFA for flow cytometry analysis.

2.7.4 Staining of CFSE-labelled cells

For the proliferation analysis, CFSE-labelled cells were harvested after the 72 hours incubation and washed twice with PBS. Then, cells were resuspended with 100µL PBS and 0.1µL LIVE/DEAD™ Fixable Red Dead Cell Stain (Invitrogen, Carlsbad, CA), and incubated for 30 minutes at room temperature protected from light. Then, cells were washed twice and resuspended with 50µL FACS buffer and stained with anti-CD3 and anti-CD8 monoclonal antibodies for 30 minutes on ice in the dark. After the staining step, cells were washed twice and fixed by incubation with 100µL of 1% PFA for 20 minutes at room temperature in the dark. Lastly, cells were washed twice and resuspended with 200µL FACS buffer for subsequent flow cytometry data acquisition.

2.8 Development of CT26-specific CD8+ T cell hybridomas

For the generation of CT26-specific CD8+ T cell hybridomas, splenocytes from Treg-depleted mice that eliminated the CT26 tumour were fused with BWZ.36/CD8α cells using polyethylene glycol (PEG).

2.8.1 PEG-mediated fusion

CT26-specific hybridomas were developed using splenocytes from Treg-depleted tumour-free mice. Briefly, tumour-free mice were re-challenged *in vivo* with 10^5 CT26 cells s.c., in order to boost the immune response and increase the frequency of CT26-specific CD8+ T cells. Seven days after re-challenge, splenocytes and tdLNs were harvested and cell suspensions from each animal were re-stimulated *in vitro* with x-ray-irradiated (10 Gy) CT26 cells in R10 supplemented with 10U/ml of recombinant mouse IL-2 (PeproTech, Rocky Hill, NJ) for 4 days. After this period of stimulation, viable T cells were recovered using a density gradient with Ficoll-Paque (GE Healthcare, Chicago, IL) by centrifugation at 2000min^{-1} for 30 minutes and removing the lymphocytic interface. Then, 3 x 10^6 live CD8+ T cells were fused with BWZ.36/CD8α fusion partners at a 1:1 T-cell:partner ratio using pre-warmed PEG (Sigma-Aldrich, Darmstadt, Germany), washed with pre-warmed serum-free medium and incubated at 37°C for eight minutes. Fused cells were washed and then cultured for 7 to 10 days in flat-bottom 96-well plates at a density of 3 x 10^5 cells/ml in 200µL R10 supplemented with 1X HAT (Sigma-Aldrich, Darmstadt, Germany) and 0.25mg/ml Hygromycin B. After this time, wells that showed signs of cell growth were cultured for 7 more days in R10 with 1X HT (Sigma-Aldrich, Darmstadt, Germany), in order to wean off HAT. Finally, the newly developed hybridomas were kept in R10 for further analysis.

2.8.2 Hybridoma testing

The specificity and sensitivity of the newly developed hybridomas was measured using a series of different activators. Activation of the *lacZ* gene was verified by activating all the clones with 5ng/ml PMA (Sigma-Aldrich, Darmstadt, Germany) plus 500ng/ml Ionomycin (Sigma-Aldrich, Darmstadt, Germany) for 4 hours. TCR-mediated signalling was checked by stimulating the hybridomas with 0.5µg/ml of soluble anti-mouse CD3ε for 16 hours at 37°C. Peptide specificity was detected by pulsing 10^5 P815 cells with the respective peptides at a concentration of 100nM prior to co-culturing with 10^5 hybridoma cells for 16 hours at 37°C and 5% CO_2. After stimulation, supernatants were discarded and 100µl of CPRG solution were added into the cells and followed by a room temperature incubation. The CPRG solution is prepared by dissolving 91mg CPRG reagent (Sigma-Aldrich, Darmstadt, Germany) in 1L of PBS containing 1.25ml NP40 and 9ml $MgCl_2$. CPRG is a substrate for the β-galactosidase produced upon *lacZ* activation, which cleaves the CPRG releasing β-galactose and chlorophenol red. This reaction leads to a colorimetric change in the buffer from yellow to increasing intensities of red that can be measured by absorbance at a wavelength of 595nm, with an additional measurement at 695nm to subtract background levels. Thus, this assay allows an easy detection of the sensitivity of the hybridomas, as the absorbance detected at 595nm is directly proportional to the levels of β-galactosidase produced by the cells, which is positively correlated with the level of cell activation. All absorbance measurements were performed in an iMark Microplate reader (BioRad, Hercules, CA) at point zero (just after adding the CPRG reagent) and every hour thereafter.

2.8.3 Sub-cloning of hybridomas

Due to overgrow of non-specific cells and to the loss of TCR expression in specific clones, hybridomas must be subcloned regularly in order to keep a batch of sensitive cells. Briefly, hybridomas were diluted at a concentration of one cell/well at final volume of 200µl of R10 in flat-bottom 96-well plates. Cells were grown for 7 to 10 days at 37°C and 5% CO_2, and every well with signs of cell growth was tested by taking 100µl of cells and co-culturing with 10^5 CT26 overnight. After a CPRG assay, only the cells that show a high sensitivity against CT26 were further expanded and frozen down to maintain the stock. This process was repeated whenever the performance of the hybridomas appeared suboptimal.

2.8.4 MHC-I Blocking assays

In order to determine the MHC-I restriction of the newly developed hybridomas, 10^5 CT26 cells were incubated with serial dilutions of anti-mouse H-2K^d (SF1-1.1), H–2D^d (34-5-8S) or H–2L^d (30-

5-7S) for one hour at 4°C before being cultured together with hybridoma cells, as described above in section 2.8.2.

2.9 Engineering of a H-2L^d/AH1 single chain trimer (SCT)

In order to monitor the frequency of AH1-specific CD8+ T cells by flow cytometry, the development of a SCT construct was tried as previously described (Mitaksov, Truscott et al. 2007).

2.9.1 Site directed mutagenesis (SDM) of H-2L^d/AH1 SCT

SDM was performed from a previously generated SCT containing the AH1 peptide linked to β2M and H-2L^d heavy chain. Different set of primers were designed in order to: rectify the open reading frame; remove the signal peptide and 5'CAP sequence and mutate position 83 in H-2L^d heavy chain from a tyrosine to a cysteine; insert an extra repetition of GGAGGTGGCGGTTCG in the β2M-heavy chain linker (BHL); and modify the peptide-β2M linker (PBL) from the amino acid sequence GGGGGGSGGSGGSGG to GCGASGGGAS. This construct will be referred hereafter as pcDNA3.1/SCT. Once the sequence of pcDNA3.1/SCT was verified, a second construct (pET28a/SCT) was designed with primers aimed to remove the transmembrane domain from the H-2L^d heavy chain and replace it with the AviTag biotinylation sequence (Beckett, Kovaleva et al. 1999), as well as to remove the β2M signal peptide. The information of all primers used for SDM and sequencing is detailed in Table 2.2.

Table 2.2 List of primers used for SDM and sequencing

Function	Sequence	Direction	Tm (°C)	%GC
Modify PBLs	GGCGGGGGTGGATCTATCCAGAAAACCCCTCAAATTC	Fwd.	67.2	54.1
	ACTTCCACCACAGCCAAATTGGTGGTAAACATAACTAG	Rv.	63.5	42.1
Modify BHL and remove H-2L^d signal peptide	AGGCAGCGGCCCACACTCGATGCGGTATTTCG	Fwd.	70.4	62.5
	CCACCCCCAGAGCCGCCGCCACCCGA	Rv.	75.8	80.8
Create the Y83C mutation in H-2L^d	GGGGCCGGAGTGTTGGGAGCGGA	Fwd.	69.9	73.9
	TCCTGCTCCATCCACGGCG	Rv.	62.7	68.4

Function	Sequence	Direction	Tm (°C)	%GC
Replace H-2L^d transmembrane domain for AviTag	GTCGAATTCTCACTCATGCCATTCAATTTTCTGTGCTTC GAAAATATCATTCAACCCGGACCCAACCATGTAGCTGT CGGTGC	Rv.	92.8	45.7
Remove the β2M signal peptide	GCTAAGCTTGCCATGGCTCGGAGCGTGACCC	Fwd.	69.8	64.5
Sequence H-2L^d	AGAGTGAACCTGAGAACCCT	Fwd.	55.2	50
	AGATAGGCTCTGTAGTACTCGG	Rv.	54.8	50
Remove the β2M signal peptide	GCTAAGCTTGCCATGGCTCGGAGCGTGACCC	Fwd.	69.8	64.5

To generate these constructs, 50µL PCR reactions were set up using KOD Hot Start polymerase (Merck, Darmstadt, Germany) and carried out according to manufacturer instructions. The reactions consisted in 5µL of 10x PCR KOD buffer, 4µL of 25mM $MgSO_4$, 5µL of 2mM dNTPs, 1.5µL of 10µM forward and reverse primers, 1µL KOD Hot Start Polymerase, and 100 to 250ng DNA template. The reaction conditions were 95°C for 2 minutes followed by 25 cycles of 95°C for 20 seconds, the respective Tm for 10 seconds, and 70°C for 2:30 minutes. After each PCR reaction, DNA was analysed by 0.6% agarose gel electrophoresis, and the fragments of the desired length were excised from the gel and purified using the QIAquick Gel Extraction kit (Qiagen, Hilden, Germany) following manufacturer instructions.

2.9.2 Restriction enzyme and DNA ligation reactions

The pcDNA3.1/SCT construct and pcDNA3.1 vector were double-digested in standard 30µL reactions consisting of dH_2O, 1x BSA, 1x buffer, 1 to 3µg DNA, 1µL HindIII and 1µL XhoI (Promega, Madison, WI). The same reaction was performed with the pET28a vector and pET28a/SCT construct, but the enzymes used for these molecules were NcoI and EcoRI (Promega, Madison, WI). All these digestion reactions were incubated at 37°C for two hours before being run on a 0.6% agarose gel electrophoresis. The DNA from the correct size was excised from the gel and purified as previously described. Ligation reactions were carried out using a 3:1 DNA to vector molar ratio with a final DNA amount of 200ng, between HindIII-XhoI double digested pcDNA3.1/SCT and pcDNA3.1 vector; and NcoI-EcoRI double digested pET28a/SCT and pET28a

vector. T4 DNA ligase (NEB, Ipswich, MA) and 10X ligase buffer were used for ligation in a final reaction of 15µL. The reactions were incubated overnight at 16°C and stored at 4°C for subsequent bacterial transformation.

2.9.3 Bacterial transformation

JM109 and BL21(DE3)pLysS competent cells were used to transform DNA constructs generated by site directed mutagenesis. For this, 5µL of ligated plasmid DNA was added to 50µL bacterial cells and incubated for 30 minutes on ice. After this time, bacteria were heat shocked at 42°C for 30 seconds and placed back on ice before adding of 250µL SOC media (Invitrogen, Carlsbad, CA). The bacterial culture was incubated for 1 hour at 37°C with shaking at 220min^{-1} before spreading 50µl on agar plates containing 100µg/ml ampicillin (for pcDNA3.1/SCT) or 50µg/ml kanamycin (for pET28a/SCT) and incubated overnight at 37°C.

2.9.4 Screening of bacterial colonies

To screen the bacterial colonies for the expression of the desired constructs, a selection of colonies were picked up and incubated in 2ml or 10ml of LB medium containing 100µg/ml ampicillin or 50µg/ml kanamycin for pcDNA3.1/SCT and pET28a/SCT, respectively. Bacteria were incubated at 37°C with 220min^{-1} shaking overnight. Plasmid DNA was purified from bacteria using QIAprep Spin Miniprep Kit (Qiagen, Hilden, Germany) following manufacturer instructions. To determine the successful incorporation of the constructs, 20µL of Miniprep plasmid DNA at a concentration of 100ng/µL were sent for sequence verification to Source BioScience LifeSciences laboratories (Nottingham, UK). Once the sequence of the constructs was verified, the bacterial culture containing the correct DNA sequences was amplified overnight at 37°C with 220min^{-1} shaking in 150ml LB medium containing 100µg/ml ampicillin for pcDNA3.1/SCT, or 300ml for LB medium with 50µg/ml kanamycin for pET28a/SCT. The QIAfilter Plasmid Maxi kit (Qiagen, Hilden, Germany) was used to purify a greater quantity of plasmid DNA, which was resuspended in 1X TE buffer and quantified by using a Nanodrop spectrophotometer (Thermo-Fisher Scientific, Waltham, MA). DNA was diluted at a final concentration of 1µg/µl for further analysis.

2.9.5 Transfection of pcDNA3.1/SCT

The pcDNA3.1/SCT construct was transfected into HeLa cells using the FuGENE®6 transfection reagent (Promega, Madison, WI). A pcDNA3.1 vector encoding the fluorescent protein mCherry was transfected alongside pcDNA3.1/SCT to verify the transfection efficiency. Briefly, HeLa cells were seeded at a concentration of 10^5 cells/ml in 2ml R10/well of a six-well cell culture plate and

incubated overnight to achieve 50 - 80% confluence. Transfection of cells was carried out following manufacturer instructions as follows: 97µL of serum free RPMI were added to 1.5ml Eppendorf tubes followed by FuGENE®6 at a 3:1 FuGENE®6 to DNA ratio (3µL FuGENE®6 for every 1µg plasmid DNA) and incubated for 5 minutes at room temperature. After this, 1µg of the plasmid DNA constructs were added and incubated at room temperature for 15 minutes. Following this incubation, the transfection mix was added drop wise into the cells and maintained at 37°C and 5% CO_2. After 24 and 48 hours, cells were harvested and analysed by flow cytometry, as previously described.

2.9.6 Induction and extraction of SCT proteins

The protein expression of the pET28a/SCT construct was carried out using Isopropyl β-D-1-thiogalactopyranoside (IPTG). Briefly, transformed BL21(DE3)pLysS competent bacteria were cultured in LB media containing Kanamycin/Chloramphenicol, and induction of monomer expression was performed by adding IPTG in the exponential phase of bacterial growth. Different incubation lengths, temperatures, and IPTG concentrations were tested, followed by a centrifugation at 500min^{-1} for 20 minutes at 4°C. The final pellet was weighted and stored at -20°C for protein extraction from bacterial inclusion bodies (IBs) using the BugBuster® (Merck, Darmstadt, Germany) extraction protocol, following manufacturer instructions. Extracted proteins were solubilized in an 8M urea or 8M guanidine buffer and quantified using Bradford assay. Aliquots of the samples were taken before and after IPTG pulse, in all the washes steps of the extraction protocol, and after urea solubilization, and were analysed by SDS-PAGE (Sodium dodecyl sulphate polyacrylamide gel electrophoresis) analysis to verify the presence of the desired protein.

2.9.7 SDS-PAGE

Protein aliquots from the previously mentioned steps were analysed in 12.5% SDS-PAGE gel electrophoresis under reducing conditions. Samples were diluted 1:4 with loading buffer containing 2-mercaptoethanol and heated at 95°C for 2 minutes. Subsequently, protein samples were loaded into a 5% Stacking/12.5% Resolving Bis/Acrylamide gel and ran for 120 V for 10-15 minutes for the stacking gel, and later at 150V for 45 to 60 minutes for the resolving gel. Once completed the electrophoresis, the gels were stained with Coomassie blue for five minutes with continuing rocking, and later de-stained with several washes of hot distilled water. De-stained gels were analysed in a BioRad Gel Doc XR+ system (BioRad, Hercules, CA).

2.9.8 Western blot analysis

For Western Blot (WB) assays, samples were previously processed by SDS-PAGE electrophoresis as previously described. For protein transfer, gels were placed alongside 0.45µm nitrocellulose membranes (GE Healthcare, Chicago, IL) and soaked in 1X transfer buffer containing 192mM glycine, 25mM Tris-Base, and 20% ethanol. Gels and membranes were stacked between Whatman® filter papers (Sigma-Aldrich, Darmstadt, Germany) and sponges, placed within a transfer cassette in a gel electrophoresis chamber, and ran at 24 V for 1 hour on ice. After this incubation, membranes were blocked using PBS-Tween 20 0.1% v/v plus 5% w/v skimmed milk overnight at room temperature. Then, membranes were incubated with rabbit polyclonal anti-human/mouse β2M for 1 hour with gentle rocking at room temperature, followed by three 15-minute washes with PBS-Tween 20. An anti-rabbit HRP was used as secondary antibody, which was diluted in PBS-Tween 20 0.1% v/v plus 1% w/v skimmed milk and loaded into the washed membranes for 1 hour at room temperature with gentle rocking. Once this incubation was finished, three additional 15-minute washes with PBS-Tween 20 were carried out, and the protein-antibody conjugates were revealed using the SuperSignal® West Pico Chemiluminescent Substrate (Thermo-Fisher Scientific, Waltham, MA). WB images were obtained and analysed using the BioRad Gel Doc XR+ system (BioRad, Hercules, CA).

2.10 Statistical analysis

For all the data generated in this study, a Shapiro-Wilk normality test was performed to verify the distribution of data. A Kruskal-Wallis test, 2-way ANOVA, or Mixed-effects analysis with Tukey's multiple comparisons test were chosen based on data distribution and grouping. A log-rank test was used for survival analysis, whereas single regression analyses were performed to determine correlations. All statistical analyses were carried out using GraphPad Prism 9.2 (GraphPad Software, La Jolla, CA).

Chapter 3 Discovery of novel CD8+ T cell epitopes from CT26 immuno-transcriptomic data

3.1 Introduction

The identification of immunogenic epitopes derived from next-generation sequencing data has become a pivotal area of investigation in cancer immunotherapy. Most of the peptides detected by such methodologies are evaluated and tested based on their predicted affinity towards MHC-I, NetMHC being the "gold standard" algorithm for such predictions (Jurtz, Paul et al. 2017). However, as this algorithm uses artificial neural networks built upon *in vitro* binding assays for predicting MHC-I binding affinities, these predictions can be greatly affected by the number and quality of *in vitro* assays included for each specific MHC-I allele. Moreover, p/MHC-I binding affinities are not the sole parameter contributing to immunogenicity, and other steps involved in APP should be considered to improve the detection of such immunogenic peptides. Indeed, novel algorithms have attempted to include different parameters to improve the prediction of immunogenicity, such as the agretopicity index that selects neoantigens based on an improved MHC-I binding compared to WT peptides (Duan, Duitama et al. 2014), or by incorporating predictors of the APP like protein cleavage and TAP transport efficiency (Kim, Kim et al. 2018). Nonetheless, most of these approaches still use a bioinformatic prediction of MHC-I binding through NetMHC as one of their inputs. Thus, in this study a PFR formula is tested that incorporates the relative abundance of the source protein from the target peptides, as well as their predicted and measured MHC-I binding affinity, to try to improve the detection of immunogenic peptides in the CT26 tumour model.

3.2 Results

3.2.1 Sorting of potential novel immunogenic peptides from CT26 immuno-transcriptomic data

The first step taken for the identification of novel CT26 epitopes included the mining of publicly available RNA-Seq and WES data (Castle, Loewer et al. 2014). From this dataset, a total of 1827 SNVs were mapped into their corresponding peptide sequence, and the predicted MHC-I restriction and binding affinity was carried out using NetMHC4.0 only in those peptides whose mutations were located outside untranslated regions. This analysis led to the identification of 253 H-2L^d peptides, 739 H-2K^d peptides, and 656 H-2D^d peptides, which were ranked based on their

predicted MHC-I affinity and the relative abundance. Remarkably, neoantigens and differentially-expressed gp70-derived peptides showed a distinct pattern when comparing these two parameters, as the majority of neoantigens were under-expressed compared to MuLV-derived peptides but showed a higher number of peptides in the high binders and low binders category, whereas only two peptides derived from the PFR were ranked as high-binders (Ld1, and Kd34; Table 3.1, **Figure 3.1**). Despite gp70-derived peptides sharing a common protein source, they have different abundance patterns due to the genetic composition of the gp70 locus in CT26 cells. Genomic analysis of CT26 cells revealed that gp70 lies in a tetraploid region of chromosome 8, harbouring three different stop codons in heterozygosity at different positions of the gp70 gene, thus suggesting that four different transcripts could be generated with different abundances (Castle, Loewer et al. 2014). Once peptides were sorted based on abundance and affinity, they were ranked based on the calculation obtained by the PFR. Interestingly, the top ranked peptides from PFR from all three alleles corresponded to gp70-derived peptides (apart from the H-2L^d-restricted neoantigen Ld3), whereas the top ranked peptides from NetMHC4.0 were all neoantigens (Table 3.1).

Based on these analyses, 18 H-2D^d, 46 H-2K^d, and 32 H-2L^d peptides were synthesised for further assays, most being 9mers (**Figure 3.2** A). These peptides shared similar MHC-I binding motifs, as observed by the overrepresentation of Proline at positions 2 and 3 for H-2L^d and H-2D^d peptides, respectively (**Figure 3.2** B and C), as well as Tyrosine at position 2 for H-2K^d peptides (**Figure 3.2** D). Based on GO functional annotation analyses, these peptides mostly derived from cytoplasmic and plasma membrane proteins, as well as from proteins participating in metal ion binding or protein binding (**Figure 3.3**). Altogether, these results indicate that the selected peptides match the common characteristics of MHC-I peptides.

As an approach towards the validation of these peptides, we matched our peptide list against a CT26-derived immunopeptidome generated by mild acid elution (MAE) (Nicholas and Bailey, Unpublished results). From the 96 selected peptides, only four matched with the MAE immunopeptidome, three H-2L^d-restricted (AH1, Ld1, and Ld24) and one H-2K^d-restricted (Kd34). Interestingly, from these matched peptides, Ld1 and Kd34 represent the top ranked PFR peptides for their respective alleles.

Overall, these results indicate that incorporating PFR into epitope discovery could improve the likelihood of detecting peptides presented by MHC-I molecules, which could play important roles in the development of CD8+ T cell responses.

Table 3.1 Peptide ranking based on NetMHC and PFR parameters.*Peptide Dd8 is a predicted high binder for H-2D^d derived from HIV-1 gp120 and was included as a negative control.

Allele	Peptide	Sequence	Source	NetMHC affinity (nM)	NetMHC Rank	PFR	PFR Rank
H-2L^d	Ld17	SPLAAPTFL	3425401B19Rik	10.1	1	0	28
	Ld18	IPQEYVLFL	Ubash3a	23.9	2	0	28
	Ld19	NPHMYAVDM	Olfr1136	27.7	3	0	28
	Ld20	NPYANSYTL	Dscam	33.6	4	0	28
	Ld7	LPQLIQVLL	Gp5	36.4	5	1	18
	Ld1	SPHQVFNL	gp70	46	7	33852	1
	Ld31	HPLWTWWPDL	gp70	264	12	1039	2
	Ld22	KPSSSWDYI	gp70	271	13	493	3
	Ld3	FPVAFCIFM	Lass6	47.9	8	29	4
	Ld2	WPDLTPDL	gp70	1764	26	23	5
	AH1	SPSYVYHQF	gp70	1748	25	6	14
H-2K^d	Kd24	KYYAHATSL	BC026439	13.6	1	0	37
	Kd25	CYAAVCKPL	Olfr1469	14.2	2	0	37
	Kd26	KYAAICKPL	Olfr884	15.4	3	0	37
	Kd2	SYETLKKSL	Haus6	18.2	4	405	6
	Kd27	RYAAICHPV	Olfr846	19.5	5	0	37
	Kd34	DYITVSNNL	gp70	22	7	72001	1
	Kd35	WFTTLISTI	gp70	54	18	6149	2
	Kd36	SYTPRCNTA	gp70	117	24	5296	3
	Kd1	QYHQLKTI	gp70	130	27	1075	4
	Kd37	YYLAAPTGT	gp70	173	29	603	5
H-2D^d	Dd17	YGPKYNPNF	Susd2	184.8	1	0.003	17
	Dd10	KGPKRDEQC	4933424B01Rik	628.3	2	0.501	6
	Dd8	IGPGRAFYT	HIV-1 gp120*	778	3	0.000	18

Allele	Peptide	Sequence	Source	NetMHC affinity (nM)	NetMHC Rank	PFR	PFR Rank
	Dd7	GQPREHYTL	Cdc73	799.2	4	0.250	8
	Dd11	PGPIKCVPI	Aen	800.8	5	0.321	7
	Dd2	PGPHRPRW	gp70	1187	7	38.461	1
H-2D^{d}	Dd16	WGPLIVLLI	gp70	1424	9	35.612	2
	GSW11	GGPESFYCASW	gp70	1404.4	8	27.475	3
	Dd1	HGPSYWGL	gp70	3200	14	7.056	4
	Dd14	TGNHPLWTW	gp70	8019	17	1.124	5

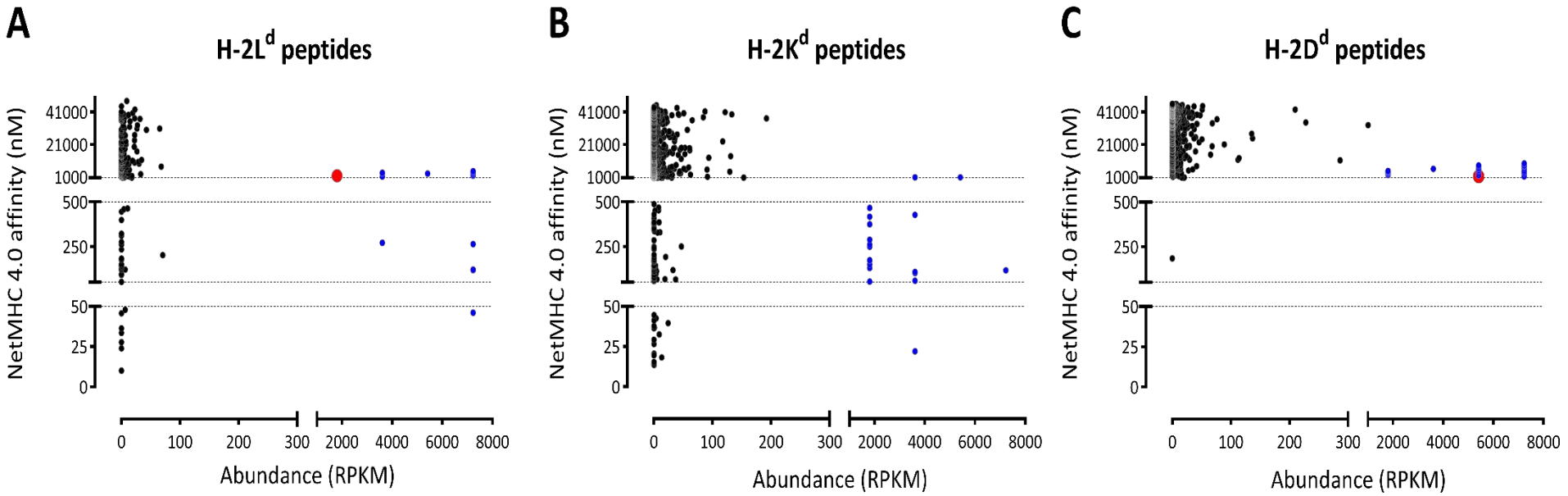

Figure 3.1 **Relationship between predicted affinity and relative abundance of the selected peptides.** From each graph, each dot represents a unique peptide. Black dots correspond to neoantigens, blue dots represent peptides derived from MuLV gp70, and red dots in Figure 3.1A and 3.1C correspond to AH1 and GSW11, respectively. Dotted lines discriminate peptides with a high predicted binding affinity (0 – 50nM), low binding affinity (50 – 500nM), and non-binders (>500nM), according to NetMHC4.0 thresholds. Abundance is expressed as RPKM, derived from CT26 transcriptomic data.

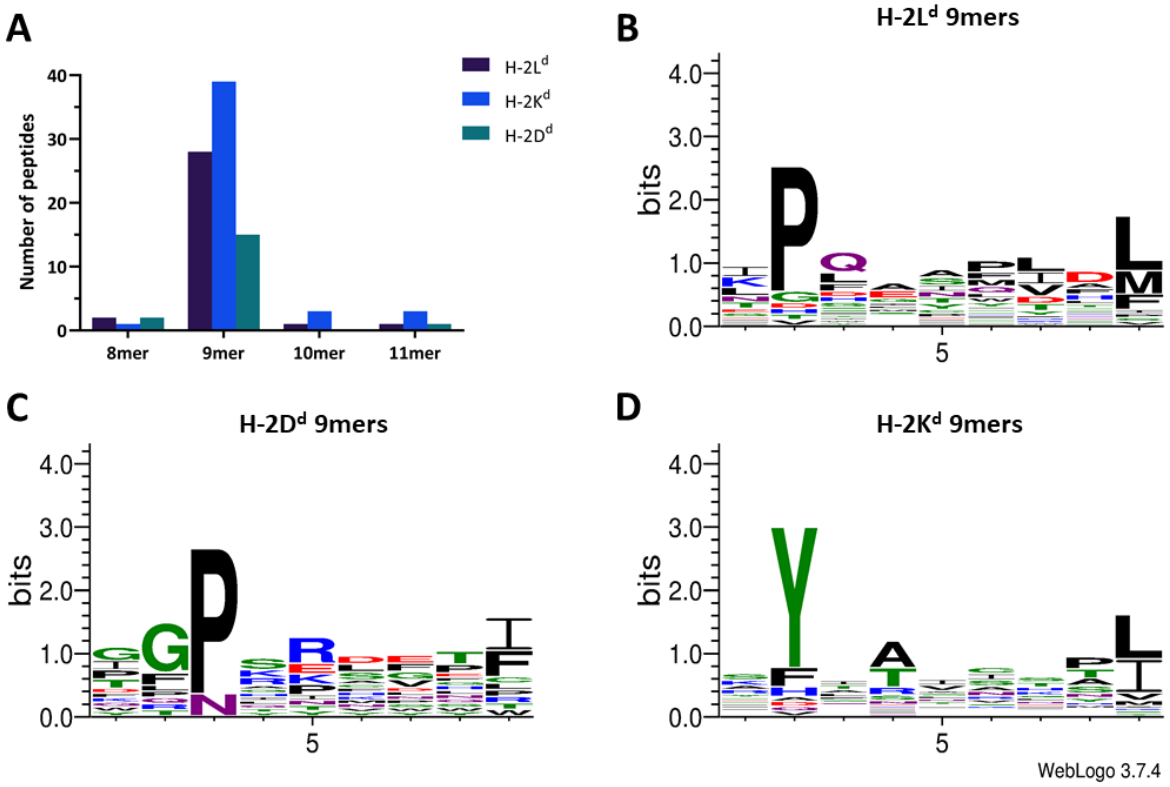

Figure 3.2 **Physicochemical characteristics of selected peptides.A.** Peptide length distribution across the three H-2 alleles. **B, C and D.** Protein logo analysis of H-2L^d (B), H-2D^d (C) and H-2K^d (D) 9mer peptides. Logo plots were performed using the WebLogo 3 server (Crooks, Hon et al. 2004)

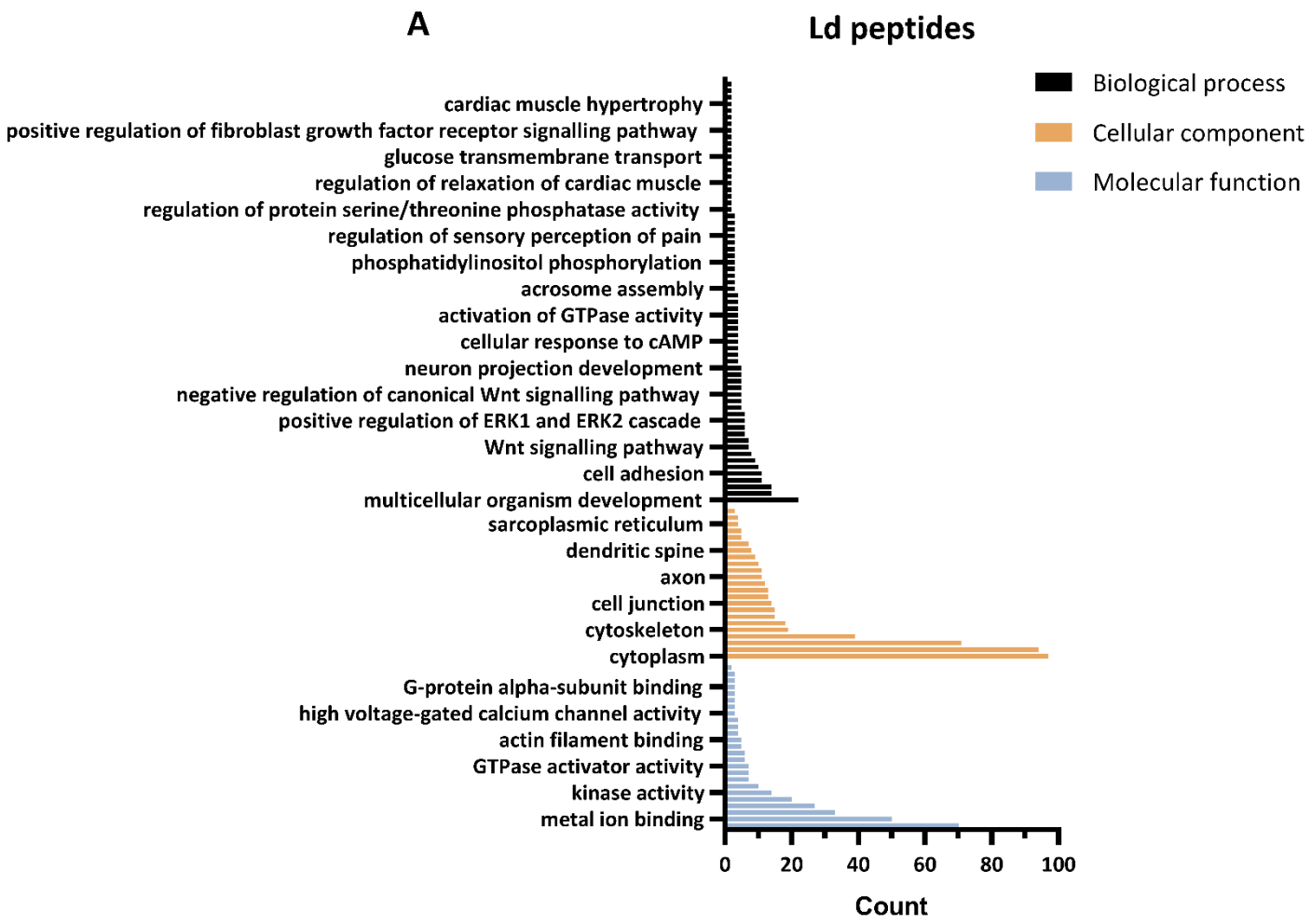
A
Ld peptides
Biological process
Cellular component
Molecular function
cardiac muscle hypertrophy
positive regulation of fibroblast growth factor receptor signalling pathway
glucose transmembrane transport
regulation of relaxation of cardiac muscle
regulation of protein serine/threonine phosphatase activity
regulation of sensory perception of pain
phosphatidylinositol phosphorylation
acrosome assembly
activation of GTPase activity
cellular response to cAMP
neuron projection development
negative regulation of canonical Wnt signalling pathway
positive regulation of ERK1 and ERK2 cascade
Wnt signalling pathway
cell adhesion
multicellular organism development
sarcoplasmic reticulum
dendritic spine
axon
cell junction
cytoskeleton
cytoplasm
G-protein alpha-subunit binding
high voltage-gated calcium channel activity
actin filament binding
GTPase activator activity
kinase activity
metal ion binding
0
20
40
60
80
100
Count

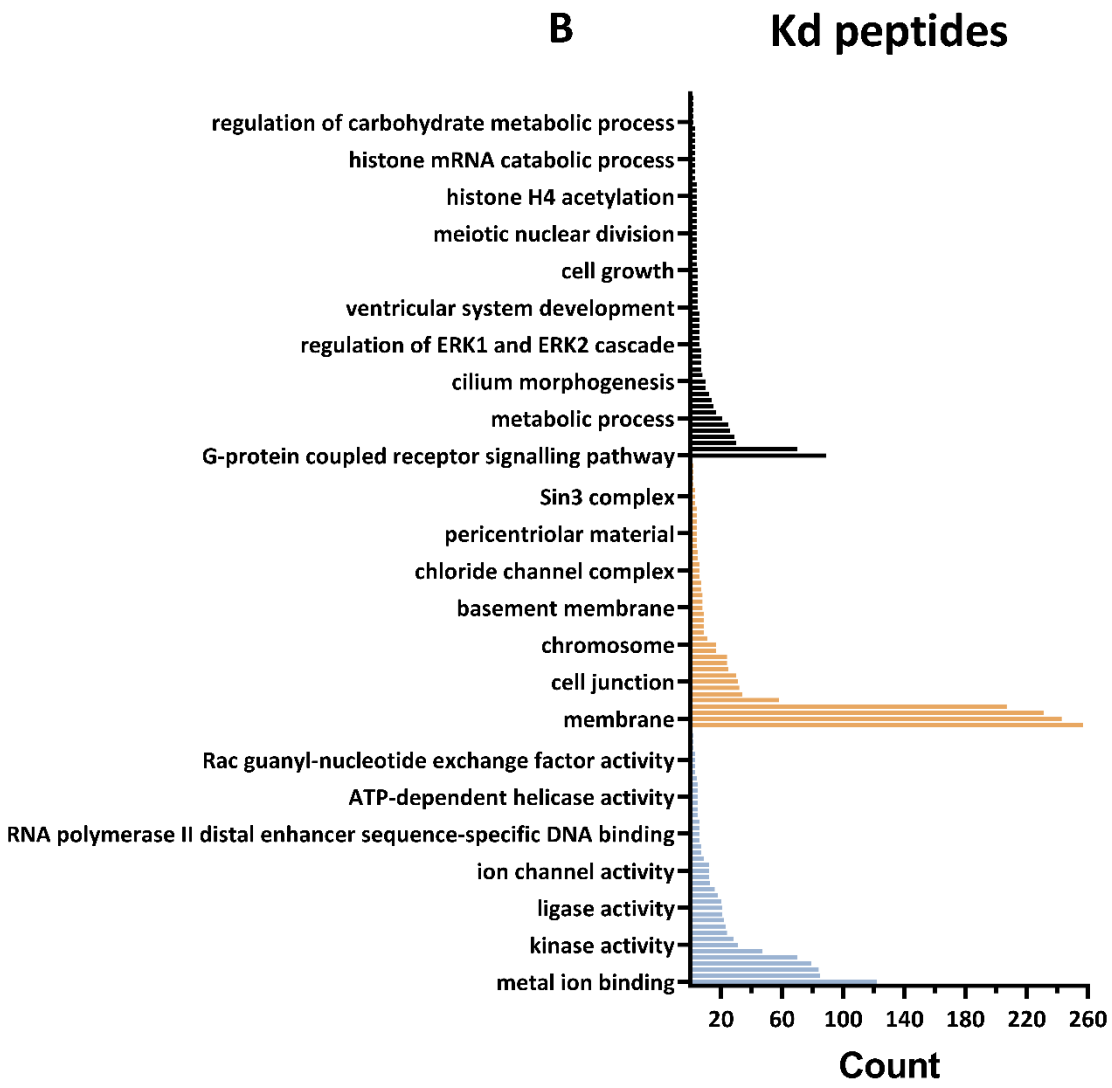
B
Kd peptides
regulation of carbohydrate metabolic process
histone mRNA catabolic process
histone H4 acetylation
meiotic nuclear division
cell growth
ventricular system development
regulation of ERK1 and ERK2 cascade
cilium morphogenesis
metabolic process
G-protein coupled receptor signalling pathway
Sin3 complex
pericentriolar material
chloride channel complex
basement membrane
chromosome
cell junction
membrane
Rac guanyl-nucleotide exchange factor activity
ATP-dependent helicase activity
RNA polymerase II distal enhancer sequence-specific DNA binding
ion channel activity
ligase activity
kinase activity
metal ion binding
20
60
100
140
180
220
260
Count

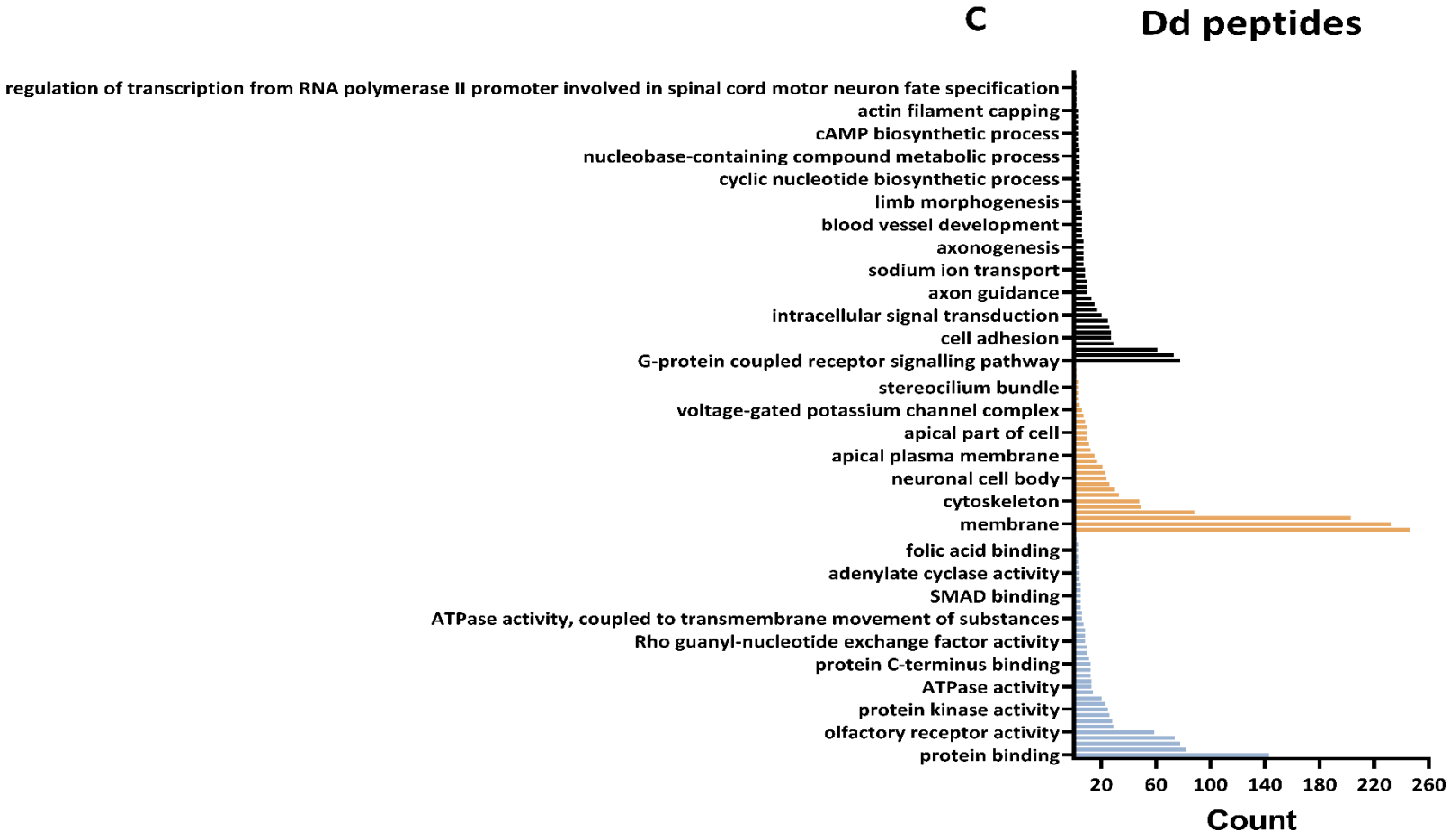

Figure 3.3 GO Functional annotation of selected peptides. The genes from which the peptides derived were analysed by GO Functional annotation focusing on Biological Process, Cellular component, and Molecular function aspects, using the DAVID platform (Huang da, Sherman et al. 2009).

3.2.2 *In vitro* measurement of peptide affinities

3.2.2.1 Verification of MHC-I overexpression in RMA-S cells

Given that the IC_{50} calculation obtained by NetMHC is predicted, the affinity of some of the selected peptides towards their respective MHC-I molecules was tested *in vitro* in BFA decay assays using RMA-S cells expressing either H-2L^d, H-2K^d or H-2D^d, as these cells overexpress MHC-I molecules at 26°C but lose this expression once incubated at 37°C. Given their intrinsic lack of TAP (De Silva, Boesteanu et al. 1999), RMA-S cells can be pulsed with external peptides to stabilize the MHC-I molecules at the cell surface, and after incubating at 37°C at different time points in the presence of BFA, the rate of MHC-I decay can be measured in a kinetic fashion by flow cytometry, thus enabling a measurement of relative peptide affinity.

First, RMA-S cells were tested to verify MHC-I overexpression after incubating at different times at 26°C. As observed in **Figure 3.4** RMA-S K^d and RMA-S D^d cells overexpressed their respective MHC-I molecules after 1 hour of 26°C incubation (**Figure 3.4** B and C). However, regarding their MFI, RMA-S D^d cells showed a constant upregulation of H-2D^d intensity until 5 hours, followed by a small decay and a further upregulation at the final time point (18 hours), whereas the peak intensity of H-2K^d expression on RMA-S K^d cells was observed at the final time point (22 hours), but these levels were similar from the 16 hours time point, indicating a plateau in the H-2K^d MFI after this time point. These kinetics were not properly performed in RMA-S L^d cells, potentially due to inefficient staining of the 30-5-7S antibody. These results indicate that, although RMA-S cells have different patterns of MHC-I overexpression, they can all increase the cell surface levels of MHC-I molecules after incubation at 26°C.

3.2.2.2 Affinity measurement of H-2-restricted peptides

Once MHC-I overexpression at 26°C was verified on RMA-S cells, the affinity of the selected peptides was measured via BFA decay assays, as described in section 2.4. For H-2K^d-restricted peptides, although the IC_{50} values obtained via BFA decay did not match the values predicted by NetMHC4.0, three peptides described as high binders by NetMHC4.0 (Kd24 = 13.6 nM, Kd26 = 15.4 nM, and Kd27 = 19.5 nM) were verified as high binders by BFA decay, as they showed IC_{50} values around 50nM. However, two NetMHC4.0 high binders (Kd25 and Kd2) displayed the highest IC_{50} among tested peptides (**Figure 3.5** A and **Figure 3.6** A), indicating an inconsistency between NetMHC4.0 affinity prediction and measured relative affinity. Moreover, all peptides derived from PFR (except for Kd35) showed IC_{50} values above 100nM, indicating that these peptides could be classified as low binders in BFA decay assays (**Figure 3.6** A). Given the discrepancy observed between the IC_{50} measurements from BFA decay and NetMHC4.0, a simple

linear regression was performed between such values, and between the peptide ranking from both approaches. Unsurprisingly, neither IC_{50} nor rank values from BFA decay positively correlated with NetMHC4.0 predictions, and only a small trend was observed in the IC_{50} correlation of these two approaches (**Figure 3.6** B and C).

Next, this same methodology was applied to the top 5 NetMHC and top 5 PFR H-2D^d-restricted peptides. As observed in **Figure 3.7**, IC_{50} values obtained by BFA decay showed an even higher discrepancy compared to NetMHC4.0. According to NetMHC4.0 predictions, all top 5 H-2D^d-restricted peptides were catalogued as non-binders, with IC_{50} values above 500 nM (except for Dd17, Table 3.1). However, BFA decay assays showed an IC_{50} for Dd11 of 39.32 nM, in sharp contrast with NetMHC4.0 (800.8 nM), indicating that this peptide could represent a high binder. Likewise, Dd16 showed a significantly lower IC_{50} via BFA decay compared to NetMHC4.0 (68.72 nM vs. 1424 nM). These observations are made evident in the simple linear regression analysis, as no correlations are observed between IC_{50} and ranking values between the two approaches (**Figure 3.7** B and C).

Lastly, BFA decay assays were performed with H-2L^d-restricted peptides. Besides the top 5 NetMHC and PFR peptides, the previously described immunodominant AH1 peptide was also included, which ranks 14th in PFR and 25th in NetMHC4.0. The exponential decay of cell surface H-2L^d expression after peptide pulsing in these assays was faster compared to the other two alleles (**Figure 3.5** C). Indeed, half of the tested peptides were categorised as non-binders, with IC_{50} values above 500nM (**Figure 3.8** A). Furthermore, one peptide was categorised as high binder by both approaches (Ld18; NetMHC4.0 = 23.9nM, BFA decay = 48.99 nM), and one peptide was catalogued as high binder by BFA decay but not NetMHC4.0 (Ld22; NetMHC4.0: 271nM, BFA decay: 23.04nM). Interestingly, the IC_{50} values obtained by these two approaches showed a significant, albeit subtle positive correlation (**Figure 3.8** B). Nonetheless, only one replicate per peptide of BFA decays using RMA-S L^d cells was performed, and more repeats are necessary to validate these observations.

Altogether, these results illustrate the significant discrepancy between *in silico* and *in vitro* calculations of p/MHC-I affinities, highlighting the importance of strong affinity measurement platforms for selecting peptides in cancer immunotherapy settings.

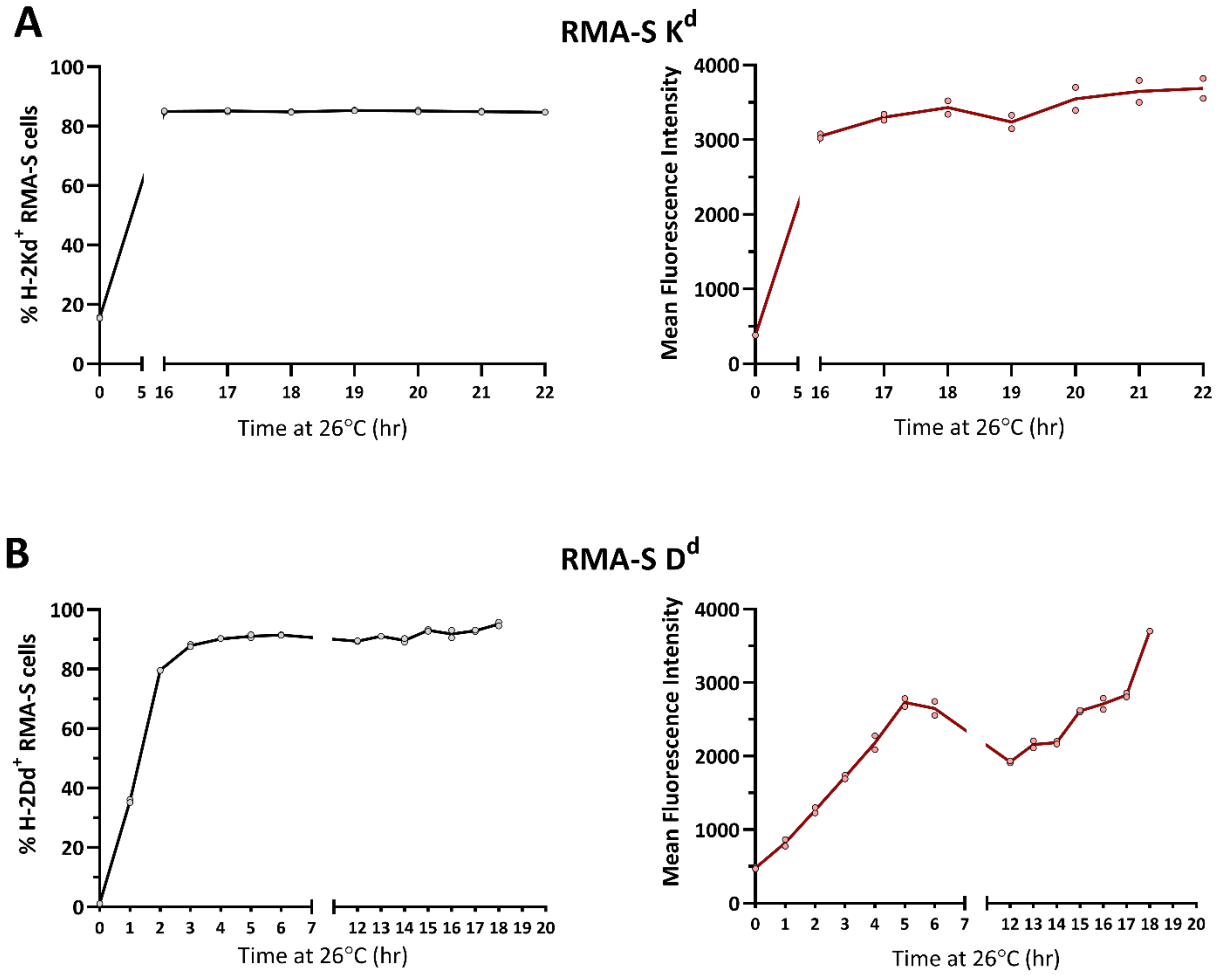

Figure 3.4 **Cell surface expression of H-2^d molecules on RMA-S cells.** RMA-S K^d (**A**) and D^d (**B**) cells were incubated at several time points at 26°C for the verification of MHC-I expression. Left graphs represent the percentage of RMA-S cells expressing the corresponding MHC-I molecule, while right graphs indicate the MHC-I MFI as detected by flow cytometry.

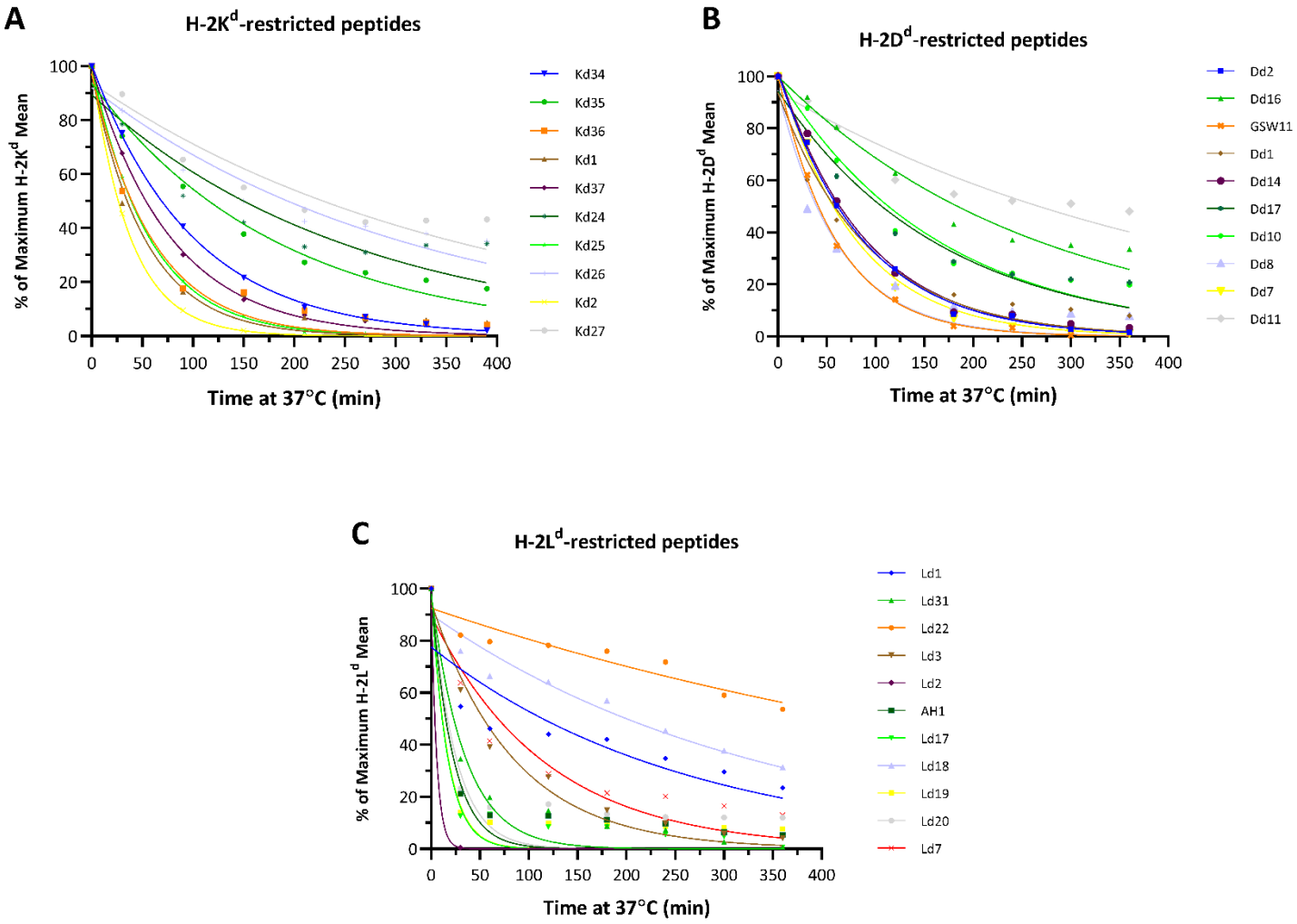

Figure 3.5 **One-phase exponential decay of H-2^d-restricted peptides.** The affinity of peptide interactions with H-2K^d (**A**), H-2D^d (**B**), or H-2L^d (**C**) were measured in RMA-S cells expressing the respective MHC-I alleles via BFA decay in the top ranked peptides from NetMHC4.0 and PFR using a one-phase exponential decay of the MHC-I MFI. Graphs are representative figures from three independent replicates for H-K^d and H-2D^d, and from one independent replicate for H-2L^d.

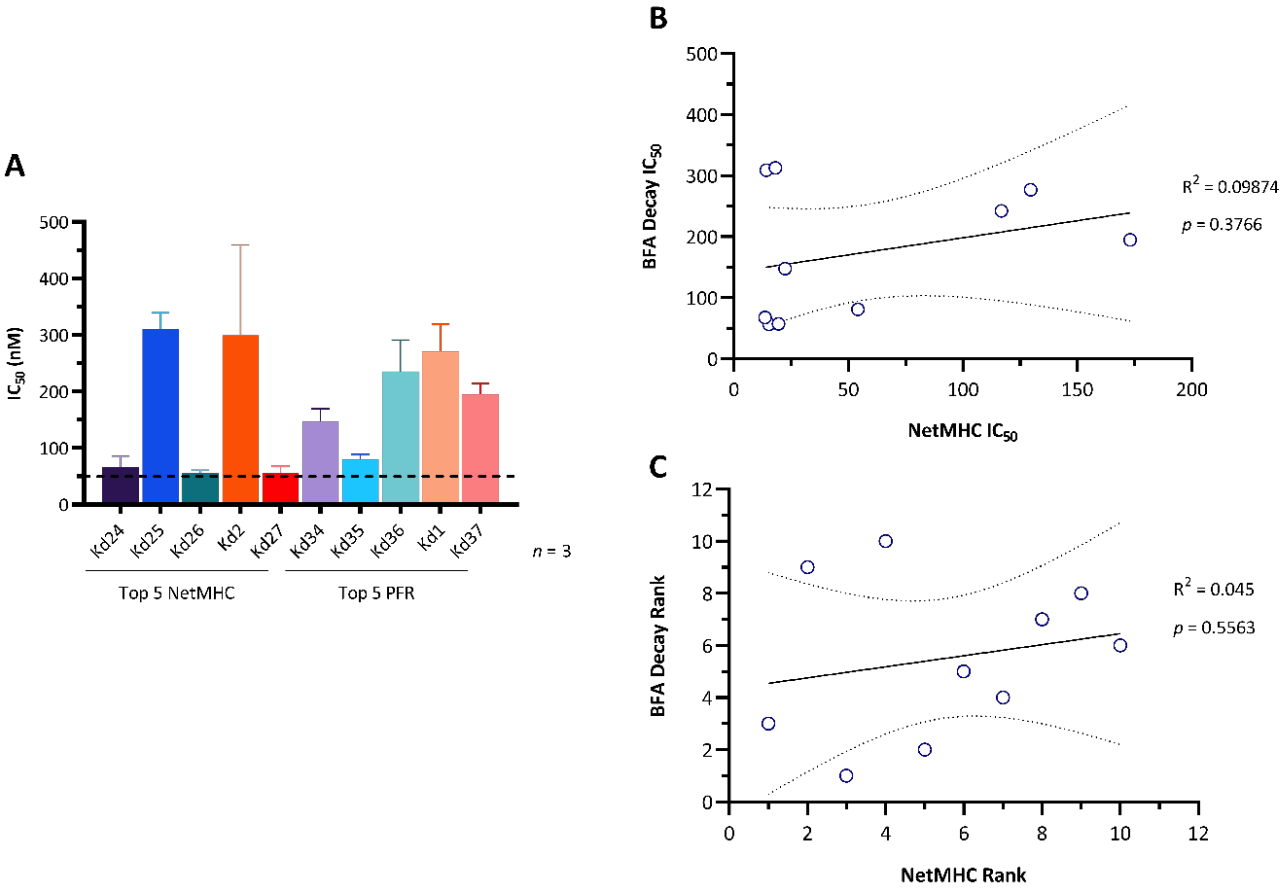

Figure 3.6 BFA decay IC_{50} measurements do not correlate with NetMHC4.0 predictions in H-2K^d-restricted peptides.A. IC_{50} values obtained from the top 5 NetMHC peptides (Left) and the top 5 PFR peptides (Right) via BFA decay assays. The dotted line discriminates peptides classified as high binders (IC_{50} <50nM) and low binders (IC_{50} >50nM). **B and C.** Correlation analysis between IC_{50} (B) and ranking values (C) obtained by NetMHC4.0 and BFA decay. Graphs depict the best-fit line (bold) as well as the standard error (dotted lines).

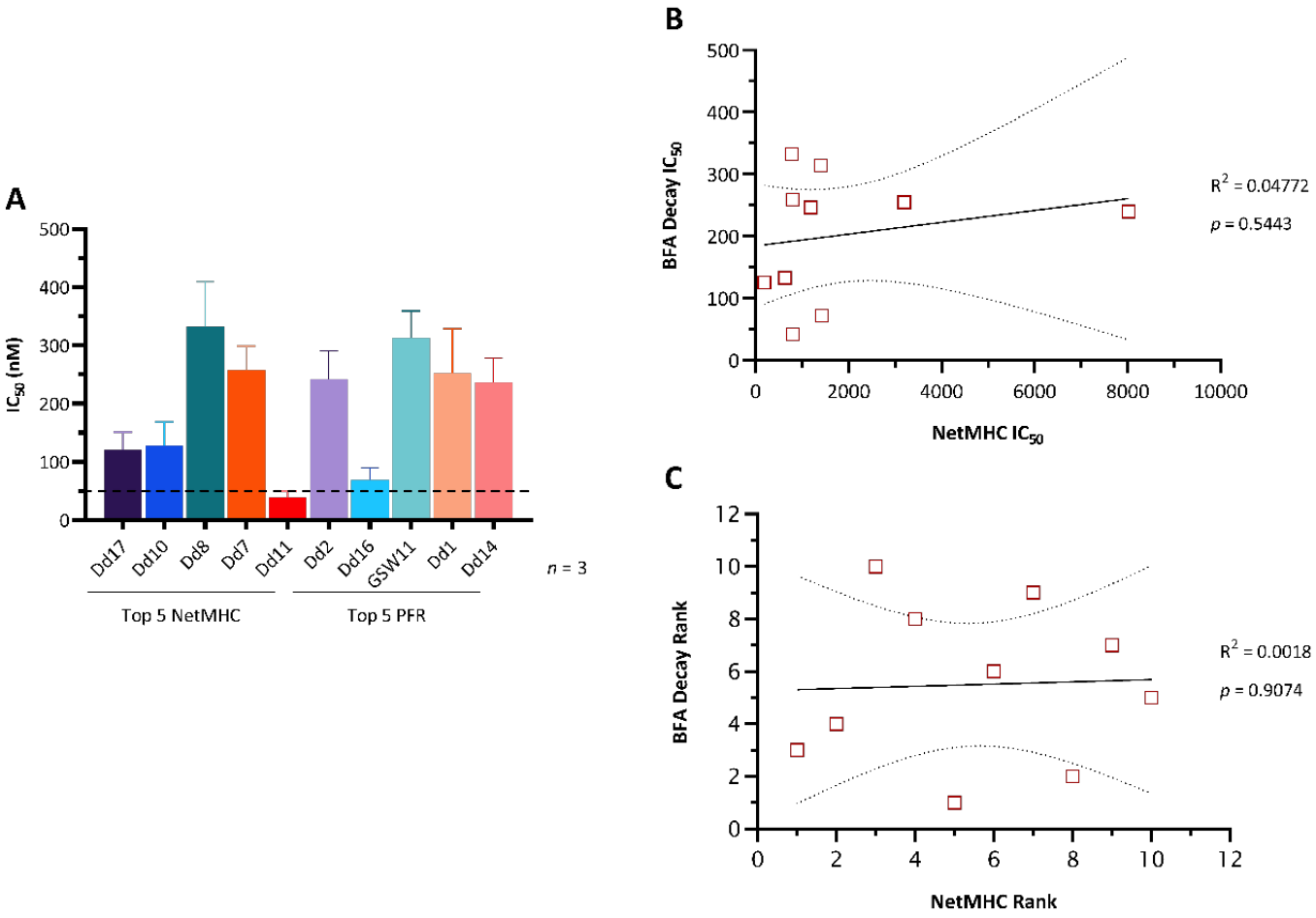

Figure 3.7 **NetMHC4.0 is not a good predictor of H-2D^d binding affinities.A.** IC_{50} values obtained from the top 5 NetMHC peptides (Left) and the top 5 PFR peptides (Right) via BFA decay assays. The dotted line discriminates peptides classified as high binders (IC_{50} <50nM) and low binders (IC_{50} >50nM). **B and C.** Correlation analysis between IC_{50} (B) and ranking values (C) obtained by NetMHC4.0 and BFA decay. Graphs depict the best-fit line (bold) as well as the standard error (dotted lines).

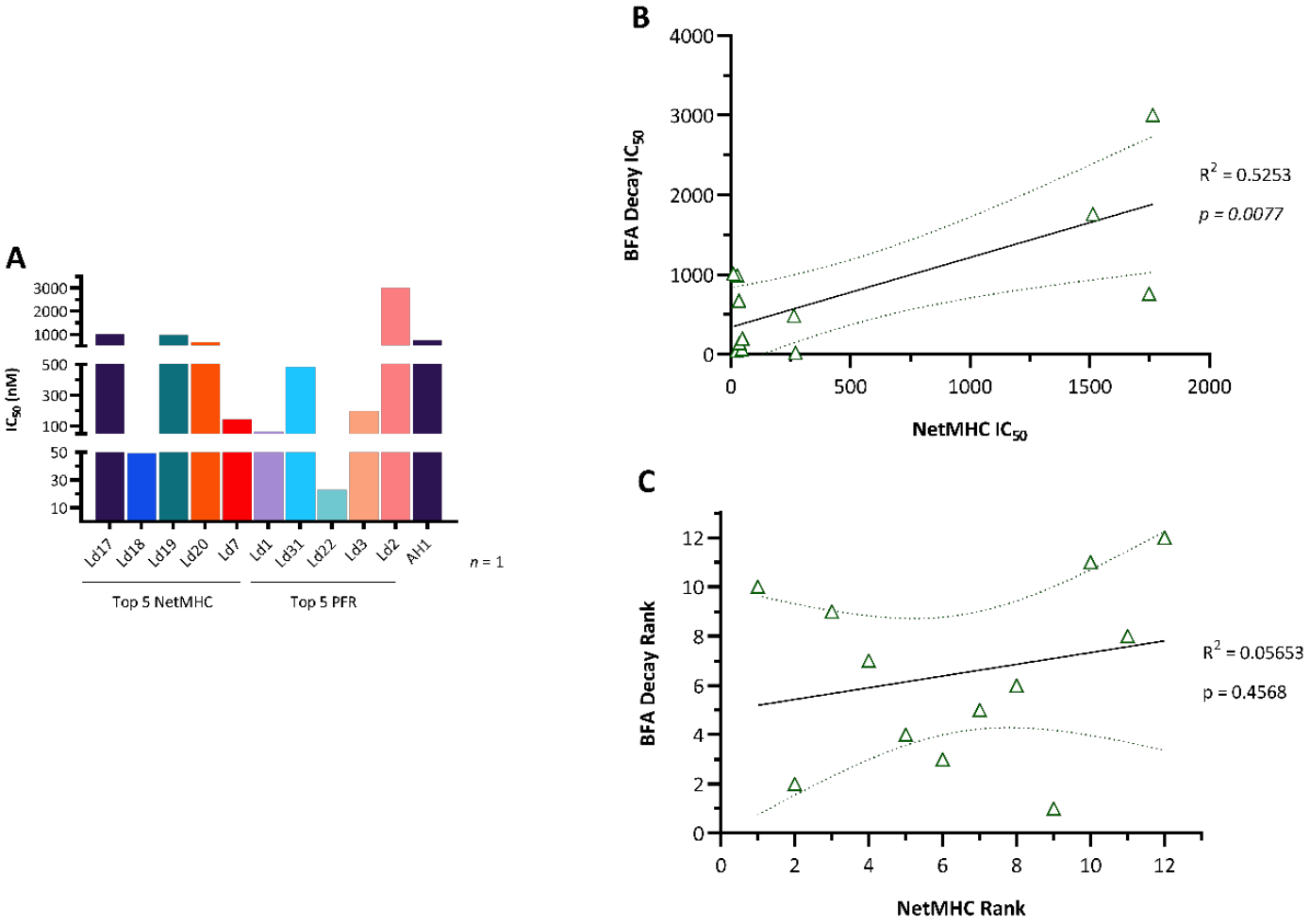

Figure 3.8 **IC_{50} measurements positively correlate with NetMHC4.0 predictions in H-2Ld-restricted peptides.A.** IC_{50} values obtained from the top 5 NetMHC peptides (Left) and the top 5 PFR peptides (plus AH1, Right) via BFA decay assays. The Y axis is segmented in three portions, distinguishing peptides classified as high binders (IC_{50} < 50nM, lower part), low binders (IC_{50} 50 – 500nM, middle part), and non-binders (IC_{50} > 500nM, top part). **B and C.** Correlation analysis between IC_{50} (B) and ranking values (C) obtained by NetMHC4.0 and BFA decay. Graphs depict the best-fit line (bold) as well as the standard error (dotted lines).

3.3 Concluding remarks

Although immunotherapeutic strategies have shown promising clinical results, the mechanisms governing the recognition of tumour-specific epitopes by CD8+ T cells in such therapies are not completely understood, and a better understanding of the determinants involved in CD8+ T cell priming and activation in cancer settings is important for the development of more specific anti-cancer approaches. Moreover, mouse pre-clinical models can represent an important tool for the study of tumour/CD8+ T cell interactions, as these models can replicate specific features observed in human cancers, such as T cell infiltration and responsiveness to checkpoint blockade (Mosely, Prime et al. 2017). Our characterisation of MHC-I-restricted peptides derived from previously published CT26 immuno-transcriptomic data (Castle, Loewer et al. 2014), by means of MHC-I predicted affinities alone, or by filtering the affinity and abundance parameters using an *in house* PFR algorithm, allowed us to identify potentially immunogenic peptides from mutated proteins (neoantigens) and over-expressed proteins (gp70-derived peptides). Although the vast majority of studies have focused on high-affinity peptides as potential immunogenic peptides, the fact that low-affinity peptides can be detected on the cell surface of CT26 cells in MAE immunopeptidomics, as observed in this study and by others (Duan, Duitama et al. 2014, Ebrahimi-Nik, Michaux et al. 2019), highlights the importance of incorporating peptides with intermediate or low predicted binding affinities in the screening of potential immunogenic peptides in cancer settings. Nonetheless, the detection of MHC-I-presented cancer-derived peptides on the cell surface of these cells is not a complete indicator of immunogenicity (Abelin, Keskin et al. 2017, Bulik-Sullivan, Busby et al. 2018), and functional analysis are essential for verifying if such peptides can activate CD8+ T cells in normal and therapeutic settings.

Chapter 4 Response mapping of novel peptides in CT26-challenged mice

4.1 Introduction

The identification of tumour antigens targeted by CD8+ T cells in immunotherapy settings represents an important field of study that can improve the success of such therapies. Indeed, high frequencies of tumour-specific CD8+ T cells infiltrating the TME have been associated with favourable outcomes in different immunotherapeutic regimes, such as checkpoint blockade with anti-CTLA-4 or anti-PD-1 (Blass and Ott 2021). As mentioned previously, RNA-Seq and WES data have played a pivotal role in the identification of novel tumour-derived epitopes targeted in immunotherapy. However, the analysis of immuno-transcriptomic data from tumour samples must be coupled with functional analysis of CD8+ T cells to determine which peptides could bypass immunological tolerance and trigger immune responses in the tumour, and therefore which peptides could represent promising therapeutic targets for novel immunotherapy approaches. Upon efficient T cell priming, immunogenic peptides induce proliferation and cytokine production of CD8+ T cells (mainly IFNγ, TNFα and IL-2). These features can be tested *in vitro* through proliferation assays, by measuring cytokine release/production using Enzyme-Linked ImmunoSpot (ELISPOT) or intracellular cytokine staining assays, allowing for the verification of immunogenicity of the candidate peptides (Roudko, Greenbaum et al. 2020). Thus, in this study the previously ranked peptides derived from CT26 immuno-transcriptomic data were tested via IFNγ intracellular cytokine staining (ICS) assays in untreated and tumour protective Treg-depleted mice, in order to determine the immunogenicity of these peptides, and if any association exists between therapeutic benefit and T cell responses against specific peptides.

4.2 Results

4.2.1 Standardisation of ICS for peptide screening

Before testing the previously described peptide library, several parameters were standardized to improve the quality of detection of the IFNγ responses by CD8+ T cells. First, SEB was considered as a potential positive control, given the fact that acting as a superantigen it can activate the TCR signalling pathway in a peptide-independent fashion (Fraser 2011). Two concentrations of SEB (0.1µg/ml and 5µg/ml) were tested in BALB/c splenocytes for 4 hours, but none of them induced significant production of IFNγ by CD8+ T cells (**Figure 4.1** A). Next, the *Canavalia ensiformis* lectin

ConA was tested at different concentrations, as it has been reported that treatment of mice splenocytes with this mitogen stimulates cytotoxic responses of CD8+ T cells (Thomsen and Jensen 1980). At a concentration of 5µg/ml ConA induced a significant increase in the levels of IFNγ by CD8+ T cells (**Figure 4.1** B), however, cells stimulated with this concentration showed a drastic morphologic change in forward and side scatter plots indicative of cell death, which can lead to a high background staining and a high frequency of false positives. In order to improve the detection of IFNγ and reduce cell stress, several combinations of concentrations of the protein kinase C activator PMA along with the Ca^{2+} ionophore ionomycin were tried, as these compounds induce a high IFNγ response in splenocytes (Ai, Li et al. 2013). Regardless of the combination used, the levels of IFNγ after PMA/Ionomycin stimulation were consistently higher compared to ConA stimulation (**Figure 4.1** C). Given these results, the combination of PMA at 5ng/ml and Ionomycin at 500ng/ml was chosen as positives controls for further ICS experiments. Furthermore, a viability dye and an isotype control were titrated to better delineate the positive gates for IFNγ responses in the CD8+ T cell population and reduce background levels. Three different dilutions of the Zombie Green™ viability dye were tried in splenocytes from naïve BALB/c mice, showing similar levels of live and dead cells (**Figure 4.2** A), from which the 1:500 dilution was chosen as it showed a low background staining (**Figure 4.2** B). Regarding the isotype control, a rat IgG1κ PE-Cy7-conjugated antibody was tested at three concentrations, and a 0.1µg/ml concentration was chosen as it led to the lowest levels of background staining (**Figure 4.2** C).

4.2.2 CD8+ T cell responses against novel peptides in CT26-challenged untreated BALB/c mice

Once the methodological pipeline for the identification of IFNγ responses from peptide-stimulated splenocytes was standardised, a peptide screening was performed using CT26-challenged untreated BALB/c mice.

First, the levels of IFNγ production by CD8+ T cells were measured at day 11 post tumour challenge in spleen and tdLNs from untreated mice (**Figure 4.3**), as this time point allows for a good delineation of progressors and regressors in therapeutic settings (See **Figure 4.9** A). In spleen, the IFNγ response pattern was consistently low across the tested peptides from the three alleles, with a slight increase in the frequency of IFNγ+ CD8+ T cells stimulated with NetMHC-ranked H-$2K^d$-restricted peptides (**Figure 4.4** B). Splenocytes stimulated with either GSW11 or AH1 showed low levels of IFNγ production, with similar frequencies of IFNγ+ CD8+ T cells (GSW11 mean = 0.066%, AH1 mean = 0.092%; **Figure 4.4** A and C). These low responses were also evident in tdLNs, as more than half of the tested mice did not show IFNγ production above the negative control background when stimulated with GSW11, AH1, or Kd34 (**Figure 4.4** D).

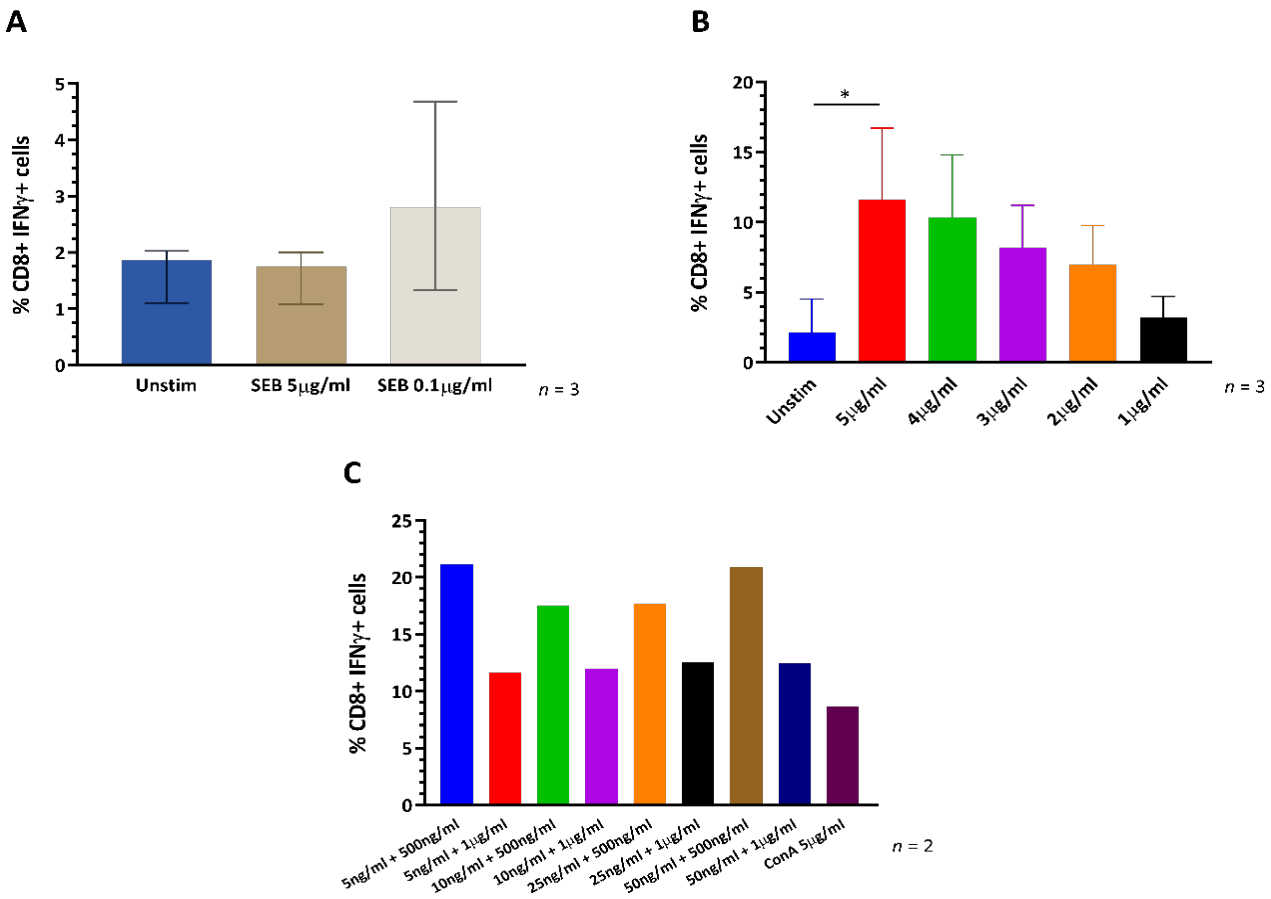

Figure 4.1 **Standardisation of the ICS positive control in BALB/c splenocytes.A.** Splenocytes from naïve BALB/c mice were incubated with indicated concentrations of SEB for 4 hours, and the levels of IFNγ production by CD8+ T cells were measured by ICS. Median and range. **B.** Titration assay of ConA for the stimulation of IFNγ production in CD8+ T cells. Median and range; Kruskal-Wallis test, $p = 0.0295$. **C.** IFNγ production towards different concentrations of PMA plus Ionomycin in CD8+ T cells from naïve BALB/c mice. Median only.

As a second approach for the validation of immunogenicity from the selected peptides, splenocytes from CT26-challenged untreated mice were pulsed with the same peptides for 72 hours and proliferation was measured by CFSE dye dilution analysis (**Figure 4.5**). The proliferation patterns of splenocytes pulsed with such peptides showed that most of the tested peptides did not induce proliferation of CD8+ T cells, as proliferation was only observed against Dd2, Dd1, Dd17, Kd34, Kd2 and Ld3 (**Figure 4.6**). Interestingly, none of these specimens showed proliferative responses against GSW11 nor AH1 (**Figure 4.6** A and D).

Lastly, to map the contribution of each tested peptide to the overall observed IFNγ production, the average frequency of IFNγ+ CD8+ T cells from three mice where all the peptides were screened was plotted. These analyses showed that untreated mice display similar IFNγ production levels across all the tested peptides, regardless of their MHC-I restriction (**Figure 4.7**). The highest response observed in splenocytes was to the neoantigen Dd17, followed by the gp70-derived peptide Kd35, and the neoantigen Kd26.

Altogether, these results suggest that CD8+ T cells do not follow immunodominant patterns in CT26-challenged untreated mice, as the frequency of IFNγ production is relatively similar across the tested peptides. Nonetheless, the finding that these cells can proliferate upon peptide stimulation may suggest these CD8+ T cells could enter an early state of dysfunction that impedes the correct production of effector cytokines following stimulation.

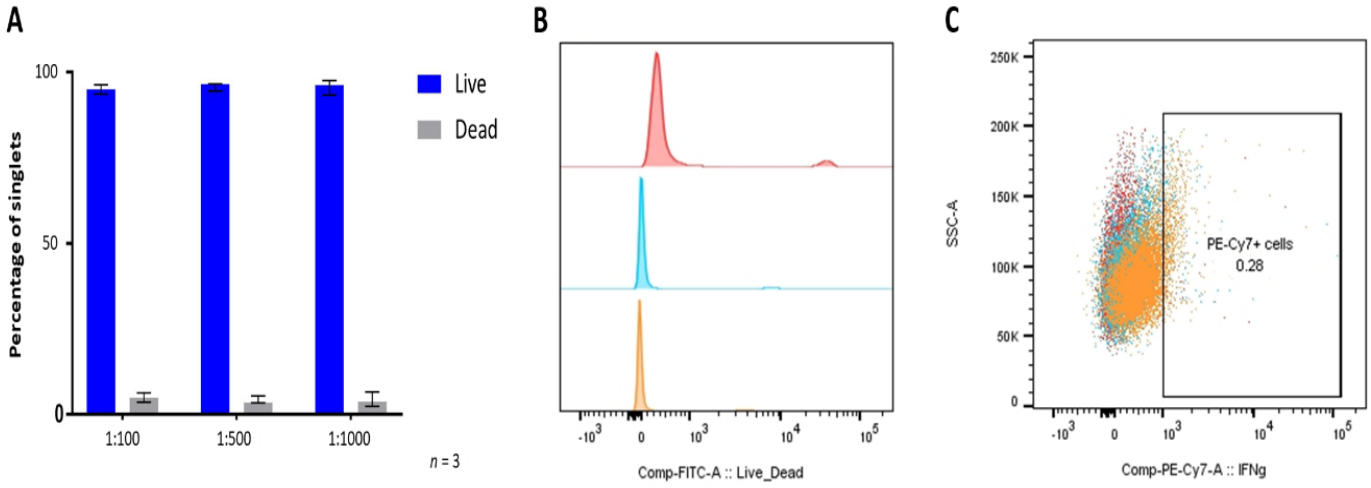

Figure 4.2 **Standardisation of Live/Dead and IFNγ positive populations.A.** Zombie Green™ viability dye was tested at 1:100, 1:500 and 1:1000 dilutions in splenocytes from BALB/c mice. The frequency of live (blue) and dead cells (grey) are depicted as median and range. **B.** Flow cytometry histograms of live and dead populations using 1:100 (red), 1:500 (blue) and 1:1000 (orange) dilutions. **C.** Percentage of PE-Cy7+ cells using 0.1µg/ml (red), 0.2µg/ml (blue) and 0.4µg/ml (orange) or the rat IgG1κ isotype control.

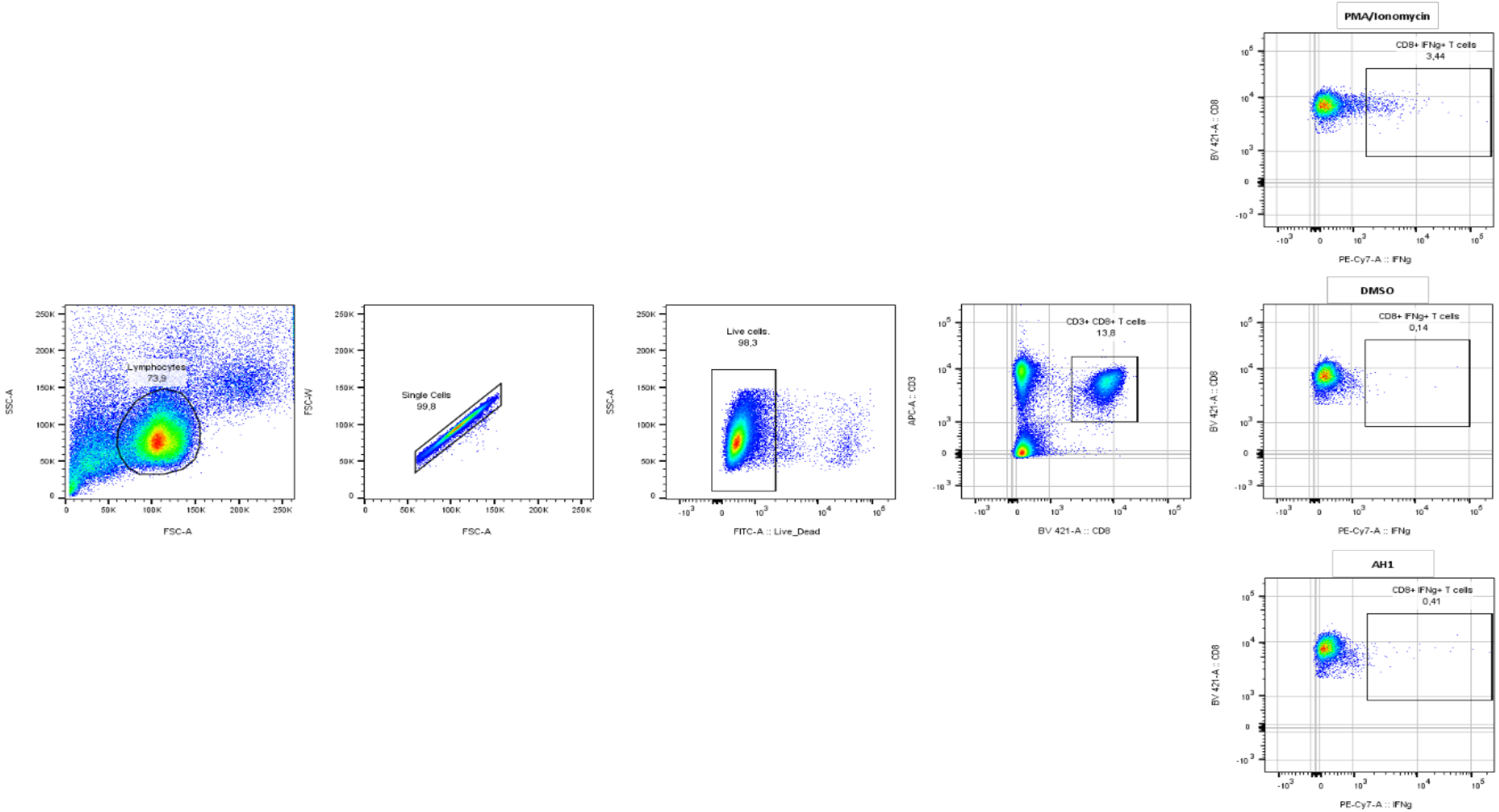
Lymphocytes
73,9
SSC-A
FSC-A
FSC-W
Single Cells
99,8
Live cells.
98,3
FITC-A :: Live_Dead
APC-A :: CD3
CD3+ CD8+ T cells
13,8
BV 421-A :: CD8
PMA/Ionomycin
CD8+ IFNg+ T cells
3,44
PE-Cy7-A :: IFNg
DMSO
CD8+ IFNg+ T cells
0,14
AH1
CD8+ IFNg+ T cells
0,41

Figure 4.3 FACS gating strategy for IFNγ responses in CD8+ T cells from spleen. Representative workflow for the detection of IFNγ+ CD8+ T cells after 4-hour peptide incubation. Plots at the right represent the positive control PMA/Ionomycin (top), the background IFNγ detection when cells were stimulated with DMSO (middle), and a prototypical IFNγ response against an immunogenic peptide, such as AH1 (bottom).

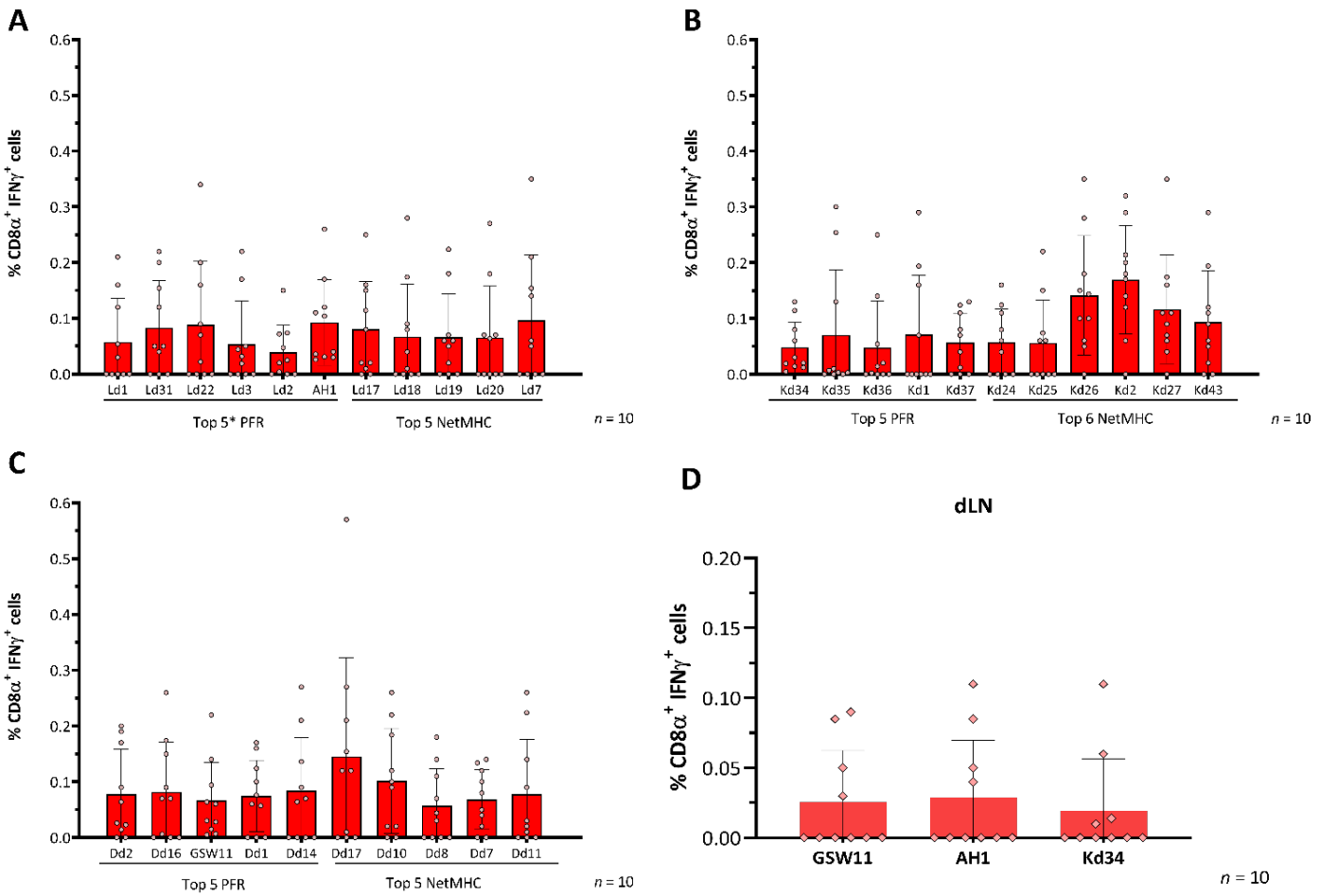

Figure 4.4 **IFNγ responses towards CT26-derived peptides in tumour-challenged mice.** BALB/c mice were challenged with 10^5 CT26 cells, and spleen and tdLNs were harvested at day 11 for the detection of IFNγ production by CD8+ T cells after 4-hour peptide stimulation with the top ranked peptides from PFR and NetMHC. Basal IFNγ responses in untreated cells (cultured with DMSO) were subtracted from each specimen, and data is represented as mean and standard deviation of the frequency of IFNγ+ CD8+ T cells splenocytes with H-2L^d (**A**), H-2K^d (**B**), and H-2D^d (**C**) peptides, as well as the frequency of IFNγ+ CD8+ T cells from tdLNs stimulated with GSW11, AH1 and Kd34 (**D**).

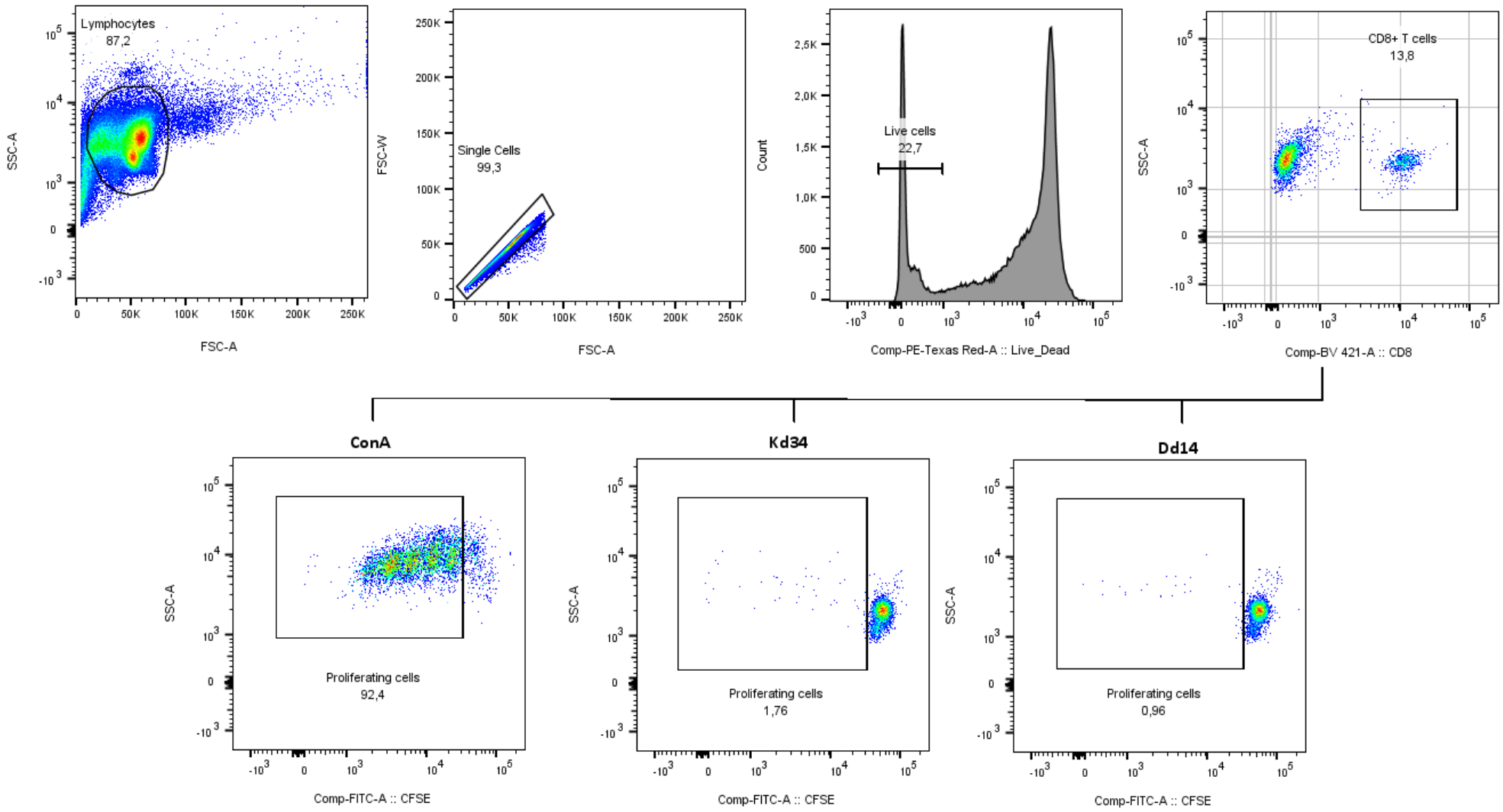
Lymphocytes
87,2
SSC-A
FSC-A
Single Cells
99,3
FSC-W
FSC-A
Live cells
22,7
Count
Comp-PE-Texas Red-A :: Live_Dead
CD8+ T cells
13,8
SSC-A
Comp-BV 421-A :: CD8
ConA
Proliferating cells
92,4
SSC-A
Comp-FITC-A :: CFSE
Kd34
Proliferating cells
1,76
SSC-A
Comp-FITC-A :: CFSE
Dd14
Proliferating cells
0,96
SSC-A
Comp-FITC-A :: CFSE

Figure 4.5 **FACS gating strategy for the detection of proliferating CD8+ T cells.** Splenocytes from untreated and Treg-depleted mice were incubated for 72 hours in the presence of CT26-derived peptides. Proliferation was measured by staining stimulated cells with CFSE and detecting the dye dilution within the live CD8+ T cell populations. The bottom three graphs depict the positive control ConA (left), a peptide that induces strong proliferation (middle), and a peptide inducing weak proliferation (right).

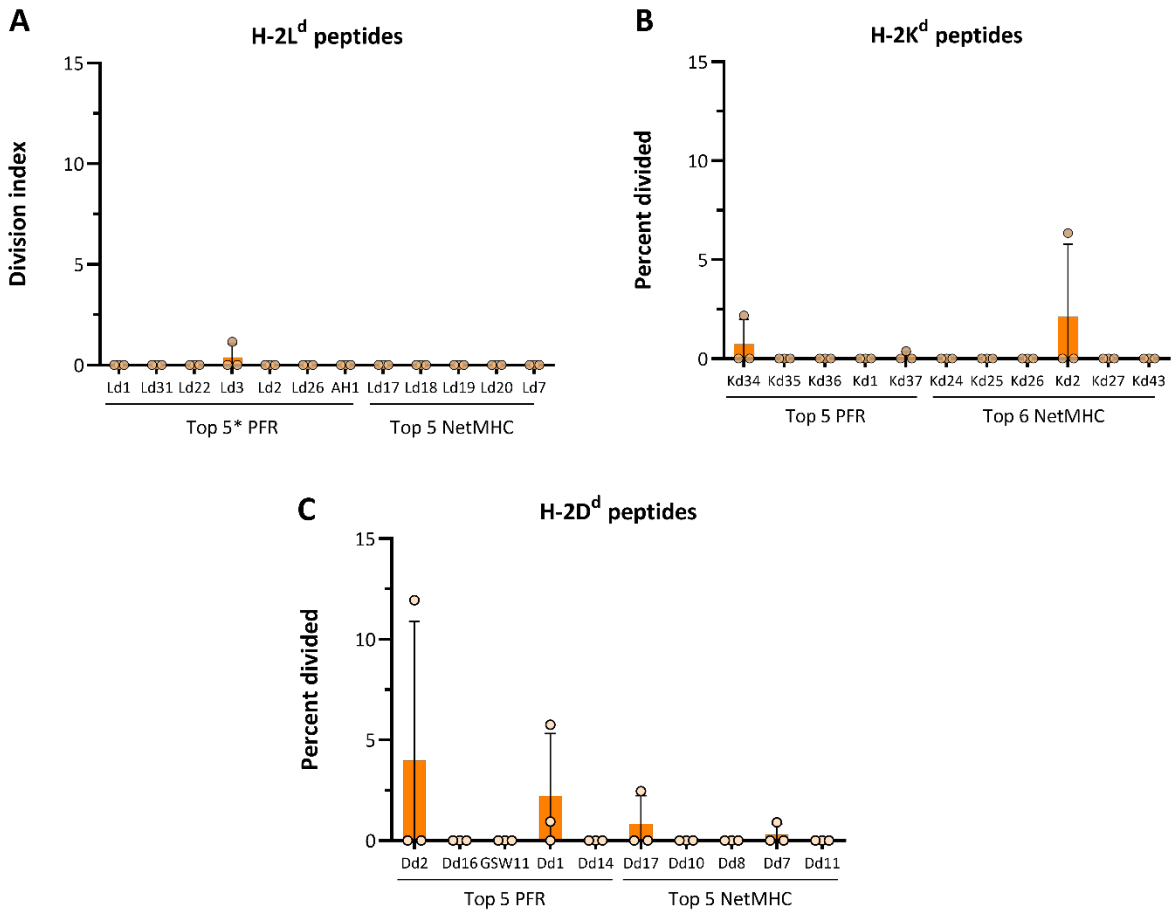

Figure 4.6 **Proliferation patterns of peptide-pulsed CD8+ T cells in untreated mice.** Splenocytes from CT26-challenged mice were incubated for 72 hours in the presence of H-2L^d- (**A**), H-2K^d- (**B**), and H-2D^d-restricted peptides (**C**). Proliferation was measured via CFSE dye dilution, using cells cultured with DMSO as a negative control. Results are depicted as mean and standard deviation of the percentage of proliferating cells from each tested peptide. N = 3.

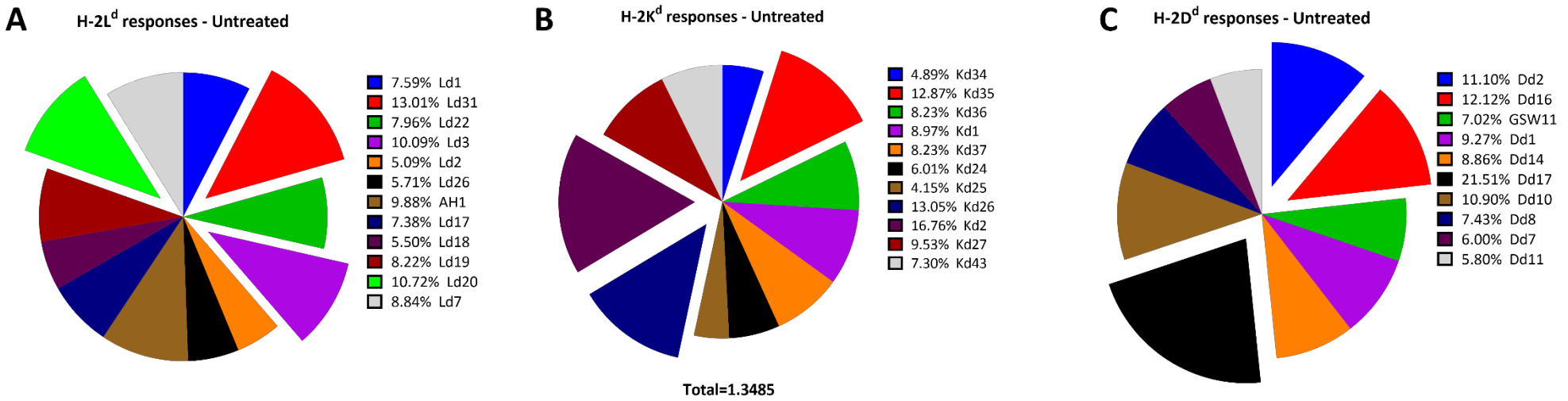

Figure 4.7 **Overall IFNγ responses against tested peptides in splenocytes from CT26-challenged untreated mice.** Average frequency of IFNγ+ CD8+ T cells from three mice against H-2L^d- (**A**), H-2K^d- (**B**), and H-2D^d-restricted peptides (**C**). Each portion represents a unique peptide, the average frequency of IFNγ+ CD8+ T cells for each specific MHC-I allele is depicted alongside the respective legends, and the total average IFNγ responses is depicted at the bottom. The three highest IFNγ responses for each allele are depicted in each graph as exploded pie portions.

4.2.3 Modulation of CD8+ T cell responses upon Treg depletion

4.2.3.1 Validation of Treg depletion strategy

The second screening approach for the peptide library was carried out using Treg-depleted CT26-challenged mice, as it has been observed that this therapeutic intervention leads to the development of strong CD8+ T cell responses able to eliminate tumours in a significant number of mice (Golgher, Jones et al. 2002), and is associated with boosting of IFNγ responses against AH1 and GSW11 (James, Yeh et al. 2010). Initially, two different Treg-depleting antibodies were used: an *in-house* produced anti-CD25 monoclonal antibody (PC61, Rat IgG1 λ), and a commercial version of the same antibody. *In vivo* depletion of Tregs was performed via i.p. injection of two different doses of these antibodies (200µg and 400µg) given twice with one-day intervals into naïve BALB/c mice, and levels of CD4+ CD25+ FOXP3+ Tregs were verified in spleen and tdLNs at day 11 after the last PC61 dose. As observed in **Figure 4.8** A, Tregs levels were significantly reduced in both spleen and mesenteric lymph nodes at all tested concentrations, regardless of the antibody, compared to untreated mice. Based on these results, all further Treg-depletion experiments were performed using 200µg of the commercial PC61. Given than previous reports have shown an *in vivo* PC61 half-life of 20 days (Tan, Reddy et al. 2013), we aimed to measure Treg levels in tumours, tdLNs and spleen from PC61-treated mice at day 30. Remarkably, PC61-treated animals showed a significantly lower frequency of Tregs in all three organs compared to control mice (**Figure 4.8** B), indicating that the PC61 therapeutic regime adopted in this study leads to a stable depletion of Tregs.

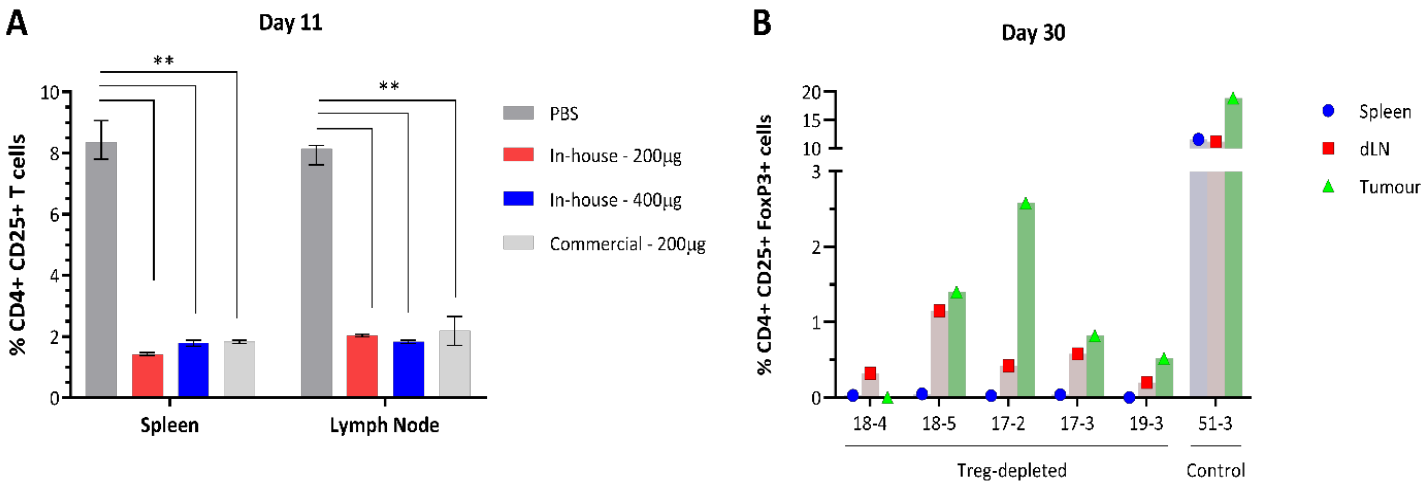

Figure 4.8 **PC61 injections lead to a significant decrease in Tregs in secondary lymphoid organs and tumours.A.** Three BALB/c mice were injected with two doses of PC61 or the equivalent volume of vehicle (PBS) as controls. Spleens and lymph nodes were harvested 11 days after the last PC61 dose, and levels of CD4+ CD25+ Tregs were measured by flow cytometry. Median and range; Kruskal-Wallis test; $p = 0.0079$. **B.** BALB/c mice were Treg-depleted with two doses of 200µg PC61 before CT26 injection. At day 30 post tumour challenge, spleen, tdLNs and tumours were harvested and levels of CD4+ CD25+ FOXP3+ Tregs were measured by flow cytometry.

After verifying the *in vivo* depletion of Tregs, we tested if the absence of these cells could confer immunity against CT26, as previously reported. For this, two doses of 200µg PC61 were injected i.p. three days and one day prior subcutaneous inoculation of 10^5 CT26 cells. This therapeutic scheme yielded a 30% level of tumour rejection in treated animals, which started to show signs of tumour regression at days 11 – 13 post-tumour challenge, reaching complete regression at days 22 - 25 (**Figure 4.9** A). Moreover, animals that did not achieve complete tumour remission (progressors) tended to reach the tumour humane endpoint at a later stage compared to untreated animals (**Figure 4.9** B), which translates into a significant increase in survival in Treg-depleted mice (**Figure 4.9** C). The lack of tumour control in PC61-treated progressors was not related to a defect in the Treg-depletion protocol, as the frequency of these cells in peripheral blood at day 11 post tumour challenge was comparable between regressors and progressors, and lower compared to untreated mice (**Figure 4.10**).

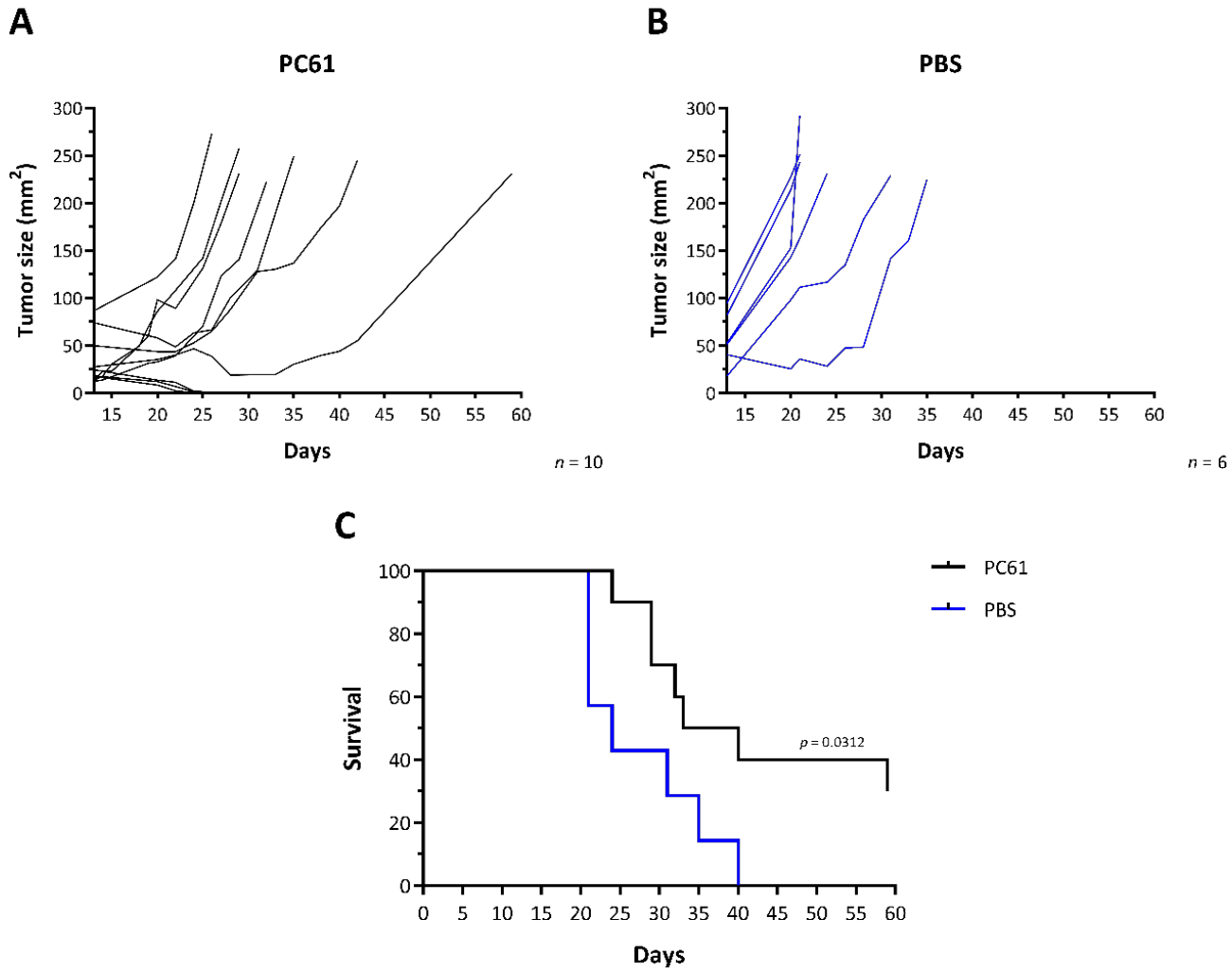

Figure 4.9 **PC61-mediated Treg depletion is associated with tumour control.**BALB/c mice were injected with two doses of 200µg of PC61 (**A**), or the equivalent vehicle volume (**B**) at days -3 and -1 prior CT26 inoculation. Each line depicts the kinetics of tumour growth in individual mouse. **C.** Survival analysis of PC61-treated mice (blue and red lines) and PBS controls (black line); log-rank test.

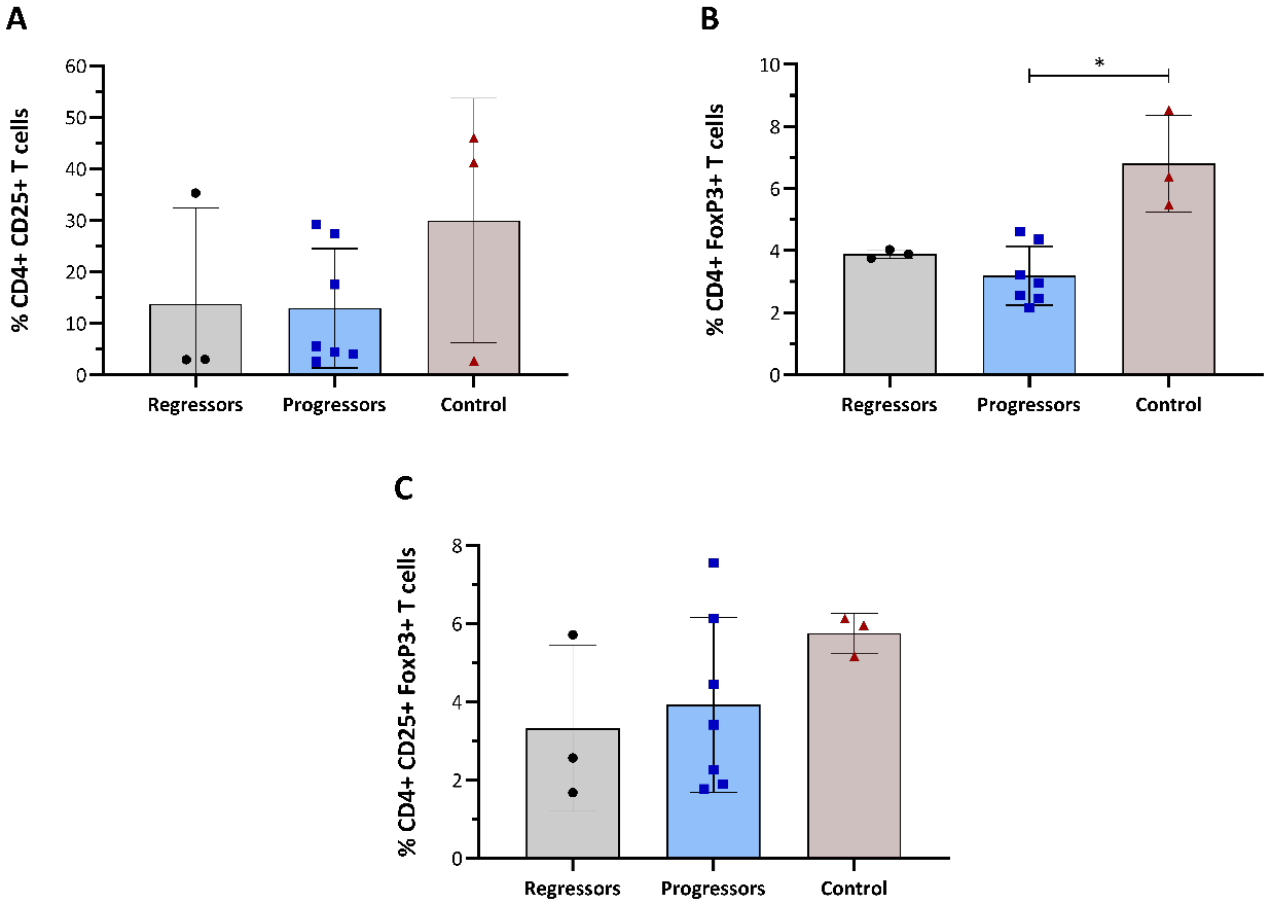

Figure 4.10 Treg levels in peripheral blood post PC61 treatment do not discriminate regressors of progressors. Peripheral blood was obtained from Treg-depleted and untreated mice at day 11 post tumour challenge via tail prick, and levels of CD4+ CD25+ (**A**), CD4+ CD4+ FOXP3+ (**B**), and CD4+ CD25+ FOXP3+ cells (**C**) were measured by flow cytometry. Mean ± standard deviation; Kruskal-Wallis test; $p = 0.0236$.

Overall, these results indicate that Treg-depletion prior to tumour challenge represents an effective therapeutic intervention leading to the elimination of CT26 tumours in a third of treated BALB/c mice.

4.2.3.2 Treg depletion broadens the CD8+ T cell responses in mice with regressing tumours

To explore the relationship between tumour control and specific peptides targeted by CD8+ T cells, splenocytes and tdLNs from CT26-challenged Treg-depleted mice were harvested at day 11 post tumour challenge and stimulated with the previously tested peptides for 4 hours for the detection of IFNγ production by CD8+ T cells. This time point was strategically chosen as tumour sizes in earlier time points do not allow for a proper delineation of regressors and progressors,

and a later time point would lead to a reduction in IFNγ production due to T cell dysfunction/exhaustion. Animals showing signs of tumour regression showed a higher frequency of IFNγ+ CD8+ T cells compared to progressors across the majority of peptides while animals showing continuous tumour growth exhibited low IFNγ production by CD8+ T cells, thus suggesting that the immune control of CT26 tumours in Treg-depleted mice could be associated with a broadening of the CD8+ T cell responses (**Figure 4.11**). As expected, IFNγ production against AH1 and GSW11 was significantly boosted in regressors compared to progressors (**Figure 4.11** A and C). Interestingly, two novel gp70-derived peptides (Kd34 and Kd37) that ranked 1st and 5th by PFR also induced significantly higher levels of IFNγ+ CD8+ T cells in regressors versus progressors (**Figure 4.11** B). These differences were not explained by a reduction in the total number of viable cells or in the frequency of CD8+ T cells from each mouse, as these levels did not differ significantly between regressors and progressors (**Figure 4.12** A and B). Moreover, besides being the best H-2K^{d} ranked peptide by PFR, Kd34 was also detected in the CT26 MAE immunopeptidome, strongly indicating that this peptide is intracellularly processed and presented by H-2K^{d}, representing a novel CT26 epitope with potential therapeutic benefit.

In general, PFR allowed for a higher detection of IFNγ responses for H-2L^{d}-restricted peptides than NetMHC, whereas the opposite was observed for H-2D^{d}- and H-2K^{d}-restricted peptides. This is evidenced by several NetMHC-ranked neo-antigens showing a significantly higher IFNγ response in regressors compared to progressors, such as Kd2, Kd26, and Kd27 (**Figure 4.11** B), as well as other peptides that although showing high IFNγ responses, were not statistically significant between the two groups (like the top 5 NetMHC-ranked H-2D^{d}-restricted peptides, **Figure 4.11** C). Nonetheless, a striking observation was made with PFR-ranked peptides, as 4 out of 16 tested peptides (25%) showed strong statistically significant ($p < 0.005$) IFNγ responses in regressors compared to progressors, whereas for NetMHC-ranked peptides, only one out of 16 tested peptides (6.25%) showed this level of significance. Importantly, this NetMHC-ranked peptide (Kd2) was ranked as top 6 by PFR. Thus, these observations, along with the fact that only PFR is able to rank GSW11 and AH1 in the top 15 ranked peptides, collectively suggest that although PFR does not outperform NetMHC for the prediction of immunogenic peptides, it significantly improves the likelihood of identifying peptides correlated with protection. This conclusion is also supported by the IFNγ responses observed against the HIV-derived peptide Dd8, which was originally included as a negative control for being a non-CT26 peptide with a predicted high affinity for H-2D^{d}, but that showed high levels of IFNγ production in regressors compared to progressors (**Figure 4.11** C). These results suggest that this peptide could represent a mimotope, considering that all peptides were tested at the same time, and that background IFNγ levels were subtracted from each peptide based on the basal levels of CD8+ IFNγ+ T cells stimulated with vehicle (DMSO). Moreover, these findings also point towards the conclusion that not all IFNγ

responses observed against NetMHC-ranked peptides are therapeutically relevant. Indeed, the top-ranked H-2L^d restricted peptide predicted by NetMHC (Ld17) showed a higher mean frequency of IFNγ+ CD8+ T cells in progressors compared to regressors (**Figure 4.11** A), indicating that Ld17-specific CD8+ T cells could participate in the lack of immune tumour control associated with Treg-depletion in these mice.

In tdLNs, given the small sizes of the organs, only a few peptides could be screened in ICS assays. Thus, GSW11, AH1, and Kd34 were chosen as targets, considering that the first two peptides are well-established CT26 epitopes, and the latter ranks first by PFR, was detected in the MAE immunopeptidome, and induces strong IFNγ responses in spleen from regressors. Although the overall responses against these three peptides were higher in regressors compared to progressors, mainly in cells stimulated with GSW11, no statistically significant differences were observed between these two groups for any of the peptides (**Figure 4.11** D). Interestingly, regressors displayed lower frequencies of CD8+ T cells in tdLNs compared to progressors, being statistically significant when compared to untreated mice (**Figure 4.12** D). These observations could indicate a higher rate of CD8+ T cell egress from tdLNs towards tumours in tumour-regressing Treg depleted mice.

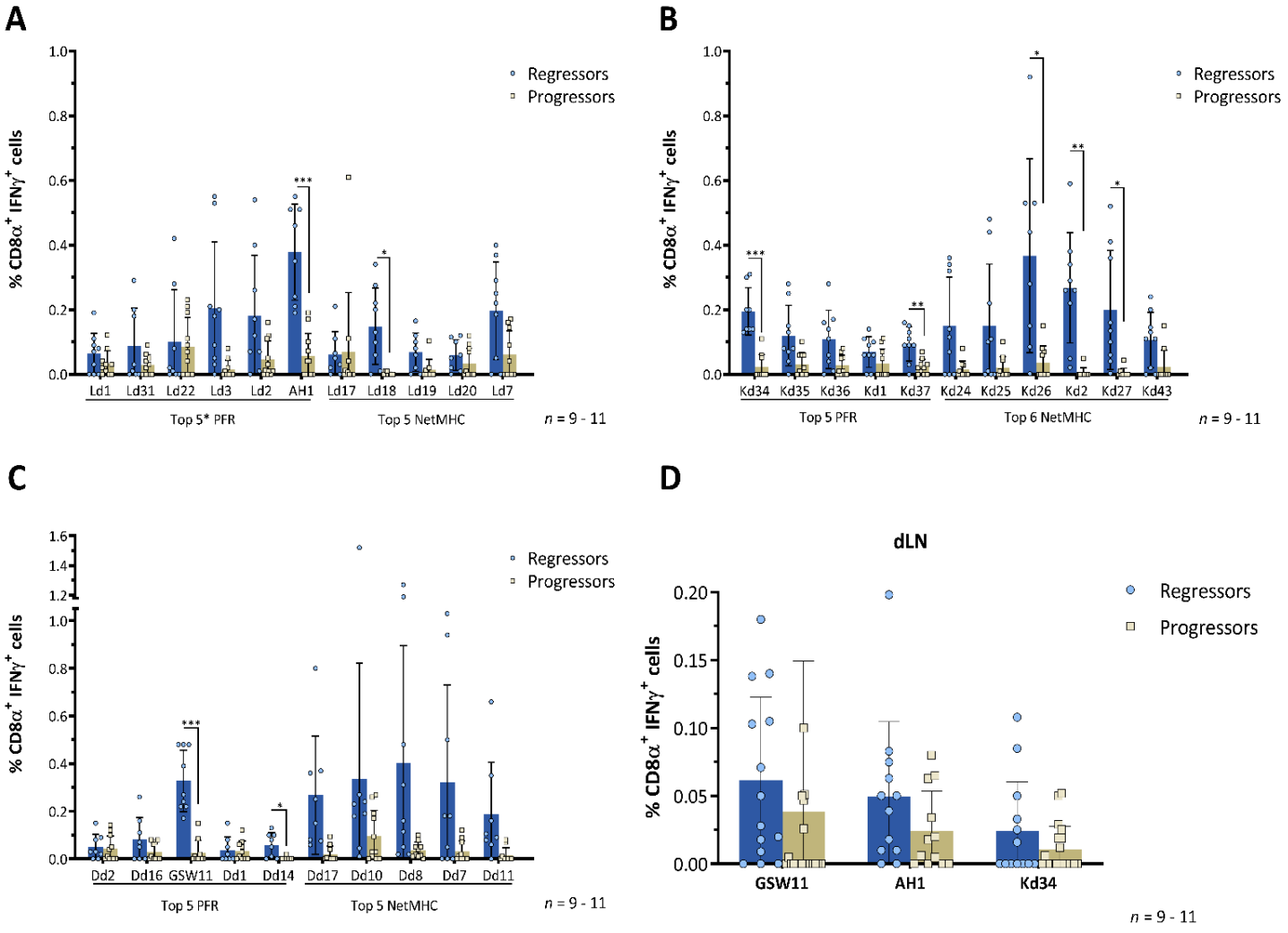

Figure 4.11 Depletion of Tregs in CT26-challenged mice leads to a broad repertoire of IFNγ responses in regressing mice. BALB/c mice were treated with two PC61 doses at days -3 and -1, and subsequently challenged with 10^5 CT26 cells. **A – C**. Spleens from regressors and progressors were harvested at day 11 post tumour challenge, and IFNγ responses against top ranked H-2L^d (**A**), H-2K^d (**B**), and H-2D^d (**C**) peptides from PFR and NetMHC4.0 were measured by flow cytometry. **D.** tdLNs responses from regressors and progressors against GSW11, AH1, and Kd34. Mean ± standard deviation; Mixed-effects analysis with Tukey's multiple comparisons test; * $p < 0.05$, ** $p < 0.005$; *** $p < 0.001$.

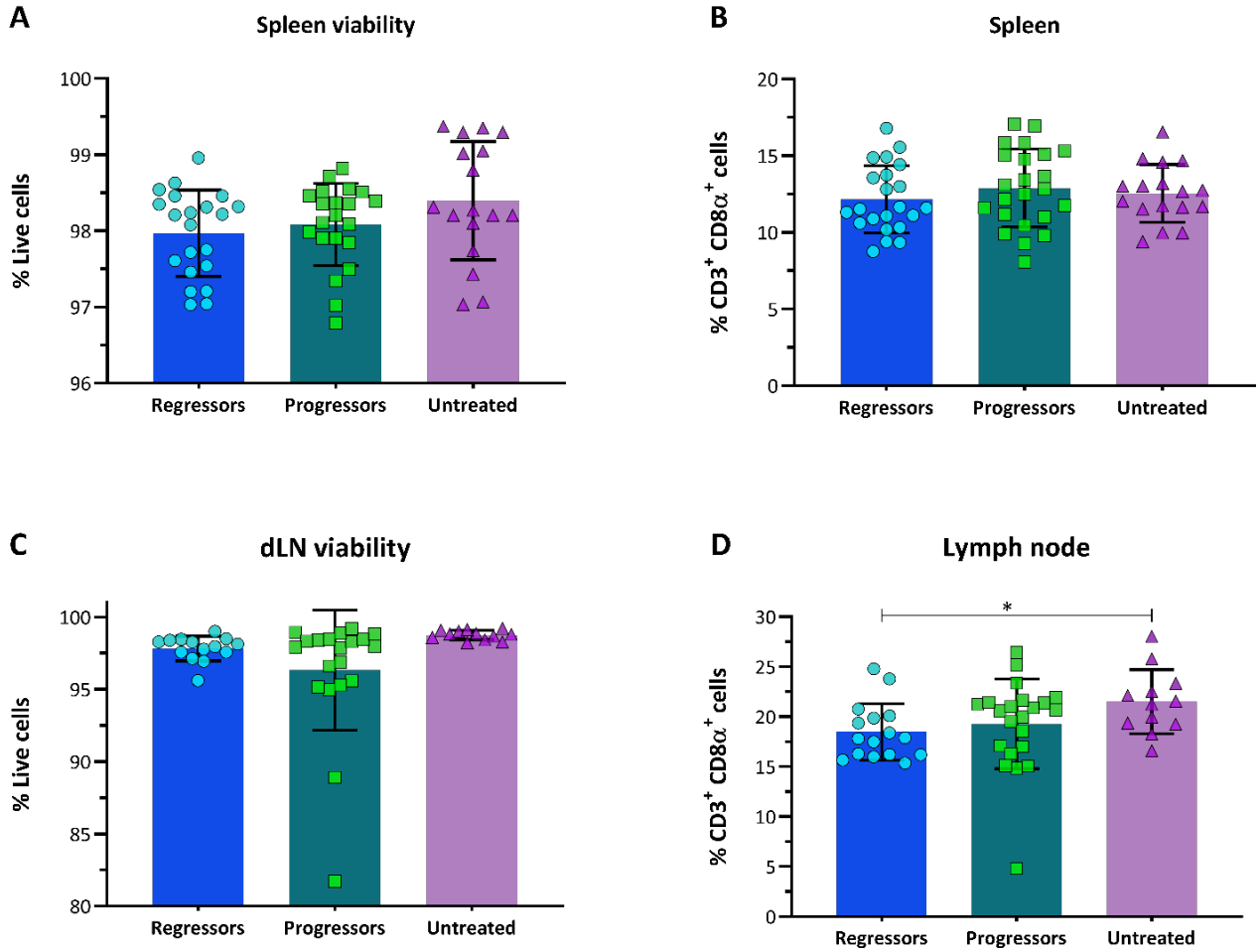

Figure 4.12 CD8+ T cell viability and frequency in organs from tested mice. Frequency of live CD8+ T cells was detected in spleen (**A**) and tdLNs (**C**) using the Zombie Green™ Fixable viability dye. Frequency of CD3+ CD8+ T cells was measured in spleen (**B**) and tdLNs (**D**) by flow cytometry. Mean ± standard deviation; Kruskal-Wallis test, p = 0.0401.

The proliferation patterns of splenocytes from regressors and progressors pulsed with the target peptides was measured in CFSE assays. Interestingly, the majority of PFR-ranked H-2L^d-restricted peptides showed a higher proliferation in regressors compared to progressors (except for Ld3 and Ld2) (**Figure 4.13** A). For H-2K^d-restricted peptides, 7 out of 11 tested peptides induced higher proliferation of CD8+ T cells in regressors versus progressors, with no discernible differences observed between PFR-ranked and NetMHC-ranked peptides (**Figure 4.13** B). However, for H-2D^d-restricted peptides, only GSW11 and Dd1 from the PFR rank exhibited higher proliferation rates in regressors compared to progressors, while 3 out of 5 NetMHC-ranked peptides showed higher proliferation responses in regressors (**Figure 4.13** C).

Interestingly, the p/MHC-I affinities measured via BFA decay did not correlate with levels of CD8+ IFNγ+ T cells across all alleles, with only a faint and non-significant correlation observed in H-2K^d-restricted peptides (**Figure 4.14** B). Conversely, the MHC-I predicted affinities for H-2L^d-restricted peptides showed a significant inverse correlation with the frequencies of CD8+ IFNγ+ T cells observed after peptide stimulation, as the lower the affinity (high IC_{50} values) the higher the induction of IFNγ production (**Figure 4.14** A). For H-2K^d and H-2D^d-restricted peptides, affinity values obtained by NetMHC showed a positive correlation with CD8+ IFNγ+ T cells, although this correlation was statistically significant only for H-2D^d (**Figure 4.14** B and C).

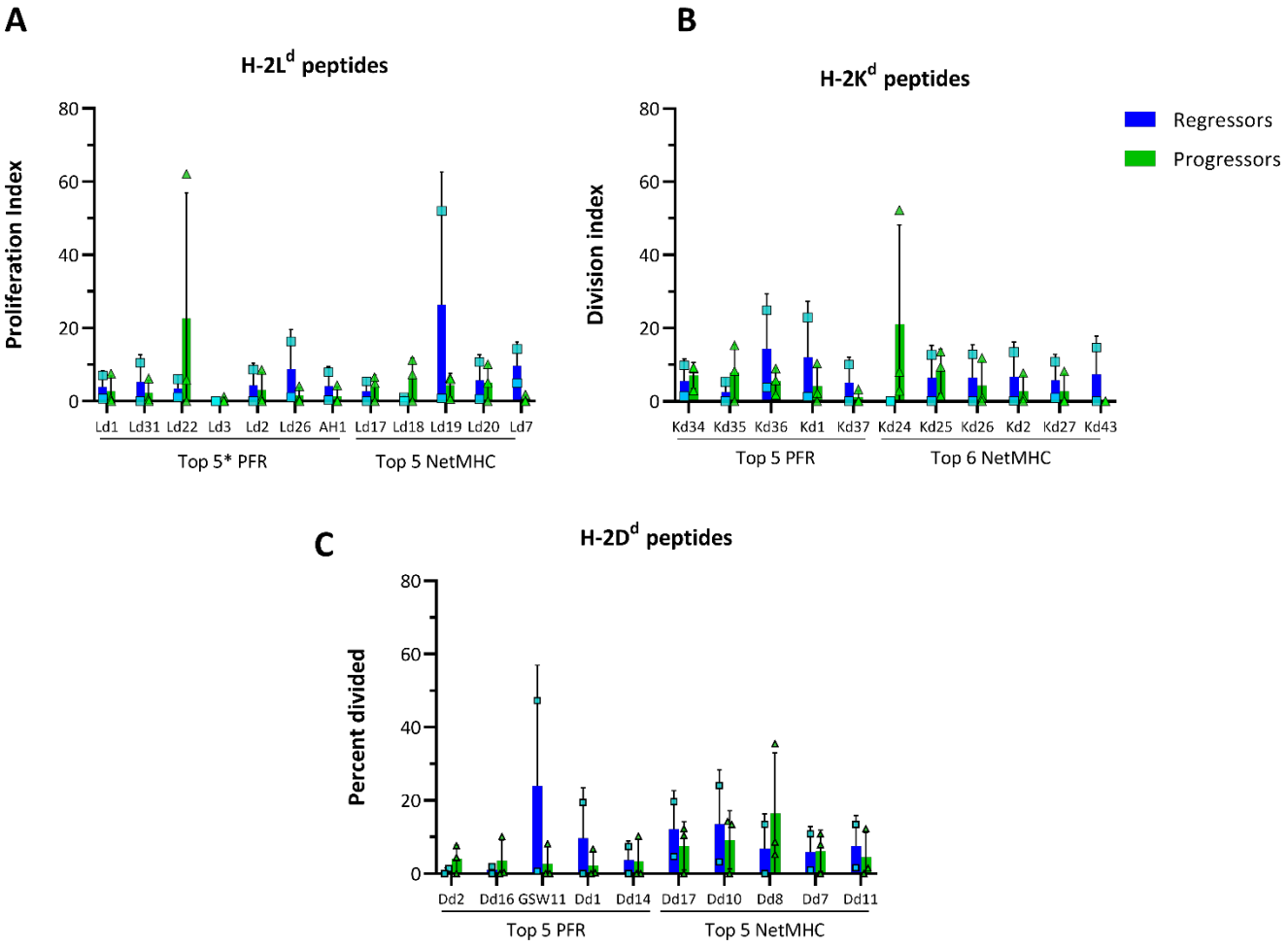

Figure 4.13 Proliferation patterns of CD8+ T cells from Treg-depleted CT26-challenged mice. Splenocytes from Treg-depleted CT26-challenged mice were incubated for 72 hours in the presence of H-2L^d- (**A**), H-2K^d- (**B**), and H-2D^d-restricted peptides (**C**). Proliferation was measured via CFSE dye dilution, using cells cultured with DMSO as a negative control. Results are depicted as mean and standard deviation of the percentage of proliferating cells from each tested peptide. N = 3.

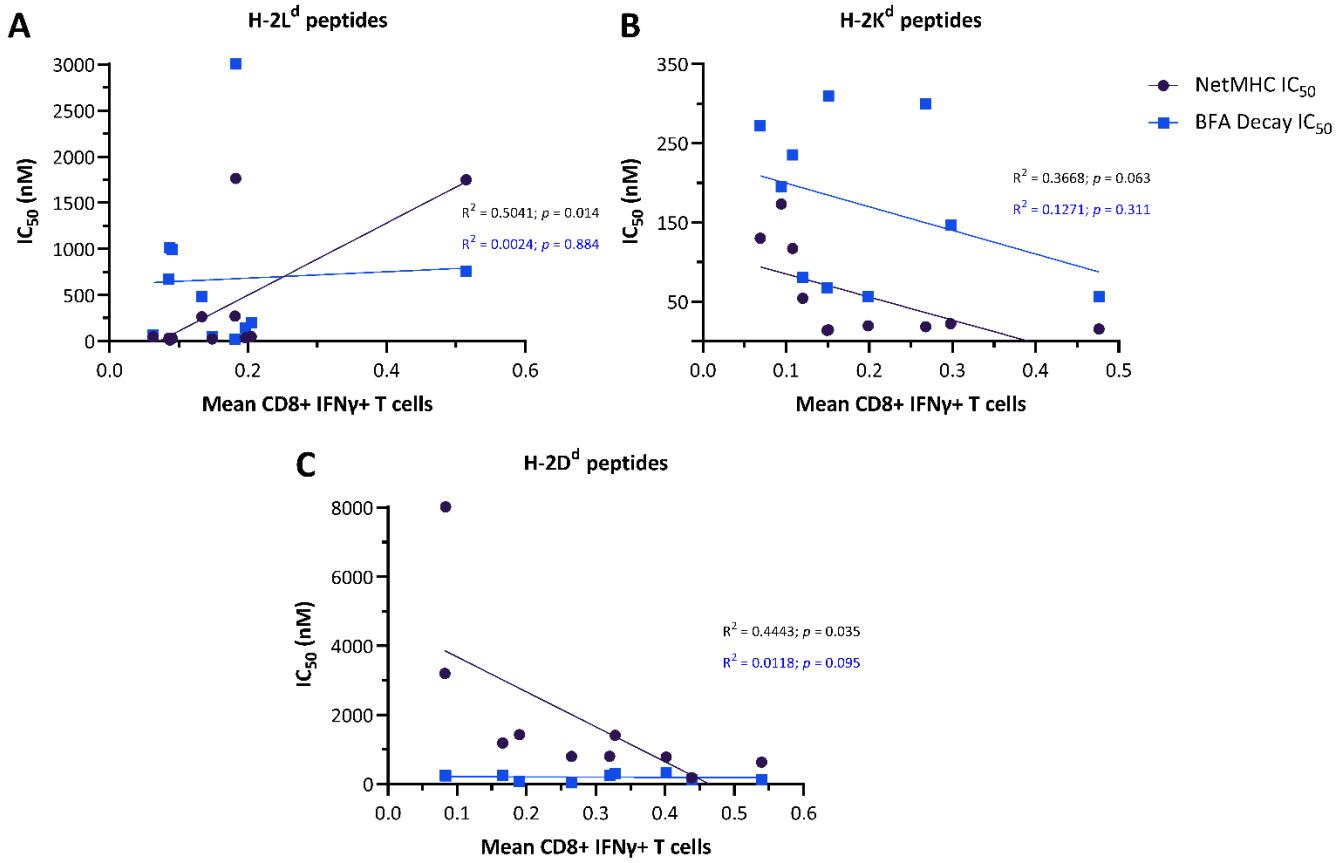

Figure 4.14 Predicted MHC-I binding affinities correlate with the rate of IFNγ production by CD8+ T cells in regressors. NetMHC (black circles) and BFA decay (blue squares) IC_{50} affinity values were correlated with the mean IFNγ+ production observed by CD8+ T cells from regressors stimulated with H-2L^d (**A**), H-2K^d (**B**), or H-2D^d (**C**) restricted peptides.

Mapping the average IFNγ responses in regressors and progressors where all the target peptides were tested showed interesting results. In regressors, just like in untreated mice, no specific predominance against allele-specific peptides were observed, but a higher total frequency of IFNγ responses was observed (**Figure 4.15**). In addition, the most predominant IFNγ responses were observed against AH1, the neoantigens Kd26 and Dd10, and the mimotope Dd8 (**Figure 4.15**). Interestingly, progressors showed predominant IFNγ production against H-2L^{d}-restricted peptides, as almost half of the observed responses were directed against these peptides (**Figure 4.16** A). Moreover, the high AH1-specific IFNγ signature observed in regressors is not present in progressors, but akin to regressors, high IFNγ production was observed with cells stimulated with the neoantigens Kd26 and Dd10 (**Figure 4.15** B and C, and **Figure 4.16** B and C), thus suggesting that NetMHC-ranked peptides may not play important roles in the CD8+ T cell-mediated clearance of CT26 tumours in Treg-depleted mice.

These results highlight that incorporating abundance alongside affinity parameters for the identification of potential immunogenic peptides results in an increased likelihood of detecting peptides with therapeutic potential. Moreover, although NetMHC-ranked peptides also showed high IFNγ responses in regressors compared to progressors, the fact that the mimotope Dd8 also induced high IFNγ production, that proliferation patterns of NetMHC-ranked peptides were higher in progressors compared to regressors, and that none of these peptides were detected by the MAE immunopeptidome, highlights that using predicted affinities alone is an insufficient approach towards the selection of immunogenic peptides with therapeutic relevance for cancer immunotherapy.

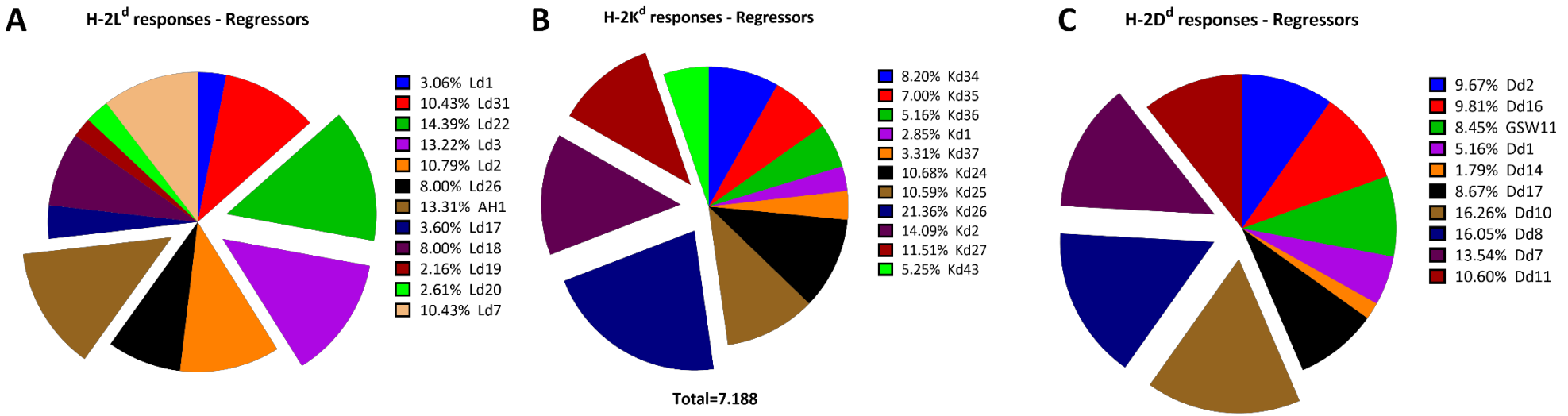

Figure 4.15 High and broad IFNγ responses against tested peptides in splenocytes from Treg-depleted regressors mice. Average frequency of IFNγ+ CD8+ T cells from five mice against H-2L^d- (**A**), H-2K^d- (**B**), and H-2D^d-restricted peptides (**C**). Each portion represents a unique peptide, the average frequency of IFNγ+ CD8+ T cells is depicted alongside the respective legends, and the total average IFNγ responses is shown at the bottom. The three highest IFNγ responses for each allele are portrayed in each graph as exploded pie portions. Grey areas in the pie charts indicate the responses against the remaining tested peptides, which are omitted for illustrative purposes.

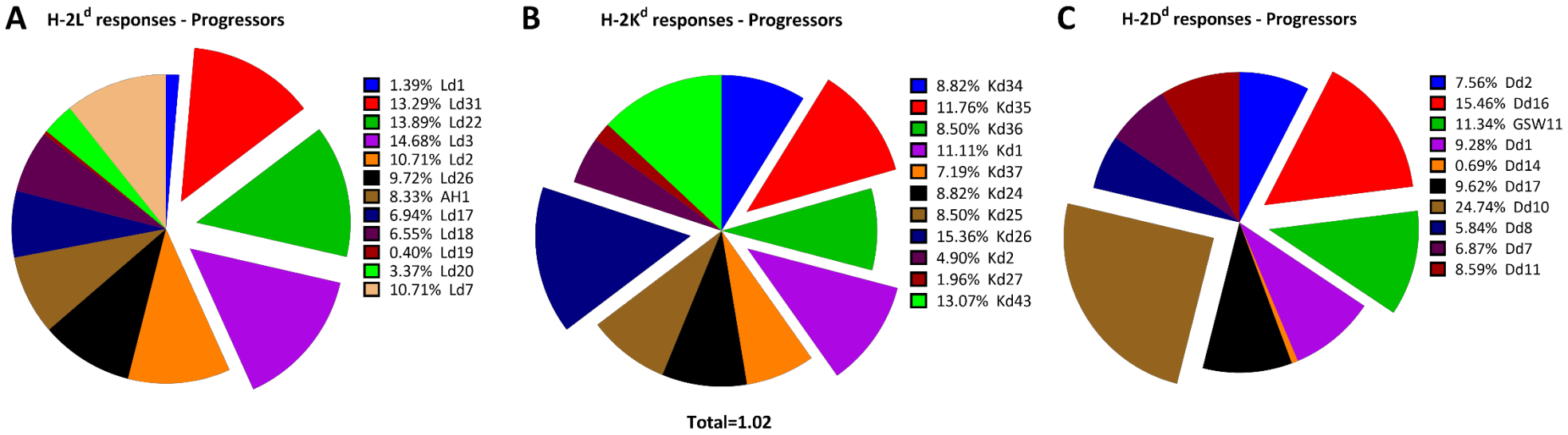

Figure 4.16 Treg-depleted progressors showed a skewed IFNγ profile against H-2L^d-restricted peptides. Average frequency of IFNγ+ CD8+ T cells from three mice against H-2L^d- (**A**), H-2K^d- (**B**), and H-2D^d-restricted peptides (**C**). Each portion represents a unique peptide, the average frequency of IFNγ+ CD8+ T cells is depicted alongside the respective legends, and the total average IFNγ responses is shown at the bottom. The three highest IFNγ responses for each allele are portrayed in each graph as exploded pie portions. Grey areas in the pie charts indicate the responses against the remaining tested peptides, which are omitted for illustrative purposes.

4.3 Concluding remarks

The evaluation of peptide immunogenicity is critical to validate the predictions of cancer-derived epitopes, regardless of the methodological strategy employed for the identification of such peptides. By comparing the amount of IFNγ production and proliferation by CD8+ T cells from CT26-challenged mice at different conditions, we could identify peptides involved in the therapeutic responses after Treg depletion and correlate such responses with the ranking predictions of two different algorithms (NetMHC and PFR). Remarkably, incorporating the relative abundance of the peptide protein source alongside the predicted MHC-I binding affinity allowed us to identify three novel immunogenic CT26-derived epitopes, which can be categorised as overexpressed TAAs, as they derive from the most abundant protein of CT26 cells (gp70). Furthermore, four neoantigens with predicted high MHC-I affinities also showed high IFNγ responses in mice responding to Treg-depletion therapy, but the fact that two of these responses (Kd26 and Dd10) were also observed in lower proportion in regressors, and that NetMHC ranking failed to identify peptides showing strong statistical differences between regressors and progressors in terms of IFNγ production, highlights that PFR could be a better predictor of therapeutically-relevant immunogenic peptides in immunotherapeutic settings, which could have great implications for the development of highly-effective cancer immunotherapy strategies in patients. These results also suggest that a potential mechanism of action of the immune-mediated control upon Treg-depletion is the broadening of anti-tumour immune responses, as observed in melanoma patients treated with ipilimumab (Kvistborg, Philips et al. 2014, Robert, Tsoi et al. 2014). Furthermore, the low IFNγ responses observed in untreated and mice with progressing tumours may suggest that other inhibitory mechanisms could block the correct activation of CD8+ T cells, such as the high frequency of T cells with an exhausted phenotype (van der Leun, Thommen et al. 2020).

Chapter 5 Immunophenotyping of novel antigen-specific CD8+ T cell populations in CT26-challenged mice

5.1 Introduction

The phenotype of TILs represents an important factor that can shape the outcome of cancer immunotherapy (van der Leun, Thommen et al. 2020). Given the remarkable plasticity and heterogeneity of T cells in health and disease, as well as the broad peptide repertoire that tumour-specific CD8+ TILs can recognise, a better understanding on the specificities and immunophenotypes of CD8+ TILs and how these cells can be affected in different cancer settings could improve the development of more targeted and better immunotherapy schemes (Lim and Zainal 2021). One of the most widely used techniques for these purposes is tetramer staining, which consists of four p/MHC-I molecules linked to a fluorochrome that enables the detection of antigen-specific T cells in tissues by flow cytometry (Christophersen 2020). Different derivates from this platform have been developed to increase sensitivity and binding affinity towards TCR molecules. Two of such technologies are Pentamers (consisting in five p/MHC-I molecules linked to a fluorochrome) and Dextramers (made of a dextran backbone carrying ten p/MHC-I molecules), which increases the sensitivity of detection of low-frequency T cell populations and significantly reduces background staining, leading to the use of these technologies for the evaluation of antigen-specific T cell populations in a wide array of cancer studies (Lynn, Sedlik et al. 2020, Stadtmauer, Fraietta et al. 2020, Stifter, Dekhtiarenko et al. 2020). Thus, we aimed to measure the levels and phenotypes of CD8+ and CD4+ T cells in Treg-depleted mice at different time points, as well as the frequency and phenotype of antigen-specific CD8+ T cells against GSW11, AH1, Kd34 and Kd37, considering that the first two peptides are well-stablished CT26 tumour antigens, and that the last two peptides are high ranked by PFR and yielded significant IFNγ responses in Treg-depleted regressors compared to progressors in ICS assays.

5.2 Results

5.2.1 Frequency, memory, and exhaustion phenotypes of CT26-infiltrating CD4+ and CD8+ T cells

For the analysis of CT26-infiltrating T cells, tumours and tdLNs from Treg-depleted mice were harvested at different strategic time points. Day 11 was chosen as this is the earliest time point that facilitates the classification of regressors and progressors, while analyses at day 27 and day 20 were performed in regressors that had eliminated the tumour, or in progressors that reached the tumour humane endpoint, respectively. Additionally, untreated CT26-challenged mice were analysed at day 11 to compare the frequency and phenotype of T cells between Treg-depleted and treatment-naïve mice.

At day 11, no significant differences were observed in the frequency of CD8+ or CD4+ TILs among the groups. However, regressors showed a higher proportion of both cell populations compared to all groups, while tumour progression in later stages was associated with a sharp decline in these cells (**Figure 5.1**). Indeed, T cells comprise around 20% of the tumour cellularity at day 11 regardless of the group; the frequency of CD4+ TILs was almost double than of CD8+ TILs, in contrast with the 2.5% frequency of these cells in tumours from progressors at day 20 (**Figure 5.1** C). This pattern was not observed in tdLNs, as all groups exhibited high numbers of CD8+ and CD4+ T cells, with frequencies in untreated mice being significantly higher compared to day 20 progressors (**Figure 5.1** B).

Next, the levels of antigen-experienced (defined by the expression of CD44) and activated (defined by the expression of PD-1) T cells were measured in the same groups and organs (**Figure 5.2**). Following the previous results, no differences in the levels of CD44+ CD8+ or CD44+ CD4+ T cells were observed at day 11 in tumours, but a significant decrease of these populations was evidenced in progressors at day 20 (**Figure 5.3** A and B). Despite the marked decrease in the T cell percentage in tumours of animals reaching endpoint, no differences were observed in the frequency of PD-1 expression on CD8+ and CD4+ T cells across all groups, as most animals displayed high levels of PD-1+ cells (**Figure 5.3** C and D). In tdLNs, specimens at late time points exhibited the highest frequency of antigen-experienced CD8+ and CD4+ T cells. Remarkably, regressors and progressors at day 11 showed the lowest percentage of CD44+ T cells in tdLNs, while these levels were slightly higher in untreated mice at the same time point (**Figure 5.3** A and B). Furthermore, untreated mice also showed the lowest levels of PD-1 expression on T cells compared to Treg-depleted mice, suggesting that the presence of Tregs in these animals is blocking activating signals on T cells that leads to the upregulation of PD-1 (**Figure 5.3** C and D).

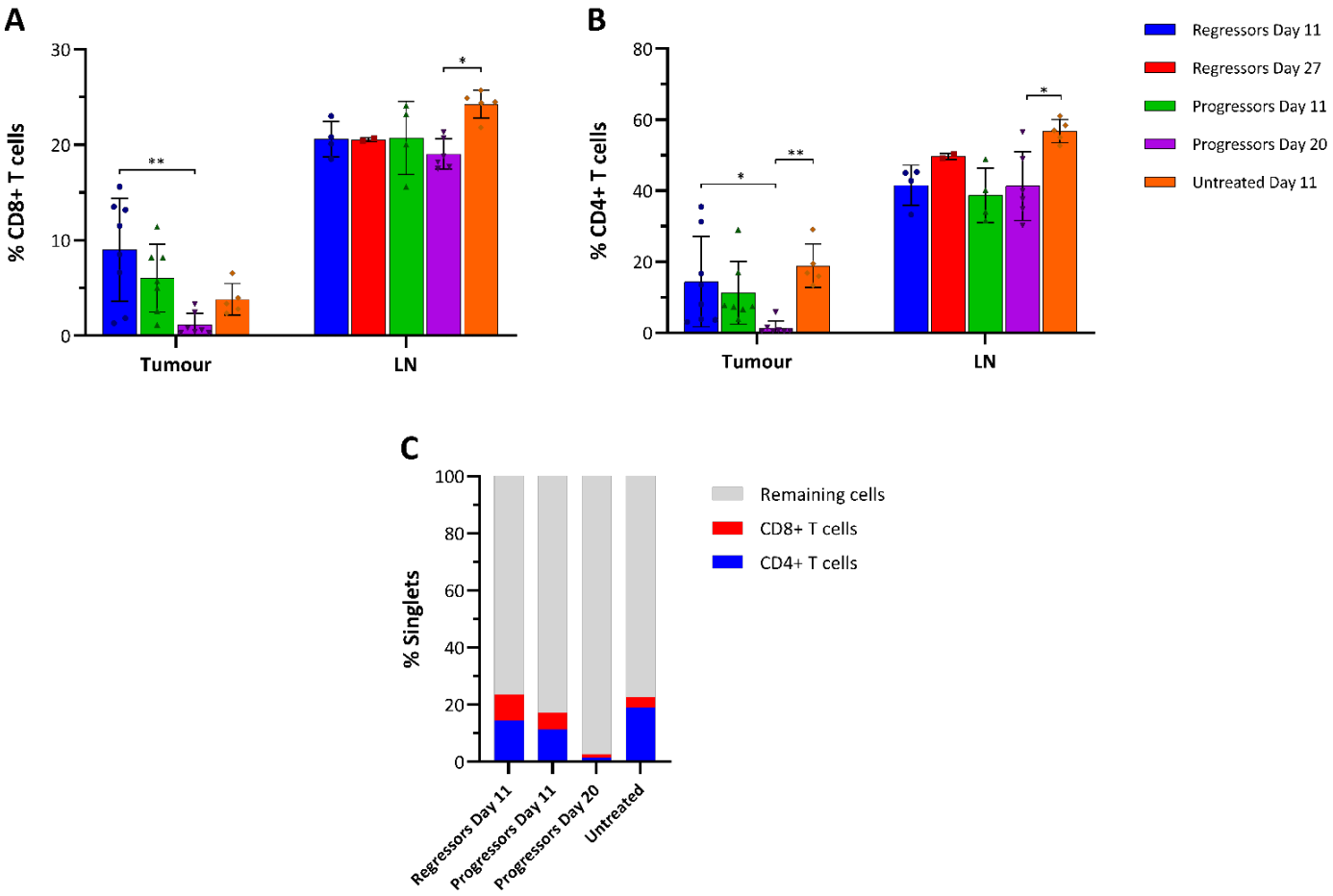

Figure 5.1 CD8+ and CD4+ T cell infiltration in tumours and tdLNs from CT26-challenged mice. Percentages of CD8+ (**A**) and CD4+ (**B**) T cells were measured in Treg-depleted and untreated mice at different time points. Mean ± standard deviation; Kruskal-Wallis test; * $p < 0.05$, ** $p < 0.005$. **C.** Cumulative frequencies of CD8+ (red) and CD4+ (blue) within the tumour.

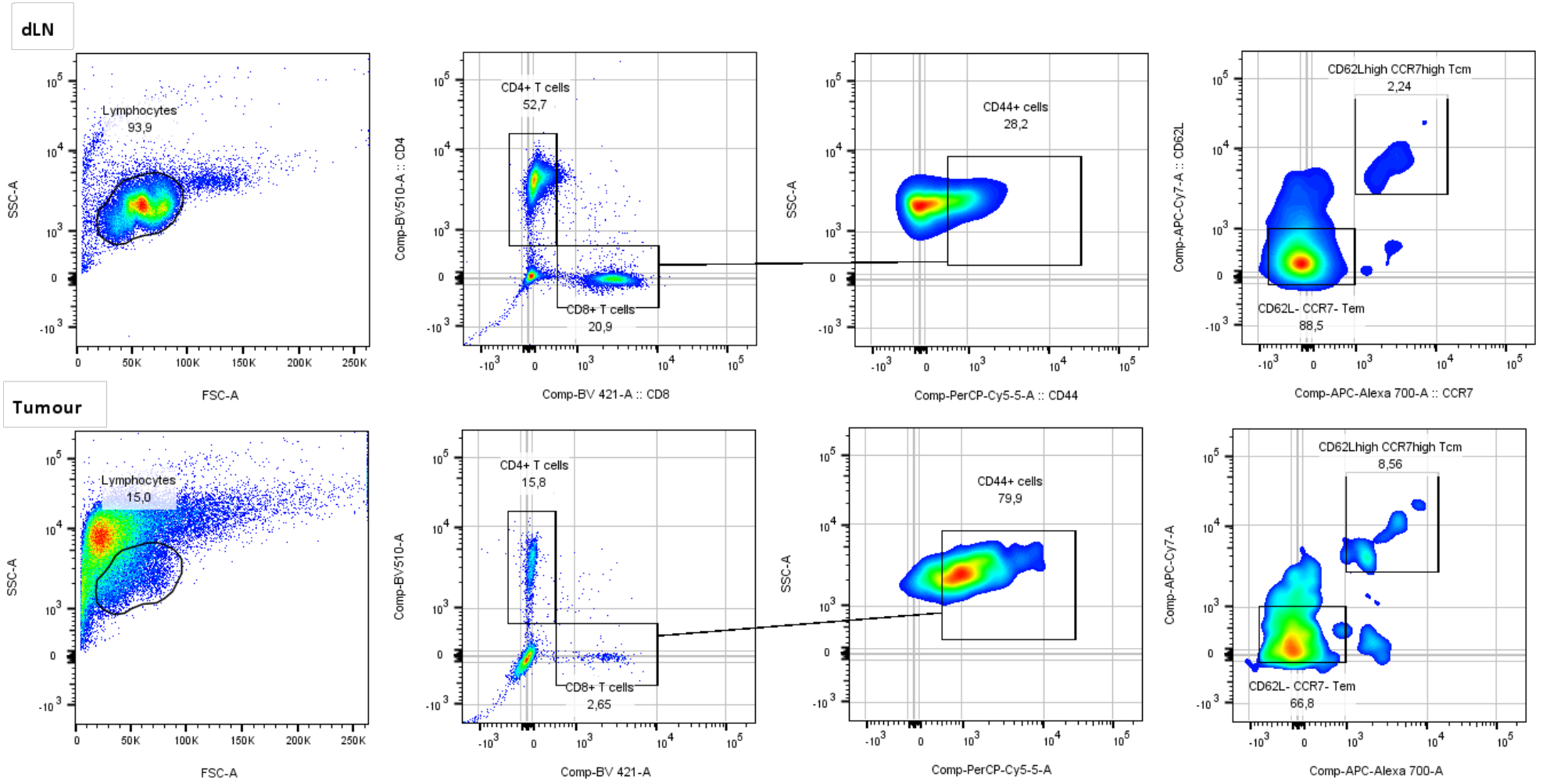
dLN
Lymphocytes
93,9
SSC-A
FSC-A
CD4+ T cells
52,7
CD8+ T cells
20,9
Comp-BV510-A :: CD4
Comp-BV 421-A :: CD8
CD44+ cells
28,2
SSC-A
Comp-PerCP-Cy5-5-A :: CD44
CD62Lhigh CCR7high Tcm
2,24
CD62L- CCR7- Tem
88,5
Comp-APC-Cy7-A :: CD62L
Comp-APC-Alexa 700-A :: CCR7
Tumour
Lymphocytes
15,0
SSC-A
FSC-A
CD4+ T cells
15,8
CD8+ T cells
2,65
Comp-BV510-A
Comp-BV 421-A
CD44+ cells
79,9
SSC-A
Comp-PerCP-Cy5-5-A
CD62Lhigh CCR7high Tcm
8,56
CD62L- CCR7- Tem
66,8
Comp-APC-Cy7-A
Comp-APC-Alexa 700-A

Figure 5.2 Methodological approach for the detection of antigen-experienced and memory subsets. Representative FACS plots from tdLNs (top) and tumours (bottom) depicting the gating strategy adopted for the detection of antigen-experienced T cells (CD44+), T_{CM} (CD62L^{high} CCR7^{high}) and T_{EM} (CD62L- CCR7-).

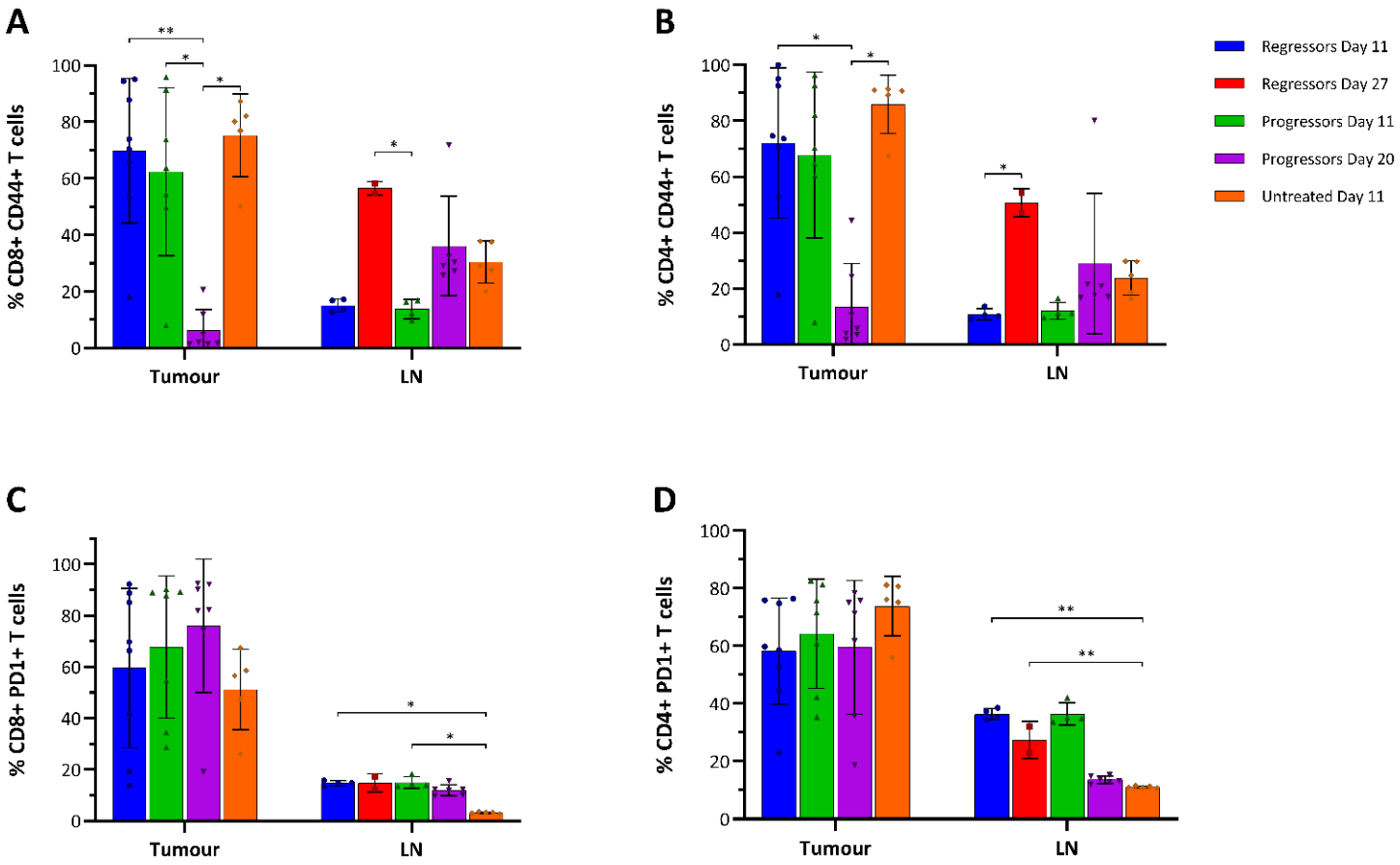

Figure 5.3 Antigen experience and activation profiles of CD8+ and CD4+ T cells in CT26-challenged mice. Frequencies of antigen-experienced (defined as CD44+) CD8+ (**A**) and CD4+ (**B**) T cells, as well as activated (defined as PD-1+) CD8+ (**C**) and CD4+ (**D**) T cells were determined in tumours and tdLNs from Treg-depleted and untreated mice at different time points. Mean ± standard deviation; Kruskal-Wallis test; * $p < 0.05$, ** $p < 0.005$.

To further evaluate the memory subtypes of T cells, levels of CD8+ and CD4+ antigen-experienced (CD44+) T_{CM} (CD62L^{high} CCR7^{high}) and T_{EM} (CD62L- CCR7-) cells were measured in these mice (**Figure 5.2**). Remarkably, both CD4+ and CD8+ T_{EM} represented the dominant phenotype in tumours across all groups (**Figure 5.4**). Furthermore, T_{CM} cells were mostly detected in CD8+ TILs from Treg-depleted mice at day 11, as these cells are virtually absent in untreated mice at the same time point. Moreover, as tumour progresses, the proportion of CD8+ T_{CM} cells in these mice also decreases, reaching levels similar to the ones observed in untreated mice at day 11 (**Figure 5.4** A). A different pattern emerges regarding CD4+ T cells, as the majority of tumour-infiltrating CD4+ CD44+ T cells are represented by the T_{EM} subset in all groups being the highest frequency of this cell population observed in untreated mice (**Figure 5.4** C). In tdLNs, a more homogeneous pattern of CD8+ and CD4+ memory subsets is observed, represented by high T_{EM} and low T_{CM} frequencies in all groups except in regressors at day 27, as less than 20% of the CD8+ and CD4+ CD44+ T cells were categorised into these two subgroups (**Figure 5.4** B and D). These results suggest that Treg depletion favours the development of CD8+ T_{CM} in the TME, and that a decline in these cells could be an indication of immune failure in mice with progressive tumours.

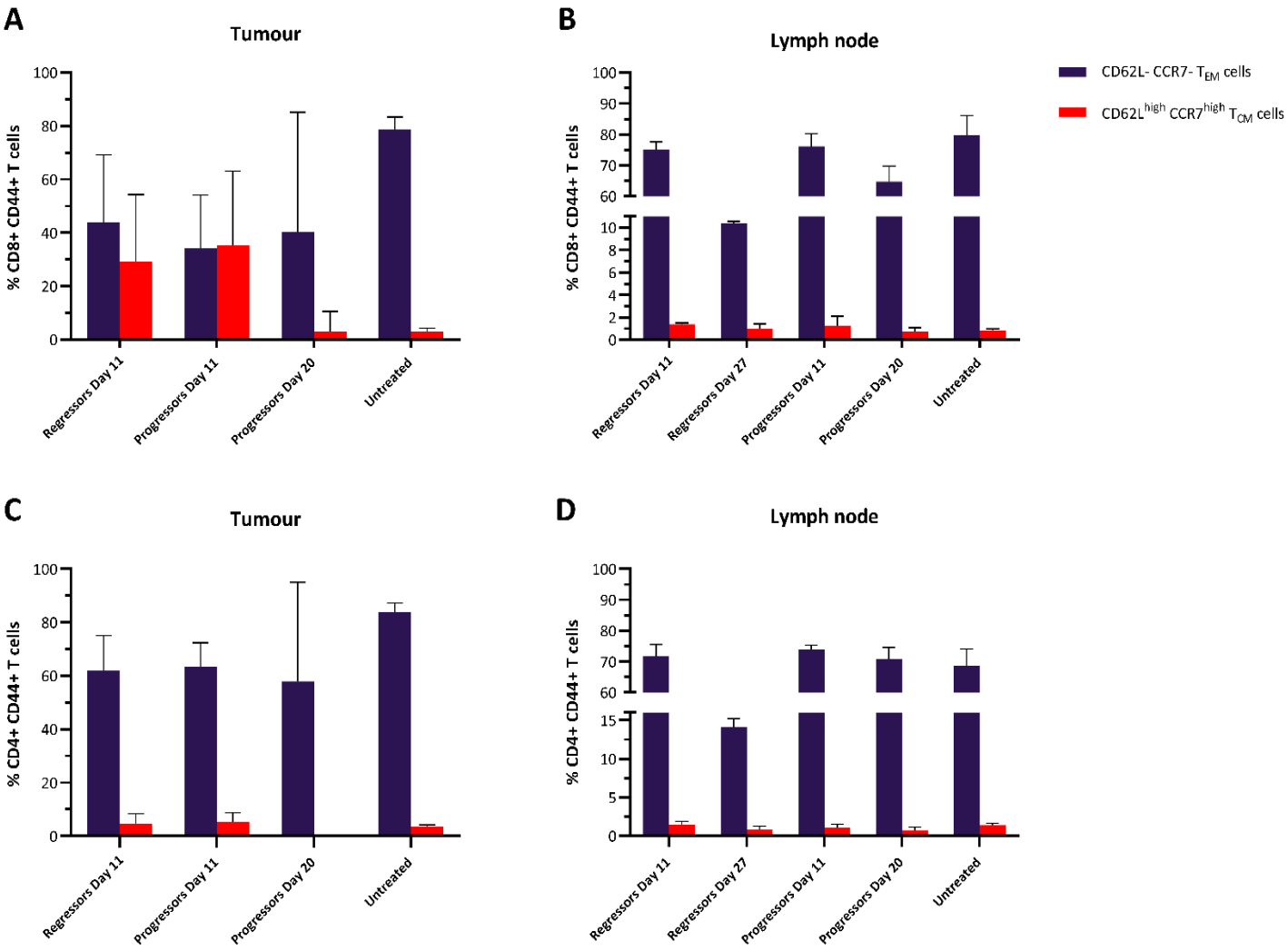

Figure 5.4 Memory subsets of CD8+ CD44+ and CD4+ CD44+ T cells in CT26-challenged mice. The frequency of T_{CM} (grey bars) and T_{EM} (gold bars) was detected from the total CD44+ population based on the levels of expression of CD62L and CCR7 in CD8+ T and CD4+ T cells from tumours (**A** and **C**, respectively), and CD8+ and CD4+ T cells from tdLNs (**B** and **D**, respectively). Mean ± standard deviation.

In order to study T cell activation and exhaustion phenotypes in these cells, levels of PD-1, TIM-3 and LAG-3 were measured in CD8+ and CD4+ T cells in Treg-depleted and untreated mice (**Figure 5.5**). Although PD-1 expression has been considered as a hallmark of T cell exhaustion (Wherry 2011), activated T cells can also express PD-1 at low levels, which gradually increases as T cells become exhausted (Thommen, Koelzer et al. 2018). Thus, the first approach for differentiating activated from exhausted T cells was the evaluation of PD-1^{high}, PD-1^{mid}, and PD-1^{low} populations in CD8+ and CD4+ T cells. Remarkably, more than 80% of the CD8+ TIL populations from all mice at all studied time points were comprised of PD-1^{mid} and PD-1^{high} cells (**Figure 5.6** A), in contrast with CD4+ TILs, where lower frequencies of PD-1^{high} and higher frequencies of PD-1^{low} T cells were observed (**Figure 5.6** C).

These observations were not replicated in tdLNs, where the majority of CD8+ and CD4+ T cells expressed low levels of PD-1, whereas PD-1^{high} cells were significantly underrepresented (**Figure 5.6** B and D), thus suggesting that the exhaustion phenotype is preferentially imprinted on CD8+ in the TME. Moreover, although the frequencies of CD8+ PD-1^{high} T cells in Treg-depleted compared to untreated mice are not statistically significant, the differential frequencies of this cell population observed between these animals suggest that in the presence of Tregs, CD8+ T cells are subject to immunoregulatory signals restricting the activation/exhaustion fate of these cells.

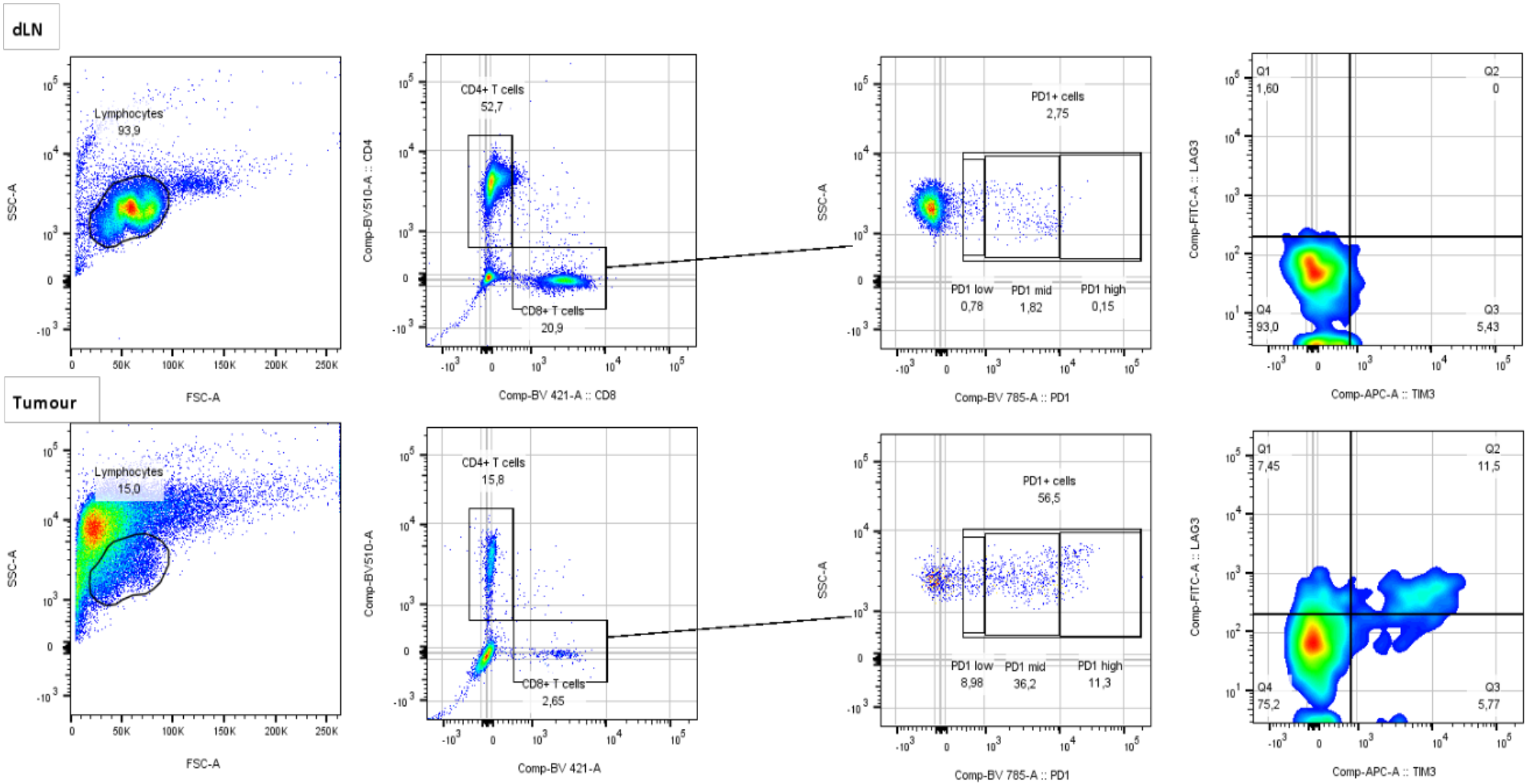
dLN
Lymphocytes
93,9
SSC-A
FSC-A
CD4+ T cells
52,7
CD8+ T cells
20,9
Comp-BV510-A :: CD4
Comp-BV 421-A :: CD8
PD1+ cells
2,75
PD1 low
0,78
PD1 mid
1,82
PD1 high
0,15
Comp-BV 785-A :: PD1
Q1
1,60
Q2
0
Q4
93,0
Q3
5,43
Comp-FITC-A :: LAG3
Comp-APC-A :: TIM3
Tumour
Lymphocytes
15,0
CD4+ T cells
15,8
CD8+ T cells
2,65
Comp-BV510-A
Comp-BV 421-A
PD1+ cells
56,5
PD1 low
8,98
PD1 mid
36,2
PD1 high
11,3
Q1
7,45
Q2
11,5
Q4
75,2
Q3
5,77

Figure 5.5 Methodological approach for the detection of activated and exhausted T cells. Representative FACS plots from tdLNs (top) and tumours (bottom) depicting the gating strategy adopted for the detection of PD-1+ cells from the total CD8+ and CD4+ T cell populations. From the PD-1+ pool, cells were categorised as PD-1^{low}, PD-1^{mid}, and PD-1^{high}, based on the intensity of the PD-1 staining. PD-1+ T cells were also evaluated for the co-expression of LAG-3 and TIM-3.

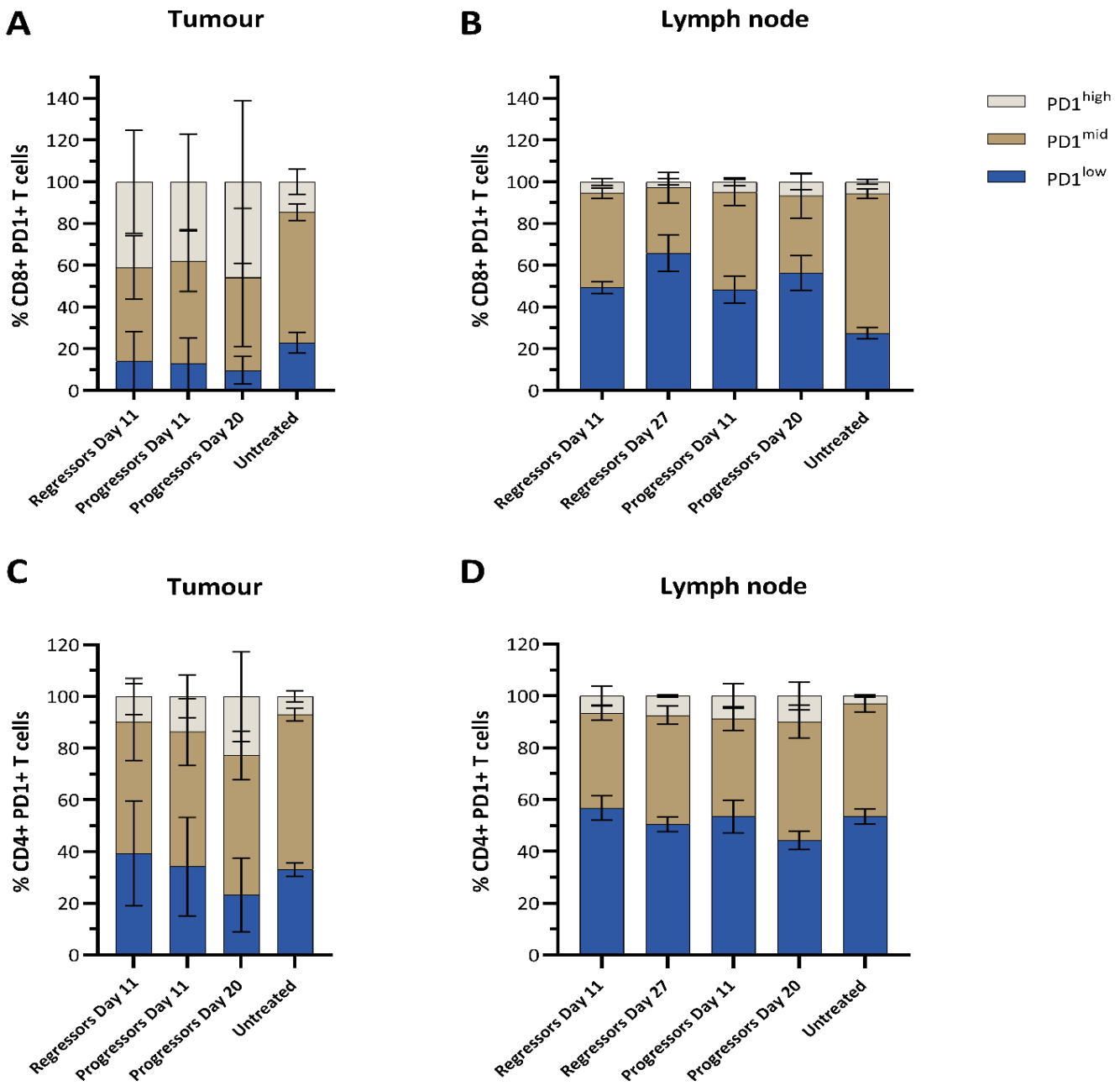

Figure 5.6 Activation/Exhaustion phenotype of T cells based on levels of expression of PD-1. Activated and exhausted T cells were differentiated based on cell-surface levels of PD-1 expression as PD-1^{low} (blue bars), PD-1^{mid} (gold bars), and PD-1^{high} (grey bars) on CD8+ T and CD4+ T cells from tumours (**A** and **C**, respectively), and CD8+ and CD4+ T cells from tdLNs (**B** and **D**, respectively). Mean ± standard deviation.

Considering that PD-1 expression does not entirely discriminate between activated and exhausted T cells, and that the development of fully-exhausted T cells in the TME is a progressive phenomenon that can develop early in tumorigenesis (Schietinger, Philip et al. 2016), a more detailed investigation into different exhaustion phenotypes was performed in CD8+ and CD4+ T cell from CT26-challenged mice. For these analysis, different combinations of TIM-3 and LAG-3 expression within the PD-1+ populations were evaluated, considering that PD-1+ TIM-3+ LAG-3- and PD-1+ TIM-3- LAG-3+ cells have been described as a "rescuable phenotype" that can be reversed into effector cells upon checkpoint blockade, whereas PD-1+ TIM-3+ LAG-3+ are considered terminally exhausted, thus incapable of exert cytotoxic functions on cancer cells with such therapies (McLane, Abdel-Hakeem et al. 2019). Based on these classifications, Treg-depleted animals at day 11 showed low levels of terminally exhausted CD4+ TILs, with levels marginally higher in CD8+ TILs. Indeed, half of the CD8+ TIL populations from Treg-depleted mice were comprised of PD-1+ cells co-expressing at least one additional marker (TIM-3 or LAG-3), while only 26.6% of CD4+ TILs showed these patterns (**Figure 5.7** A and C). Interestingly, and following the observations from **Figure 5.6**, untreated mice showed low levels of CD8+ TILs expressing either TIM-3, LAG-3, or a combination of both within the PD-1+ compartment (20.36% on average, **Figure 5.7** A), further indicating that the absence of Tregs in the TME promotes the development of partially exhausted T cells. On the other hand, CD8+ and CD4+ T cells from tdLNs displayed low levels of exhausted cells, as most of the PD-1+ T cells from all the study groups did not express either TIM-3 or LAG-3 (**Figure 5.7** B and D). TIM-3/LAG-3 double-positive T cells were mostly enriched in the PD-1^{high} compartment, followed by PD-1^{mid} cells, and lastly PD-1^{low} cells, which showed the lowest frequency of TIM-3+ LAG-3+ cells, further strengthening the notion that PD-1^{low} cells represent activated T cells rather than exhausted cells (**Figure 5.8**).

Overall, this initial approximation about the T cell immune compartment in CT26 tumours indicates that although tumour-infiltrating CD4+ T cells are almost double in frequency CD8+ T cells in frequency, the latter cell population exhibit higher expression of phenotypic traits associated with tumour immune recognition. Moreover, the contrasting results observed between tdLNs and tumours highlight the biological importance of the TME in imprinting specific activation/exhaustion phenotypes of TILs.

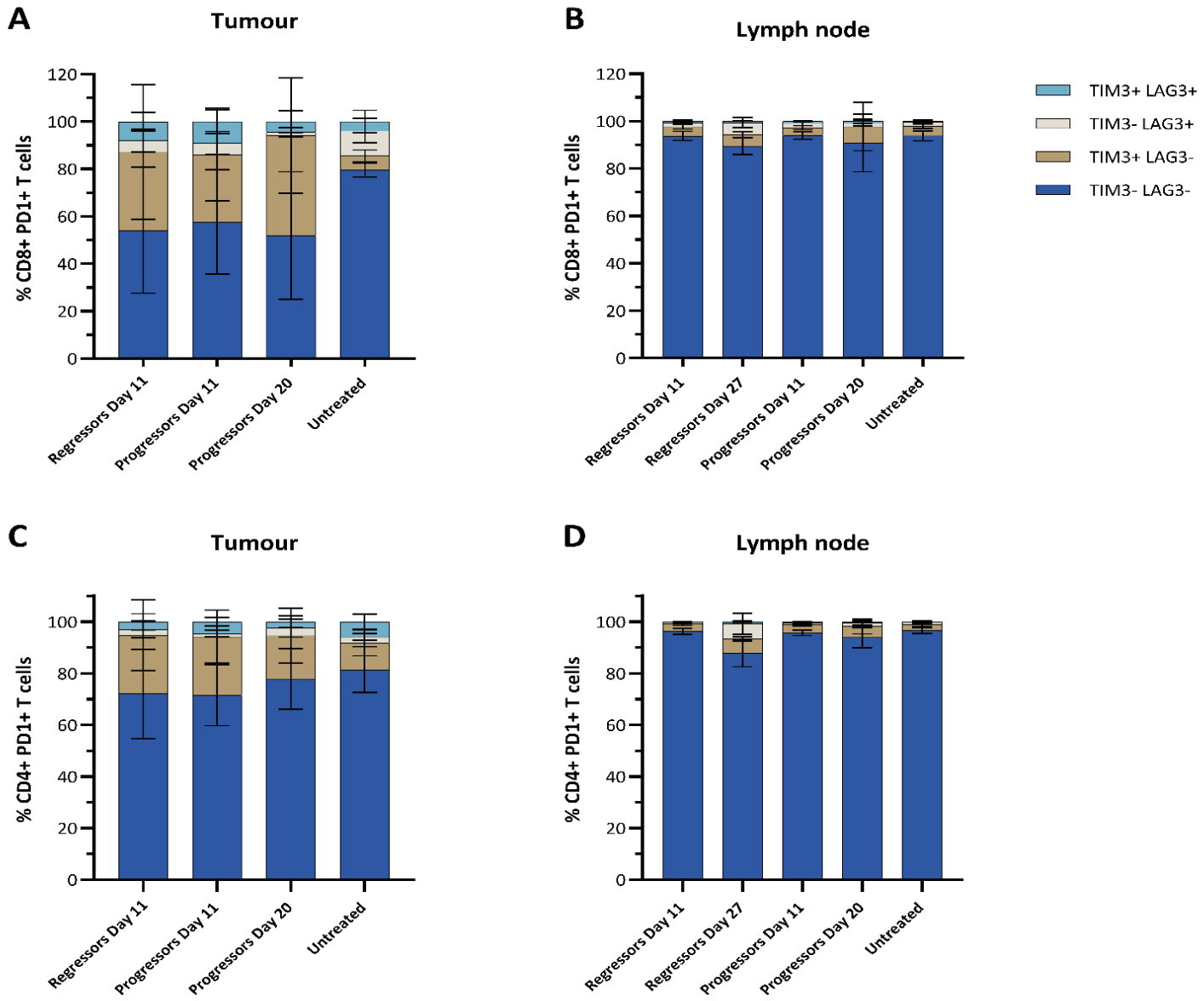

Figure 5.7 **Rescuable and Terminally-exhausted phenotypes in PD-1+ T cells.** The frequencies of "rescuable" T cells (TIM-3+ LAG-3-, gold bars; TIM-3- LAG-3+, grey bars) and terminally-exhausted T cells (TIM-3+ LAG-3+, light blue bars) were evaluated from the total PD-1+ populations in CD8+ T and CD4+ T cells from tumours (**A** and **C**, respectively), and CD8+ and CD4+ T cells from tdLNs (**B** and **D**, respectively). Mean ± standard deviation.

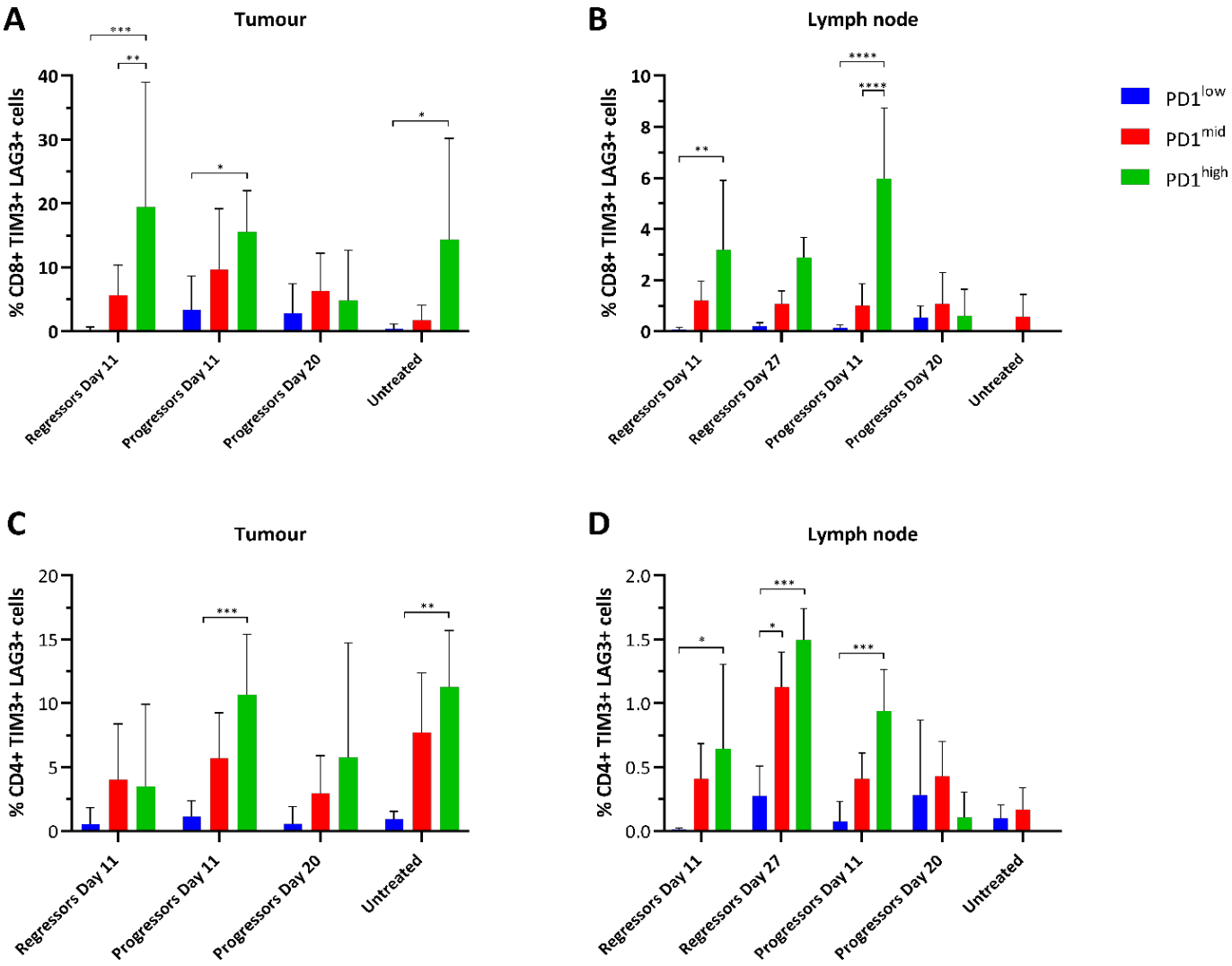

Figure 5.8 **High levels of PD-1 expression are associated with co-expression of TIM-3 and LAG-3.** TIM-3-LAG-3 double-positive cells were measured within the in PD-1^{low} (blue bars), PD-1^{mid} (red bards), and PD-1^{high} (green bars) in CD8+ T and CD4+ T cells from tumours (**A** and **C**, respectively), and CD8+ and CD4+ T cells from tdLNs (**B** and **D**, respectively). Mean and standard deviation; 2-way ANOVA; * $p < 0.05$, ** $p < 0.005$, *** $p < 0.0005$, **** $p < 0.0001$.

5.2.2 Phenotypic traits of CT26-specific CD8+ T cells

In order to explore the frequency and phenotypes of antigen-specific CD8+ T cells in CT26-challenged mice, tumours and tdLNs samples were stained with an *in house* GSW11 tetramer, a commercial AH1 pentamer, and two commercial dextramers against Kd34 and Kd37 (**Figure 5.9**). Following tetramer/pentamer/dextramer staining, all samples were stained with the same monoclonal antibodies used in the previous figures. First, the frequency of antigen-specific CD8+ T cells against these four peptides was determined in the five tested groups. As expected, GSW11-specific cells were the dominant population of CD8+ T cells in both TILs and tdLNs in all groups, representing on average 39.1% and 56.7% of the total CD8+ TILs at day 11 in regressors and progressors, respectively (**Figure 5.10** A and C). Kd34-specific CD8+ TILs represented the second most frequent population, being these cells preferentially enriched in Treg-depleted mice at day 11 (**Figure 5.10** A). AH1-specific CD8+ T cells were observed at small frequencies in both organs in all groups, whereas Kd37-specific CD8+ T cells were only observed in Treg-depleted mice at day 11 followed by a marked decrease in the frequencies of these cells at later time points (**Figure 5.10** C).

Although Kd37-specific CD8+ T cells were the least frequent population in tumours at all time points, these cells represented the second-most abundant cells in tdLNs from Treg-depleted and untreated mice at day 11 (**Figure 5.10** B), suggesting that Kd37-specific CD8+ T cells could be preferentially excluded from the tumour bed in CT26-challenged mice, or suffering a higher degree of cell death upon entering the tumour bed. Lastly, when compiling the average frequencies of antigen-specific CD8+ TILs across groups, Treg-depleted progressors at day 11 showed a higher frequency of antigen-specific CD8+ TILs than regressors at day 11, as 23.4% of the total CD8+ TIL population was not categorised by any of the tetramer/pentamer/dextramer used in regressors, compared to only 5.47% in progressors (**Figure 5.10** C). Overall, these initial observations indicate that GSW11 induces the immunodominant CD8+ T cell responses in CT26-challenged mice, but that the abundance of these cells does not discriminate regressors and progressors in Treg-depleted mice.

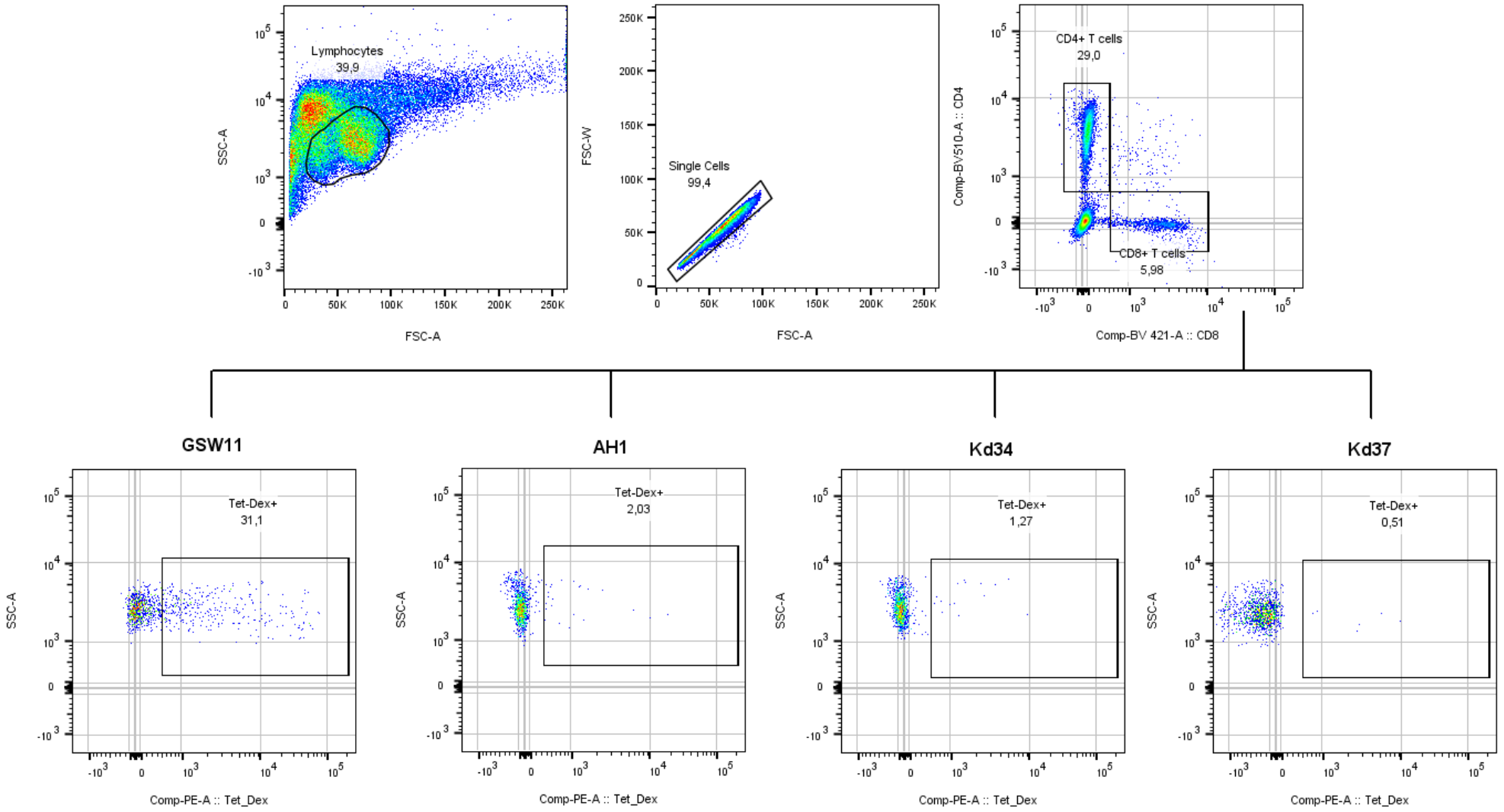
Lymphocytes
39,9
SSC-A
FSC-A
Single Cells
99,4
FSC-W
FSC-A
CD4+ T cells
29,0
CD8+ T cells
5,98
Comp-BV510-A :: CD4
Comp-BV 421-A :: CD8
GSW11
Tet-Dex+
31,1
AH1
Tet-Dex+
2,03
Kd34
Tet-Dex+
1,27
Kd37
Tet-Dex+
0,51
SSC-A
Comp-PE-A :: Tet_Dex

Figure 5.9 Gating strategy for the evaluation of antigen-specific CD8+ T cells in CT26-challenged mice. Representative FACS plot from a tumour sample, depicting the gating strategy for the detection of GSW11-, AH1-, Kd34-, and Kd37-specific CD8+ T cells.

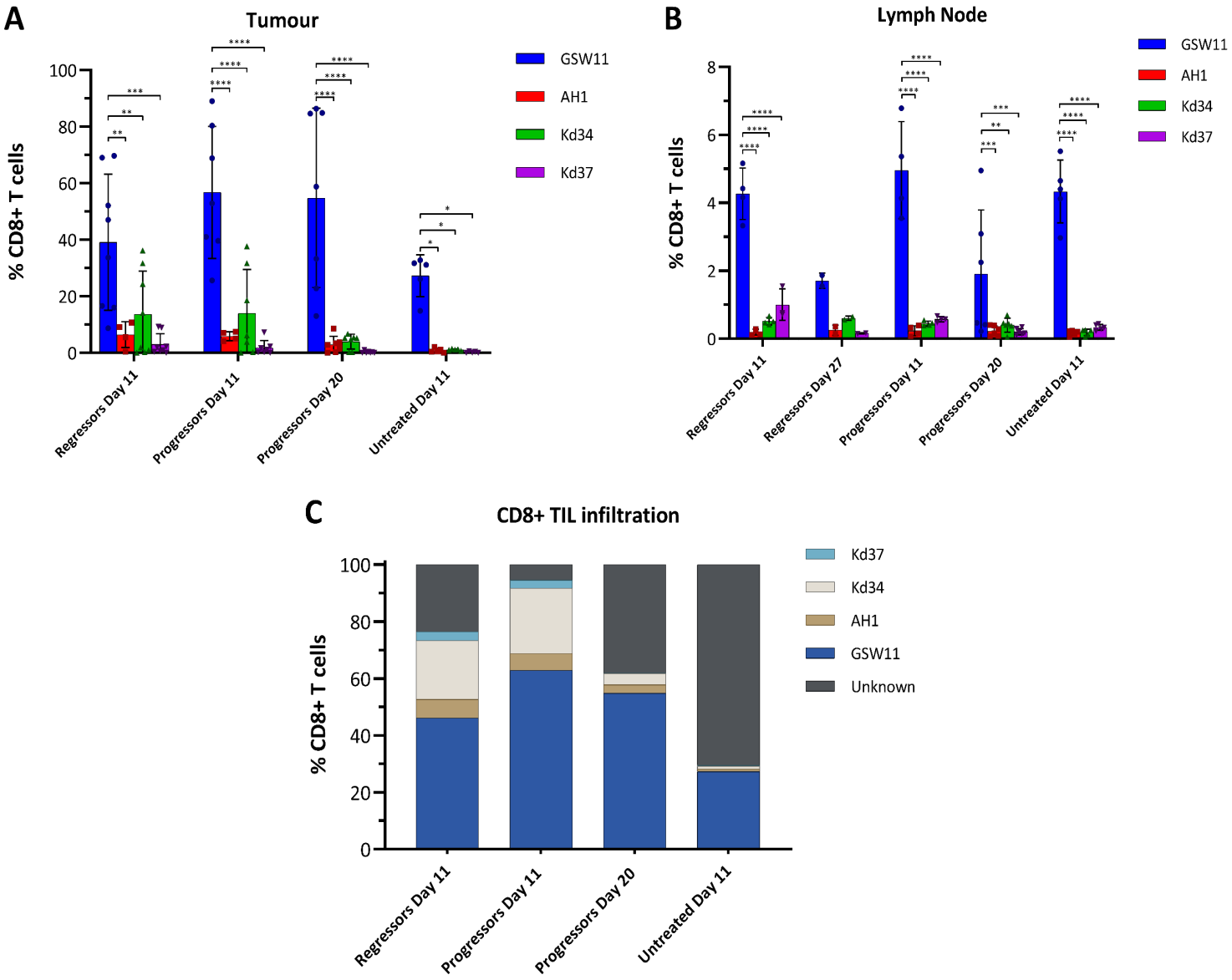

Figure 5.10 GSW11 represents the immunodominant CD8+ T cell epitope in CT26-challenged mice.A and B. Frequency of antigen-specific CD8+ T cells from tumours (**A**) and tdLNs (**B**) of Treg-depleted and untreated mice. Mean ± standard deviation; 2-way ANOVA; * $p < 0.05$, ** $p < 0.005$, *** $p < 0.0005$, **** $p < 0.0001$. **C.** Average frequencies of antigen-specific CD8+ TILs in CT26 tumours from Treg-depleted and untreated mice.

Next, the frequency of antigen-experienced and memory subtypes was determined in CT26-specific cells. As seen in **Figure 5.11**, although no significant differences were detected among epitopes, all antigen-specific CD8+ TILs showed a high expression of CD44 in all groups, except for progressors at day 20, where a drastic decrease in the frequencies of these cells was observed (**Figure 5.11** A). In contrast, in tdLNs from Treg-depleted mice at day 11, AH1-specific CD8+ T cells displayed the highest expression of CD44 among the four epitopes, while GSW11-specific CD8+ T cells showed the lowest frequencies of this cell population in the same group of mice (**Figure 5.11** B). Remarkably, these findings were not replicated in untreated mice at the same time point, as CD8+ T cells against any of the peptides displayed similar levels of CD44 expression (**Figure 5.11** B). Regarding T_{CM} and T_{EM} levels, tumours from Treg-depleted mice at day 11 exhibited a higher infiltration of antigen-specific T_{CM} cells, while these cells were observed at low frequencies in untreated mice for GSW11- and Kd34-specific CD8+ TILs (**Figure 5.12** A). Remarkably, only GSW11-specific CD8+ TILs showed a higher proportion of T_{EM} compared T_{CM} in regressors (**Figure 5.12** A), which suggests that this effector phenotype could be associated with the immune control of the tumour observed in these mice. A more homogeneous pattern was observed in tdLNs, as surprisingly T_{EM} accounted for the majority of antigen-specific CD8+ CD44+ T cells, with the exception of Kd37-specific CD8+ T cells, where T_{CM} predominated in regressors at days 11 and 27, and in progressors at day 11 (**Figure 5.12** B). These results further suggest that Treg-depletion favours the infiltration and/or development of antigen-specific CD8+ T_{CM} cells, but that the development of these two memory subtypes follows different paths depending on the antigen specificity of CD8+ TILs.

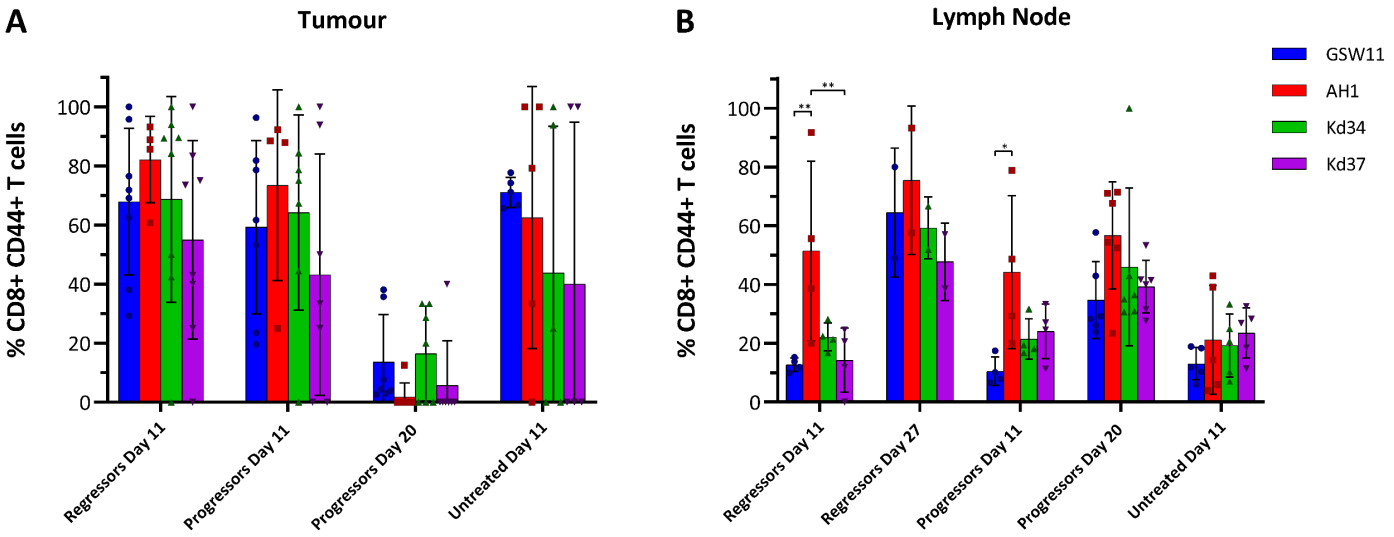

Figure 5.11 Antigen experience among CT26-specific CD8+ T cells. Levels of CD8+ CD44+ T cells were determined in tumours (**A**) and tdLNs (**B**) from Treg-depleted or untreated CT26-challenged mice at different time points. Mean ± standard deviation; 2-way ANOVA; * $p < 0.05$, ** $p < 0.005$.

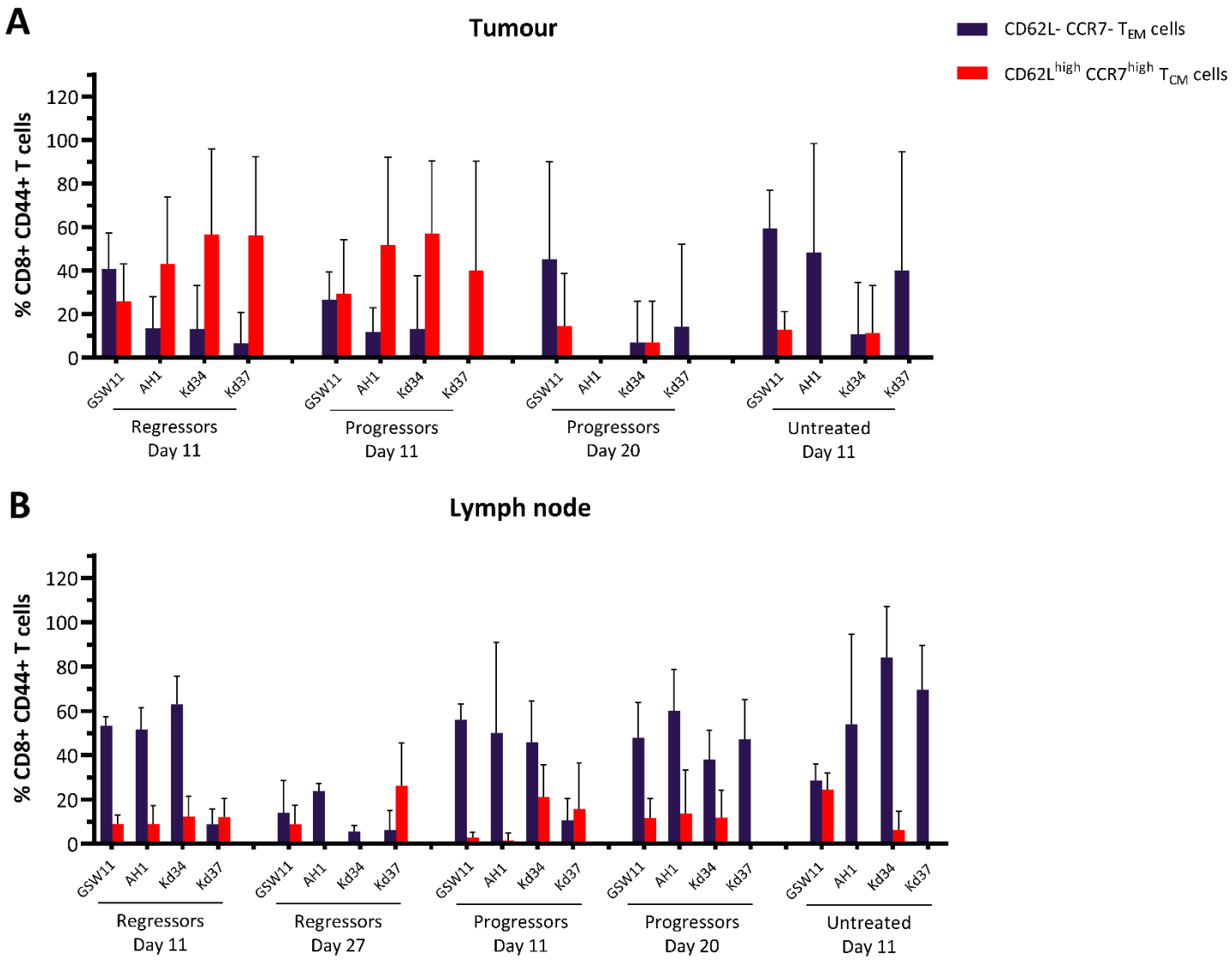

Figure 5.12 CD8+ T_{CM} cells are enriched in Treg-depleted mice at day 11. Frequencies of T_{EM} (black bars) and T_{CM} (red bars) were determined from the antigen-specific CD8+ CD44+ T cell pool in tumours (**A**) and tdLNs (**B**). Mean ± standard deviation.

Lastly, the levels of activation/exhaustion were determined in these antigen-specific cells. The proportion of cells expressing PD-1 was consistently high across the four antigen-specific CD8+ T cell populations in tumours from Treg-depleted mice, with the exception of progressors at day 20, where Kd37-specific CD8+ TILs showed significantly lower frequencies of PD-1+ cells compared to GSW11-, AH1-, and Kd34-specific cells. This low frequency of Kd37-specific PD-1+ cells was also evidenced in untreated mice, where these levels were significantly lower to the frequency of Kd37-spefic PD-1+ cells in Treg-depleted mice at day 11 (**Figure 5.13** A). Tumour-draining lymph nodes from Treg-depleted mice at day 11 also showed high frequencies of CD8+ PD-1+ T cells across the four epitopes, being the highest values observed in AH1- and Kd37-specific CD8+ T cells (**Figure 5.13** B). Although previous analysis revealed that the bulk CD8+ PD-1+ T cell population from tdLNs in untreated mice at day 11 were significantly lower compared to Treg-depleted mice (**Figure 5.3** C), this behaviour was only replicated in AH1- and Kd37-specific CD8+ T cells, as GSW11- and Kd34-specific CD8+ T cells showed similar levels of PD-1 expression to Treg-depleted mice (**Figure 5.13** B). In terms of the different subpopulations of PD-1+ cells, antigen-specific CD8+ T cells showed similar results compared to previous observations obtained in bulk CD8+ T cells, where a high frequency of PD-1^{high} and PD-1^{mid} CD8+ TILs was observed in Treg-depleted mice, while untreated mice displayed low frequencies of PD-1^{high} CD8+ T cells. Moreover, despite the significant decrease of antigen-specific CD8+ T cells in progressors at day 20, the remaining CD8+ TILs were mostly categorised as PD-1^{high} and PD-1^{mid} (**Figure 5.14** A). Despite the congruency between bulk and antigen-specific CD8+ T cell data of PD-1 expression in tumours, a slight discrepancy was evidenced in tdLNs, where the majority of antigen-specific CD8+ T cells were PD-1^{mid}. Only in tdLNs from progressors at day 20, AH1-specific CD8+ T cells showed a higher frequency of PD-1^{high} than PD-1^{mid} (**Figure 5.14** B). Interestingly, Kd37-specific PD-1+ CD8+ TILs showed a high expression of the inhibitory receptors TIM-3 and LAG-3, as less than 10% of these cells did not express any of these markers in Treg-depleted mice, while none of the PD-1+ CD8+ TILs specific against this peptide expressed TIM-3 or LAG-3 in untreated mice (**Figure 5.15** A). These results were also observed in tdLNs, as 97.9% and 86.6% of Kd37-specific PD-1+ CD8+ T cells expressed TIM-3 or LAG-3 (**Figure 5.15** B). Regarding the other antigen-specific CD8+ TILs, the results obtained in tumours partially matched the observations from the bulk analysis of CD8+ T cells, where a higher proportion of PD-1+ CD8+ TILs expressing TIM-3 and/or LAG-3 was evidenced in Treg-depleted mice compared to untreated mice (**Figure 5.15** A). Nonetheless, the overall panorama in tdLNs was sharply different between bulk and antigen-specific CD8+ T cells. Similar to bulk CD8+ T cells analysis, GSW11-specific (and to a lesser extent Kd34-specific) CD8+ T cells in tdLNs displayed low levels of TIM-3 or LAG-3 expression. In contrast, and similar to Kd37-specific CD8+ T cells, AH1-specific CD8+ T cells from Treg-depleted mice showed high levels of TIM-3 and LAG-3 (**Figure 5.15** B). These results suggest that not all CT26-specific T cells follow the

same pathways for the development of exhaustion, where GSW11- and Kd34-specific CD8+ T cells are primed in tdLNs into a mostly activated phenotype which transitions to exhaustion in the TME, whereas AH1- and Kd37-specific CD8+ T cells might enter the TME with a preestablished exhaustion phenotype.

Then, we evaluated if co-expression of TIM-3 and LAG-3 in the different PD-1+ subpopulations from antigen-specific CD8+ T cells mimicked the findings obtained from the bulk analysis. As observed in bulk CD8+ T cell populations, antigen-specific CD8+ PD-1^{high} TILs from Treg-depleted and untreated mice at day 11 showed the highest frequency of TIM-3/LAG-3 double-positive cells, followed by CD8+ PD-1^{mid} TILs (**Figure 5.16** A). Interestingly, in animals reaching tumour endpoint, only PD-1^{mid} and PD-1^{low} CD8+ TILS co-expressed TIM-3 and LAG-3, suggesting that the pool of PD-1^{high} TIM-3+ LAG-3+ cells could have been deleted in these mice as tumour progressed (**Figure 5.16** A). Analysis from tdLNs showed more discordant results when compared to bulk CD8+ T cells, as only GSW11-specific CD8+ T cells from regressors and progressors at day 11, and AH1-specific CD8+ T cells from regressors at day 11 showed high levels of TIM-3/LAG-3 co-expression within the PD-1^{high} population (**Figure 5.16** B). Remarkably, for AH1-specific CD8+ T cells, the TIM-3/LAG-3 expression pattern was reversed in progressors at day 11, where most cells expressing these two markers were PD-1^{low}, followed by PD-1^{mid}. This was also the case for GSW11-specific CD8+ T cells from progressors at day 20, and for AH1-specific CD8+ T cells from progressors at day 20 and untreated mice at day 11 (**Figure 5.16** B).

Altogether, these results suggest that although the TME can exert strong immunoregulatory signals that affect CD8+ T cell activation and effector function, the process of exhaustion/dysfunction follows an antigen-specific pattern where CD8+ T cell populations enter differential exhaustion pathways based on their epitope restriction.

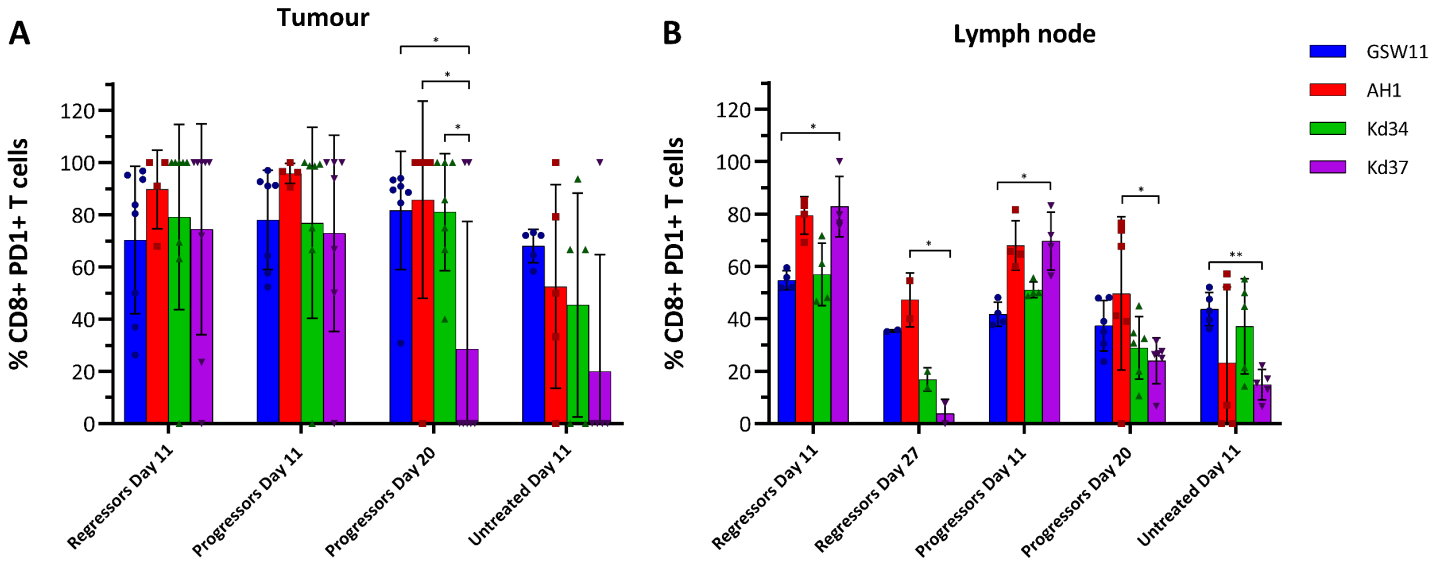

Figure 5.13 Treg-depleted mice exhibit high levels of PD-1 expression in antigen-specific cells. Frequencies of antigen-specific CD8+ PD-1+ T cells were determined in tumours (**A**) and tdLNs (**B**) from Treg depleted and untreated mice at different time points. Mean ± standard; 2-way ANOVA; * $p < 0.05$, ** $p < 0.005$.

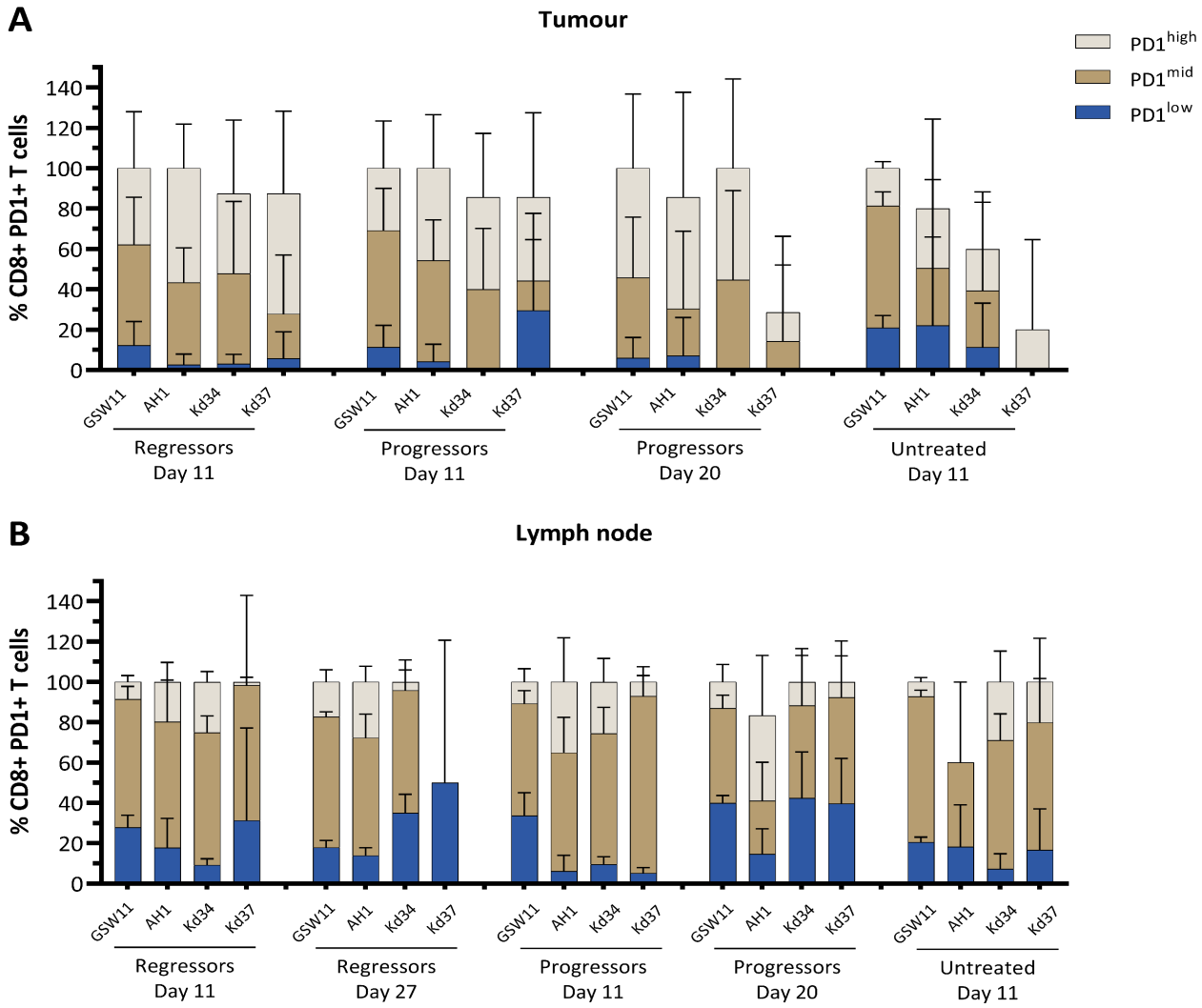

Figure 5.14 PD-1 levels of expression in antigen-specific CD8+ T cells. CD8+ T cells were categorised based on their cell-surface levels of PD-1 expression as PD-1^{low} (blue bars), PD-1^{mid} (gold bars), and PD-1^{high} (grey bars) on CD8+ T from tumours (**A**) and tdLNs (**B**). Mean and standard deviation.

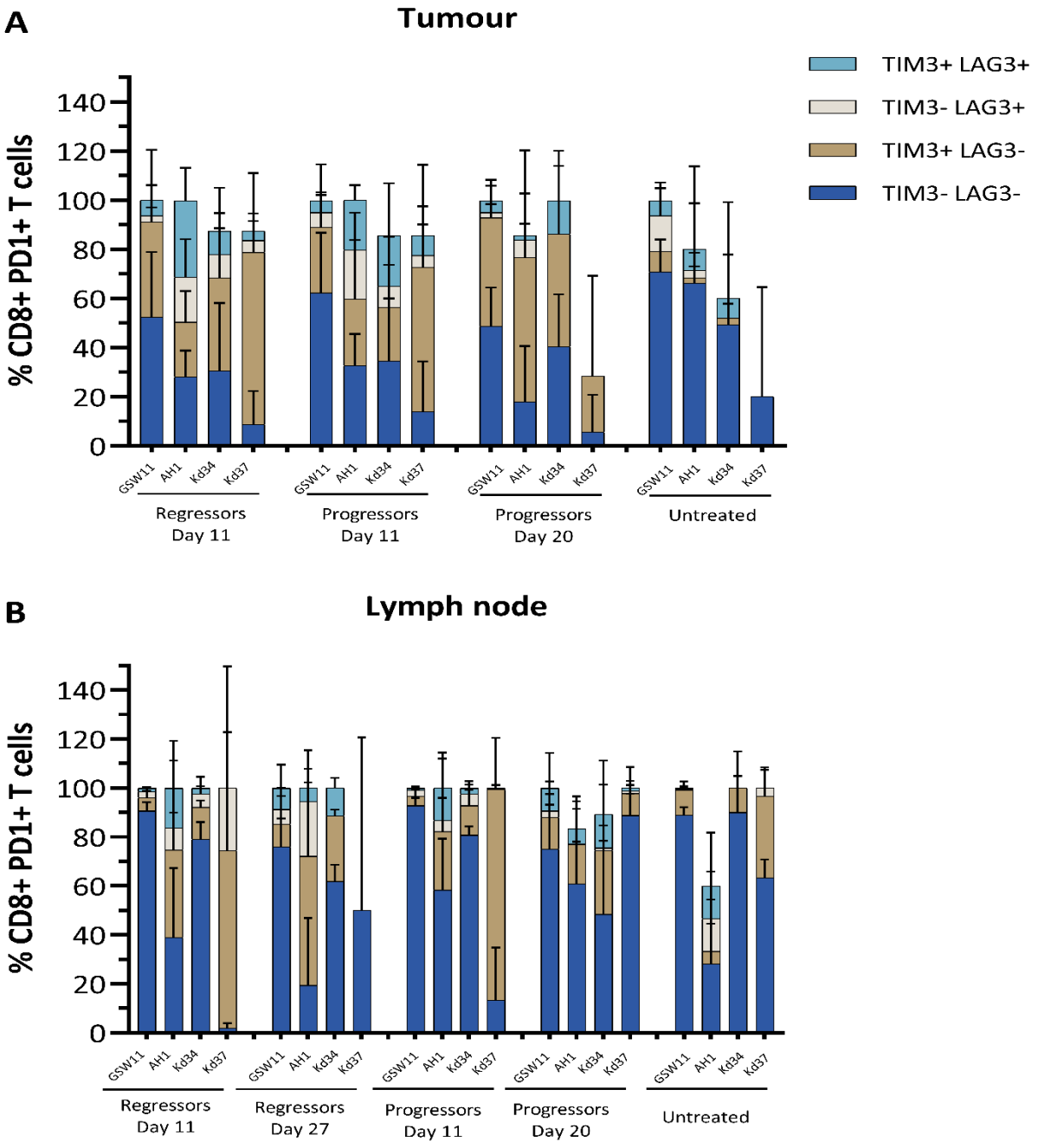

Figure 5.15 The expression of inhibitory receptors in PD-1+ CD8+ T cells is preferentially confined to the tumour. The frequencies of "rescuable" T cells (TIM-3+ LAG-3-, gold bars; TIM-3- LAG-3+, grey bars) and terminally-exhausted T cells (TIM-3+ LAG-3+, light blue bars) were evaluated from the total PD-1+ populations in antigen-specific CD8+ T cells from tumours (**A**) and tdLNs (**B**). Mean ± standard deviation.

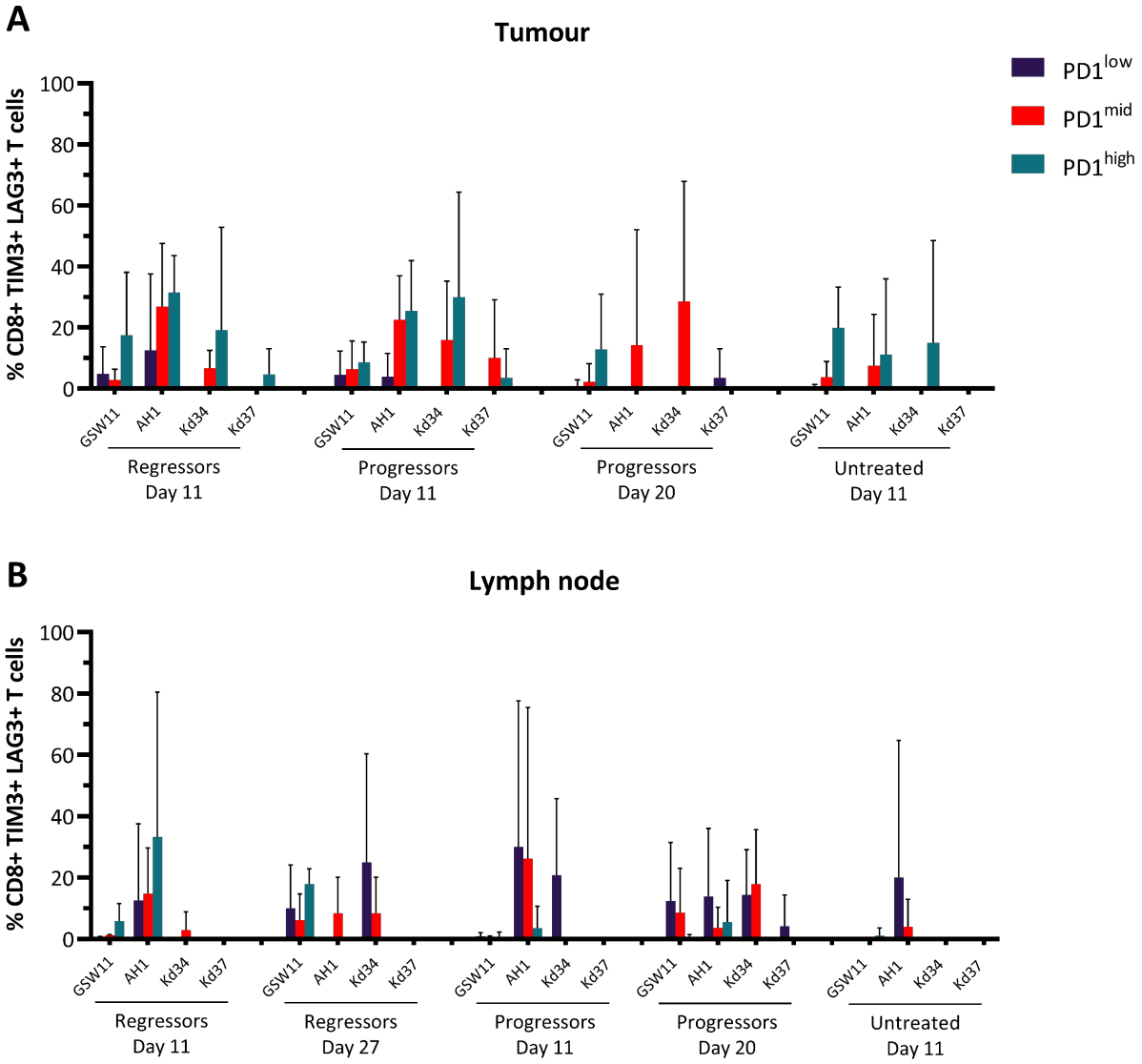

Figure 5.16 Terminally-exhausted antigen-specific CD8+ TILs are enriched in the PD-1^{high} compartment. Levels of TIM-3/LAG-3 co-expression were determined in PD-1^{low} (black bars), PD-1^{mid} (red bars), and PD-1^{high} (dark green bars) CD8+ T cells from tumours (**A**) and tdLNs (**B**). Mean and standard deviation.

5.3 Concluding remarks

The analysis of antigen-specific CD8+ TILs in CT26-challenged mice allowed us to verify that the PFR-ranked Kd34 and Kd37 peptides are true novel CD8+ T cell specificities in this tumour model. Although these four peptides derive from the same retroviral protein, GSW11 represents the immunodominant response in CT26 tumours, considering the high frequencies of GSW11-specific CD8+ TILs, as well as the consistent IFNγ production by CD8+ T cell splenocytes stimulated with this peptide in Treg depleted mice showing tumour regression, while AH1, Kd34, and Kd37 are most likely subdominant responses that get boosted upon Treg depletion. Interestingly, these four populations of CT26-specific CD8+ TILs share similar phenotypic traits, with these cells showing relatively similar frequencies of antigen-experienced, memory phenotypes, and activation/exhaustion profiles within groups, indicating that although GSW11-specific CD8+ T cells are the most prevalent cell population, all of these cells are potentially imprinted with the same effector functions in the TME. Nonetheless, further studies are required in order to better characterise phenotypic traits of these antigen-specific cells, as well as their relevance in the elimination of CT26 tumours in therapeutic settings.

Chapter 6 General discussion

Cancer immunotherapy has represented a significant breakthrough in the treatment of several types of cancer, with long and durable clinical responses observed in a substantial proportion of treated patients, depending on the cancer type, and chosen immunotherapeutic regime (Waldman, Fritz et al. 2020). Despite these encouraging outcomes, more research is needed in order to improve the success of these therapies. One of the most critical components that could potentially benefit current and novel immunotherapy advances relies in the identification of cancer-derived epitopes recognised by CD8+ T cells in tumours, as these cells are considered the primary effectors in the anti-tumour immune response (Gonzales Carazas, Pinto et al. 2021); however, the identification of such epitopes for clinical settings is a complex endeavour, as the characteristics that better define peptide immunogenicity are still not well understood (Dersh, Holly et al. 2021). Thus, using immuno-transcriptomic data from the widely tested CT26 pre-clinical tumour model, we aimed to identify novel immunogenic CD8+ T cell epitopes in untreated and Treg-depleted mice aided by a peptide filter relation (PFR) algorithm, and comparing it to widely used predictions of MHC-I binding affinities.

The vast majority of studies aimed to discover immunogenic peptides from different diseases (including cancer) have been based on bioinformatic pipelines inferring the affinities between peptides and their respective MHC-I molecule. Several algorithms have been developed for this purpose, which can be roughly classified into: i) methods based on sequence-scoring functions (such as SYFPEITHI (Rammensee, Bachmann et al. 1999) and MixMHCpred 2.0.1 (Gfeller, Guillaume et al. 2018)), ii) methods based on machine-learning algorithms (including NetMHCpan 4.0 (Jurtz, Paul et al. 2017) and MHCflurry 2.0 (O'Donnell, Rubinsteyn et al. 2020)), and iii) methods that integrate different binding predictions (like NetMHCcons 1.1 (Karosiene, Lundegaard et al. 2012) and IEDB analysis resource-consensus (IEDB-AR-Consensus, (Dhanda, Mahajan et al. 2019)). Besides their inherent differences in model construction, not all these algorithms yield results in comparable fashions, as some models like SYFPEITHI predicts a binomial outcome of binder/non-binder, whereas the results obtained by models like NetMHC4.0 can indicate a range of affinities based on IC_{50} and ranking calculations, thus representing a daunting choice for researchers at the point of selecting the most appropriate method for MHC-I binding predictions. Importantly, a recent systematic study aimed at evaluating the performance of different MHC-I binding affinity prediction tools using a curated database of peptides with experimentally detected affinities concluded that the better performances for the prediction of MHC-I affinities were MixMHCpred 2.0.1, NetMHCpan 4.0, and NetMHCcons 1.1, with no discernible differences between these three models (Mei, Li et al. 2020).

Despite the recent improvements of these algorithms, using just the predicted affinity of a peptide for MHC-I molecules is not sufficient to classify a peptide as immunogenic or not, as other factors can also play an influential role into the immunogenicity of a peptide, such as MHC-I binding stability, abundance of the precursor protein, efficient intracellular processing by the APP machinery, and T cell recognition (Calis, Maybeno et al. 2013). The *in vitro* identification and validation of cancer-derived immunogenic peptides for clinical use is expensive and laborious, hence several studies have attempted to develop algorithms able to incorporate many of the aforementioned parameters for the prediction of peptide immunogenicity. POPI and POPISK were the first platforms based on identifying immunogenicity based on physicochemical characteristics of peptides (Tung and Ho 2007, Tung, Ziehm et al. 2011), which remarkably did not include affinity predictions in their algorithms. PAAQD incorporates amino acid pairwise contact potentials and quantum topological molecular similarity, thus considering amino acid contact sites between peptides and MHC molecules and physicochemical properties of adjacent amino acids within peptides (Saethang, Hirose et al. 2013). Regarding cancer neoantigens, Duan *et al.* proposed a differential agretopicity index (DAI), which consists in the subtraction of the NetMHC IC_{50} value from WT peptides to the values of the mutated neoepitopes, in order to reflect how peptide-binding determinants in neoepitopes differ from WT (Duan, Duitama et al. 2014). More recent approaches for prediction of immunogenicity have been constructed based on peptides obtained by LC-MS, with the rationale that these peptides have gone through all antigen-processing steps and are most likely to represent immunogenic peptides (Blass and Ott 2021). Among these, EDGE (Bulik-Sullivan, Busby et al. 2018) and APPM (Hao, Wei et al. 2021) have proven to improve the prediction of immunogenicity when benchmarked against classical MHC-I prediction algorithms, such as MHCflurry and NetMHC4.0. Despite this, LC-MS-derived peptide data can be skewed towards high-affinity peptides, as potentially immunogenic low-affinity peptides could be lost during the washing steps prior to peptide elution (Abella, Antunes et al. 2020). Furthermore, LC-MS has well-known inability to properly detect cysteine-rich peptides (Abelin, Keskin et al. 2017). Indeed, different LC-MS studies performed with CT26 cells have failed to identify GSW11, potentially due to its low binding affinity towards H-2D^{d} and its sequence (GGPESFY**C**ASW) (Laumont, Vincent et al. 2018).

In our study, we used a PFR model that does not predict binding nor immunogenicity *per se*, but rather the abundance of cell-surface p/MHC-I complexes considering the processes leading to the selection of peptides forming such stable complexes (known as peptide optimization), in which the peptide off-rate from MHC-I molecules is influenced by protein abundance, MHC-I binding affinity, and the proofreading activities of tapasin (Dalchau, Phillips et al. 2011). Importantly, this dynamical systems model was benchmarked in an *in vitro* study where peptides with different off-

rates and abundances would compete for MHC-I binding, concluding that low-affinity peptides can outcompete high-affinity ones and be presented at the cell surface if the abundance of the former is significantly higher than the latter (Boulanger, Eccleston et al. 2018), suggesting that a low-affinity peptide could be presented by MHC-I molecules and trigger immune responses if the intracellular abundance of its source protein is high enough. This observation has also been made in LC-MS studies using MHC-I mono-allelic cell lines, where a 10-fold increase in protein expression could approximately compensate for a 90% decrease in binding potential to MHC-I molecules (Abelin, Keskin et al. 2017). This association was observed in our dataset, as gp70-derived peptides occupied the top rank positions based on PFR sorting, even when some peptides showed low predicted affinities for MHC-I binding (Table 3.1). This hypothesis was moderately supported by LC-MS data, where the four matching peptides were ranked higher in PFR than in NetMHC4.0, further suggesting that binding affinity alone is a poor predictor for antigen presentation. A striking observation from NetMHC4.0-ranked peptides was the relative expression of the source proteins from predicted high-affinity peptides, as the majority of them had negligible gene expression in CT26 cells (**Figure 3.1**), which could explain why none of these neoantigens were detected by LC-MS experiments. Regardless of the algorithm used for the filtering strategies, all peptides displayed classical H-2^{d}-binding characteristics. For H-2L^{d}-restricted peptides, the majority of peptides displayed a proline at P2 and a C-terminal hydrophobic motif predominantly represented by leucine, phenylalanine and methionine (**Figure 3.2** B), in accordance with classical H-2L^{d}-restricted 9mers obtained from peptide elution and high performance liquid chromatography (HPLC) analysis of H-2L^{d}-transfected cells (Corr, Boyd et al. 1992). H-2K^{d}-restricted peptides had an overrepresentation of tyrosine at P2 (**Figure 3.2** D), as this amino acid is the main anchoring site for H-2K^{d} binding to the B pocket, as well as a high prevalence of leucine and isoleucine at P9 which is a secondary anchoring site binding the F pocket of H-2K^{d} (Mitaksov and Fremont 2006). Although studies have suggested the presence of a third H-2K^{d} anchoring site at the C pocket by the overrepresentation of serine, valine, and threonine at P5 (Suri, Walters et al. 2006), no such motifs were observed among our peptides. Lastly, H-2D^{d}-presented peptides showed enrichment of amino acids known to participate in the four-motif binding of peptides to this MHC-I molecule (Corr, Boyd et al. 1993): Glycine at P2, Proline at P3, Arginine at P5, Isoleucine at P9 (**Figure 3.2** C).

The biggest discrepancies regarding peptide biochemistry were between predicted MHC-I affinity and BFA decay assays. NetMHC predictions are mostly built upon biological data of p/MHC-I interactions using purified proteins, such as surface plasmon resonance and fluorescence polarisation (Andreatta and Nielsen 2016), thus not accounting for interactions between peptides and MHC-I molecules at the cellular level. In contrast, BFA decay assays using cells lacking a functional APP machinery, such as RMA-S, allow for the measurement of MHC-I downregulation

when pulsed with exogenous peptides, thus representing a more physiological technique to measure p/MHC-I interactions in cells (Saini, Ostermeir et al. 2013, Okiyama, Hasegawa et al. 2015). Modified versions of BFA decay assays have been performed in different cancer studies, leading to the identification of immunogenic peptides derived from breast cancer TAAs (Tang, Zhou et al. 2015, Das, Eisel et al. 2019) and HPV proteins (Ohlschlager, Osen et al. 2003). Although the previously mentioned studies found immunogenic peptides within the pool of high binders, this behaviour is not always replicated, as observed in a study of spontaneous thymoma in p53-KO mice, where peptides from overexpressed antigens with intermediate binding affinities induced the strongest CD8+ T cell responses (Andersen, Ruhwald et al. 2003). Altogether, this evidence indicates that modelling immunogenicity *in silico* from experimental data represents a challenging endeavour. Immunogenicity of a peptide is mainly dependent on the correct antigen presentation of the peptide on tumour cells, as well as on the presence of T cell precursors able to recognise the peptide and trigger an immune response. The former can be modelled through MHC-I binding-affinity predictors and APP predictors, as well as by LC-MS studies, but does not cover the T cell factor. Meanwhile, the latter requires peptide immunisation strategies (such as vaccinations) that oftentimes overlook antigen presentations steps that must occur before the induction of an immunogenic T cell response. Furthermore, immunising with a high-affinity peptide could render this approach useless if that peptide is derived from a low-abundant (or suppressed) protein in the tumour, or if the peptide is not properly presented by the APP machinery.

In order to verify the immunogenicity of PFR- and NetMHC-ranked peptides from our study, we sought to stimulate splenocytes from CT26-challenged mice without any therapeutic intervention, or Treg-depleted. This second approach was used as previous results from our group have revealed that depletion of Tregs prior tumour challenge using the anti-CD25 antibody PC61 leads to tumour elimination and generation of memory CD8+ T cell responses in 73% of treated animals (Golgher, Jones et al. 2002), and is associated with boosted IFNγ responses against AH1 and GSW11 (James, Yeh et al. 2010). Although initial investigations about the mechanism of action of PC61 suggested that this antibody exerted its therapeutic functions by functional inactivation of Tregs via internalisation and/or shedding of CD25, which deprives Tregs from crucial survival signalling mediated by IL-2 (Kohm, McMahon et al. 2006), further studies have confirmed that PC61 induces a depletion of the Treg populations from peripheral blood and secondary lymphoid organs in a mechanism dependent on FcγRIII and antibody-dependent cell phagocytosis (ADCP) mediated by monocytes and macrophages, reaching its peak depletion activities by day 8, and starting to return to basal levels at day 22 (Setiady, Coccia et al. 2010). These observations are consistent with our data, where we observed a sharp and significant reduction in the frequency of

Tregs at day 11 in spleen, mesenteric lymph nodes, and peripheral blood (**Figure 4.8** and **Figure 4.10**). Despite the successful depletion of Tregs by PC61, only 30% of CT26-challenged mice treated with this antibody showed complete regression of tumour growth (**Figure 4.9**). Although these results did not match the rates of tumour regression previously observed in our group, these observations are not entirely surprising considering that PC61 can also bind to CD25 expressed on T_{EFF} and hinder the proliferation of these cells by inhibiting IL-2 signalling (Solomon, Amann et al. 2020). Furthermore, besides binding the activator FcγRIII, PC61 can also interact with the inhibitory FcγRIIb, which can be overexpressed in the myeloid compartment of the TME and prevent Treg depletion in the tumour bed (Arce Vargas, Furness et al. 2017).

In splenocytes and tdLNs from untreated mice at day 11 post tumour challenge, no obvious production of IFNγ or proliferation was observed in CD8+ T cells against any of the tested peptides, regardless of their abundance or MHC-I binding affinities (**Figure 4.4** and **Figure 4.6**). These observations are not surprising considering that tumour-specific CD8+ T cells can enter a state of dysfunctionality as early as 8 days after tumour engraftment (Schietinger, Philip et al. 2016). Nonetheless, and as described in Section 1.2, cancer-specific CD8+ T cells enter a dysfunctional phenotype in a step-wise approach, where they first exhibit an unexpected high rate of proliferation, followed by a fast decrease in this proliferation capacity and a continuous inability to produce effector cytokines like IFNγ and TNFα (Li, van der Leun et al. 2019). This can explain why in certain mice we observed some proliferation when stimulated with certain peptides (mainly AH1, GSW11, Ld20 and Kd34), but negligible IFNγ production. Furthermore, the presence of immune regulators in untreated mice (such as Tregs) can impede the correct activation of T cells. In this context, mouse tumour models have shown that PC61-mediated Treg-depletion can significantly increase the proportion of IFNγ+ in CD8+ T cells from spleen (Huss, Pellerin et al. 2016) and tumours (Turnis, Sawant et al. 2016, Arce Vargas, Furness et al. 2017). Indeed, overall IFNγ responses were higher in Treg-depleted regressors compared to untreated, being the average sum of detected IFNγ responses almost double in the former compared to the latter (7.18% vs. 3.77%, **Figure 4.7** and **Figure 4.15**). Remarkably, progressors showed similar IFNγ production patterns compared to untreated mice, despite the fact that Treg levels were similar in both PC61-treated groups (**Figure 4.16**), suggesting that additional inhibitory mechanisms, such as a high expression of inhibitory receptors on the cell surface of CD8+ T cells and/or tumour stroma could be blocking the correct activation of CT26-specific CD8+ T cells. This high production of IFNγ by CD8+ T cells from regressors can also explain the immune control of tumour growth observed in these mice. Overacre-Delgoffe *et al.* described a “fragile” phenotype of Tregs characterised by the expression of Neuropilin-1 (Nrp1) that retain FOXP3 expression but lose suppressive functions, where high amounts of IFNγ within the TME represent an important inducer of this

phenotype (Overacre-Delgoffe, Chikina et al. 2017). Thus, in the absence of Tregs, CD8+ T cells can be appropriately activated in the TME and secondary lymphoid organs, leading to a high production of IFNγ upon stimulation with CT26-derived peptides, which can further decrease the suppressive functions of Tregs by the induction of a "fragile" phenotype.

When ranking the potential immunogenic peptides from the CT26 immuno-transcriptome, two main observations were made: i) peptides derived from the most overexpressed protein in CT26 (gp70) ranked higher by PFR despite some of them having low predicted MHC-I binding affinities, and ii) neoantigens were highly ranked by NetMHC, despite the low abundance of their source transcripts. The gp70 glycoprotein from the ecotropic MuLV was first described as an overexpressed TAA in the MCA-induced MethA fibrosarcoma model (DeLeo, Shiku et al. 1977), and further studies have confirmed a high expression of this retroviral element in CT26, B16, 4T1 and A20 murine tumour models (Scrimieri, Askew et al. 2013). In normal BALB/c mice, the pattern of gp70 expression is heterogeneous, with a trend of an increased production of this retroviral protein as the mice get older (> 8 months old), whereas only 12% of BALB/c mice are MuLV-positive in early life (1 - 5 months old) (McCubrey and Risser 1982). Furthermore, recent publications have shown a faint to absent production of gp70-derived peptides (mainly AH1) in thymus isolated from 5- to 8-week-old BALB/c mice (Laumont, Vincent et al. 2018), thus suggesting that peptides derived from this endogenous retroviral product might induce an incomplete negative selection in the thymus, leading to the generation of gp70-specific CD8+ and CD4+ T cells that could play important roles in the immune control of tumours where gp70 is overexpressed. Indeed, and as previously mentioned, the only two described immunogenic peptides recognised by CD8+ T cells in the CT26 tumour model (AH1 and GSW11) derive from this MuLV protein (Huang, Gulden et al. 1996, James, Yeh et al. 2010), as well as conformation-dependent epitope recognised by CD4+ T cells that derives from the gp70 precursor gp90 (Golgher, Korangy et al. 2001). Furthermore, a study using $gp70^{-/-}$ mice showed that upon tumour challenge with CT26, half of the animals showed no signs of tumour growth, splenocytes had stronger IFNγ production and cytotoxic and activities against CT26 cells when stimulated with the AH1 peptide compared to splenocytes from normal mice, and a 4- to 5-fold increase in the frequency of high-avidity AH1-specific CD8+ TILs was observed in mice were tumour control was not achieved (McWilliams, Sullivan et al. 2008). This evidence partially contradicts the previous observations about gp70 expression in BALB/c thymus, as it suggests that in normal mice gp70-specific T cells might not be developed due to thymic negative selection, and that only when gp70 is absent from these mice since birth, they can induce strong anti-tumour responses against CT26. Nonetheless, the presence of anti-gp70 CD8+ T cell responses in gp70-sufficient mice indicates that these cells can be developed in the thymus, although with differential TCR affinities/avidities.

During negative selection, double-positive or single-positive thymocytes expressing TCRs with high affinities towards self-antigens are deleted (Klein, Kyewski et al. 2014). Thus, in the CT26 tumour model in BALB/c mice, gp70-specific T cells participating in immune control could harbour TCR with low affinities, which has been demonstrated for GSW11-specific CD8+ T cells in CT26-challenged Treg-depleted mice (Sugiyarto, Prossor et al. 2021), as well as mice treated with anti-PD-1 (Sugiyarto, Unpublished data). In humans, tumour-specific CD8+ T cell responses towards overexpressed HERV have also been reported. Different HERV-E-derived peptides have shown immunogenic potential in clear cell renal cell carcinoma (Takahashi, Harashima et al. 2008, Cherkasova, Scrivani et al. 2016), and overexpression of HERV-H has been positively correlated with type II IFN responses, CD8+ T cell effector function, and immune checkpoint activity (Rooney, Shukla et al. 2015, Kong, Rose et al. 2019). Collectively, this evidence highlights the importance of studying CD8+ T cell responses against endogenous retroviruses overexpressed in tumours, as targeting these peptides in clinical settings could represent an attractive approach for the development of immunotherapeutic strategies across a large number of patients.

From our screening assays, five gp70-derived peptides (GSW11, AH1, Kd34, Kd37 and Dd14) induced significantly higher IFNγ responses in regressors compared to progressors, being one of these (Kd34) top ranked by the PFR algorithm. Nonetheless, CD8+ T cells stimulated with Kd34, Kd37, or Dd14, showed lower IFNγ production compared to cells stimulated with GSW11 or AH1 in regressors (**Figure 4.11**). Importantly, besides AH1, Kd34 was the only peptide detected in the CT26 MAE immunopeptidome, thus indicating that this peptide represents a true novel immunogenic epitope in CT26. A plausible explanation about why the other novel immunogenic epitopes were not detected in the MAE immunopeptide lies in the MHC-I affinities of these peptides, measured at 194.7nM and 236.6nM for Kd37 and Dd14, respectively (**Figure 3.6** and **Figure 3.7**), thus being classified as low-binders. These observations have been shared in preclinical studies with mouse MC-38 and TRAMP-C1 cell lines using LC-MS for the identification of immunogenic peptides, as only 0.54% of the predicted immunogenic peptides were identified by this methodology; all of the identified peptides derived from highly-abundant proteins and displayed high predicted binding affinities towards their respective MHC-I molecule (Yadav, Jhunjhunwala et al. 2014). However, MHC-I binding affinity alone cannot fully explain why a peptide can be detected by LC-MS strategies, as a recent study using the MethA fibrosarcoma cell line showed that this methodology can detect peptides usually categorised as non-binders (IC_{50} > 500nM) (Ebrahimi-Nik, Michaux et al. 2019), thus pointing at other factors, such as correct antigen processing of these peptides, for the inability to detect them at the cell surface of CT26 cells by LC-MS. Lastly, from these five gp70-derived peptides, three of them (AH1, GSW11 and Kd37) induced higher (but subtle) proliferation rates in CD8+ T cells from regressors compared to progressors while the opposite was observed for Kd34 and Dd14 (**Figure 4.13**). An important

aspect of these IFNγ and proliferation assays lies in the use of spleens and tdLNs as a source of tumour-specific CD8+ T cells, as previous studies have shown that the frequencies of such cells in these secondary lymphoid organs are ten-times lower than in tumours (Fehlings, Simoni et al. 2017). Despite this drawback, the high cellularity of these organs (mostly spleen) allows for an easier screening of a large number of peptides in a single mouse, while compromising the sensibility in detecting subdominant responses. These results collectively support the notion that mainly GSW11 (and in less extent AH1) represent the immunodominant epitopes in CT26, whereas the newly identified epitopes could be considered as subdominant.

The identification of neoantigens has proven useful for the development of vaccines, as neoantigen-based strategies have been associated with favourable clinical outcomes in different types of preclinical models and human cancers (Li, Sobral et al. 2018, Hilf, Kuttruff-Coqui et al. 2019, Liu, Shao et al. 2021). However, their identification is laborious, as less than 1% of somatic mutations in tumour cells will result in the generation of mutated peptides that can be presented by MHC-I molecules (Schumacher and Schreiber 2015). Although the vast majority of potential neoantigens described in this study were considered as non-binders by NetMHC (**Figure 3.1**), the top-ranked peptides using this algorithm were all neoantigens (Table 3.1), which remarkably derived from low-abundant transcripts in CT26 cells. From these, we observed significant high IFNγ production by CD8+ T cells from regressors when stimulated with Ld18, Kd26, Kd2 and Kd27, with high responses also observed for NetMHC-ranked H-2D^{d}-restricted peptides (**Figure 4.11**). Ld18 derives from the UBASH3A protein (Ubiquitin-associated (UBA) and Src homology 3 (SH3) domain containing A), which is mainly expressed on T cells acting as a negative regulator (Ge, Paisie et al. 2019), and high levels of UBASH3A expression have been associated with good prognosis in patients with HNSCC (Wang, Tian et al. 2021). Kd26 and Kd27 derive from the olfactory receptors Olfr884 and Olfr846, respectively, both of them having no current biological relevance in any human or murine cancers. Lastly, Kd2 is found within the HAUS6 (HAUS augmin-like complex subunit 6) protein, which plays important roles in the formation of the mitotic spindle (Larsson, Jafferali et al. 2018) and in brain development (Viais, Farina-Mosquera et al. 2021). Remarkably, HAUS6 has been used for molecular stratification of breast cancer (MotieGhader, Masoudi-Sobhanzadeh et al. 2020), and has been described as an essential protein in functional screens of high-grade serous ovarian cancer cell lines (Gusev, Lawrenson et al. 2019). Nonetheless, HAUS6 expression in CT26 is low, suggesting that this protein is dispensable for the tumorigenic activities of this cell line. Despite showing strong IFNγ responses in spleen from Treg-depleted regressors, and having high measured affinities (only Kd2 showed an IC_{50} > 50nM, **Figure 3.6**), none of these peptides were detected by the MAE immunopeptidome, which could be associated with the low abundance of their respective mRNA transcripts, as LC-MS techniques can

be biased towards peptides derived from high-abundant transcripts (Garcia-Garijo, Fajardo et al. 2019). Collectively, our results highlight the potential use of the PFR algorithm for the detection of therapeutically-relevant cancer-derived epitopes, indicating that MHC-I binding affinity alone is a poor predictor of such epitopes. A recent consortium analysis of determinants of cancer-derived peptide immunogenicity elegantly described that the three main features affecting the immunogenicity of a given peptide are MHC-I binding affinity, abundance of the source protein in tumours, and MHC-I binding stability, and that ranking potential immunogenic peptides using only MHC-I binding affinities resulted in a precision <20% (Wells, van Buuren et al. 2020). From these characteristics, MHC-I binding affinity and intracellular abundance are incorporated in the PFR model, strengthening the observation that cell-surface p/MHC-I abundance is a good indicator of immunogenic peptides in clinical settings. The therapeutic responses observed by top-ranked PFR peptides could be explained by the priming of T cells with different avidities. Previous studies in our lab using the CT26 tumour model have shown that high abundant peptides can prime both low- and high-avidity T cells, while low abundant peptides preferentially prime high-avidity T cells. Furthermore, low-avidity T cells have been associated with protection in Treg-depleted (Sugiyarto, Prossor et al. 2021) and PD-1 treated mice (Sugiyarto, Unpublished results). In this last regard, a recent study reported a preferential suppression of low-avidity T cells by PD-1, and that checkpoint blockade with anti-PD-1 in the E.G7 thymoma mouse model potentiated the responses of low-avidity T cells (Shimizu, Sugiura et al. 2021). Thus, a more detailed investigation regarding the avidity patterns of PFR-ranked peptides that significantly boosted IFNγ responses in regressors is necessary to corroborate this hypothesis.

Besides the identification of cytokine production and proliferation responses against candidate immunogenic peptides, the detection of antigen-specific T cells infiltrating the tumour bed represents a critical step towards the validation of peptide immunogenicity, and identifying which antigens are responsible for inducing strong and durable immune responses in the tumour bed can improve the development of more targeted immunotherapeutic strategies. Thus, and based on the previous IFNγ and proliferation screenings, we aimed to evaluate the frequencies and phenotypes of CT26-specific CD8+ T cells in untreated and Treg-depleted mice, focusing on GSW11, AH1, Kd34 and Kd37. Overall, we observed that in CT26 tumours, regardless of the therapeutic intervention, CD4+ T cells are most abundant immune cell population, almost doubling the frequencies of CD8+ T cells (**Figure 5.1** C). These observations are in line with previous publications using this same tumour model, which have shown that the majority of CD4+ TILs are Tregs (Yu, Bhattacharya et al. 2018, Zhong, Myers et al. 2020).Given that PC61-treated mice still show low levels of intertumoral Tregs (**Figure 4.8** B), but that total CD4+ T cell levels are comparable to untreated mice, our results suggest that these cells could be represented by

conventional T helper cells rather than Tregs. Despite this inflamed phenotype, CT26 tumours show lower T cell infiltration than human colorectal cancers (Zhong, Myers et al. 2020), which could be explained by a relatively low production of T cell-attracting chemokines in the TME, such as CX3CL1 and CXCL10, as well as by the overexpression of proteins associated with extracellular matrix remodelling, such as fibronectin and the receptor tyrosine kinase AXL, which can create dense areas in the tumour that physically prevent T cells from entering (Yu, Bhattacharya et al. 2018). Despite these barriers that can hinder T cell infiltration in tumours, no differences were observed at the frequencies of total CD8+ or CD4+ TILs in treated or untreated mice, and only regressors at day 11 showed a trend towards a high CD8+ T cell infiltration without reaching statistical significance when compared to untreated mice at the same time point (**Figure 5.1** A), thus indicating that a failed T cell infiltration into the TME does not explain why only a third of PC61-treated animals show complete tumour regression. Interestingly, Angelova *et al.* have shown that in patients with colorectal cancer, the frequencies of CD8+ TILs increase from stage I to III, but sharply decline in stage IV (Angelova, Charoentong et al. 2015), which correlates with the decrease of CD8+ TILs observed in progressors at day 27 (**Figure 5.1** A), suggesting that the decrease in the total T cell infiltrate in Treg-depleted mice without clinical benefit could be a result of a deletion of these cells, potentially via apoptosis. Although pre-clinical studies have shown that animals achieving tumour regression upon combined anti-CTLA-4/PD-1 checkpoint blockade display a higher frequency of antigen-specific CD8+ TILs compared to non-responders (Principe, Kidman et al. 2020), no such differences were observed in our study for any of the four CT26-derived epitopes tested, as progressors showed an even higher frequency of GSW11-specific CD8+ TILs than regressors (**Figure 5.10** A). Although the total frequencies of CD8+ and CD4+ T cells in tdLNs were higher compared to tumours, CT26-specific cells were ten-times less frequent in tdLNs (**Figure 5.10** B), in line with previous reports regarding the frequencies of endogenous neoepitope-specific CD8+ T cells in the MCA-induced T3 sarcoma model (Fehlings, Simoni et al. 2017), and in adoptive-transfer studies using OT-1 T cells and B16-OVA melanoma cells (Martinez-Usatorre, Donda et al. 2018). These results are consistent with the role of tdLNs as a priming rather than an effector site, serving as an important source of immune cells in the surrounding cancer tissues (Quintana, Peg et al. 2021). Tetramer-staining assays revealed a predominance of GSW11-specific CD8+ T cells in both tumours and tdLNs compared to the other tested epitopes, indicating that GSW11 induces the immunodominant CD8+ T cell responses in CT26 challenged mice (**Figure 5.10** C). Despite this, previous investigations in our group have shown that GSW11-specific CD8+ TILs are highly dysfunctional, showing impaired IFNγ production upon *in vitro* peptide restimulation (Sugiyarto, Prossor et al. 2021). These observations indicate that although GSW11-specific CD8+ T cells represent the dominant CT26-specific population in both tumours and tdLNs, the accumulation of these cells in these organs does not allow complete

differentiation between regressors and progressors. Furthermore, the low frequencies of non-GSW11/-AH1/-Kd34/-Kd37 cells in progressors compared to regressors at day 11 could indicate that the former could have a more restricted CD8+ T cell response in tumours, allowing for the easy selection of immune escape mutations against these four epitopes. In contrast, the relatively high frequency of CD8+ T cells of unknown specificities in regressors at day 11 might indicate that these animals mount broader CD8+ T cells responses restricted against epitopes that are yet to be identified.

Memory T cells represent an important subset of T cells in the anti-cancer immune response, as they can serve as a quick source of tumour-specific T_{EFF} in the case of tumour recurrence, and different subset of memory T cells have been associated with good prognosis in human cancers (Principe, Kidman et al. 2020). Our first approximation for the detection of memory T cells relied on measuring of CD44 expression levels on bulk CD4+ and CD8+ T cells, as this marker is upregulated on T cells upon antigen stimulation (Samji and Khanna 2017). Indeed, the majority of CD8+ and CD4+ TILs expressed CD44, while these cells were lower in tdLNs (**Figure 5.3** A and B), being these findings also observed in the four populations of CT26-specific CD8+ TILs (**Figure 5.11** A). This is consistent with previously published data, where the highest frequencies of CD44+ CD8+ T cells were observed within the antigen-specific population (Fehlings, Simoni et al. 2017). The fact that not all CD8+ TILs express CD44 could suggest that these CD44- cells are bystanders, which have been well characterised in patients with NSCLC, colorectal cancer, melanoma, and ovarian cancer (Erkes, Smith et al. 2017, Simoni, Becht et al. 2018, Scheper, Kelderman et al. 2019). Interestingly, AH1-specific CD8+ T cells from tdLNs showed the highest CD44 expression in all groups, but more evidently in Treg-depleted mice at day 11 (**Figure 5.11** B). This behaviour could be associated with the strength of the TCR-p/MHC interaction, as studies have reported that adoptively transferred OT-1 T cells in mice challenged with B16 cells expressing a modified SIINFEKL peptide with low affinity towards the TCR (but not towards MHC-I) showed an impaired production of memory cells, thus suggesting that CD44 expression could be avidity-dependent (Martinez-Usatorre, Donda et al. 2018). Although AH1, is considered as a poor-binder towards H-2L^d by both NetMHC4.0 predictions and BFA decay assays, the avidity of AH1-specific T cell clones towards CT26 cells has not been explored, and these measurements could shed lights into why these cells are preferentially primed in tdLNs of Treg-depleted mice.

One particular feature from our analysis represents the abundance of CD8+ T_{EM} over T_{CM} in tumours, but particularly in tdLNs (**Figure 5.4** A). The findings in tumour samples are not surprising, considering that CD8+ T_{EM} cells have higher cytotoxic activities compared to T_{CM} (Han, Khatwani et al. 2020), and that CD8+ T_{EM} cells are abundant in different mouse (Engels, Engelhard et al. 2013, Principe, Kidman et al. 2020) and human cancers (Angelova, Charoentong et al. 2015,

Thommen, Schreiner et al. 2015, Giraldo, Becht et al. 2017). Remarkably, in the B16 and MC38 mouse models, Treg inactivation using an anti-IL-35 antibody is associated with increased frequencies of T_{EM} and potentiation of IFNγ responses in the TME (Turnis, Sawant et al. 2016). Furthermore, high HERV expression in patients with clear-cell renal cell carcinoma (ccRCC) has been associated with T_{EM} immune signatures (Smith, Beckermann et al. 2018), which suggests that the combination of Treg depletion and overexpression of MuLV in the CT26 tumour model may favour the development of T_{EM} cells over T_{EM}. The lower frequencies of both CD8+ and CD4+ T_{CM} in tdLNs and higher in tumours are unexpected, considering that these cells are preferentially located in lymph nodes (Mueller, Gebhardt et al. 2013). A potential explanation of this phenomenon in the tumour samples is the formation of TLSs, as both T_{CM} and T_{EM} have been associated with these structures in melanoma (Cabrita, Lauss et al. 2020). Furthermore, the presence of TLSs could also play an important role into the mechanism of action of the Treg-depletion therapy, as very low numbers of T_{CM} cells are detected in untreated mice, as well as in mice reaching the humane endpoint, both in the bulk CD8+ T cell populations and in antigen-specific CD8+ TILs (**Figure 5.4** and **Figure 5.12**). Boosting of CD8+ T_{CM} cells in immunotherapeutic settings has been associated with immune control in different mouse models (Enamorado, Iborra et al. 2017, Wu, Zhu et al. 2017, Li, Cong et al. 2021), thus indicating that a potential mechanism involved in the CT26 immune clearance observed in Treg-depleted mice could be the preferential expansion of CD8+ T_{CM} cells in the TME. Lastly, a significant proportion of CD44+ T cells could not be categorized as either T_{EM} or T_{CM} (**Figure 5.2**). These cells could represent T_{SCM}, which are often categorised as $CD44^{-/low}$ CD62L+. Krishna *et al.* described that $CD44^{low}$ CD62L+ CD39- CD69- TCF1+ T_{SCM} can proliferate upon polyclonal TCR stimulation and give rise to other effector populations, and that adoptive transfer of gp100-specific Pmel-1 T cells with this phenotype into mice challenged with gp100-B16 melanoma leads to a significantly delayed tumour growth without complete regression (Krishna, Lowery et al. 2020). The presence of T_{SCM} could explain why the majority of CD4+ and CD8+ antigen-experienced T cells from tdLNs in regressors at day 27 were not categorised as either T_{EM} or T_{CM}, and further studies investigating the role of other memory populations are important to further evaluate the contribution of these subpopulations in the immune control of CT26 tumours upon Treg depletion.

A critical feature of cancers is their capacity to evade the immune system through a myriad of mechanisms, being the induction of T cell dysfunction in the TME one of the most widely studied and therapeutically targeted (Waldman, Fritz et al. 2020). One of the main markers used for the identification of exhausted T cells is PD-1, as antibodies blocking this inhibitory receptor have been associated with the recovery of effector functions by exhausted T cells in the Lymphocytic choriomeningitis (LCMV) chronic viral model, as well as in mice and human cancers (McLane,

Abdel-Hakeem et al. 2019). In this study we observed than on average more than half of the total CD8+ and CD4+ TIL populations, as well as antigen-specific CD8+ TILs, express PD-1 across all groups (**Figure 5.3** C and D, and **Figure 5.13** A). These high patterns of PD-1 expression in TILs have been evidenced in mouse (Hailemichael, Dai et al. 2013, Fehlings, Simoni et al. 2017) and human cancers (Thommen, Schreiner et al. 2015, Giraldo, Becht et al. 2017, Kansy, Concha-Benavente et al. 2017). Interestingly, total CD4+ and CD8+ T cells in tdLNs expressing PD-1+ were significantly lower in untreated mice compared to Treg-depleted (**Figure 5.3** C and D), and these observations were particularly evident for AH1-specific and Kd37-specific CD8+ T cells from these tissues (**Figure 5.13** B). Although the majority of studies tend to categorise PD-1+ T cells as exhausted, the expression of this marker is also indicative of T cell activation, as evidenced in PD-1+ NY-ESO-1-specific CD8+ T cells that are able to proliferate and produce effector cytokines upon *in vitro* peptide restimulation (Fourcade, Sun et al. 2010). Based on our observations, it is plausible to infer that in the presence of Tregs, both CD8+ and CD4+ T cells in tdLNs are not properly activated, leading to a reduced expression of PD-1 on these cells.

Considering its role on T cell activation, several investigators have used the cell-surface levels of PD-1 expression to discriminate activated and exhausted T cells. First described in the LCMV model, these different subsets have been termed as rescuable T cells (PD-1$^{low/mid}$ T-bet^{high}), which respond to checkpoint blockade, and terminally-exhausted T cells (PD-1^{high} Eomes^{high}) that are unresponsive to these therapies (Blackburn, Shin et al. 2008, Im, Hashimoto et al. 2016). Recent investigations in this chronic viral model have shown that PD-1^{mid} CD8+ T cells show signs of proliferation via Ki67 staining, while PD-1^{high} are non-proliferative (Beltra, Manne et al. 2020). These observations have been translated in cancer, as CD8+ PD-1^{high} TILs from NSCLC and ovarian cancer patients showed a failed production of IL-2, TNFα and IFNγ upon polyclonal activation, whereas PD-1$^{low/mid}$ showed normal production of these cytokines (Thommen, Koelzer et al. 2018, Salas-Benito, Conde et al. 2021). In this study, the total CD4+ and CD8+ T cell populations in tumours were preferentially enriched in the PD-1^{mid} and PD-1^{high} compartments in Treg-depleted mice, while untreated mice showed low frequencies of PD-1^{high} cells (**Figure 5.6** A and C). Interestingly, PD-1^{high} were almost absent in tdLNs, as almost half of the CD4+ and CD8+ PD-1+ populations had low expression of this inhibitory receptor (**Figure 5.6** B and D), thus indicating that in these tissues PD-1+ cells represent activated rather than exhausted T cells. Contrary to findings using checkpoint blockade in mouse tumour models, where this therapy leads to a significant increase in the frequency of antigen-specific PD-1^{low} cells in the TME (Fehlings, Simoni et al. 2017), no discernible differences were observed in the levels of PD-1^{low} cells among antigen-specific CD8+ T cells across groups (**Figure 5.14** A). This suggest that checkpoint blockade and Treg depletion may have different mechanisms in potentiating anti-tumour CD8+ T cell responses, where in the absence of Tregs in the TME, CD8+ T cells might proliferate and activate in a

polyclonal fashion, leading to a fast upregulation of inhibitory receptors like PD-1 (Gonzalez-Navajas, Fan et al. 2021). Moreover, the high frequencies of PD-1^{high} antigen-specific CD8+ TILs in progressors at day 20 could explain the significant decrease of CD8+ T cells observed in these mice, as these cells have a transcriptional profile enriched in proteins involved in apoptosis (Miller, Sen et al. 2019).

The establishment of a terminally-exhausted phenotype follows a dynamical process where T cells start losing effector functions and express inhibitory receptors upon constant antigen stimulation (Waldman, Fritz et al. 2020). Two of the most widely studied inhibitory receptors are TIM-3 and LAG-3, as the expression of these markers is associated with terminally exhausted T cells in the LCMV model (Abdel-Hakeem, Manne et al. 2021) and human cancers (Oliveira, Stromhaug et al. 2021). In mouse models, expression of TIM-3 and/or LAG-3 is restricted to PD-1+ T cells, and antigen-specific CD8+ PD-1+ TILs expressing at least one of these two markers have an impaired production of effector cytokines (Fourcade, Sun et al. 2010, Miller, Sen et al. 2019) and have been associated with the development of metastasis (Zhou, Munger et al. 2011). We have observed that half of the total CD8+ PD-1+ TIL populations express TIM-3 and/or LAG-3 in Treg depleted mice, in contrast with ~20% of CD4+ PD-1+ TILs in the same group, and less than 10% in both bulk CD8+ and CD4+ PD-1+ T cells in tdLNs (**Figure 5.7**). These values are similar to the frequencies of CD8+ PD-1+ TILs expressing these inhibitory markers in B16 melanoma, MC38 colon carcinoma, and T3 sarcoma models, where the CD8+ PD-1+ T cells expressing inhibitory receptors range from 25 – 60%, being these cells preferentially located in tumours compared to tdLNs (Woo, Turnis et al. 2012, Fehlings, Simoni et al. 2017). Furthermore, and in accordance with previous reports in NSCLC patients (Thommen, Koelzer et al. 2018), the total and antigen-specific CD8+ PD-1+ T cell populations co-expressing TIM-3 and LAG-3 were preferentially observed in the PD-1^{high} population (**Figure 5.8** and **Figure 5.16**), which indicates that these cells are terminally exhausted. Although the continuous antigen stimulation and immunoregulatory milieu in the TME significantly contribute to the preferential development of T cell exhaustion in tumours (Dolina, Van Braeckel-Budimir et al. 2021), metabolic cues can also affect the expression of inhibitory receptors in tumour-infiltrating T cells, and can explain the high frequencies of T cells expressing PD-1, TIM-3 and/or LAG-3 in tumours compared to tdLNs. Within the TME, T cells develop a reduced capacity for glucose uptake along with a loss of functional mitochondrial mass (Scharping, Menk et al. 2016), and these stressors along with tissue hypoxia commonly observed within tumours have been associated with the development of PD-1^{high} TIM-3+ LAG-3+ CD8+ TILs in the B16 melanoma model (Scharping, Rivadeneira et al. 2021). Despite this immunosuppressive microenvironment being observed preferentially in the tumour bed, we also observed remarkably high frequencies of antigen-specific PD-1+ CD8+ T cells in tdLNs expressing TIM-3 or LAG-3, mostly for AH1- and Kd37-specific CD8+ T cells, while these values were low in the bulk analysis, as well

as in GSW11- and Kd34-specific CD8+ T cells in these tissues (**Figure 5.7** and **Figure 5.15**). Studies using the OVA-transfected AE17 mesothelioma tumour model revealed that ~15% of OVA-specific PD-1+ CD8+ T cells in tdLNs did not express other inhibitory receptors, such as TIM-3 and TIGIT, while more than 95% of the bulk CD8+ T cells from these tissues did not express such receptors (Dammeijer, van Gulijk et al. 2020). These results, along with our observations, strongly suggest that the exhaustion phenotype can be imprinted in tdLNs in tumour-specific T cells. However, the fact that GSW11- and Kd34-specific CD8+ T cells did not replicate this behaviour, suggests that the continuous development of an exhaustion phenotype is an antigen-specific phenomenon. Although high frequencies of CD8+ PD-1+ TILs expressing TIM-3+ and/or LAG-3+ have been associated with poor prognosis and unresponsiveness to checkpoint blockade in NSCLC (Thommen, Koelzer et al. 2018), ccRCC (Giraldo, Becht et al. 2017), melanoma (Oliveira, Stromhaug et al. 2021), and breast cancer (Liu, Qi et al. 2021), no significant differences in these cell populations were observed between regressors and progressors, both in the total CD8+ T cell populations and in antigen-specific CD8+ TILs (**Figure 5.5** and **Figure 5.12**), indicating that an overexpression of exhausted cells in the TME of progressors is not associated with the lack of immune control towards CT26 tumour observed in these Treg-depleted mice.

Collectively, the results obtained in this study allowed us to identify novel immunogenic peptides in the CT26 tumour model implicated in the therapeutic response observed after Treg depletion, by filtering the abundance of the source protein and the predicted MHC-I binding affinities using the *in house* PFR formula. Remarkably, this PFR filtering outperformed NetMHC predictions for the detection of immunogenic peptides with low predicted binding affinities, such as GSW11 and AH1, highlighting the drawbacks for predicting immunogenicity using affinity measurements alone. The two novel CT26 epitopes (Kd34 and Kd37), were confirmed via IFNγ production, proliferation assays, and dextramer staining of CT26 tumours, where the low frequencies of these cells compared to GSW11-specific CD8+ TILs suggest that these two peptides induce subdominant T cell responses in this tumour model. Moreover, the presence of different memory and activation/exhaustion phenotypes in these antigen-specific CD8+ T cell populations indicate that the immune control of CT26 tumours is associated with specific phenotypic imprinting in tdLNs and tumours (**Figure 6.1**). Nonetheless, several questions still remain unanswered from our project, and addressing these issues would significantly improve our understanding of antigen presentation of immunogenic peptides in this tumour model. The role of tapasin in the presentation of these peptides was assumed as equal for all peptides and the three H-2^d alleles, while in human settings certain HLA-I alleles show a remarkable tapasin-dependency (van Hateren and Elliott 2021). Such investigations could be carried out via surface plasmon resonance using anti-tapasin antibodies and detecting the off-rate of different tapasin/H-2^d/peptide combinations.

Moreover, a very low number of MAE-detected peptides matched our list of PFR- or NetMHC-ranked peptides, even across different MAE strategies used by various groups (Laumont, Vincent et al. 2018). Different immunopeptidomics approaches, i.e., by using immunoprecipitates of H-2^d molecules as a source of peptides rather than whole cells, could improve the detection of novel immunogenic peptides in CT26 cells. This study was conducted using the *in vivo* depletion of Tregs as a therapeutic approach; however, this strategy is not yet applicable to humans, due to the importance of Tregs in maintaining tissue homeostasis and to the exacerbated autoimmune manifestations observed in humans lacking these cells (Georgiev, Charbonnier et al. 2019). Thus, it would be important to evaluate if the novel CT26-derived epitopes observed in this study can also induce strong IFNγ responses in common immunotherapeutic strategies, such as checkpoint blockade with anti-CTLA-4 and/or anti-PD-1, and if PFR ranking can accurately predict peptides associated with immune control in these therapeutic settings. Despite the significant increase of IFNγ responses in regressors, as well as the tumour infiltration of CD8+ T cells against the four tested peptides, no direct correlations of protection can be made against a specific peptide. For this, vaccination strategies containing these peptides prior CT26 inoculation could shed lights into which specific peptide or group of peptides are the main responsible in mediated tumour control upon Treg depletion and/or checkpoint blockade. Lastly, even in settings where gp70 is considered a foreign antigen in gp$70^{-/-}$ mice, only 50% of these animals achieve immune control of CT26 growth in the absence of therapy (McWilliams, Sullivan et al. 2008), thus suggesting that other non-gp70 peptides can also participate in the anti-tumour CD8+ T cell responses against this cancer. In this regard, neoantigens could represent attractive candidate of immunogenic peptides, considering that we observed high IFNγ responses against several neoantigens, despite the significant low abundance of these peptides in the CT26 proteome. Thus, it is imperative to evaluate via tetramer assays and/or vaccination approaches if these peptides are boosted in immunotherapy settings in CT26.

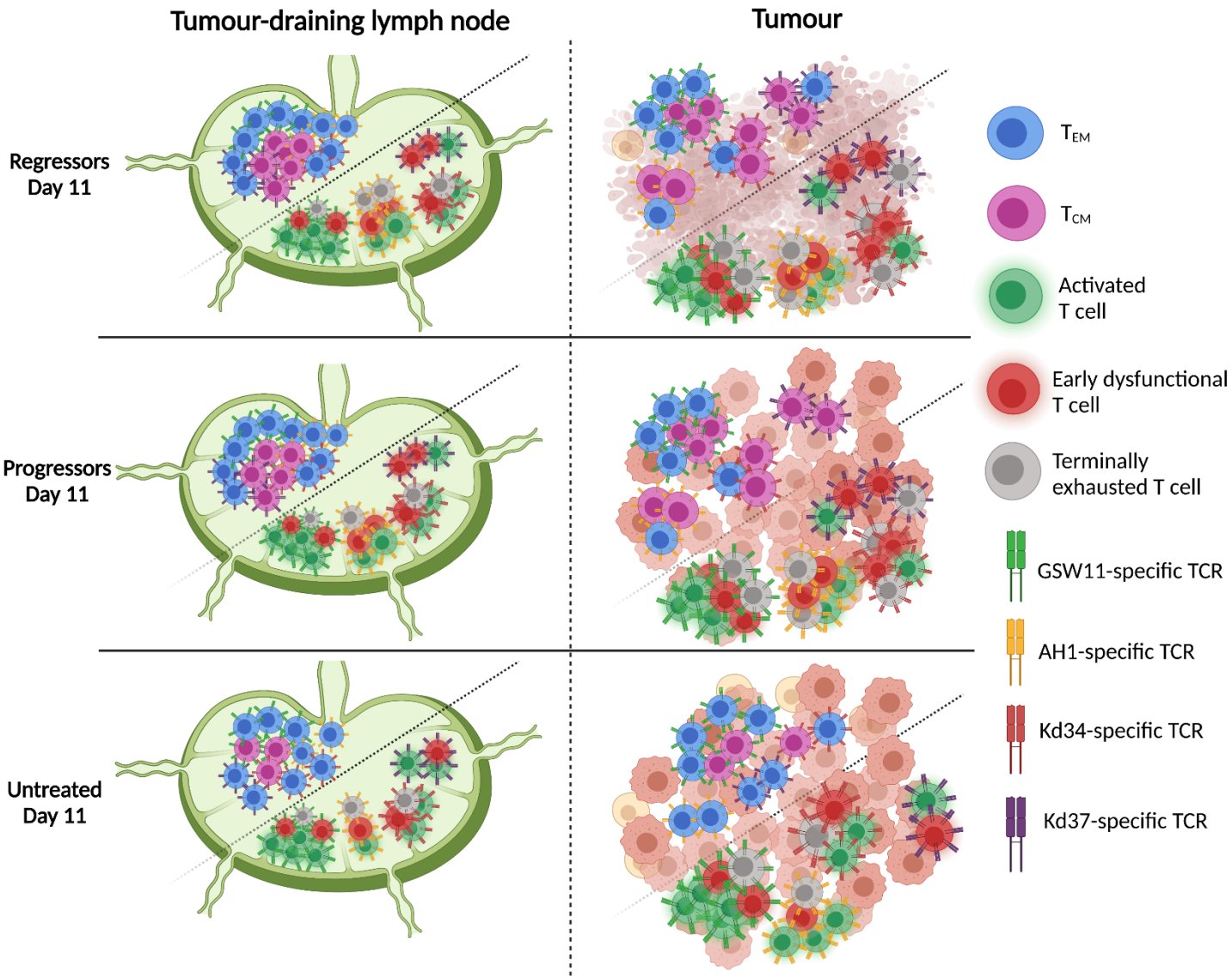

Figure 6.1 Immunological landscape of antigen-specific CD8+ T cell populations in CT26 tumours. Summary of the main phenotypic findings in GSW11-, AH1-, Kd34-, and Kd37-specific CD8+ T cells in tdLNs and tumours from Treg-depleted or untreated mice at day 11 post tumour challenge. For illustration purposes, activated T cells (in green) refer to PD-1+ TIM-3- LAG-3-, early dysfunctional T cells (in red) comprises PD-1+ T cells expressing either TIM-3 or LAG-3, while terminally exhausted T cells (in grey) includes PD-1+ TIM-3+ LAG-3+ T cells. The main observations from these phenotypic analysis include the overrepresentation of T_{CM} cells in tumours from Treg-depleted animals, as well as a decreased proportion of terminally exhausted T cells in untreated mice compared to their Treg-depleted counterparts.

Appendix A Generation of a non-GSW11 non-AH1 CT26-specific T cell hybridoma

The first approach taken towards deciphering novel CT26-derived epitopes was based in the production of T cell hybridomas using cells from Treg-depleted mice. For this, Treg-depleted mice that had cleared the initial CT26 tumour were rechallenged with 10^5 CT26 cells *in vivo* for seven days. Then, splenocytes were harvested and stimulated with irradiated CT26 cells *in vitro* in the presence of IL-2 for 4 additional days. These two re-stimulation steps were carried out to boost proliferation of CT26-specific T cells, thus increasing the likelihood of capturing T cell clones specific against this tumour. Once the re-stimulation steps were completed, fusions were performed between stimulated splenocytes and BWZ.36/CD8α and kept in R10 supplemented with 1X HAT for 10 days. After this period, from the 672 clones plated 99 clones showed signs of cell growth and were used for activation assays. First, the activation of the *lacZ* gene was verified by stimulating these clones with PMA/Ionomycin for 4 hours. From the initial 99 clones, 41 showed activation of the *lacZ* gene with this approach (**Figure 6.2** A), which were used for subsequent assays. These clones were then activated with P815 cells pulsed with AH1 or GSW11 peptides at a final concentration of 100nM; however, none of the clones reacted against these peptides (**Figure 6.2** B and C). Because of this, cells were activated with soluble anti-mouse CD3ε at a final concentration of 0.5μg/ml to verify that the TCR signalling pathway was functional, showing that only two of the 41 clones responded with this stimulus (**Figure 6.2** D). Finally, to verify the specificity of the clones, 10^5 CT26 cells were co-cultured with the same number of hybridoma cells overnight. Interestingly, only one of the clones responded against CT26 (Clone C3, **Figure 6.2** E), although this clone did not show signs of activation with soluble anti-mouse CD3ε (**Figure 6.2** D, Blue line). As a control, the previously developed GSW11-specific CCD2Z hybridomas were stimulated with CT26 cells as previously described. As observed in **Figure 6.2** F, CCD2Z hybridomas display a faster kinetics in the activation of *lacZ* compared to C3, suggesting that the latter hybridomas could be specific against low abundant peptides. To verify the expression of CD8α, CD3 and TCRβ, all clones were stained with fluorescent-labelled monoclonal antibodies against these molecules and analysed by flow cytometry. The clones showed a highly variable pattern of expression of the three molecules. Particularly for CD8α, three clones showed that only less than 2% of the cells expressed this molecule (**Figure 6.3** B). For CD3 and TCRβ, the mean frequency of expression among clones was 58.55% and 58.47%, respectively (**Figure 6.3** A and C). The CT26-specific clone C3 showed that 40.1% of cells expressed the three markers (**Figure 6.3** D).

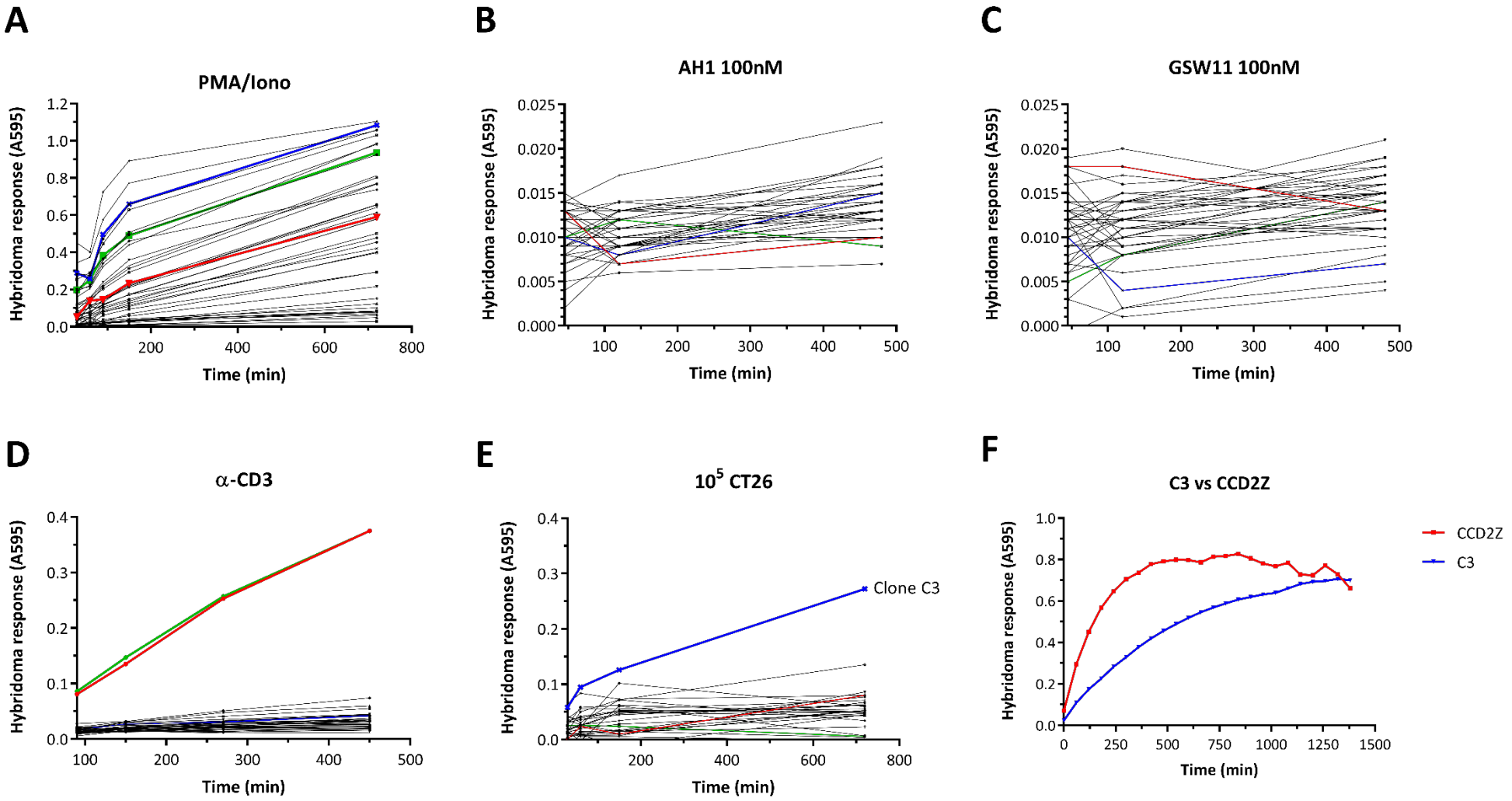
A
PMA/Iono
Hybridoma response (A595)
Time (min)
B
AH1 100nM
Hybridoma response (A595)
Time (min)
C
GSW11 100nM
Hybridoma response (A595)
Time (min)
D
α-CD3
Hybridoma response (A595)
Time (min)
E
10^5 CT26
Clone C3
Hybridoma response (A595)
Time (min)
F
C3 vs CCD2Z
CCD2Z
C3
Hybridoma response (A595)
Time (min)

Figure 6.2 **Development of a CT26-specific CD8+ T cell hybridoma.A.** The 99 growing clones obtained after fusion of BWZ.36/CD8α cells and splenocytes from CT26-immune mice were stimulated with 5ng/ml PMA plus 500ng/ml ionomycin for four hours. **B and C.** Peptide stimulation of the 41 responsive clones observed after PMA/Ionomycin stimulation with 10^5 P815 cells pulsed with 100nM of AH1 (B) or GSW11 (C) peptides overnight. **D.** Activation of the 41 responsive clones using soluble anti-mouse CD3ε at a final concentration of 0.5µg/ml overnight. **E.** Stimulation of the 41 reactive clones with 10^5 CT26 cells overnight. In figures A to E, the blue lines represent the C3 clone, whereas the green and red lines correspond to the clones activated only by soluble anti-mouse CD3ε. **F.** Comparison of the responsive profile of CCD2Z (golden line) and C3 (blue line) hybridomas against 10^5 CT26 cells overnight. In all experiments, supernatants were discarded after the mentioned time points, and a CPRG assay was performed as described in Section 2.8.2.

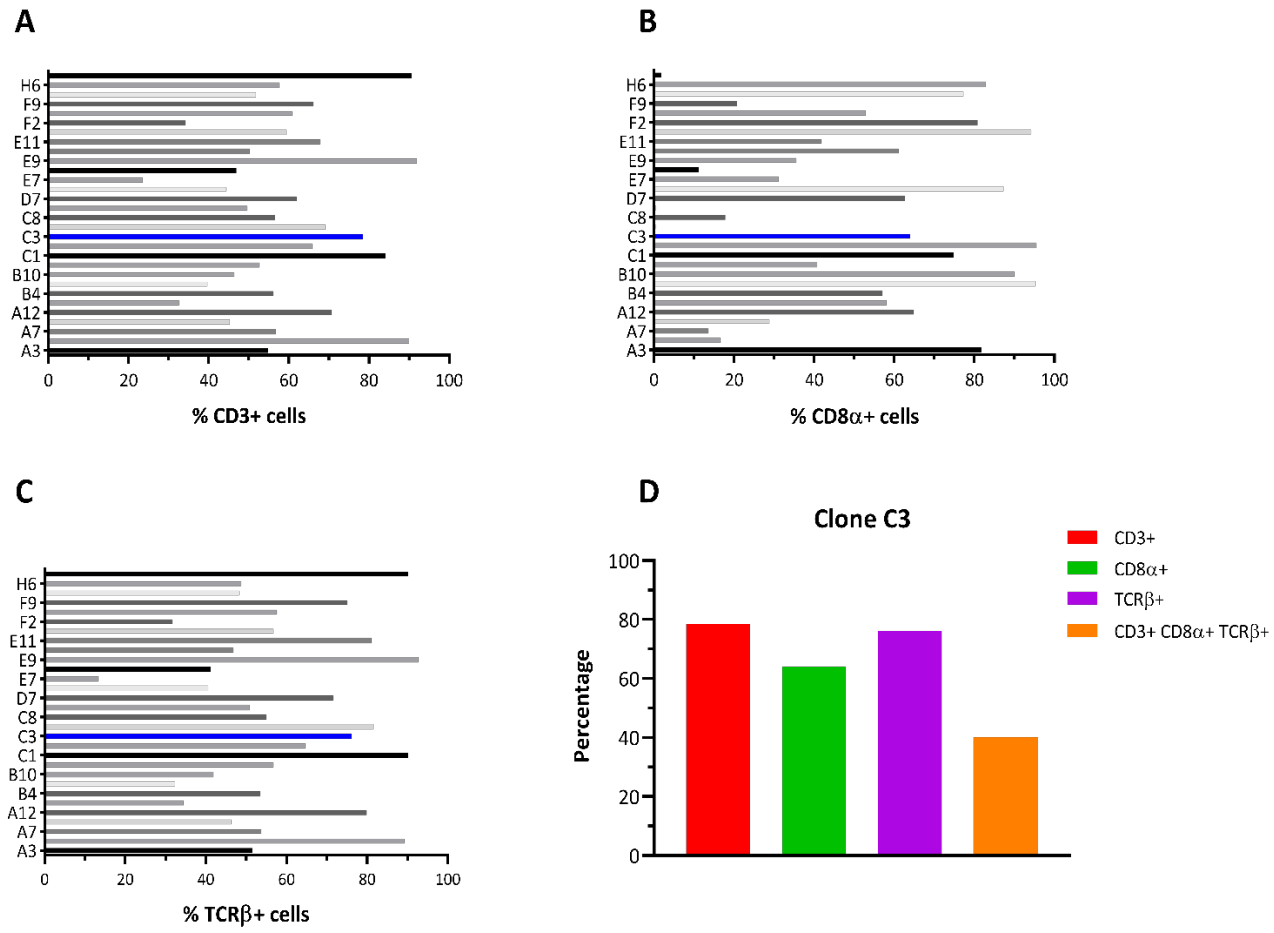

Figure 6.3 **The C3 hybridoma express classical T cell markers.** The responsive hybridomas were stained with fluorescent-labelled monoclonal antibodies against CD3 (**A**), CD8α (**B**) and TCRβ (**C**), and the frequency of positive cells was analysed by flow cytometry. **D.** Frequency of CD3+ CD8α+ TCRβ+ cells in the novel CT26-specific C3 hybridoma.

Altogether, these results show that the newly developed C3 hybridoma is CT26 specific, express surface markers associated with TCR activation, and do not react against the immunodominant AH1 and GSW11 epitopes, thus representing an important tool for deciphering novel CD8+ T cell epitopes in this tumour model.

The development of the non-GSW11/AH1 CT26-specific C3 hybridoma represents an exciting tool for the identification of novel CT26 specificities, as large peptide screenings can be done relatively easy using this cell line. As a first attempt to decipher the specificity of the C3 hybridoma, four different C3 clones were incubated overnight with P815 cells pulsed with 29 different gp70-derived peptides. This first screening was focused on gp70 as this is the most overexpressed protein in CT26, and since the GSW11 and AH1 peptides derive from this viral protein, it is likely that other CD8+ T cell epitopes can be derived from gp70. CPRG analysis showed that none of the 29 gp70-derived peptides was able to activate any of the clones, as no discernible differences

were observed between cells stimulated with these peptides and cell co-cultured with P815 alone (**Figure 6.4**). In addition, in order to identify the MHC-I-restriction of the C3 hybridoma, MHC-I molecules were blocked in CT26 cells by pre-incubating these cells with anti-H-2D^d, -H-2K^d, or –H–2L^d antibodies at different concentrations prior co-culture with C3 cells. As a positive control, CCD2Z cells were incubated with H-2D^d-blocked GSW11-pulsed P815 cells. Strikingly, none of these antibodies was able to block C3 activation, whereas CCD2Z cells cultured with H-2D^d-blocked P815 cells show a dose-dependent decrease of activation (**Figure 6.5** A). These results are not explained by a lack of expression of MHC-I molecules in CT26 cells, as flow cytometry analysis confirmed that these cells have a high expression of H-2K^d, moderate expression of H-2D^d, and low expression of H-2L^d (**Figure 6.5** B). Overall, these results suggest that the non-GSW11/AH1 C3 hybridoma could be activated by peptides presented in non-classical MHC-I molecules, but further experiments must be performed to prove this hypothesis.

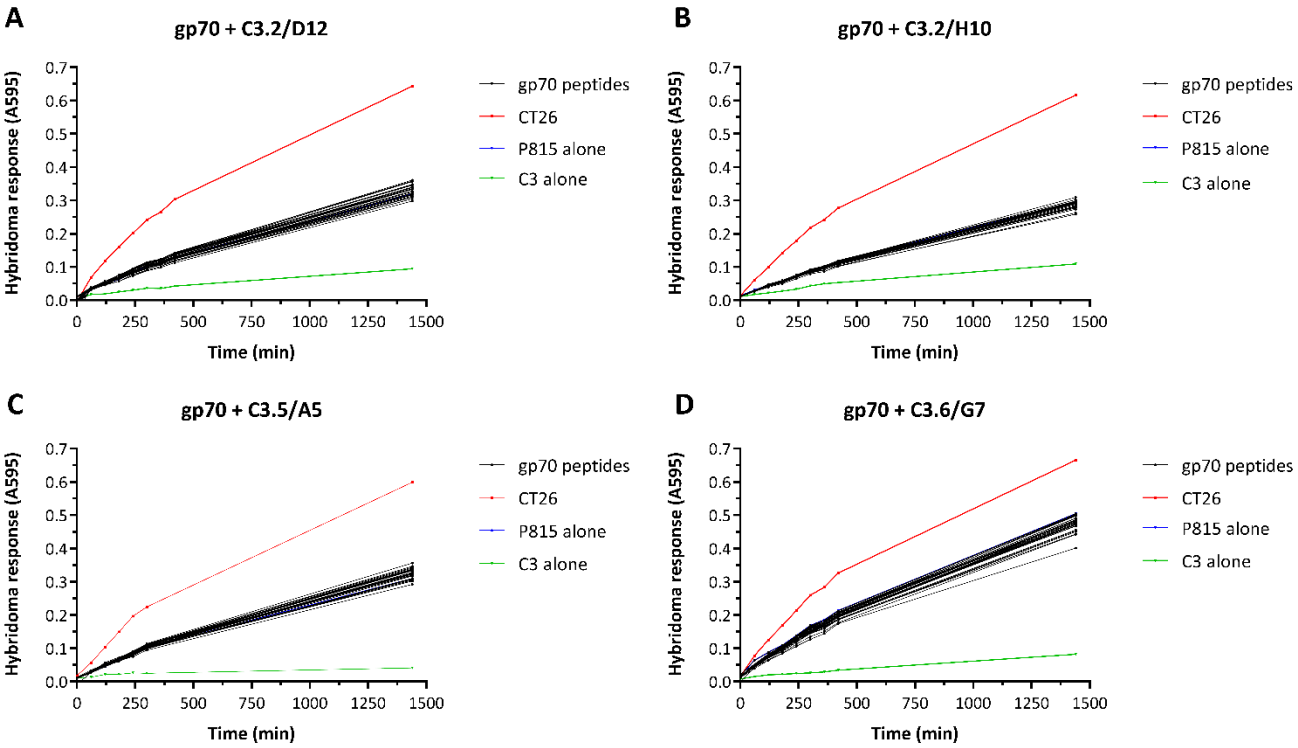

Figure 6.4 **C3 peptide stimulation with gp70-derived epitopes.** The seven clones with a high anti-CT26 sensitivity were stimulated overnight with 10^5 peptide-pulsed P815 cells at a final concentration of 100nM (Black lines), P815 cells alone (Blue lines), 10^5 CT26 cells as positive control (Red lines), or with no stimulus as negative control (Green lines), followed by a CPRG assay in order to verify cell activation.

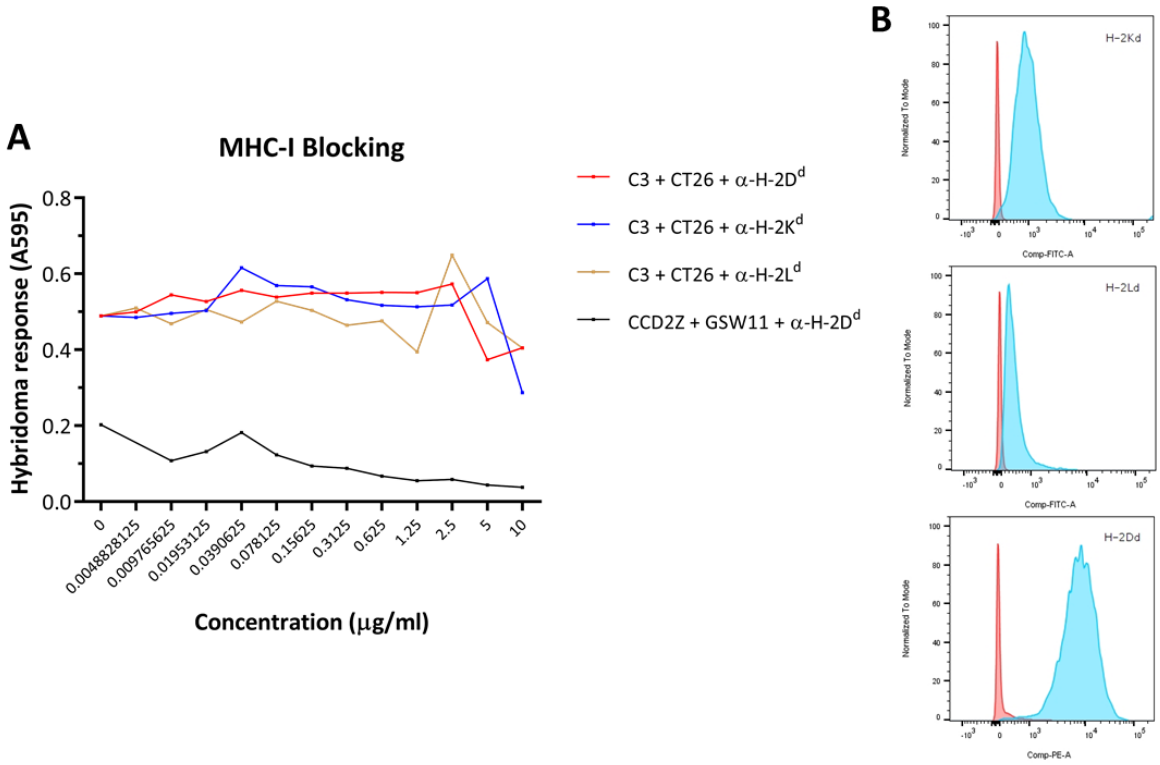

Figure 6.5 **The C3 hybridoma is not restricted by classical MHC-I molecules.A.** C3 cells were incubated with H-2D^d- (Red line), -H-2K^d- (Blue line) or H-2L^d-blocked CT26 cells overnight (Golden line) using serial dilutions of the antibodies. As a control, the CCD2Z hybridoma was incubated with H-2D^d-blocked GSW11-pulsed P815 cells (Black line). **B.** Surface expression of H-2K^d (top), H-2L^d (middle) and H-2D^d (bottom) in CT26 cells measured by flow cytometry. Red histograms represent the background fluorescence levels in unstained cells, whereas blue histograms depict the level of expression of these molecules in CT26 cells.

T cell hybridomas represent highly specific, reliable, reproducible, and useful cell lines that can be grown exponentially to screen a large number of peptides or libraries. In addition, their independence to co-stimulatory signals and the ability to quantitatively measure the TCR responses to peptide-MHC complexes in APCs, highlights the advantages of using these cell lines for the determination of novel CD8+ T cell epitopes (Canaday 2013). From the initial 672 clones derived from the fusion of CT26-activated splenocytes and BWZ.36/CD8α cells, we observed growth in 99 of them (14.7%). In similar assays performed in the group, the growth rate was between 20.3% and 26.5% (Yeh 2005), indicating that, although the current percent of positive clones is lower, it is similar to what has been previously described. Remarkably, only one of the 99 clones were specific against CT26, and did not recognize the previously described AH1 and GSW11 epitopes (**Figure 6.2**). In the experiments that led to the development of the GSW11-specific CCD2Z hybridoma, only 4 out of 192 clones was specific for CT26 (Yeh 2005), for which the low

numbers of CT26-specific clones in this study is not surprising, as not all T cell populations in spleen are specific against CT26. The development of CD8+ T cell hybridomas has been useful for the identification of new cancer epitopes, as it helped to the identification of GSW11 in CT26 (James, Yeh et al. 2010), as well as to gp100-derived peptides from the B16 melanoma model (Cafri, Sharbi-Yunger et al. 2013). Nonetheless, CD8+ T cell hybridomas present some drawbacks. These cells are not suitable to use *in vivo*, given their immortal phenotype that can lead to the development of tumours in mice (Canaday 2013). In the specific case of T cell hybridomas generated by fusing with the BW5147 cell line or derivatives (such as BWZ.36/CD8α), one cannot guarantee that the TCR observed in the fused cells are entirely derived from the T cell, as BW5147 cells still retain some components of the TCR signalling pathway (Canaday 2013). Additionally, BW5147 cells can negatively affect the immortalization of the effector function of T cells, as their genome simultaneously imposes, albeit not completely, its own programming on the hybridomas (Kubota and Iwabuchi 2014). Moreover, the antigen sensitivity of these cells is not constant, as it starts dropping after culturing for long periods of time (between 4 to 6 weeks, (Canaday 2013)), for which subcloning of the hybridomas is necessary in order to maintain a highly sensitive population. Despite all these potential disadvantages, T cell hybridomas are an easy tool to detect new epitopes in tumour models, and the development of a non-GSW11 and non-AH1 T cell hybridoma in this study represents an exciting finding that can improve our understanding about the mechanisms of immune recognition in CT26.

As an exploration about the MHC-I restriction of the newly developed C3 hybridoma, we blocked the classic H-2L^d, H-2K^d and H-2D^d molecules from CT26 cells using monoclonal antibodies prior co-culture with C3 cells. Strikingly, none of these antibodies were able to block C3 activation. The positive control for this experiment showed that culturing P815 cells with the same anti-H-2D^d antibody prior GSW11 pulse was able to block the activation of CCD2Z cells in a dose dependent fashion (**Figure 6.5**), confirming that the anti-H-2D^d clone is blocking MHC-I. Given these results, is reasonable to speculate that the C3 hybridoma is not restricted by H-2D^d; however, the lack of controls for the blocking activity of the anti-H-2L^d and anti-H-2K^d antibodies does not completely rule out that the C3 hybridoma is not restricted by these molecules. The clones of the monoclonal antibodies against H-2L^d and H-2K^d can explain these observations, as these antibodies recognize peptides located in the α3 domain of the MHC-I, and therefore do not interfere directly with TCR engagement. However, the α3 domain of MHC-I molecules is also important for the TCR signalling pathway as it interacts with CD8 leading to the recruitment of the tyrosine kinase LCK to the immunological synapse. This kinase is responsible for the phosphorylation of the immunoreceptor tyrosine-based activation motifs (ITAM) of the CD3 chains, which triggers a series of signalling events resulting in T cell activation (Gaud, Lesourne et al. 2018). As the C3 T cell hybridoma

expresses CD8α, it is imperative to determine if the signalling pathway associated with this molecule is functional in this cell line. Lastly, based on the previously mentioned data, it is plausible to infer that the C3 hybridoma is restricted by non-classical MHC-I molecules, such as H-2Qa1, H-2T1a and H-2M, as these molecules also associate with β2M and can present peptides to CD8+ T cells (Stuart 2015). Nagarajan *et al.* have shown that sensitization of WT C57BL/6 mice with ERAAP-KO splenocytes leads to the development of a Qa-1^{b}-restricted CD8+ T cell response, which was detected using a T cell hybridoma (Nagarajan, Gonzalez et al. 2012). Therefore, it is necessary to design and perform experiments to verify if the C3 hybridoma is restricted by non-classical MHC-I.

Appendix B Engineering of an H-2L^d/AH1 Single chain trimer (SCT)

SCTs represent valuable tools for the *ex vivo* monitoring of peptide-specific CD8+ T cells, as they allow to perform extensive immunophenotypic studies in T cells specific for low-affinity p/MHC-I complexes (Hansen, Connolly et al. 2010). Thus, we aimed to develop an H-2L^d/AH1 SCT, considering that an H-2D^d/GSW11 SCT previously develop in the group has facilitated the identification of low-avidity GSW11-specific CD8+ T cells that play crucial roles in tumour clearance in immunotherapy settings (Sugiyarto, Prossor et al. 2021). The first construct generated consisted of the AH1 peptide flanked between the β2M signal peptide and the peptide-β2M linker (PBM), followed by β2M, a β2M-heavy chain linker (BHL), and the H-2L^d heavy-chain sequence (**Figure 6.6** A). The H-2L^d heavy chain sequence from this construct does not include the respective signal peptide, and contains a mutation at position 83 of the heavy chain, changing a tyrosine for a cysteine, which facilitates the formation of a disulphide bridge with a cysteine in the BHL, stabilizing the union of the peptide to H-2L^d (Mitaksov, Truscott et al. 2007). This initial construct was successfully cloned into a HindIII-XhoI double digested pcDNA3.1 vector, which was further amplified and used in transfection analysis for the verification of cellular refolding of the construct. For this, the newly developed H-2L^d/AH1 SCT was transfected into HeLa cells, and the levels of cell surface H-2L^d were measured by flow cytometry, while a pcDNA3.1 vector encoding mCherry was used as a control to verify transfection efficiency. After 24hr of transfection, there were negligible levels of H-2L^d in cell surface; however, the SCT was detectable at low levels after 48hr of transfection (**Figure 6.7** A). This data is not related with a poor transfection efficiency, since the expression of mCherry was observed at each time points post-transfection (**Figure 6.7** B). Although the transfection efficiency was not high, the results obtained in this experiment suggest that the H-2L^d/AH1 SCT can be properly refolded by the cellular machinery.

Once the cellular refolding of the newly developed SCT was verified, this construct was edited to remove the β2m signal peptide and replace the H-2L^d transmembrane domain for the AviTag biotinylation sequence (**Figure 6.6** B), which was successfully inserted into the pET28a protein expression vector using overlapping-extension PCR and transformed into competent BL21(DE3)pLysS bacteria for further protein expression.

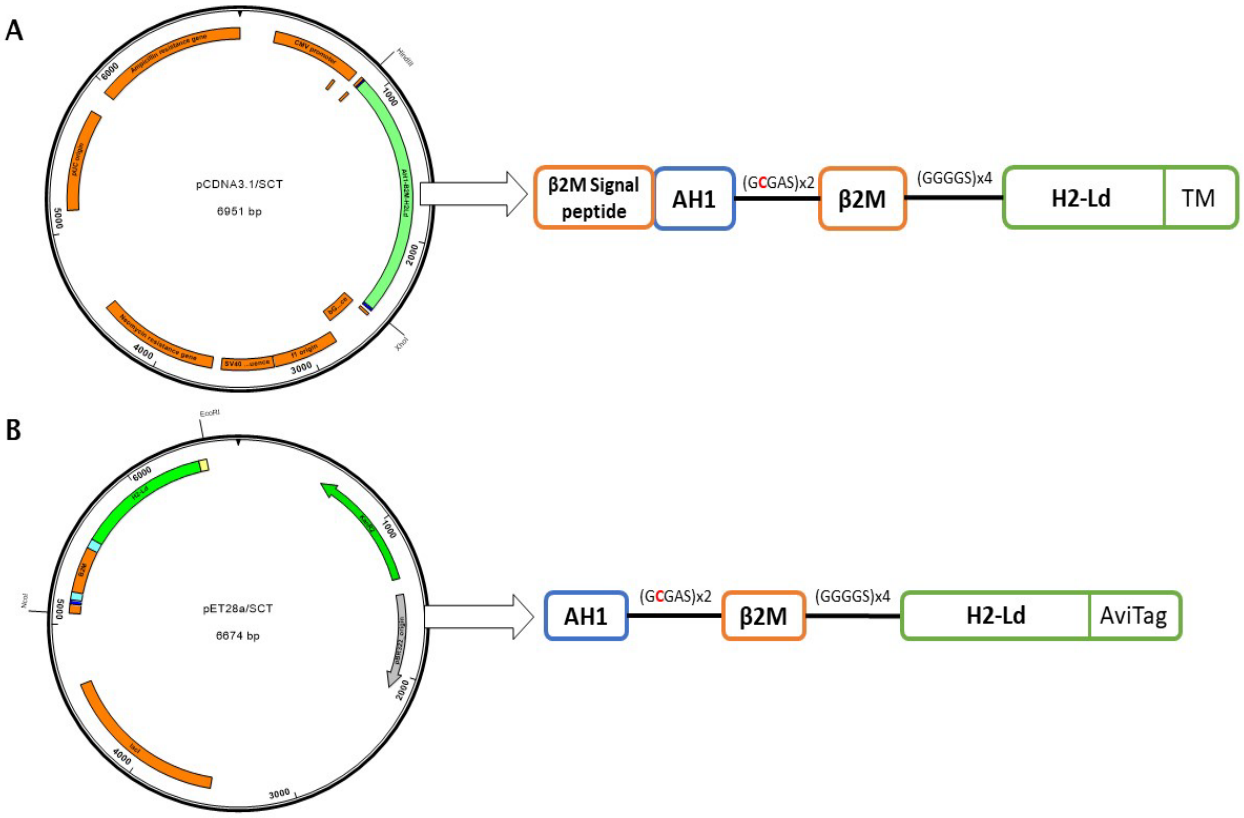

Figure 6.6 **Schematic representation of H-2L^d/AH1 SCT constructs.A.** Left: Positional location of pcDNA3.1/SCT within the pcDNA3.1 vector. Right: Detailed representation of the DNA organization of the SCT. **B.** Left: Positional location of pET28a/SCT within the pET28a vector. Right: Detailed representation of the DNA organization of the SCT. This SCT differ from the pcDNA3.1/SCT as it does not contain the β2M signal peptide, and the transmembrane domain of H-2L^d is replaced by the AviTag biotinylation sequence.

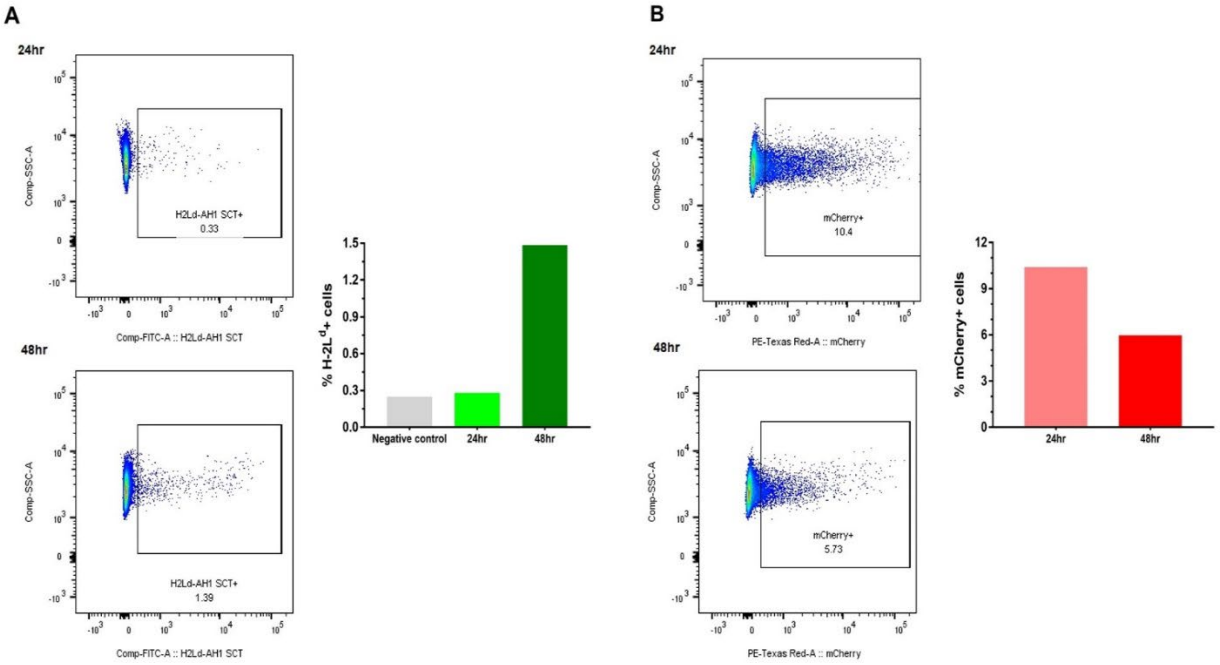

Figure 6.7 **The H-2L^d/AH1 SCT can be refolded and expressed by eucaryotic cells.A.** Left. Flow cytometry analysis of HeLa cells transfected with the H-2L^d/AH1 SCT at 24 (top) or 48 hours (bottom) post transfection, stained with a FITC-conjugated anti-H-2L^d monoclonal antibody. Right. Summary of the frequency of H-2L^d+ cells in HeLa cells after 24 or 48 hours after H-2L^d/AH1 SCT transfection, and untransfected cells as negative control. **B.** Left. Expression of mCherry after 24 (top) and 48 hours (bottom) post-transfection into HeLa cells. Right. Evaluation of transfection efficiency by the measurement of mCherry+ cells after 24 or 48 hours of transfection.

For the induction of protein expression of the H-2L^d/AH1 SCT construct, transformed BL21(DE3)pLysS bacteria were pulsed with 1mM IPTG in the exponential phase of growth, and incubated for hours at 37°C. After induction, bacteria were pelleted and protein IBs were extracted using the BugBuster protocol, as described in section 2.9.6. This initial induction protocol showed a deficient yield of the expected ~53 kDa protein (**Figure 6.8** A), as well as high abundance of contaminating proteins in the IBs that persisted after extraction (**Figure 6.8** B). Thus, we explored different conditions of IPTG induction to improve the yield and quality of the purified proteins. The first approach consisted in performing the protein induction at room temperature for the same time, in order to reduce contaminating proteins in IBs. As observed in **Figure 6.9**, this approach marginally induced the expression of the SCT construct, but significantly reduced the presence of non-specific proteins in the purified product. Consequently, all the IPTG inductions performed in subsequent experiments were performed at room temperature.

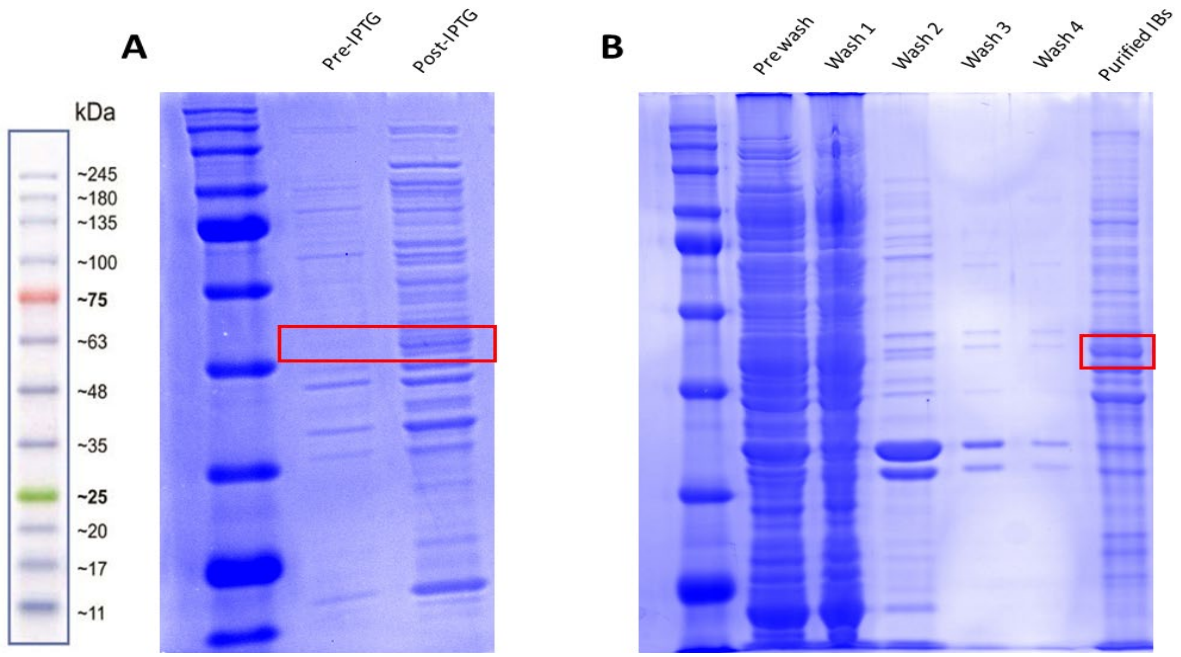

Figure 6.8 **The H-2L^d/AH1 SCT construct is not properly expressed in normal IPTG induction conditions.A.** Samples of transformed BL21(DE3)pLysS bacteria were taken before and after pulsing with 1mM IPTG. Sample volumes were normalised according to the optical density (O.D) value obtained at the moment of adding IPTG. **B.** SDS-PAGE analysis of the different washing steps during IBs extraction, and of the final purified IB product. Red squares indicate the H-2L^d/AH1 SCT proteins.

In order to determine if the final concentration of IPTG in the bacterial culture affected the expression of the H-2L^d/AH1 SCT, different concentrations of IPTG were tested at room temperature for 4 hours. Under these conditions, we observed that a final concentration of 0.5mM IPTG resulted in the highest protein expression with relatively low expression of contaminating proteins and was chosen for next assays (**Figure 6.10**). Despite the relative improvements in SCT expression, this construct was poorly solubilised using conventional urea and guanidine solubilisation buffers (**Figure 6.11** A), and the fraction of solubilised protein containing β2M was significantly underrepresented compared to the previously-developed GSW11-SCT (**Figure 6.11** B). Thus, considering these drawbacks and the prioritisation of other assays in this project, no further assays were carried out with this H-2L^d/AH1 SCT construct.

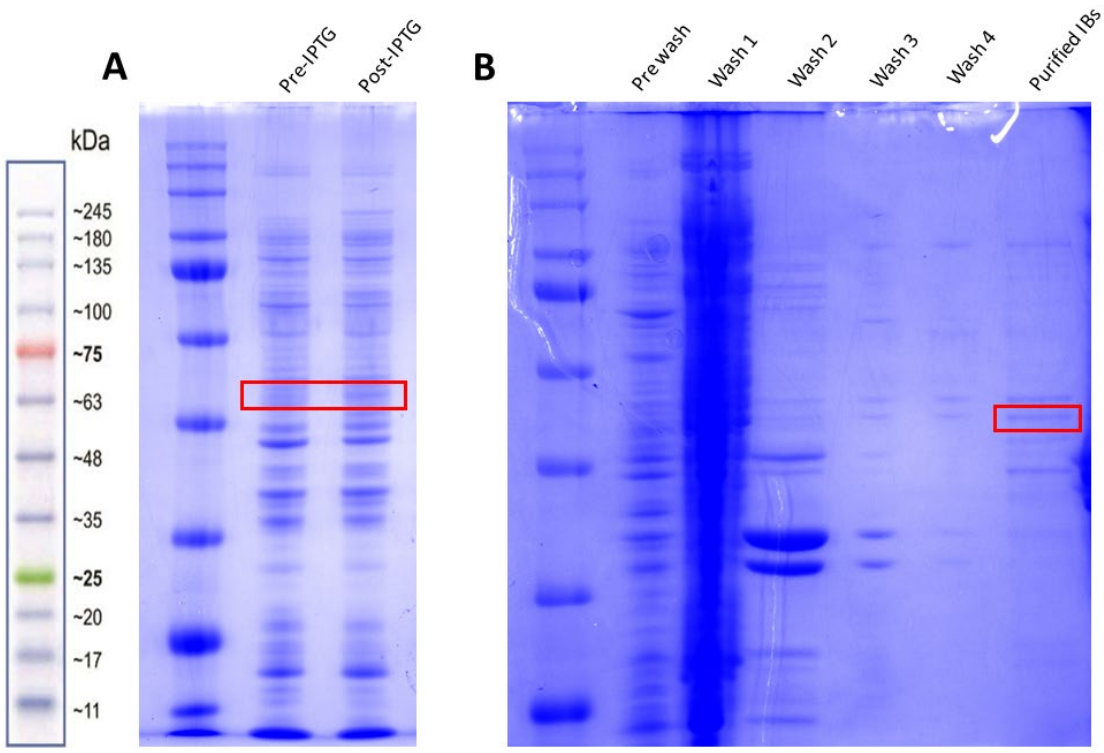

Figure 6.9 **Room temperature IPTG induction reduces background proteins in IBs.A.** Samples of transformed BL21(DE3)pLysS bacteria were taken before and after pulsing with 1mM IPTG. Sample volumes were normalised according to the O.D value obtained at the moment of adding IPTG. **B.** SDS-PAGE analysis of the different washing steps during IBs extraction, and of the final purified IB product. Red squares indicate the H-2L^{d}/AH1 SCT proteins.

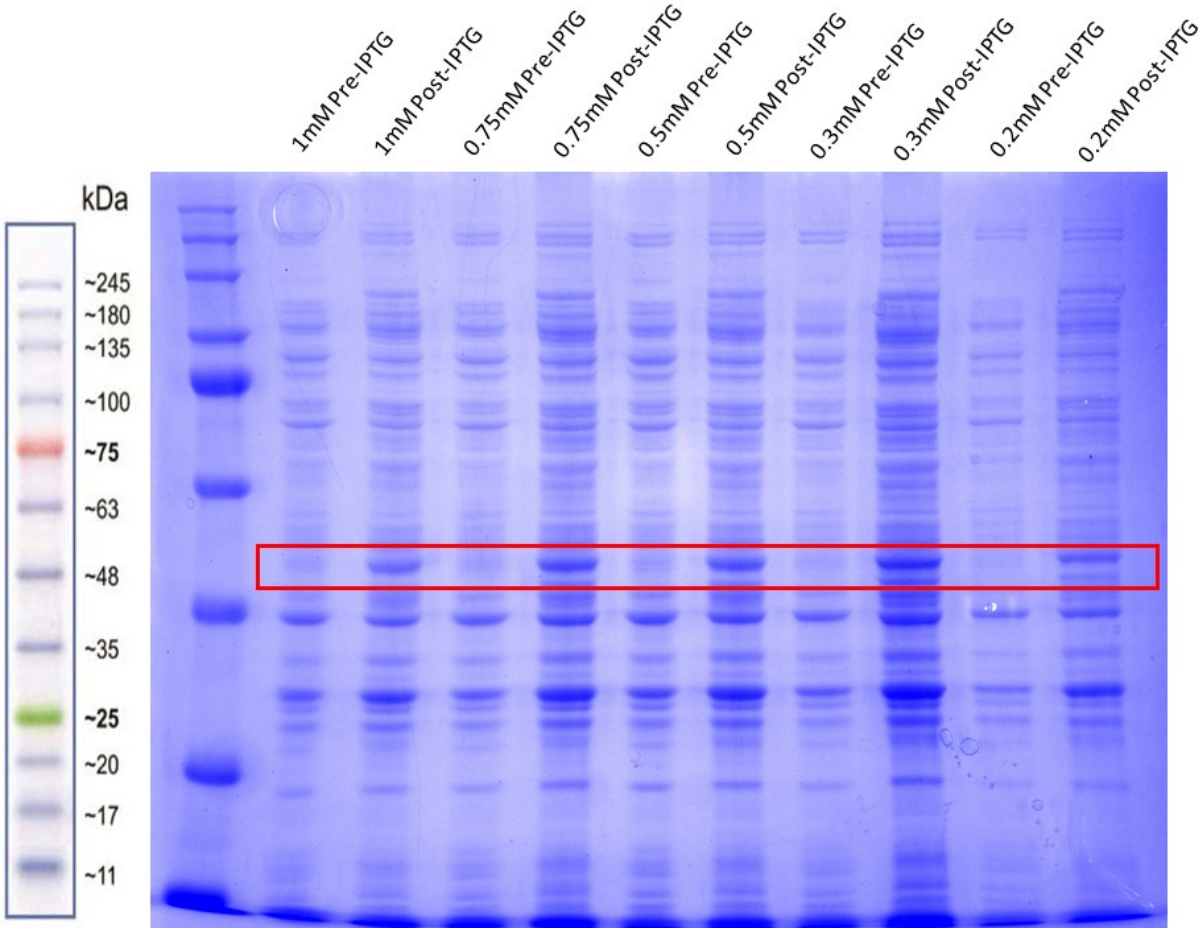

Figure 6.10 Low concentrations of IPTG results in high SCT expression. SDS-PAGE analysis of transformed BL21(DE3)pLysS bacteria pulsed with different concentrations of IPTG at room temperature for 4 hours. Red squares indicate the H-2L^{d}/AH1 SCT proteins.

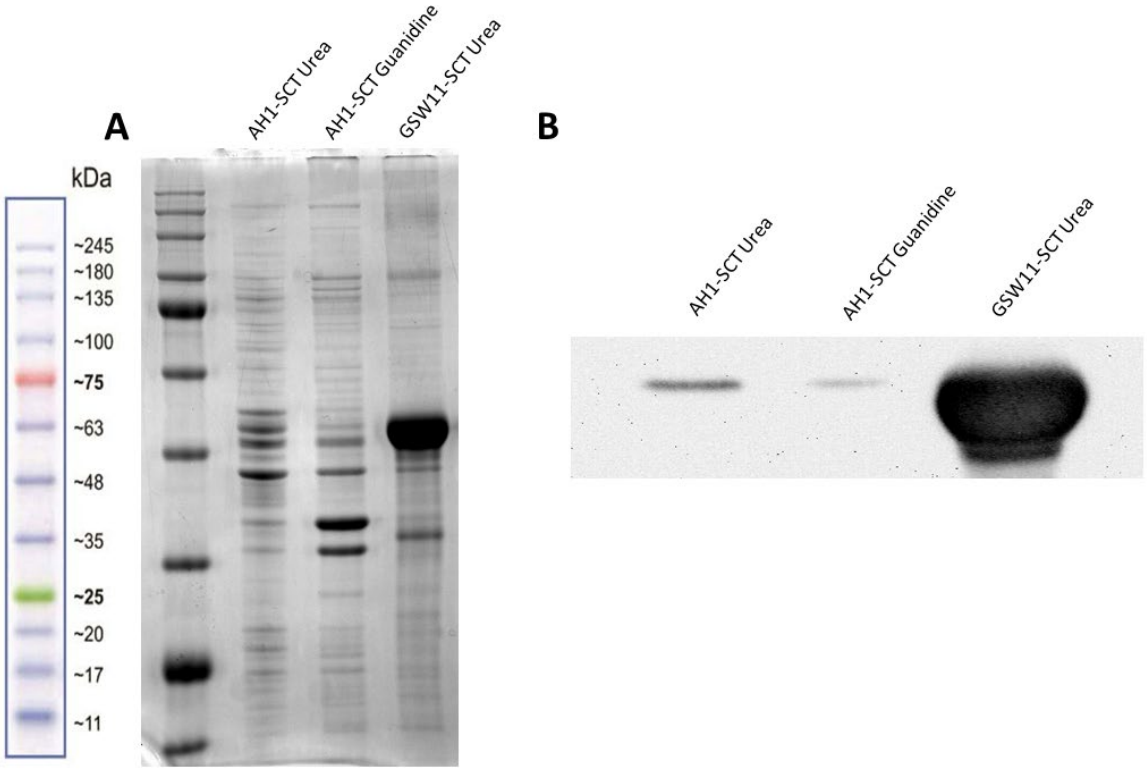

Figure 6.11 The H-2L^d/AH1 SCT construct is poorly represented in IPTG-induced IBs.A. SDS-PAGE analysis of H-2L^d/AH1 SCT solubilised with 8M urea or 8M guanidine. The H-2D^d/GSW11 SCT construct was used as comparison. **B.** Western-Blot analysis of mouse β2M in the AH1 and GSW11 IBs. In this experiment, 0.5µg of protein were loaded into each well.

Bibliography

Abdel-Hakeem, M. S., S. Manne, J. C. Beltra, E. Stelekati, Z. Chen, K. Nzingha, M. A. Ali, J. L. Johnson, J. R. Giles, D. Mathew, A. R. Greenplate, G. Vahedi and E. J. Wherry (2021). "Epigenetic scarring of exhausted T cells hinders memory differentiation upon eliminating chronic antigenic stimulation." Nat Immunol **22**(8): 1008-1019.

Abelin, J. G., D. B. Keskin, S. Sarkizova, C. R. Hartigan, W. Zhang, J. Sidney, J. Stevens, W. Lane, G. L. Zhang, T. M. Eisenhaure, K. R. Clauser, N. Hacohen, M. S. Rooney, S. A. Carr and C. J. Wu (2017). "Mass Spectrometry Profiling of HLA-Associated Peptidomes in Mono-allelic Cells Enables More Accurate Epitope Prediction." Immunity **46**(2): 315-326.

Abella, J. R., D. A. Antunes, C. Clementi and L. E. Kavraki (2020). "Large-Scale Structure-Based Prediction of Stable Peptide Binding to Class I HLAs Using Random Forests." Front Immunol **11**: 1583.

Agata, Y., A. Kawasaki, H. Nishimura, Y. Ishida, T. Tsubata, H. Yagita and T. Honjo (1996). "Expression of the PD-1 antigen on the surface of stimulated mouse T and B lymphocytes." Int Immunol **8**(5): 765-772.

Ai, W., H. Li, N. Song, L. Li and H. Chen (2013). "Optimal method to stimulate cytokine production and its use in immunotoxicity assessment." Int J Environ Res Public Health **10**(9): 3834-3842.

Andersen, M. L., M. Ruhwald, M. H. Nissen, S. Buus and M. H. Claesson (2003). "Self-peptides with intermediate capacity to bind and stabilize MHC class I molecules may be immunogenic." Scand J Immunol **57**(1): 21-27.

Andreatta, M. and M. Nielsen (2016). "Gapped sequence alignment using artificial neural networks: application to the MHC class I system." Bioinformatics **32**(4): 511-517.

Angelova, M., P. Charoentong, H. Hackl, M. L. Fischer, R. Snajder, A. M. Krogsdam, M. J. Waldner, G. Bindea, B. Mlecnik, J. Galon and Z. Trajanoski (2015). "Characterization of the immunophenotypes and antigenomes of colorectal cancers reveals distinct tumor escape mechanisms and novel targets for immunotherapy." Genome Biol **16**: 64.

Annibaldi, A. and H. Walczak (2020). "Death Receptors and Their Ligands in Inflammatory Disease and Cancer." Cold Spring Harb Perspect Biol **12**(9).

Appay, V., D. C. Douek and D. A. Price (2008). "CD8+ T cell efficacy in vaccination and disease." Nat Med **14**(6): 623-628.

Arce Vargas, F., A. J. S. Furness, I. Solomon, K. Joshi, L. Mekkaoui, M. H. Lesko, E. Miranda Rota, R. Dahan, A. Georgiou, A. Sledzinska, A. Ben Aissa, D. Franz, M. Werner Sunderland, Y. N. S. Wong, J. Y. Henry, T. O'Brien, D. Nicol, B. Challacombe, S. A. Beers, T. C. Melanoma, T. C. Renal, T. C. Lung, S. Turajlic, M. Gore, J. Larkin, C. Swanton, K. A. Chester, M. Pule, J. V. Ravetch, T. Marafioti, K. S. Peggs and S. A. Quezada (2017). "Fc-Optimized Anti-CD25 Depletes Tumor-Infiltrating Regulatory T Cells and Synergizes with PD-1 Blockade to Eradicate Established Tumors." Immunity **46**(4): 577-586.

Ayers, M., J. Lunceford, M. Nebozhyn, E. Murphy, A. Loboda, D. R. Kaufman, A. Albright, J. D. Cheng, S. P. Kang, V. Shankaran, S. A. Piha-Paul, J. Yearley, T. Y. Seiwert, A. Ribas and T. K. McClanahan (2017). "IFN-gamma-related mRNA profile predicts clinical response to PD-1 blockade." J Clin Invest **127**(8): 2930-2940.

Azizi, E., A. J. Carr, G. Plitas, A. E. Cornish, C. Konopacki, S. Prabhakaran, J. Nainys, K. Wu, V. Kiseliovas, M. Setty, K. Choi, R. M. Fromme, P. Dao, P. T. McKenney, R. C. Wasti, K. Kadaveru, L. Mazutis, A. Y. Rudensky and D. Pe'er (2018). "Single-Cell Map of Diverse Immune Phenotypes in the Breast Tumor Microenvironment." Cell **174**(5): 1293-1308 e1236.

Baumgaertner, P., C. Costa Nunes, A. Cachot, H. Maby-El Hajjami, L. Cagnon, M. Braun, L. Derre, J. P. Rivals, D. Rimoldi, S. Gnjatic, S. Abed Maillard, P. Marcos Mondejar, M. P. Protti, E. Romano, O. Michielin, P. Romero, D. E. Speiser and C. Jandus (2016). "Vaccination of stage III/IV melanoma patients with long NY-ESO-1 peptide and CpG-B elicits robust CD8(+) and CD4(+) T-cell responses with multiple specificities including a novel DR7-restricted epitope." Oncoimmunology **5**(10): e1216290.

Beckett, D., E. Kovaleva and P. J. Schatz (1999). "A minimal peptide substrate in biotin holoenzyme synthetase-catalyzed biotinylation." Protein Sci **8**(4): 921-929.

Beckhove, P., M. Feuerer, M. Dolenc, F. Schuetz, C. Choi, N. Sommerfeldt, J. Schwendemann, K. Ehlert, P. Altevogt, G. Bastert, V. Schirrmacher and V. Umansky (2004). "Specifically activated memory T cell subsets from cancer patients recognize and reject xenotransplanted autologous tumors." J Clin Invest **114**(1): 67-76.

Beltra, J. C., S. Manne, M. S. Abdel-Hakeem, M. Kurachi, J. R. Giles, Z. Chen, V. Casella, S. F. Ngiow, O. Khan, Y. J. Huang, P. Yan, K. Nzingha, W. Xu, R. K. Amaravadi, X. Xu, G. C. Karakousis, T. C. Mitchell, L. M. Schuchter, A. C. Huang and E. J. Wherry (2020). "Developmental Relationships of Four Exhausted CD8(+) T Cell Subsets Reveals Underlying Transcriptional and Epigenetic Landscape Control Mechanisms." Immunity **52**(5): 825-841 e828.

Bhat, M. Y., H. S. Solanki, J. Advani, A. A. Khan, T. S. Keshava Prasad, H. Gowda, S. Thiyagarajan and A. Chatterjee (2018). "Comprehensive network map of interferon gamma signaling." J Cell Commun Signal **12**(4): 745-751.

Binnewies, M., A. M. Mujal, J. L. Pollack, A. J. Combes, E. A. Hardison, K. C. Barry, J. Tsui, M. K. Ruhland, K. Kersten, M. A. Abushawish, M. Spasic, J. P. Giurintano, V. Chan, A. I. Daud, P. Ha, C. J. Ye, E. W. Roberts and M. F. Krummel (2019). "Unleashing Type-2 Dendritic Cells to Drive Protective Antitumor CD4(+) T Cell Immunity." Cell **177**(3): 556-571 e516.

Blackburn, S. D., H. Shin, G. J. Freeman and E. J. Wherry (2008). "Selective expansion of a subset of exhausted CD8 T cells by alphaPD-L1 blockade." Proc Natl Acad Sci U S A **105**(39): 15016-15021.

Blass, E. and P. A. Ott (2021). "Advances in the development of personalized neoantigen-based therapeutic cancer vaccines." Nat Rev Clin Oncol **18**(4): 215-229.

Boulanger, D. S. M., R. C. Eccleston, A. Phillips, P. V. Coveney, T. Elliott and N. Dalchau (2018). "A Mechanistic Model for Predicting Cell Surface Presentation of Competing Peptides by MHC Class I Molecules." Front Immunol **9**: 1538.

Brummelman, J., E. M. C. Mazza, G. Alvisi, F. S. Colombo, A. Grilli, J. Mikulak, D. Mavilio, M. Alloisio, F. Ferrari, E. Lopci, P. Novellis, G. Veronesi and E. Lugli (2018). "High-dimensional single cell analysis identifies stem-like cytotoxic CD8(+) T cells infiltrating human tumors." J Exp Med **215**(10): 2520-2535.

Brunet, J. F., F. Denizot, M. F. Luciani, M. Roux-Dosseto, M. Suzan, M. G. Mattei and P. Golstein (1987). "A new member of the immunoglobulin superfamily--CTLA-4." Nature **328**(6127): 267-270.

Bulik-Sullivan, B., J. Busby, C. D. Palmer, M. J. Davis, T. Murphy, A. Clark, M. Busby, F. Duke, A. Yang, L. Young, N. C. Ojo, K. Caldwell, J. Abhyankar, T. Boucher, M. G. Hart, V. Makarov, V. T. Montpreville, O. Mercier, T. A. Chan, G. Scagliotti, P. Bironzo, S. Novello, N. Karachaliou, R. Rosell, I. Anderson, N. Gabrail, J. Hrom, C. Limvarapuss, K. Choquette, A. Spira, R. Rousseau, C. Voong, N.

A. Rizvi, E. Fadel, M. Frattini, K. Jooss, M. Skoberne, J. Francis and R. Yelensky (2018). "Deep learning using tumor HLA peptide mass spectrometry datasets improves neoantigen identification." Nat Biotechnol.

Buonaguro, L., A. Petrizzo, M. L. Tornesello and F. M. Buonaguro (2011). "Translating tumor antigens into cancer vaccines." Clin Vaccine Immunol **18**(1): 23-34.

Burnet, F. M. (1970). "The concept of immunological surveillance." Prog Exp Tumor Res **13**: 1-27.

Butterfield, L. H., A. Ribas, V. B. Dissette, S. N. Amarnani, H. T. Vu, D. Oseguera, H. J. Wang, R. M. Elashoff, W. H. McBride, B. Mukherji, A. J. Cochran, J. A. Glaspy and J. S. Economou (2003). "Determinant spreading associated with clinical response in dendritic cell-based immunotherapy for malignant melanoma." Clin Cancer Res **9**(3): 998-1008.

Cabrita, R., M. Lauss, A. Sanna, M. Donia, M. Skaarup Larsen, S. Mitra, I. Johansson, B. Phung, K. Harbst, J. Vallon-Christersson, A. van Schoiack, K. Lovgren, S. Warren, K. Jirstrom, H. Olsson, K. Pietras, C. Ingvar, K. Isaksson, D. Schadendorf, H. Schmidt, L. Bastholt, A. Carneiro, J. A. Wargo, I. M. Svane and G. Jonsson (2020). "Tertiary lymphoid structures improve immunotherapy and survival in melanoma." Nature **577**(7791): 561-565.

Cafri, G., A. Sharbi-Yunger, E. Tzehoval and L. Eisenbach (2013). "Production of LacZ inducible T cell hybridoma specific for human and mouse gp100(2)(5)(-)(3)(3) peptides." PLoS One **8**(2): e55583.

Calis, J. J., M. Maybeno, J. A. Greenbaum, D. Weiskopf, A. D. De Silva, A. Sette, C. Kesmir and B. Peters (2013). "Properties of MHC class I presented peptides that enhance immunogenicity." PLoS Comput Biol **9**(10): e1003266.

Campbell, D. J. and M. A. Koch (2011). "Phenotypical and functional specialization of FOXP3+ regulatory T cells." Nat Rev Immunol **11**(2): 119-130.

Canaday, D. H. (2013). "Production of CD4(+) and CD8(+) T cell hybridomas." Methods Mol Biol **960**: 297-307.

Castle, J. C., M. Loewer, S. Boegel, J. de Graaf, C. Bender, A. D. Tadmor, V. Boisguerin, T. Bukur, P. Sorn, C. Paret, M. Diken, S. Kreiter, O. Tureci and U. Sahin (2014). "Immunomic, genomic and transcriptomic characterization of CT26 colorectal carcinoma." BMC Genomics **15**: 190.

Castro, A., K. Ozturk, R. M. Pyke, S. Xian, M. Zanetti and H. Carter (2019). "Elevated neoantigen levels in tumors with somatic mutations in the HLA-A, HLA-B, HLA-C and B2M genes." BMC Med Genomics **12**(Suppl 6): 107.

Chabner, B. A. and T. G. Roberts, Jr. (2005). "Timeline: Chemotherapy and the war on cancer." Nat Rev Cancer **5**(1): 65-72.

Chan, T. A., M. Yarchoan, E. Jaffee, C. Swanton, S. A. Quezada, A. Stenzinger and S. Peters (2019). "Development of tumor mutation burden as an immunotherapy biomarker: utility for the oncology clinic." Ann Oncol **30**(1): 44-56.

Chang, H. F., H. Bzeih, C. Schirra, P. Chitirala, M. Halimani, E. Cordat, E. Krause, J. Rettig and V. Pattu (2016). "Endocytosis of Cytotoxic Granules Is Essential for Multiple Killing of Target Cells by T Lymphocytes." J Immunol **197**(6): 2473-2484.

Chao, J. L. and P. A. Savage (2018). "Unlocking the Complexities of Tumor-Associated Regulatory T Cells." J Immunol **200**(2): 415-421.

Chen, D. S. and I. Mellman (2013). "Oncology meets immunology: the cancer-immunity cycle." Immunity **39**(1): 1-10.

Cherkasova, E., C. Scrivani, S. Doh, Q. Weisman, Y. Takahashi, N. Harashima, H. Yokoyama, R. Srinivasan, W. M. Linehan, M. I. Lerman and R. W. Childs (2016). "Detection of an Immunogenic HERV-E Envelope with Selective Expression in Clear Cell Kidney Cancer." Cancer Res **76**(8): 2177-2185.

Chew, G. L., A. E. Campbell, E. De Neef, N. A. Sutliff, S. C. Shadle, S. J. Tapscott and R. K. Bradley (2019). "DUX4 Suppresses MHC Class I to Promote Cancer Immune Evasion and Resistance to Checkpoint Blockade." Dev Cell **50**(5): 658-671 e657.

Chiang, M. C., K. M. Tullett, Y. S. Lee, A. Idris, Y. Ding, K. J. McDonald, A. Kassianos, I. M. Leal Rojas, V. Jeet, M. H. Lahoud and K. J. Radford (2016). "Differential uptake and cross-presentation of soluble and necrotic cell antigen by human DC subsets." Eur J Immunol **46**(2): 329-339.

Christophersen, A. (2020). "Peptide-MHC class I and class II tetramers: From flow to mass cytometry." HLA **95**(3): 169-178.

Clancy-Thompson, E., C. A. Devlin, P. M. Tyler, M. M. Servos, L. R. Ali, K. S. Ventre, M. A. Bhuiyan, P. T. Bruck, M. E. Birnbaum and S. K. Dougan (2018). "Altered Binding of Tumor Antigenic Peptides to MHC Class I Affects CD8(+) T Cell-Effector Responses." Cancer Immunol Res **6**(12): 1524-1536.

Clarke, J., B. Panwar, A. Madrigal, D. Singh, R. Gujar, O. Wood, S. J. Chee, S. Eschweiler, E. V. King, A. S. Awad, C. J. Hanley, K. J. McCann, S. Bhattacharyya, E. Woo, A. Alzetani, G. Seumois, G. J. Thomas, A. P. Ganesan, P. S. Friedmann, T. Sanchez-Elsner, F. Ay, C. H. Ottensmeier and P. Vijayanand (2019). "Single-cell transcriptomic analysis of tissue-resident memory T cells in human lung cancer." J Exp Med **216**(9): 2128-2149.

Colvin, R. A., G. S. Campanella, J. Sun and A. D. Luster (2004). "Intracellular domains of CXCR3 that mediate CXCL9, CXCL10, and CXCL11 function." J Biol Chem **279**(29): 30219-30227.

Corr, M., L. F. Boyd, S. R. Frankel, S. Kozlowski, E. A. Padlan and D. H. Margulies (1992). "Endogenous peptides of a soluble major histocompatibility complex class I molecule, H-2Lds: sequence motif, quantitative binding, and molecular modeling of the complex." J Exp Med **176**(6): 1681-1692.

Corr, M., L. F. Boyd, E. A. Padlan and D. H. Margulies (1993). "H-2Dd exploits a four residue peptide binding motif." J Exp Med **178**(6): 1877-1892.

Coulie, P. G., B. J. Van den Eynde, P. van der Bruggen and T. Boon (2014). "Tumour antigens recognized by T lymphocytes: at the core of cancer immunotherapy." Nat Rev Cancer **14**(2): 135-146.

Couzin-Frankel, J. (2013). "Breakthrough of the year 2013. Cancer immunotherapy." Science **342**(6165): 1432-1433.

Cretney, E., K. Takeda, H. Yagita, M. Glaccum, J. J. Peschon and M. J. Smyth (2002). "Increased susceptibility to tumor initiation and metastasis in TNF-related apoptosis-inducing ligand-deficient mice." J Immunol **168**(3): 1356-1361.

Crooks, G. E., G. Hon, J. M. Chandonia and S. E. Brenner (2004). "WebLogo: a sequence logo generator." Genome Res **14**(6): 1188-1190.

Cukalac, T., J. Chadderton, W. Zeng, J. G. Cullen, W. T. Kan, P. C. Doherty, D. C. Jackson, S. J. Turner and N. L. La Gruta (2014). "The influenza virus-specific CTL immunodominance hierarchy in mice is determined by the relative frequency of high-avidity T cells." J Immunol **192**(9): 4061-4068.

Dalchau, N., A. Phillips, L. D. Goldstein, M. Howarth, L. Cardelli, S. Emmott, T. Elliott and J. M. Werner (2011). "A peptide filtering relation quantifies MHC class I peptide optimization." PLoS Comput Biol **7**(10): e1002144.

Dammeijer, F., M. van Gulijk, E. E. Mulder, M. Lukkes, L. Klaase, T. van den Bosch, M. van Nimwegen, S. P. Lau, K. Latupeirissa, S. Schetters, Y. van Kooyk, L. Boon, A. Moyaart, Y. M. Mueller, P. D. Katsikis, A. M. Eggermont, H. Vroman, R. Stadhouders, R. W. Hendriks, J. V. Thusen, D. J. Grunhagen, C. Verhoef, T. van Hall and J. G. Aerts (2020). "The PD-1/PD-L1-Checkpoint Restrains T cell Immunity in Tumor-Draining Lymph Nodes." Cancer Cell **38**(5): 685-700 e688.

Das, K., D. Eisel, M. Vormehr, K. Muller-Decker, A. Hommertgen, D. Jager, I. Zornig, M. Feuerer, A. Kopp-Schneider, W. Osen and S. B. Eichmuller (2019). "A transplantable tumor model allowing investigation of NY-BR-1-specific T cell responses in HLA-DRB1*0401 transgenic mice." BMC Cancer **19**(1): 914.

Davis, J. E., M. J. Smyth and J. A. Trapani (2001). "Granzyme A and B-deficient killer lymphocytes are defective in eliciting DNA fragmentation but retain potent in vivo anti-tumor capacity." Eur J Immunol **31**(1): 39-47.

de Saint Basile, G., G. Menasche and A. Fischer (2010). "Molecular mechanisms of biogenesis and exocytosis of cytotoxic granules." Nat Rev Immunol **10**(8): 568-579.

De Silva, A. D., A. Boesteanu, R. Song, N. Nagy, E. Harhaj, C. V. Harding and S. Joyce (1999). "Thermolabile H-2Kb molecules expressed by transporter associated with antigen processing-deficient RMA-S cells are occupied by low-affinity peptides." J Immunol **163**(8): 4413-4420.

DeLeo, A. B., H. Shiku, T. Takahashi, M. John and L. J. Old (1977). "Cell surface antigens of chemically induced sarcomas of the mouse. I. Murine leukemia virus-related antigens and alloantigens on cultured fibroblasts and sarcoma cells: description of a unique antigen on BALB/c Meth A sarcoma." J Exp Med **146**(3): 720-734.

Dersh, D., J. Holly and J. W. Yewdell (2021). "A few good peptides: MHC class I-based cancer immunosurveillance and immunoevasion." Nat Rev Immunol **21**(2): 116-128.

Dhanda, S. K., S. Mahajan, S. Paul, Z. Yan, H. Kim, M. C. Jespersen, V. Jurtz, M. Andreatta, J. A. Greenbaum, P. Marcatili, A. Sette, M. Nielsen and B. Peters (2019). "IEDB-AR: immune epitope database-analysis resource in 2019." Nucleic Acids Res **47**(W1): W502-W506.

Dhatchinamoorthy, K., J. D. Colbert and K. L. Rock (2021). "Cancer Immune Evasion Through Loss of MHC Class I Antigen Presentation." Front Immunol **12**: 636568.

Di Caro, G., F. Bergomas, F. Grizzi, A. Doni, P. Bianchi, A. Malesci, L. Laghi, P. Allavena, A. Mantovani and F. Marchesi (2014). "Occurrence of tertiary lymphoid tissue is associated with T-cell infiltration and predicts better prognosis in early-stage colorectal cancers." Clin Cancer Res **20**(8): 2147-2158.

Dighe, A. S., E. Richards, L. J. Old and R. D. Schreiber (1994). "Enhanced in vivo growth and resistance to rejection of tumor cells expressing dominant negative IFN gamma receptors." Immunity **1**(6): 447-456.

Djenidi, F., J. Adam, A. Goubar, A. Durgeau, G. Meurice, V. de Montpreville, P. Validire, B. Besse and F. Mami-Chouaib (2015). "CD8+CD103+ tumor-infiltrating lymphocytes are tumor-specific tissue-resident memory T cells and a prognostic factor for survival in lung cancer patients." J Immunol **194**(7): 3475-3486.

Dolina, J. S., N. Van Braeckel-Budimir, G. D. Thomas and S. Salek-Ardakani (2021). "CD8(+) T Cell Exhaustion in Cancer." Front Immunol **12**: 715234.

Dong, H., S. E. Strome, D. R. Salomao, H. Tamura, F. Hirano, D. B. Flies, P. C. Roche, J. Lu, G. Zhu, K. Tamada, V. A. Lennon, E. Celis and L. Chen (2002). "Tumor-associated B7-H1 promotes T-cell apoptosis: a potential mechanism of immune evasion." Nat Med **8**(8): 793-800.

Du, X., F. Tang, M. Liu, J. Su, Y. Zhang, W. Wu, M. Devenport, C. A. Lazarski, P. Zhang, X. Wang, P. Ye, C. Wang, E. Hwang, T. Zhu, T. Xu, P. Zheng and Y. Liu (2018). "A reappraisal of CTLA-4 checkpoint blockade in cancer immunotherapy." Cell Res **28**(4): 416-432.

Duan, F., J. Duitama, S. Al Seesi, C. M. Ayres, S. A. Corcelli, A. P. Pawashe, T. Blanchard, D. McMahon, J. Sidney, A. Sette, B. M. Baker, Mandoiu, II and P. K. Srivastava (2014). "Genomic and bioinformatic profiling of mutational neoepitopes reveals new rules to predict anticancer immunogenicity." J Exp Med **211**(11): 2231-2248.

Dunn, G. P., A. T. Bruce, H. Ikeda, L. J. Old and R. D. Schreiber (2002). "Cancer immunoediting: from immunosurveillance to tumor escape." Nat Immunol **3**(11): 991-998.

Dunn, G. P., C. M. Koebel and R. D. Schreiber (2006). "Interferons, immunity and cancer immunoediting." Nat Rev Immunol **6**(11): 836-848.

Duraiswamy, J., K. M. Kaluza, G. J. Freeman and G. Coukos (2013). "Dual blockade of PD-1 and CTLA-4 combined with tumor vaccine effectively restores T-cell rejection function in tumors." Cancer Res **73**(12): 3591-3603.

Dutoit, V., V. Rubio-Godoy, P. Y. Dietrich, A. L. Quiqueres, V. Schnuriger, D. Rimoldi, D. Lienard, D. Speiser, P. Guillaume, P. Batard, J. C. Cerottini, P. Romero and D. Valmori (2001). "Heterogeneous T-cell response to MAGE-A10(254-262): high avidity-specific cytolytic T lymphocytes show superior antitumor activity." Cancer Res **61**(15): 5850-5856.

Ebrahimi-Nik, H., J. Michaux, W. L. Corwin, G. L. Keller, T. Shcheglova, H. Pak, G. Coukos, B. M. Baker, Mandoiu, II, M. Bassani-Sternberg and P. K. Srivastava (2019). "Mass spectrometry driven exploration reveals nuances of neoepitope-driven tumor rejection." JCI Insight **5**.

Enamorado, M., S. Iborra, E. Priego, F. J. Cueto, J. A. Quintana, S. Martinez-Cano, E. Mejias-Perez, M. Esteban, I. Melero, A. Hidalgo and D. Sancho (2017). "Enhanced anti-tumour immunity requires the interplay between resident and circulating memory CD8(+) T cells." Nat Commun **8**: 16073.

Engels, B., V. H. Engelhard, J. Sidney, A. Sette, D. C. Binder, R. B. Liu, D. M. Kranz, S. C. Meredith, D. A. Rowley and H. Schreiber (2013). "Relapse or eradication of cancer is predicted by peptide-major histocompatibility complex affinity." Cancer Cell **23**(4): 516-526.

Erkes, D. A., C. J. Smith, N. A. Wilski, S. Caldeira-Dantas, T. Mohgbeli and C. M. Snyder (2017). "Virus-Specific CD8(+) T Cells Infiltrate Melanoma Lesions and Retain Function Independently of PD-1 Expression." J Immunol **198**(7): 2979-2988.

Eroglu, Z., D. W. Kim, X. Wang, L. H. Camacho, B. Chmielowski, E. Seja, A. Villanueva, K. Ruchalski, J. A. Glaspy, K. B. Kim, W. J. Hwu and A. Ribas (2015). "Long term survival with cytotoxic T lymphocyte-associated antigen 4 blockade using tremelimumab." Eur J Cancer **51**(17): 2689-2697.

Facciabene, A., G. T. Motz and G. Coukos (2012). "T-regulatory cells: key players in tumor immune escape and angiogenesis." Cancer Res **72**(9): 2162-2171.

Fairfax, B. P., C. A. Taylor, R. A. Watson, I. Nassiri, S. Danielli, H. Fang, E. A. Mahe, R. Cooper, V. Woodcock, Z. Traill, M. H. Al-Mossawi, J. C. Knight, P. Klenerman, M. Payne and M. R. Middleton (2020). "Peripheral CD8(+) T cell characteristics associated with durable responses to immune checkpoint blockade in patients with metastatic melanoma." Nat Med **26**(2): 193-199.

Fehlings, M., Y. Simoni, H. L. Penny, E. Becht, C. Y. Loh, M. M. Gubin, J. P. Ward, S. C. Wong, R. D. Schreiber and E. W. Newell (2017). "Checkpoint blockade immunotherapy reshapes the high-dimensional phenotypic heterogeneity of murine intratumoural neoantigen-specific CD8(+) T cells." Nat Commun **8**(1): 562.

Finnberg, N., A. J. Klein-Szanto and W. S. El-Deiry (2008). "TRAIL-R deficiency in mice promotes susceptibility to chronic inflammation and tumorigenesis." J Clin Invest **118**(1): 111-123.

Forde, P. M., J. E. Chaft, K. N. Smith, V. Anagnostou, T. R. Cottrell, M. D. Hellmann, M. Zahurak, S. C. Yang, D. R. Jones, S. Broderick, R. J. Battafarano, M. J. Velez, N. Rekhtman, Z. Olah, J. Naidoo, K. A. Marrone, F. Verde, H. Guo, J. Zhang, J. X. Caushi, H. Y. Chan, J. W. Sidhom, R. B. Scharpf, J. White, E. Gabrielson, H. Wang, G. L. Rosner, V. Rusch, J. D. Wolchok, T. Merghoub, J. M. Taube, V. E. Velculescu, S. L. Topalian, J. R. Brahmer and D. M. Pardoll (2018). "Neoadjuvant PD-1 Blockade in Resectable Lung Cancer." N Engl J Med **378**(21): 1976-1986.

Fourcade, J., Z. Sun, M. Benallaoua, P. Guillaume, I. F. Luescher, C. Sander, J. M. Kirkwood, V. Kuchroo and H. M. Zarour (2010). "Upregulation of Tim-3 and PD-1 expression is associated with tumor antigen-specific CD8+ T cell dysfunction in melanoma patients." J Exp Med **207**(10): 2175-2186.

Francisco, L. M., P. T. Sage and A. H. Sharpe (2010). "The PD-1 pathway in tolerance and autoimmunity." Immunol Rev **236**: 219-242.

Franciszkiewicz, K., A. Le Floc'h, M. Boutet, I. Vergnon, A. Schmitt and F. Mami-Chouaib (2013). "CD103 or LFA-1 engagement at the immune synapse between cytotoxic T cells and tumor cells promotes maturation and regulates T-cell effector functions." Cancer Res **73**(2): 617-628.

Fraser, J. D. (2011). "Clarifying the mechanism of superantigen toxicity." PLoS Biol **9**(9): e1001145.

Freeman, G. J., A. J. Long, Y. Iwai, K. Bourque, T. Chernova, H. Nishimura, L. J. Fitz, N. Malenkovich, T. Okazaki, M. C. Byrne, H. F. Horton, L. Fouser, L. Carter, V. Ling, M. R. Bowman, B. M. Carreno, M. Collins, C. R. Wood and T. Honjo (2000). "Engagement of the PD-1 immunoinhibitory receptor by a novel B7 family member leads to negative regulation of lymphocyte activation." J Exp Med **192**(7): 1027-1034.

Fritsch, E. F., M. Rajasagi, P. A. Ott, V. Brusic, N. Hacohen and C. J. Wu (2014). "HLA-binding properties of tumor neoepitopes in humans." Cancer Immunol Res **2**(6): 522-529.

Future II Study Group (2007). "Quadrivalent vaccine against human papillomavirus to prevent high-grade cervical lesions." N Engl J Med **356**(19): 1915-1927.

Galluzzi, L., E. Vacchelli, J. M. Bravo-San Pedro, A. Buque, L. Senovilla, E. E. Baracco, N. Bloy, F. Castoldi, J. P. Abastado, P. Agostinis, R. N. Apte, F. Aranda, M. Ayyoub, P. Beckhove, J. Y. Blay, L. Bracci, A. Caignard, C. Castelli, F. Cavallo, E. Celis, V. Cerundolo, A. Clayton, M. P. Colombo, L. Coussens, M. V. Dhodapkar, A. M. Eggermont, D. T. Fearon, W. H. Fridman, J. Fucikova, D. I. Gabrilovich, J. Galon, A. Garg, F. Ghiringhelli, G. Giaccone, E. Gilboa, S. Gnjatic, A. Hoos, A. Hosmalin, D. Jager, P. Kalinski, K. Karre, O. Kepp, R. Kiessling, J. M. Kirkwood, E. Klein, A. Knuth, C. E. Lewis, R. Liblau, M. T. Lotze, E. Lugli, J. P. Mach, F. Mattei, D. Mavilio, I. Melero, C. J. Melief, E. A. Mittendorf, L. Moretta, A. Odunsi, H. Okada, A. K. Palucka, M. E. Peter, K. J. Pienta, A. Porgador, G. C. Prendergast, G. A. Rabinovich, N. P. Restifo, N. Rizvi, C. Sautes-Fridman, H. Schreiber, B. Seliger, H. Shiku, B. Silva-Santos, M. J. Smyth, D. E. Speiser, R. Spisek, P. K. Srivastava, J. E. Talmadge, E. Tartour, S. H. Van Der Burg, B. J. Van Den Eynde, R. Vile, H. Wagner, J. S. Weber, T. L. Whiteside, J. D. Wolchok, L. Zitvogel, W. Zou and G. Kroemer (2014). "Classification of current anticancer immunotherapies." Oncotarget **5**(24): 12472-12508.

Ganesan, A. P., J. Clarke, O. Wood, E. M. Garrido-Martin, S. J. Chee, T. Mellows, D. Samaniego-Castruita, D. Singh, G. Seumois, A. Alzetani, E. Woo, P. S. Friedmann, E. V. King, G. J. Thomas, T. Sanchez-Elsner, P. Vijayanand and C. H. Ottensmeier (2017). "Tissue-resident memory features are linked to the magnitude of cytotoxic T cell responses in human lung cancer." Nat Immunol **18**(8): 940-950.

Gao, J., L. Z. Shi, H. Zhao, J. Chen, L. Xiong, Q. He, T. Chen, J. Roszik, C. Bernatchez, S. E. Woodman, P. L. Chen, P. Hwu, J. P. Allison, A. Futreal, J. A. Wargo and P. Sharma (2016). "Loss of IFN-gamma Pathway Genes in Tumor Cells as a Mechanism of Resistance to Anti-CTLA-4 Therapy." Cell **167**(2): 397-404 e399.

Garcia-Garijo, A., C. A. Fajardo and A. Gros (2019). "Determinants for Neoantigen Identification." Front Immunol **10**: 1392.

Gardner, A. and B. Ruffell (2016). "Dendritic Cells and Cancer Immunity." Trends Immunol **37**(12): 855-865.

Garris, C. S., S. P. Arlauckas, R. H. Kohler, M. P. Trefny, S. Garren, C. Piot, C. Engblom, C. Pfirschke, M. Siwicki, J. Gungabeesoon, G. J. Freeman, S. E. Warren, S. Ong, E. Browning, C. G. Twitty, R. H. Pierce, M. H. Le, A. P. Algazi, A. I. Daud, S. I. Pai, A. Zippelius, R. Weissleder and M. J. Pittet (2018). "Successful Anti-PD-1 Cancer Immunotherapy Requires T Cell-Dendritic Cell Crosstalk Involving the Cytokines IFN-gamma and IL-12." Immunity **49**(6): 1148-1161 e1147.

Gattinoni, L., C. A. Klebanoff, D. C. Palmer, C. Wrzesinski, K. Kerstann, Z. Yu, S. E. Finkelstein, M. R. Theoret, S. A. Rosenberg and N. P. Restifo (2005). "Acquisition of full effector function in vitro paradoxically impairs the in vivo antitumor efficacy of adoptively transferred CD8+ T cells." J Clin Invest **115**(6): 1616-1626.

Gattinoni, L., X. S. Zhong, D. C. Palmer, Y. Ji, C. S. Hinrichs, Z. Yu, C. Wrzesinski, A. Boni, L. Cassard, L. M. Garvin, C. M. Paulos, P. Muranski and N. P. Restifo (2009). "Wnt signaling arrests effector T cell differentiation and generates CD8+ memory stem cells." Nat Med **15**(7): 808-813.

Gaud, G., R. Lesourne and P. E. Love (2018). "Regulatory mechanisms in T cell receptor signalling." Nat Rev Immunol **18**(8): 485-497.

Ge, Y., T. K. Paisie, S. Chen and P. Concannon (2019). "UBASH3A Regulates the Synthesis and Dynamics of TCR-CD3 Complexes." J Immunol **203**(11): 2827-2836.

Georgiev, P., L. M. Charbonnier and T. A. Chatila (2019). "Regulatory T Cells: the Many Faces of Foxp3." J Clin Immunol **39**(7): 623-640.

Germain, C., S. Gnjatic, F. Tamzalit, S. Knockaert, R. Remark, J. Goc, A. Lepelley, E. Becht, S. Katsahian, G. Bizouard, P. Validire, D. Damotte, M. Alifano, P. Magdeleinat, I. Cremer, J. L. Teillaud, W. H. Fridman, C. Sautes-Fridman and M. C. Dieu-Nosjean (2014). "Presence of B cells in tertiary lymphoid structures is associated with a protective immunity in patients with lung cancer." Am J Respir Crit Care Med **189**(7): 832-844.

Gfeller, D., P. Guillaume, J. Michaux, H. S. Pak, R. T. Daniel, J. Racle, G. Coukos and M. Bassani-Sternberg (2018). "The Length Distribution and Multiple Specificity of Naturally Presented HLA-I Ligands." J Immunol **201**(12): 3705-3716.

Giraldo, N. A., E. Becht, Y. Vano, F. Petitprez, L. Lacroix, P. Validire, R. Sanchez-Salas, A. Ingels, S. Oudard, A. Moatti, B. Buttard, S. Bourass, C. Germain, X. Cathelineau, W. H. Fridman and C. Sautes-Fridman (2017). "Tumor-Infiltrating and Peripheral Blood T-cell Immunophenotypes Predict Early Relapse in Localized Clear Cell Renal Cell Carcinoma." Clin Cancer Res **23**(15): 4416-4428.

Goc, J., C. Germain, T. K. Vo-Bourgais, A. Lupo, C. Klein, S. Knockaert, L. de Chaisemartin, H. Ouakrim, E. Becht, M. Alifano, P. Validire, R. Remark, S. A. Hammond, I. Cremer, D. Damotte, W. H. Fridman, C. Sautes-Fridman and M. C. Dieu-Nosjean (2014). "Dendritic cells in tumor-associated tertiary lymphoid structures signal a Th1 cytotoxic immune contexture and license the positive prognostic value of infiltrating CD8+ T cells." Cancer Res **74**(3): 705-715.

Gocher, A. M., C. J. Workman and D. A. A. Vignali (2021). "Interferon-gamma: teammate or opponent in the tumour microenvironment?" Nat Rev Immunol.

Golgher, D., E. Jones, F. Powrie, T. Elliott and A. Gallimore (2002). "Depletion of CD25+ regulatory cells uncovers immune responses to shared murine tumor rejection antigens." Eur J Immunol **32**(11): 3267-3275.

Golgher, D., F. Korangy, B. Gao, K. Gorski, E. Jaffee, M. Edidin, D. M. Pardoll and T. Elliott (2001). "An immunodominant MHC class II-restricted tumor antigen is conformation dependent and binds to the endoplasmic reticulum chaperone, calreticulin." J Immunol **167**(1): 147-155.

Gonzales Carazas, M. M., J. A. Pinto and F. L. Casado (2021). "Biological bases of cancer immunotherapy." Expert Rev Mol Med **23**: e3.

Gonzalez-Navajas, J. M., D. D. Fan, S. Yang, F. M. Yang, B. Lozano-Ruiz, L. Shen and J. Lee (2021). "The Impact of Tregs on the Anticancer Immunity and the Efficacy of Immune Checkpoint Inhibitor Therapies." Front Immunol **12**: 625783.

Grasso, C. S., J. Tsoi, M. Onyshchenko, G. Abril-Rodriguez, P. Ross-Macdonald, M. Wind-Rotolo, A. Champhekar, E. Medina, D. Y. Torrejon, D. S. Shin, P. Tran, Y. J. Kim, C. Puig-Saus, K. Campbell, A. Vega-Crespo, M. Quist, C. Martignier, J. J. Luke, J. D. Wolchok, D. B. Johnson, B. Chmielowski, F. S. Hodi, S. Bhatia, W. Sharfman, W. J. Urba, C. L. Slingluff, Jr., A. Diab, J. Haanen, S. M. Algarra, D. M. Pardoll, V. Anagnostou, S. L. Topalian, V. E. Velculescu, D. E. Speiser, A. Kalbasi and A. Ribas (2020). "Conserved Interferon-gamma Signaling Drives Clinical Response to Immune Checkpoint Blockade Therapy in Melanoma." Cancer Cell **38**(4): 500-515 e503.

Griswold, D. P. and T. H. Corbett (1975). "A colon tumor model for anticancer agent evaluation." Cancer **36**(6 Suppl): 2441-2444.

Guo, X., Y. Zhang, L. Zheng, C. Zheng, J. Song, Q. Zhang, B. Kang, Z. Liu, L. Jin, R. Xing, R. Gao, L. Zhang, M. Dong, X. Hu, X. Ren, D. Kirchhoff, H. G. Roider, T. Yan and Z. Zhang (2018). "Global characterization of T cells in non-small-cell lung cancer by single-cell sequencing." Nat Med **24**(7): 978-985.

Gusev, A., K. Lawrenson, X. Lin, P. C. Lyra, Jr., S. Kar, K. C. Vavra, F. Segato, M. A. S. Fonseca, J. M. Lee, T. Pejovic, G. Liu, C. Ovarian Cancer Association, B. Y. Karlan, M. L. Freedman, H. Noushmehr, A. N. Monteiro, P. D. P. Pharoah, B. Pasaniuc and S. A. Gayther (2019). "A transcriptome-wide association study of high-grade serous epithelial ovarian cancer identifies new susceptibility genes and splice variants." Nat Genet **51**(5): 815-823.

Hailemichael, Y., Z. Dai, N. Jaffarzad, Y. Ye, M. A. Medina, X. F. Huang, S. M. Dorta-Estremera, N. R. Greeley, G. Nitti, W. Peng, C. Liu, Y. Lou, Z. Wang, W. Ma, B. Rabinovich, R. T. Sowell, K. S. Schluns, R. E. Davis, P. Hwu and W. W. Overwijk (2013). "Persistent antigen at vaccination sites induces tumor-specific CD8(+) T cell sequestration, dysfunction and deletion." Nat Med **19**(4): 465-472.

Hammer, G. E., F. Gonzalez, M. Champsaur, D. Cado and N. Shastri (2006). "The aminopeptidase ERAAP shapes the peptide repertoire displayed by major histocompatibility complex class I molecules." Nat Immunol **7**(1): 103-112.

Han, J., N. Khatwani, T. G. Searles, M. J. Turk and C. V. Angeles (2020). "Memory CD8(+) T cell responses to cancer." Semin Immunol **49**: 101435.

Hanahan, D. and R. A. Weinberg (2011). "Hallmarks of cancer: the next generation." Cell **144**(5): 646-674.

Haniffa, M., M. Collin and F. Ginhoux (2013). "Ontogeny and functional specialization of dendritic cells in human and mouse." Adv Immunol **120**: 1-49.

Hansen, T. H., J. M. Connolly, K. G. Gould and D. H. Fremont (2010). "Basic and translational applications of engineered MHC class I proteins." Trends Immunol **31**(10): 363-369.

Hanson, H. L., D. L. Donermeyer, H. Ikeda, J. M. White, V. Shankaran, L. J. Old, H. Shiku, R. D. Schreiber and P. M. Allen (2000). "Eradication of established tumors by CD8+ T cell adoptive immunotherapy." Immunity **13**(2): 265-276.

Hao, Q., P. Wei, Y. Shu, Y. G. Zhang, H. Xu and J. N. Zhao (2021). "Improvement of Neoantigen Identification Through Convolution Neural Network." Front Immunol **12**: 682103.

Hargadon, K. M., C. E. Johnson and C. J. Williams (2018). "Immune checkpoint blockade therapy for cancer: An overview of FDA-approved immune checkpoint inhibitors." Int Immunopharmacol **62**: 29-39.

Higashikawa, K., K. Yagi, K. Watanabe, S. Kamino, M. Ueda, M. Hiromura and S. Enomoto (2014). "64Cu-DOTA-anti-CTLA-4 mAb enabled PET visualization of CTLA-4 on the T-cell infiltrating tumor tissues." PLoS One **9**(11): e109866.

Hildner, K., B. T. Edelson, W. E. Purtha, M. Diamond, H. Matsushita, M. Kohyama, B. Calderon, B. U. Schraml, E. R. Unanue, M. S. Diamond, R. D. Schreiber, T. L. Murphy and K. M. Murphy (2008). "Batf3 deficiency reveals a critical role for CD8alpha+ dendritic cells in cytotoxic T cell immunity." Science **322**(5904): 1097-1100.

Hilf, N., S. Kuttruff-Coqui, K. Frenzel, V. Bukur, S. Stevanovic, C. Gouttefangeas, M. Platten, G. Tabatabai, V. Dutoit, S. H. van der Burg, P. Thor Straten, F. Martinez-Ricarte, B. Ponsati, H. Okada, U. Lassen, A. Admon, C. H. Ottensmeier, A. Ulges, S. Kreiter, A. von Deimling, M. Skardelly, D. Migliorini, J. R. Kroep, M. Idorn, J. Rodon, J. Piro, H. S. Poulsen, B. Shraibman, K. McCann, R. Mendrzyk, M. Lower, M. Stieglbauer, C. M. Britten, D. Capper, M. J. P. Welters, J. Sahuquillo, K. Kiesel, E. Derhovanessian, E. Rusch, L. Bunse, C. Song, S. Heesch, C. Wagner, A. Kemmer-Bruck, J. Ludwig, J. C. Castle, O. Schoor, A. D. Tadmor, E. Green, J. Fritsche, M. Meyer, N. Pawlowski, S. Dorner, F. Hoffgaard, B. Rossler, D. Maurer, T. Weinschenk, C. Reinhardt, C. Huber, H. G. Rammensee, H. Singh-Jasuja, U. Sahin, P. Y. Dietrich and W. Wick (2019). "Actively personalized vaccination trial for newly diagnosed glioblastoma." Nature **565**(7738): 240-245.

Hinrichs, C. S., R. Spolski, C. M. Paulos, L. Gattinoni, K. W. Kerstann, D. C. Palmer, C. A. Klebanoff, S. A. Rosenberg, W. J. Leonard and N. P. Restifo (2008). "IL-2 and IL-21 confer opposing differentiation programs to CD8+ T cells for adoptive immunotherapy." Blood **111**(11): 5326-5333.

Hiraoka, N., Y. Ino, R. Yamazaki-Itoh, Y. Kanai, T. Kosuge and K. Shimada (2015). "Intratumoral tertiary lymphoid organ is a favourable prognosticator in patients with pancreatic cancer." Br J Cancer **112**(11): 1782-1790.

Hu, W., R. Sun, L. Chen, X. Zheng and J. Jiang (2019). "Prognostic significance of resident CD103(+)CD8(+)T cells in human colorectal cancer tissues." Acta Histochem **121**(5): 657-663.

Hu, Z., P. A. Ott and C. J. Wu (2018). "Towards personalized, tumour-specific, therapeutic vaccines for cancer." Nat Rev Immunol **18**(3): 168-182.

Huang, A. Y., P. H. Gulden, A. S. Woods, M. C. Thomas, C. D. Tong, W. Wang, V. H. Engelhard, G. Pasternack, R. Cotter, D. Hunt, D. M. Pardoll and E. M. Jaffee (1996). "The immunodominant

major histocompatibility complex class I-restricted antigen of a murine colon tumor derives from an endogenous retroviral gene product." Proc Natl Acad Sci U S A **93**(18): 9730-9735.

Huang da, W., B. T. Sherman and R. A. Lempicki (2009). "Systematic and integrative analysis of large gene lists using DAVID bioinformatics resources." Nat Protoc **4**(1): 44-57.

Huang, R. R., J. Jalil, J. S. Economou, B. Chmielowski, R. C. Koya, S. Mok, H. Sazegar, E. Seja, A. Villanueva, J. Gomez-Navarro, J. A. Glaspy, A. J. Cochran and A. Ribas (2011). "CTLA4 blockade induces frequent tumor infiltration by activated lymphocytes regardless of clinical responses in humans." Clin Cancer Res **17**(12): 4101-4109.

Huang, Y., N. Obholzer, R. Fayad and L. Qiao (2005). "Turning on/off tumor-specific CTL response during progressive tumor growth." J Immunol **175**(5): 3110-3116.

Huss, D. J., A. F. Pellerin, B. P. Collette, A. K. Kannan, L. Peng, A. Datta, B. T. Wipke and J. D. Fontenot (2016). "Anti-CD25 monoclonal antibody Fc variants differentially impact regulatory T cells and immune homeostasis." Immunology **148**(3): 276-286.

Hwang, E. S., S. J. Szabo, P. L. Schwartzberg and L. H. Glimcher (2005). "T helper cell fate specified by kinase-mediated interaction of T-bet with GATA-3." Science **307**(5708): 430-433.

Im, S. J., M. Hashimoto, M. Y. Gerner, J. Lee, H. T. Kissick, M. C. Burger, Q. Shan, J. S. Hale, J. Lee, T. H. Nasti, A. H. Sharpe, G. J. Freeman, R. N. Germain, H. I. Nakaya, H. H. Xue and R. Ahmed (2016). "Defining CD8+ T cells that provide the proliferative burst after PD-1 therapy." Nature **537**(7620): 417-421.

Ishida, Y., Y. Agata, K. Shibahara and T. Honjo (1992). "Induced expression of PD-1, a novel member of the immunoglobulin gene superfamily, upon programmed cell death." EMBO J **11**(11): 3887-3895.

Iwai, Y., S. Terawaki and T. Honjo (2005). "PD-1 blockade inhibits hematogenous spread of poorly immunogenic tumor cells by enhanced recruitment of effector T cells." Int Immunol **17**(2): 133-144.

James, E., I. Bailey, G. Sugiyarto and T. Elliott (2013). "Induction of protective antitumor immunity through attenuation of ERAAP function." J Immunol **190**(11): 5839-5846.

James, E., A. Yeh, C. King, F. Korangy, I. Bailey, D. S. Boulanger, B. J. Van den Eynde, N. Murray and T. J. Elliott (2010). "Differential suppression of tumor-specific CD8+ T cells by regulatory T cells." J Immunol **185**(9): 5048-5055.

Jhunjhunwala, S., C. Hammer and L. Delamarre (2021). "Antigen presentation in cancer: insights into tumour immunogenicity and immune evasion." Nat Rev Cancer **21**(5): 298-312.

Johnston, R. J., L. Comps-Agrar, J. Hackney, X. Yu, M. Huseni, Y. Yang, S. Park, V. Javinal, H. Chiu, B. Irving, D. L. Eaton and J. L. Grogan (2014). "The immunoreceptor TIGIT regulates antitumor and antiviral CD8(+) T cell effector function." Cancer Cell **26**(6): 923-937.

Jordan, K. R., R. H. McMahan, C. B. Kemmler, J. W. Kappler and J. E. Slansky (2010). "Peptide vaccines prevent tumor growth by activating T cells that respond to native tumor antigens." Proc Natl Acad Sci U S A **107**(10): 4652-4657.

Junwei, W., Z. Xiumin, Y. Jing, Y. Shoujing and L. Zengshan (2016). "In vivo enhancement of the MAGE-specific cellular immune response by a recombinant MAGE1-MAGE3-TBHSP70 tumor vaccine." Cancer Cell Int **16**: 45.

Jurtz, V., S. Paul, M. Andreatta, P. Marcatili, B. Peters and M. Nielsen (2017). "NetMHCpan-4.0: Improved Peptide-MHC Class I Interaction Predictions Integrating Eluted Ligand and Peptide Binding Affinity Data." J Immunol **199**(9): 3360-3368.

Kalergis, A. M., N. Boucheron, M. A. Doucey, E. Palmieri, E. C. Goyarts, Z. Vegh, I. F. Luescher and S. G. Nathenson (2001). "Efficient T cell activation requires an optimal dwell-time of interaction between the TCR and the pMHC complex." Nat Immunol **2**(3): 229-234.

Kansy, B. A., F. Concha-Benavente, R. M. Srivastava, H. B. Jie, G. Shayan, Y. Lei, J. Moskovitz, J. Moy, J. Li, S. Brandau, S. Lang, N. C. Schmitt, G. J. Freeman, W. E. Gooding, D. A. Clump and R. L. Ferris (2017). "PD-1 Status in CD8(+) T Cells Associates with Survival and Anti-PD-1 Therapeutic Outcomes in Head and Neck Cancer." Cancer Res **77**(22): 6353-6364.

Kaplan, D. H., V. Shankaran, A. S. Dighe, E. Stockert, M. Aguet, L. J. Old and R. D. Schreiber (1998). "Demonstration of an interferon gamma-dependent tumor surveillance system in immunocompetent mice." Proc Natl Acad Sci U S A **95**(13): 7556-7561.

Karosiene, E., C. Lundegaard, O. Lund and M. Nielsen (2012). "NetMHCcons: a consensus method for the major histocompatibility complex class I predictions." Immunogenetics **64**(3): 177-186.

Kawano, M., I. Itonaga, T. Iwasaki and H. Tsumura (2013). "Enhancement of antitumor immunity by combining anti-cytotoxic T lymphocyte antigen-4 antibodies and cryotreated tumor lysate-pulsed dendritic cells in murine osteosarcoma." Oncol Rep **29**(3): 1001-1006.

Khodadoust, M. S., N. Olsson, L. E. Wagar, O. A. Haabeth, B. Chen, K. Swaminathan, K. Rawson, C. L. Liu, D. Steiner, P. Lund, S. Rao, L. Zhang, C. Marceau, H. Stehr, A. M. Newman, D. K. Czerwinski, V. E. Carlton, M. Moorhead, M. Faham, H. E. Kohrt, J. Carette, M. R. Green, M. M. Davis, R. Levy, J. E. Elias and A. A. Alizadeh (2017). "Antigen presentation profiling reveals recognition of lymphoma immunoglobulin neoantigens." Nature **543**(7647): 723-727.

Kim, S., H. S. Kim, E. Kim, M. G. Lee, E. C. Shin, S. Paik and S. Kim (2018). "Neopepsee: accurate genome-level prediction of neoantigens by harnessing sequence and amino acid immunogenicity information." Ann Oncol **29**(4): 1030-1036.

Kim, S. W., P. Goedegebuure and W. E. Gillanders (2016). "Mammaglobin-A is a target for breast cancer vaccination." Oncoimmunology **5**(2): e1069940.

Kirkwood, J. M., P. Lorigan, P. Hersey, A. Hauschild, C. Robert, D. McDermott, M. A. Marshall, J. Gomez-Navarro, J. Q. Liang and C. A. Bulanhagui (2010). "Phase II trial of tremelimumab (CP-675,206) in patients with advanced refractory or relapsed melanoma." Clin Cancer Res **16**(3): 1042-1048.

Klebanoff, C. A., L. Gattinoni, P. Torabi-Parizi, K. Kerstann, A. R. Cardones, S. E. Finkelstein, D. C. Palmer, P. A. Antony, S. T. Hwang, S. A. Rosenberg, T. A. Waldmann and N. P. Restifo (2005). "Central memory self/tumor-reactive CD8+ T cells confer superior antitumor immunity compared with effector memory T cells." Proc Natl Acad Sci U S A **102**(27): 9571-9576.

Klebanoff, C. A., Z. Yu, L. N. Hwang, D. C. Palmer, L. Gattinoni and N. P. Restifo (2009). "Programming tumor-reactive effector memory CD8+ T cells in vitro obviates the requirement for in vivo vaccination." Blood **114**(9): 1776-1783.

Klein, L., B. Kyewski, P. M. Allen and K. A. Hogquist (2014). "Positive and negative selection of the T cell repertoire: what thymocytes see (and don't see)." Nat Rev Immunol **14**(6): 377-391.

Kohm, A. P., J. S. McMahon, J. R. Podojil, W. S. Begolka, M. DeGutes, D. J. Kasprowicz, S. F. Ziegler and S. D. Miller (2006). "Cutting Edge: Anti-CD25 monoclonal antibody injection results in the

functional inactivation, not depletion, of CD4+CD25+ T regulatory cells." J Immunol **176**(6): 3301-3305.

Kondo, T., M. Ando, N. Nagai, W. Tomisato, T. Srirat, B. Liu, S. Mise-Omata, M. Ikeda, S. Chikuma, H. Nishimasu, O. Nureki, M. Ohmura, N. Hayakawa, T. Hishiki, R. Uchibori, K. Ozawa and A. Yoshimura (2020). "The NOTCH-FOXM1 Axis Plays a Key Role in Mitochondrial Biogenesis in the Induction of Human Stem Cell Memory-like CAR-T Cells." Cancer Res **80**(3): 471-483.

Kong, Y., C. M. Rose, A. A. Cass, A. G. Williams, M. Darwish, S. Lianoglou, P. M. Haverty, A. J. Tong, C. Blanchette, M. L. Albert, I. Mellman, R. Bourgon, J. Greally, S. Jhunjhunwala and H. Chen-Harris (2019). "Transposable element expression in tumors is associated with immune infiltration and increased antigenicity." Nat Commun **10**(1): 5228.

Krishna, S., F. J. Lowery, A. R. Copeland, E. Bahadiroglu, R. Mukherjee, L. Jia, J. T. Anibal, A. Sachs, S. O. Adebola, D. Gurusamy, Z. Yu, V. Hill, J. J. Gartner, Y. F. Li, M. Parkhurst, B. Paria, P. Kvistborg, M. C. Kelly, S. L. Goff, G. Altan-Bonnet, P. F. Robbins and S. A. Rosenberg (2020). "Stem-like CD8 T cells mediate response of adoptive cell immunotherapy against human cancer." Science **370**(6522): 1328-1334.

Kubota, K. and K. Iwabuchi (2014). "Phenotypic changes in growth-arrested T cell hybrids: a possible avenue to produce functional T cell hybridoma." Front Immunol **5**: 229.

Kurtulus, S., K. Sakuishi, S. F. Ngiow, N. Joller, D. J. Tan, M. W. Teng, M. J. Smyth, V. K. Kuchroo and A. C. Anderson (2015). "TIGIT predominantly regulates the immune response via regulatory T cells." J Clin Invest **125**(11): 4053-4062.

Kvistborg, P., D. Philips, S. Kelderman, L. Hageman, C. Ottensmeier, D. Joseph-Pietras, M. J. Welters, S. van der Burg, E. Kapiteijn, O. Michielin, E. Romano, C. Linnemann, D. Speiser, C. Blank, J. B. Haanen and T. N. Schumacher (2014). "Anti-CTLA-4 therapy broadens the melanoma-reactive CD8+ T cell response." Sci Transl Med **6**(254): 254ra128.

Ladoire, S., F. Martin and F. Ghiringhelli (2011). "Prognostic role of FOXP3+ regulatory T cells infiltrating human carcinomas: the paradox of colorectal cancer." Cancer Immunol Immunother **60**(7): 909-918.

Larsson, V. J., M. H. Jafferali, B. Vijayaraghavan, R. A. Figueroa and E. Hallberg (2018). "Mitotic spindle assembly and gamma-tubulin localisation depend on the integral nuclear membrane protein Samp1." J Cell Sci **131**(8).

Laumont, C. M., K. Vincent, L. Hesnard, E. Audemard, E. Bonneil, J. P. Laverdure, P. Gendron, M. Courcelles, M. P. Hardy, C. Cote, C. Durette, C. St-Pierre, M. Benhammadi, J. Lanoix, S. Vobecky, E. Haddad, S. Lemieux, P. Thibault and C. Perreault (2018). "Noncoding regions are the main source of targetable tumor-specific antigens." Sci Transl Med **10**(470).

Le Floc'h, A., A. Jalil, I. Vergnon, B. Le Maux Chansac, V. Lazar, G. Bismuth, S. Chouaib and F. Mami-Chouaib (2007). "Alpha E beta 7 integrin interaction with E-cadherin promotes antitumor CTL activity by triggering lytic granule polarization and exocytosis." J Exp Med **204**(3): 559-570.

Leach, D. R., M. F. Krummel and J. P. Allison (1996). "Enhancement of antitumor immunity by CTLA-4 blockade." Science **271**(5256): 1734-1736.

Lee, H. J., J. Y. Kim, I. A. Park, I. H. Song, J. H. Yu, J. H. Ahn and G. Gong (2015). "Prognostic Significance of Tumor-Infiltrating Lymphocytes and the Tertiary Lymphoid Structures in HER2-Positive Breast Cancer Treated With Adjuvant Trastuzumab." Am J Clin Pathol **144**(2): 278-288.

Lennerz, V., M. Fatho, C. Gentilini, R. A. Frye, A. Lifke, D. Ferel, C. Wolfel, C. Huber and T. Wolfel (2005). "The response of autologous T cells to a human melanoma is dominated by mutated neoantigens." Proc Natl Acad Sci U S A **102**(44): 16013-16018.

Li, A. W., M. C. Sobral, S. Badrinath, Y. Choi, A. Graveline, A. G. Stafford, J. C. Weaver, M. O. Dellacherie, T. Y. Shih, O. A. Ali, J. Kim, K. W. Wucherpfennig and D. J. Mooney (2018). "A facile approach to enhance antigen response for personalized cancer vaccination." Nat Mater **17**(6): 528-534.

Li, G., B. Iyer, V. B. S. Prasath, Y. Ni and N. Salomonis (2021). "DeepImmuno: deep learning-empowered prediction and generation of immunogenic peptides for T-cell immunity." Brief Bioinform.

Li, H., A. M. van der Leun, I. Yofe, Y. Lubling, D. Gelbard-Solodkin, A. C. J. van Akkooi, M. van den Braber, E. A. Rozeman, J. Haanen, C. U. Blank, H. M. Horlings, E. David, Y. Baran, A. Bercovich, A. Lifshitz, T. N. Schumacher, A. Tanay and I. Amit (2019). "Dysfunctional CD8 T Cells Form a Proliferative, Dynamically Regulated Compartment within Human Melanoma." Cell **176**(4): 775-789 e718.

Li, Y., Y. Cong, M. Jia, Q. He, H. Zhong, Y. Zhao, H. Li, M. Yan, J. You, J. Liu, L. Chen, H. Hang and S. Wang (2021). "Targeting IL-21 to tumor-reactive T cells enhances memory T cell responses and anti-PD-1 antibody therapy." Nat Commun **12**(1): 951.

Lim, K. P. and N. S. Zainal (2021). "Monitoring T Cells Responses Mounted by Therapeutic Cancer Vaccines." Front Mol Biosci **8**: 623475.

Linette, G. P., D. Zhang, F. S. Hodi, E. P. Jonasch, S. Longerich, C. P. Stowell, I. J. Webb, H. Daley, R. J. Soiffer, A. M. Cheung, S. G. Eapen, S. V. Fee, K. M. Rubin, A. J. Sober and F. G. Haluska (2005). "Immunization using autologous dendritic cells pulsed with the melanoma-associated antigen gp100-derived G280-9V peptide elicits CD8+ immunity." Clin Cancer Res **11**(21): 7692-7699.

Lissina, A., L. A. Chakrabarti, M. Takiguchi and V. Appay (2016). "TCR clonotypes: molecular determinants of T-cell efficacy against HIV." Curr Opin Virol **16**: 77-85.

Liu, C., J. Shao, Y. Dong, Q. Xu, Z. Zou, F. Chen, J. Yan, J. Liu, S. Li, B. Liu and J. Shen (2021). "Advanced HCC Patient Benefit From Neoantigen Reactive T Cells Based Immunotherapy: A Case Report." Front Immunol **12**: 685126.

Liu, Q., Y. Qi, J. Zhai, X. Kong, X. Wang, Z. Wang, Y. Fang and J. Wang (2021). "Molecular and Clinical Characterization of LAG3 in Breast Cancer Through 2994 Samples." Front Immunol **12**: 599207.

Lizee, G., W. W. Overwijk, L. Radvanyi, J. Gao, P. Sharma and P. Hwu (2013). "Harnessing the power of the immune system to target cancer." Annu Rev Med **64**: 71-90.

Ljunggren, H. G. and K. Karre (1985). "Host resistance directed selectively against H-2-deficient lymphoma variants. Analysis of the mechanism." J Exp Med **162**(6): 1745-1759.

Lopez, J. A., O. Susanto, M. R. Jenkins, N. Lukoyanova, V. R. Sutton, R. H. Law, A. Johnston, C. H. Bird, P. I. Bird, J. C. Whisstock, J. A. Trapani, H. R. Saibil and I. Voskoboinik (2013). "Perforin forms transient pores on the target cell plasma membrane to facilitate rapid access of granzymes during killer cell attack." Blood **121**(14): 2659-2668.

Lynn, G. M., C. Sedlik, F. Baharom, Y. Zhu, R. A. Ramirez-Valdez, V. L. Coble, K. Tobin, S. R. Nichols, Y. Itzkowitz, N. Zaidi, J. M. Gammon, N. J. Blobel, J. Denizeau, P. de la Rochere, B. J. Francica, B. Decker, M. Maciejewski, J. Cheung, H. Yamane, M. G. Smelkinson, J. R. Francica, R. Laga, J. D. Bernstock, L. W. Seymour, C. G. Drake, C. M. Jewell, O. Lantz, E. Piaggio, A. S. Ishizuka and R. A.

Seder (2020). "Peptide-TLR-7/8a conjugate vaccines chemically programmed for nanoparticle self-assembly enhance CD8 T-cell immunity to tumor antigens." Nat Biotechnol **38**(3): 320-332.

Malik, B. T., K. T. Byrne, J. L. Vella, P. Zhang, T. B. Shabaneh, S. M. Steinberg, A. K. Molodtsov, J. S. Bowers, C. V. Angeles, C. M. Paulos, Y. H. Huang and M. J. Turk (2017). "Resident memory T cells in the skin mediate durable immunity to melanoma." Sci Immunol **2**(10).

Manieri, N. A., E. Y. Chiang and J. L. Grogan (2017). "TIGIT: A Key Inhibitor of the Cancer Immunity Cycle." Trends Immunol **38**(1): 20-28.

Manjarrez-Orduno, N., L. C. Menard, S. Kansal, P. Fischer, B. Kakrecha, C. Jiang, M. Cunningham, D. Greenawalt, V. Patel, M. Yang, R. Golhar, J. A. Carman, S. Lezhnin, H. Dai, P. S. Kayne, S. J. Suchard, S. H. Bernstein and S. G. Nadler (2018). "Circulating T Cell Subpopulations Correlate With Immune Responses at the Tumor Site and Clinical Response to PD1 Inhibition in Non-Small Cell Lung Cancer." Front Immunol **9**: 1613.

Martinez-Lostao, L., A. Anel and J. Pardo (2015). "How Do Cytotoxic Lymphocytes Kill Cancer Cells?" Clin Cancer Res **21**(22): 5047-5056.

Martinez-Usatorre, A., A. Donda, D. Zehn and P. Romero (2018). "PD-1 Blockade Unleashes Effector Potential of Both High- and Low-Affinity Tumor-Infiltrating T Cells." J Immunol **201**(2): 792-803.

Matsushita, H., M. D. Vesely, D. C. Koboldt, C. G. Rickert, R. Uppaluri, V. J. Magrini, C. D. Arthur, J. M. White, Y. S. Chen, L. K. Shea, J. Hundal, M. C. Wendl, R. Demeter, T. Wylie, J. P. Allison, M. J. Smyth, L. J. Old, E. R. Mardis and R. D. Schreiber (2012). "Cancer exome analysis reveals a T-cell-dependent mechanism of cancer immunoediting." Nature **482**(7385): 400-404.

Maude, S. L., D. T. Teachey, D. L. Porter and S. A. Grupp (2015). "CD19-targeted chimeric antigen receptor T-cell therapy for acute lymphoblastic leukemia." Blood **125**(26): 4017-4023.

Maute, R. L., S. R. Gordon, A. T. Mayer, M. N. McCracken, A. Natarajan, N. G. Ring, R. Kimura, J. M. Tsai, A. Manglik, A. C. Kruse, S. S. Gambhir, I. L. Weissman and A. M. Ring (2015). "Engineering high-affinity PD-1 variants for optimized immunotherapy and immuno-PET imaging." Proc Natl Acad Sci U S A **112**(47): E6506-6514.

Mayoux, M., A. Roller, V. Pulko, S. Sammicheli, S. Chen, E. Sum, C. Jost, M. F. Fransen, R. B. Buser, M. Kowanetz, K. Rommel, I. Matos, S. Colombetti, A. Belousov, V. Karanikas, F. Ossendorp, P. S. Hegde, D. S. Chen, P. Umana, M. Perro, C. Klein and W. Xu (2020). "Dendritic cells dictate responses to PD-L1 blockade cancer immunotherapy." Sci Transl Med **12**(534).

McCubrey, J. and R. Risser (1982). "Genetic interactions in the spontaneous production of endogenous murine leukemia virus in low leukemic mouse strains." J Exp Med **156**(2): 337-349.

McLane, L. M., M. S. Abdel-Hakeem and E. J. Wherry (2019). "CD8 T Cell Exhaustion During Chronic Viral Infection and Cancer." Annu Rev Immunol **37**: 457-495.

McWilliams, J. A., R. T. Sullivan, K. R. Jordan, R. H. McMahan, C. B. Kemmler, M. McDuffie and J. E. Slansky (2008). "Age-dependent tolerance to an endogenous tumor-associated antigen." Vaccine **26**(15): 1863-1873.

Mei, S., F. Li, A. Leier, T. T. Marquez-Lago, K. Giam, N. P. Croft, T. Akutsu, A. I. Smith, J. Li, J. Rossjohn, A. W. Purcell and J. Song (2020). "A comprehensive review and performance evaluation of bioinformatics tools for HLA class I peptide-binding prediction." Brief Bioinform **21**(4): 1119-1135.

Metkar, S. S., B. Wang, E. Catalan, G. Anderluh, R. J. Gilbert, J. Pardo and C. J. Froelich (2011). "Perforin rapidly induces plasma membrane phospholipid flip-flop." PLoS One **6**(9): e24286.

Michot, J. M., C. Bigenwald, S. Champiat, M. Collins, F. Carbonnel, S. Postel-Vinay, A. Berdelou, A. Varga, R. Bahleda, A. Hollebecque, C. Massard, A. Fuerea, V. Ribrag, A. Gazzah, J. P. Armand, N. Amellal, E. Angevin, N. Noel, C. Boutros, C. Mateus, C. Robert, J. C. Soria, A. Marabelle and O. Lambotte (2016). "Immune-related adverse events with immune checkpoint blockade: a comprehensive review." Eur J Cancer **54**: 139-148.

Miller, B. C., D. R. Sen, R. Al Abosy, K. Bi, Y. V. Virkud, M. W. LaFleur, K. B. Yates, A. Lako, K. Felt, G. S. Naik, M. Manos, E. Gjini, J. R. Kuchroo, J. J. Ishizuka, J. L. Collier, G. K. Griffin, S. Maleri, D. E. Comstock, S. A. Weiss, F. D. Brown, A. Panda, M. D. Zimmer, R. T. Manguso, F. S. Hodi, S. J. Rodig, A. H. Sharpe and W. N. Haining (2019). "Subsets of exhausted CD8(+) T cells differentially mediate tumor control and respond to checkpoint blockade." Nat Immunol **20**(3): 326-336.

Mitaksov, V. and D. H. Fremont (2006). "Structural definition of the H-2Kd peptide-binding motif." J Biol Chem **281**(15): 10618-10625.

Mitaksov, V., S. M. Truscott, L. Lybarger, J. M. Connolly, T. H. Hansen and D. H. Fremont (2007). "Structural engineering of pMHC reagents for T cell vaccines and diagnostics." Chem Biol **14**(8): 909-922.

Mitchell, D., S. Chintala and M. Dey (2018). "Plasmacytoid dendritic cell in immunity and cancer." J Neuroimmunol **322**: 63-73.

Mojic, M., K. Takeda and Y. Hayakawa (2017). "The Dark Side of IFN-gamma: Its Role in Promoting Cancer Immunoevasion." Int J Mol Sci **19**(1).

Morgan, R. A., N. Chinnasamy, D. Abate-Daga, A. Gros, P. F. Robbins, Z. Zheng, M. E. Dudley, S. A. Feldman, J. C. Yang, R. M. Sherry, G. Q. Phan, M. S. Hughes, U. S. Kammula, A. D. Miller, C. J. Hessman, A. A. Stewart, N. P. Restifo, M. M. Quezado, M. Alimchandani, A. Z. Rosenberg, A. Nath, T. Wang, B. Bielekova, S. C. Wuest, N. Akula, F. J. McMahon, S. Wilde, B. Mosetter, D. J. Schendel, C. M. Laurencot and S. A. Rosenberg (2013). "Cancer regression and neurological toxicity following anti-MAGE-A3 TCR gene therapy." J Immunother **36**(2): 133-151.

Mosely, S. I., J. E. Prime, R. C. Sainson, J. O. Koopmann, D. Y. Wang, D. M. Greenawalt, M. J. Ahdesmaki, R. Leyland, S. Mullins, L. Pacelli, D. Marcus, J. Anderton, A. Watkins, J. Coates Ulrichsen, P. Brohawn, B. W. Higgs, M. McCourt, H. Jones, J. A. Harper, M. Morrow, V. Valge-Archer, R. Stewart, S. J. Dovedi and R. W. Wilkinson (2017). "Rational Selection of Syngeneic Preclinical Tumor Models for Immunotherapeutic Drug Discovery." Cancer Immunol Res **5**(1): 29-41.

MotieGhader, H., Y. Masoudi-Sobhanzadeh, S. H. Ashtiani and A. Masoudi-Nejad (2020). "mRNA and microRNA selection for breast cancer molecular subtype stratification using meta-heuristic based algorithms." Genomics **112**(5): 3207-3217.

Motz, G. T. and G. Coukos (2013). "Deciphering and reversing tumor immune suppression." Immunity **39**(1): 61-73.

Mueller, S. N., T. Gebhardt, F. R. Carbone and W. R. Heath (2013). "Memory T cell subsets, migration patterns, and tissue residence." Annu Rev Immunol **31**: 137-161.

Muntjewerff, E. M., L. D. Meesters and G. van den Bogaart (2020). "Antigen Cross-Presentation by Macrophages." Front Immunol **11**: 1276.

Muraoka, D., N. Seo, T. Hayashi, Y. Tahara, K. Fujii, I. Tawara, Y. Miyahara, K. Okamori, H. Yagita, S. Imoto, R. Yamaguchi, M. Komura, S. Miyano, M. Goto, S. I. Sawada, A. Asai, H. Ikeda, K. Akiyoshi,

N. Harada and H. Shiku (2019). "Antigen delivery targeted to tumor-associated macrophages overcomes tumor immune resistance." J Clin Invest **129**(3): 1278-1294.

Myers, J. A. and J. S. Miller (2021). "Exploring the NK cell platform for cancer immunotherapy." Nat Rev Clin Oncol **18**(2): 85-100.

Nagarajan, N. A., D. A. de Verteuil, D. Sriranganadane, W. Yahyaoui, P. Thibault, C. Perreault and N. Shastri (2016). "ERAAP Shapes the Peptidome Associated with Classical and Nonclassical MHC Class I Molecules." J Immunol **197**(4): 1035-1043.

Nagarajan, N. A., F. Gonzalez and N. Shastri (2012). "Nonclassical MHC class Ib-restricted cytotoxic T cells monitor antigen processing in the endoplasmic reticulum." Nat Immunol **13**(6): 579-586.

Neefjes, J., M. L. Jongsma, P. Paul and O. Bakke (2011). "Towards a systems understanding of MHC class I and MHC class II antigen presentation." Nat Rev Immunol **11**(12): 823-836.

O'Donnell, T. J., A. Rubinsteyn and U. Laserson (2020). "MHCflurry 2.0: Improved Pan-Allele Prediction of MHC Class I-Presented Peptides by Incorporating Antigen Processing." Cell Syst **11**(1): 42-48 e47.

Ohlschlager, P., W. Osen, K. Dell, S. Faath, R. L. Garcea, I. Jochmus, M. Muller, M. Pawlita, K. Schafer, P. Sehr, C. Staib, G. Sutter and L. Gissmann (2003). "Human papillomavirus type 16 L1 capsomeres induce L1-specific cytotoxic T lymphocytes and tumor regression in C57BL/6 mice." J Virol **77**(8): 4635-4645.

Ohno, Y., Y. Toyoshima, H. Yurino, N. Monma, H. Xiang, K. Sumida, S. Kaneumi, S. Terada, S. Hashimoto, K. Ikeo, S. Homma, H. Kawamura, N. Takahashi, A. Taketomi and H. Kitamura (2017). "Lack of interleukin-6 in the tumor microenvironment augments type-1 immunity and increases the efficacy of cancer immunotherapy." Cancer Science **108**(10): 1959-1966.

Okiyama, N., H. Hasegawa, T. Oida, S. Hirata, H. Yokozeki, M. Fujimoto, N. Miyasaka and H. Kohsaka (2015). "Experimental myositis inducible with transfer of dendritic cells presenting a skeletal muscle C protein-derived CD8 epitope peptide." Int Immunol **27**(7): 327-332.

Oliveira, G., K. Stromhaug, S. Klaeger, T. Kula, D. T. Frederick, P. M. Le, J. Forman, T. Huang, S. Li, W. Zhang, Q. Xu, N. Cieri, K. R. Clauser, S. A. Shukla, D. Neuberg, S. Justesen, G. MacBeath, S. A. Carr, E. F. Fritsch, N. Hacohen, M. Sade-Feldman, K. J. Livak, G. M. Boland, P. A. Ott, D. B. Keskin and C. J. Wu (2021). "Phenotype, specificity and avidity of antitumour CD8(+) T cells in melanoma." Nature.

Onizuka, S., I. Tawara, J. Shimizu, S. Sakaguchi, T. Fujita and E. Nakayama (1999). "Tumor rejection by in vivo administration of anti-CD25 (interleukin-2 receptor alpha) monoclonal antibody." Cancer Res **59**(13): 3128-3133.

Ott, P. A., Z. Hu, D. B. Keskin, S. A. Shukla, J. Sun, D. J. Bozym, W. Zhang, A. Luoma, A. Giobbie-Hurder, L. Peter, C. Chen, O. Olive, T. A. Carter, S. Li, D. J. Lieb, T. Eisenhaure, E. Gjini, J. Stevens, W. J. Lane, I. Javeri, K. Nellaiappan, A. M. Salazar, H. Daley, M. Seaman, E. I. Buchbinder, C. H. Yoon, M. Harden, N. Lennon, S. Gabriel, S. J. Rodig, D. H. Barouch, J. C. Aster, G. Getz, K. Wucherpfennig, D. Neuberg, J. Ritz, E. S. Lander, E. F. Fritsch, N. Hacohen and C. J. Wu (2017). "An immunogenic personal neoantigen vaccine for patients with melanoma." Nature **547**(7662): 217-221.

Overacre-Delgoffe, A. E., M. Chikina, R. E. Dadey, H. Yano, E. A. Brunazzi, G. Shayan, W. Horne, J. M. Moskovitz, J. K. Kolls, C. Sander, Y. Shuai, D. P. Normolle, J. M. Kirkwood, R. L. Ferris, G. M. Delgoffe, T. C. Bruno, C. J. Workman and D. A. A. Vignali (2017). "Interferon-gamma Drives Treg Fragility to Promote Anti-tumor Immunity." Cell **169**(6): 1130-1141 e1111.

Palmer, D. C., S. Balasubramaniam, K. Hanada, C. Wrzesinski, Z. Yu, S. Farid, M. R. Theoret, L. N. Hwang, C. A. Klebanoff, L. Gattinoni, A. L. Goldstein, J. C. Yang and N. P. Restifo (2004). "Vaccine-stimulated, adoptively transferred CD8+ T cells traffic indiscriminately and ubiquitously while mediating specific tumor destruction." J Immunol **173**(12): 7209-7216.

Palucka, A. K. and L. M. Coussens (2016). "The Basis of Oncoimmunology." Cell **164**(6): 1233-1247.

Palucka, K. and J. Banchereau (2012). "Cancer immunotherapy via dendritic cells." Nat Rev Cancer **12**(4): 265-277.

Pan, J., M. Zhang, J. Wang, Q. Wang, D. Xia, W. Sun, L. Zhang, H. Yu, Y. Liu and X. Cao (2004). "Interferon-gamma is an autocrine mediator for dendritic cell maturation." Immunol Lett **94**(1-2): 141-151.

Pardo, J., R. Wallich, P. Martin, C. Urban, A. Rongvaux, R. A. Flavell, A. Mullbacher, C. Borner and M. M. Simon (2008). "Granzyme B-induced cell death exerted by ex vivo CTL: discriminating requirements for cell death and some of its signs." Cell Death Differ **15**(3): 567-579.

Park, S. Y., J. W. Seol, Y. J. Lee, J. H. Cho, H. S. Kang, I. S. Kim, S. H. Park, T. H. Kim, J. H. Yim, M. Kim, T. R. Billiar and D. W. Seol (2004). "IFN-gamma enhances TRAIL-induced apoptosis through IRF-1." Eur J Biochem **271**(21): 4222-4228.

Peggs, K. S., S. A. Quezada, C. A. Chambers, A. J. Korman and J. P. Allison (2009). "Blockade of CTLA-4 on both effector and regulatory T cell compartments contributes to the antitumor activity of anti-CTLA-4 antibodies." J Exp Med **206**(8): 1717-1725.

Peng, W., J. Q. Chen, C. Liu, S. Malu, C. Creasy, M. T. Tetzlaff, C. Xu, J. A. McKenzie, C. Zhang, X. Liang, L. J. Williams, W. Deng, G. Chen, R. Mbofung, A. J. Lazar, C. A. Torres-Cabala, Z. A. Cooper, P. L. Chen, T. N. Tieu, S. Spranger, X. Yu, C. Bernatchez, M. A. Forget, C. Haymaker, R. Amaria, J. L. McQuade, I. C. Glitza, T. Cascone, H. S. Li, L. N. Kwong, T. P. Heffernan, J. Hu, R. L. Bassett, Jr., M. W. Bosenberg, S. E. Woodman, W. W. Overwijk, G. Lizee, J. Roszik, T. F. Gajewski, J. A. Wargo, J. E. Gershenwald, L. Radvanyi, M. A. Davies and P. Hwu (2016). "Loss of PTEN Promotes Resistance to T Cell-Mediated Immunotherapy." Cancer Discov **6**(2): 202-216.

Peng, W., C. Liu, C. Xu, Y. Lou, J. Chen, Y. Yang, H. Yagita, W. W. Overwijk, G. Lizee, L. Radvanyi and P. Hwu (2012). "PD-1 blockade enhances T-cell migration to tumors by elevating IFN-gamma inducible chemokines." Cancer Res **72**(20): 5209-5218.

Perret, R. and F. Ronchese (2008). "Effector CD8+ T cells activated in vitro confer immediate and long-term tumor protection in vivo." Eur J Immunol **38**(10): 2886-2895.

Platanias, L. C. (2005). "Mechanisms of type-I- and type-II-interferon-mediated signalling." Nat Rev Immunol **5**(5): 375-386.

Postow, M. A., M. K. Callahan and J. D. Wolchok (2015). "Immune Checkpoint Blockade in Cancer Therapy." J Clin Oncol **33**(17): 1974-1982.

Presotto, D., E. Erdes, M. N. Duong, M. Allard, P. O. Regamey, M. Quadroni, M. A. Doucey, N. Rufer and M. Hebeisen (2017). "Fine-Tuning of Optimal TCR Signaling in Tumor-Redirected CD8 T Cells by Distinct TCR Affinity-Mediated Mechanisms." Front Immunol **8**: 1564.

Prieto, P. A., J. C. Yang, R. M. Sherry, M. S. Hughes, U. S. Kammula, D. E. White, C. L. Levy, S. A. Rosenberg and G. Q. Phan (2012). "CTLA-4 blockade with ipilimumab: long-term follow-up of 177 patients with metastatic melanoma." Clin Cancer Res **18**(7): 2039-2047.

Principe, N., J. Kidman, S. Goh, C. M. Tilsed, S. A. Fisher, V. S. Fear, C. A. Forbes, R. M. Zemek, A. Chopra, M. Watson, I. M. Dick, L. Boon, R. A. Holt, R. A. Lake, A. K. Nowak, W. J. Lesterhuis, A. M.

McDonnell and J. Chee (2020). "Tumor Infiltrating Effector Memory Antigen-Specific CD8(+) T Cells Predict Response to Immune Checkpoint Therapy." Front Immunol **11**: 584423.

Pritchard, A. L., J. G. Burel, M. A. Neller, N. K. Hayward, J. A. Lopez, M. Fatho, V. Lennerz, T. Wolfel and C. W. Schmidt (2015). "Exome Sequencing to Predict Neoantigens in Melanoma." Cancer Immunol Res **3**(9): 992-998.

Qifeng, S., C. Bo, J. Xingtao, P. Chuanliang and Z. Xiaogang (2011). "Methylation of the promoter of human leukocyte antigen class I in human esophageal squamous cell carcinoma and its histopathological characteristics." J Thorac Cardiovasc Surg **141**(3): 808-814.

Quezada, S. A., K. S. Peggs, T. R. Simpson, Y. Shen, D. R. Littman and J. P. Allison (2008). "Limited tumor infiltration by activated T effector cells restricts the therapeutic activity of regulatory T cell depletion against established melanoma." J Exp Med **205**(9): 2125-2138.

Quintana, A., V. Peg, A. Prat, T. Moline, G. Villacampa, L. Pare, P. Galvan, R. Dientsmann, P. Schmid, G. Curigliano, E. Munoz-Couselo, J. Perez-Garcia, M. Marti, J. Blanco-Heredia, C. D. Anjos, M. Vazquez, L. De Mattos-Arruda and J. Cortes (2021). "Immune analysis of lymph nodes in relation to the presence or absence of tumor infiltrating lymphocytes in triple-negative breast cancer." Eur J Cancer **148**: 134-145.

Ralph, P., M. A. Moore and K. Nilsson (1976). "Lysozyme synthesis by established human and murine histiocytic lymphoma cell lines." J Exp Med **143**(6): 1528-1533.

Ramagopal, U. A., W. Liu, S. C. Garrett-Thomson, J. B. Bonanno, Q. Yan, M. Srinivasan, S. C. Wong, A. Bell, S. Mankikar, V. S. Rangan, S. Deshpande, A. J. Korman and S. C. Almo (2017). "Structural basis for cancer immunotherapy by the first-in-class checkpoint inhibitor ipilimumab." Proc Natl Acad Sci U S A **114**(21): E4223-E4232.

Rammensee, H., J. Bachmann, N. P. Emmerich, O. A. Bachor and S. Stevanovic (1999). "SYFPEITHI: database for MHC ligands and peptide motifs." Immunogenetics **50**(3-4): 213-219.

Rashidian, M., J. R. Ingram, M. Dougan, A. Dongre, K. A. Whang, C. LeGall, J. J. Cragnolini, B. Bierie, M. Gostissa, J. Gorman, G. M. Grotenbreg, A. Bhan, R. A. Weinberg and H. L. Ploegh (2017). "Predicting the response to CTLA-4 blockade by longitudinal noninvasive monitoring of CD8 T cells." J Exp Med **214**(8): 2243-2255.

Reiser, J. and A. Banerjee (2016). "Effector, Memory, and Dysfunctional CD8(+) T Cell Fates in the Antitumor Immune Response." J Immunol Res **2016**: 8941260.

Revell, P. A., W. J. Grossman, D. A. Thomas, X. Cao, R. Behl, J. A. Ratner, Z. H. Lu and T. J. Ley (2005). "Granzyme B and the downstream granzymes C and/or F are important for cytotoxic lymphocyte functions." J Immunol **174**(4): 2124-2131.

Ribas, A., R. Kefford, M. A. Marshall, C. J. Punt, J. B. Haanen, M. Marmol, C. Garbe, H. Gogas, J. Schachter, G. Linette, P. Lorigan, K. L. Kendra, M. Maio, U. Trefzer, M. Smylie, G. A. McArthur, B. Dreno, P. D. Nathan, J. Mackiewicz, J. M. Kirkwood, J. Gomez-Navarro, B. Huang, D. Pavlov and A. Hauschild (2013). "Phase III randomized clinical trial comparing tremelimumab with standard-of-care chemotherapy in patients with advanced melanoma." J Clin Oncol **31**(5): 616-622.

Rice, J., S. Buchan and F. K. Stevenson (2002). "Critical components of a DNA fusion vaccine able to induce protective cytotoxic T cells against a single epitope of a tumor antigen." J Immunol **169**(7): 3908-3913.

Robbins, P. F., S. H. Kassim, T. L. Tran, J. S. Crystal, R. A. Morgan, S. A. Feldman, J. C. Yang, M. E. Dudley, J. R. Wunderlich, R. M. Sherry, U. S. Kammula, M. S. Hughes, N. P. Restifo, M. Raffeld, C. C. Lee, Y. F. Li, M. El-Gamil and S. A. Rosenberg (2015). "A pilot trial using lymphocytes genetically

engineered with an NY-ESO-1-reactive T-cell receptor: long-term follow-up and correlates with response." Clin Cancer Res **21**(5): 1019-1027.

Robert, L., C. Harview, R. Emerson, X. Wang, S. Mok, B. Homet, B. Comin-Anduix, R. C. Koya, H. Robins, P. C. Tumeh and A. Ribas (2014). "Distinct immunological mechanisms of CTLA-4 and PD-1 blockade revealed by analyzing TCR usage in blood lymphocytes." Oncoimmunology **3**: e29244.

Robert, L., J. Tsoi, X. Wang, R. Emerson, B. Homet, T. Chodon, S. Mok, R. R. Huang, A. J. Cochran, B. Comin-Anduix, R. C. Koya, T. G. Graeber, H. Robins and A. Ribas (2014). "CTLA4 blockade broadens the peripheral T-cell receptor repertoire." Clin Cancer Res **20**(9): 2424-2432.

Rock, K. L., D. J. Farfan-Arribas, J. D. Colbert and A. L. Goldberg (2014). "Re-examining class-I presentation and the DRiP hypothesis." Trends Immunol **35**(4): 144-152.

Rodriguez-Perea, A. L., E. D. Arcia, C. M. Rueda and P. A. Velilla (2016). "Phenotypical characterization of regulatory T cells in humans and rodents." Clin Exp Immunol **185**(3): 281-291.

Roider, E., S. Jellbauer, B. Kohn, C. Berchtold, M. Partilla, D. H. Busch, H. Russmann and K. Panthel (2011). "Invasion and destruction of a murine fibrosarcoma by Salmonella-induced effector CD8 T cells as a therapeutic intervention against cancer." Cancer Immunol Immunother **60**(3): 371-380.

Romano, E., M. Kusio-Kobialka, P. G. Foukas, P. Baumgaertner, C. Meyer, P. Ballabeni, O. Michielin, B. Weide, P. Romero and D. E. Speiser (2015). "Ipilimumab-dependent cell-mediated cytotoxicity of regulatory T cells ex vivo by nonclassical monocytes in melanoma patients." Proc Natl Acad Sci U S A **112**(19): 6140-6145.

Rooney, M. S., S. A. Shukla, C. J. Wu, G. Getz and N. Hacohen (2015). "Molecular and genetic properties of tumors associated with local immune cytolytic activity." Cell **160**(1-2): 48-61.

Rosenberg, S. A. and M. E. Dudley (2004). "Cancer regression in patients with metastatic melanoma after the transfer of autologous antitumor lymphocytes." Proc Natl Acad Sci U S A **101 Suppl 2**: 14639-14645.

Rosenberg, S. A., J. C. Yang and N. P. Restifo (2004). "Cancer immunotherapy: moving beyond current vaccines." Nat Med **10**(9): 909-915.

Roudko, V., B. Greenbaum and N. Bhardwaj (2020). "Computational Prediction and Validation of Tumor-Associated Neoantigens." Front Immunol **11**: 27.

Rozeman, E. A., E. P. Hoefsmit, I. L. M. Reijers, R. P. M. Saw, J. M. Versluis, O. Krijgsman, P. Dimitriadis, K. Sikorska, B. A. van de Wiel, H. Eriksson, M. Gonzalez, A. Torres Acosta, L. G. Grijpink-Ongering, K. Shannon, J. Haanen, J. Stretch, S. Ch'ng, O. E. Nieweg, H. A. Mallo, S. Adriaansz, R. M. Kerkhoven, S. Cornelissen, A. Broeks, W. M. C. Klop, C. L. Zuur, W. J. van Houdt, D. S. Peeper, A. J. Spillane, A. C. J. van Akkooi, R. A. Scolyer, T. N. M. Schumacher, A. M. Menzies, G. V. Long and C. U. Blank (2021). "Survival and biomarker analyses from the OpACIN-neo and OpACIN neoadjuvant immunotherapy trials in stage III melanoma." Nat Med **27**(2): 256-263.

Ruffell, B., D. Chang-Strachan, V. Chan, A. Rosenbusch, C. M. Ho, N. Pryer, D. Daniel, E. S. Hwang, H. S. Rugo and L. M. Coussens (2014). "Macrophage IL-10 blocks CD8+ T cell-dependent responses to chemotherapy by suppressing IL-12 expression in intratumoral dendritic cells." Cancer Cell **26**(5): 623-637.

Rycaj, K., J. B. Plummer, B. Yin, M. Li, J. Garza, L. Radvanyi, L. M. Ramondetta, K. Lin, G. L. Johanning, D. G. Tang and F. Wang-Johanning (2015). "Cytotoxicity of human endogenous retrovirus K-specific T cells toward autologous ovarian cancer cells." Clin Cancer Res **21**(2): 471-483.

Sade-Feldman, M., K. Yizhak, S. L. Bjorgaard, J. P. Ray, C. G. de Boer, R. W. Jenkins, D. J. Lieb, J. H. Chen, D. T. Frederick, M. Barzily-Rokni, S. S. Freeman, A. Reuben, P. J. Hoover, A. C. Villani, E. Ivanova, A. Portell, P. H. Lizotte, A. R. Aref, J. P. Eliane, M. R. Hammond, H. Vitzthum, S. M. Blackmon, B. Li, V. Gopalakrishnan, S. M. Reddy, Z. A. Cooper, C. P. Paweletz, D. A. Barbie, A. Stemmer-Rachamimov, K. T. Flaherty, J. A. Wargo, G. M. Boland, R. J. Sullivan, G. Getz and N. Hacohen (2018). "Defining T Cell States Associated with Response to Checkpoint Immunotherapy in Melanoma." Cell **175**(4): 998-1013 e1020.

Saethang, T., O. Hirose, I. Kimkong, V. A. Tran, X. T. Dang, L. A. Nguyen, T. K. Le, M. Kubo, Y. Yamada and K. Satou (2013). "PAAQD: Predicting immunogenicity of MHC class I binding peptides using amino acid pairwise contact potentials and quantum topological molecular similarity descriptors." J Immunol Methods **387**(1-2): 293-302.

Sahin, U. and O. Tureci (2018). "Personalized vaccines for cancer immunotherapy." Science **359**(6382): 1355-1360.

Saini, S. K., K. Ostermeir, V. R. Ramnarayan, H. Schuster, M. Zacharias and S. Springer (2013). "Dipeptides promote folding and peptide binding of MHC class I molecules." Proc Natl Acad Sci U S A **110**(38): 15383-15388.

Saito, T., H. Wada, M. Yamasaki, H. Miyata, H. Nishikawa, E. Sato, S. Kageyama, H. Shiku, M. Mori and Y. Doki (2014). "High expression of MAGE-A4 and MHC class I antigens in tumor cells and induction of MAGE-A4 immune responses are prognostic markers of CHP-MAGE-A4 cancer vaccine." Vaccine **32**(45): 5901-5907.

Sakaguchi, S., T. Yamaguchi, T. Nomura and M. Ono (2008). "Regulatory T cells and immune tolerance." Cell **133**(5): 775-787.

Salama, P., M. Phillips, F. Grieu, M. Morris, N. Zeps, D. Joseph, C. Platell and B. Iacopetta (2009). "Tumor-infiltrating FOXP3+ T regulatory cells show strong prognostic significance in colorectal cancer." J Clin Oncol **27**(2): 186-192.

Salas-Benito, D., E. Conde, I. Tamayo-Uria, U. Mancheno, E. Elizalde, D. Garcia-Ros, J. M. Aramendia, J. C. Muruzabal, J. Alcaide, F. Guillen-Grima, J. A. Minguez, J. Amores-Tirado, A. Gonzalez-Martin, P. Sarobe, J. J. Lasarte, M. Ponz-Sarvise, C. E. De Andrea and S. Hervas-Stubbs (2021). "The mutational load and a T-cell inflamed tumour phenotype identify ovarian cancer patients rendering tumour-reactive T cells from PD-1(+) tumour-infiltrating lymphocytes." Br J Cancer **124**(6): 1138-1149.

Samji, T. and K. M. Khanna (2017). "Understanding memory CD8(+) T cells." Immunol Lett **185**: 32-39.

Sanchez-Paulete, A. R., F. J. Cueto, M. Martinez-Lopez, S. Labiano, A. Morales-Kastresana, M. E. Rodriguez-Ruiz, M. Jure-Kunkel, A. Azpilikueta, M. A. Aznar, J. I. Quetglas, D. Sancho and I. Melero (2016). "Cancer Immunotherapy with Immunomodulatory Anti-CD137 and Anti-PD-1 Monoclonal Antibodies Requires BATF3-Dependent Dendritic Cells." Cancer Discov **6**(1): 71-79.

Sanderson, S. and N. Shastri (1994). "LacZ inducible, antigen/MHC-specific T cell hybrids." Int Immunol **6**(3): 369-376.

Santos, P. M. and L. H. Butterfield (2018). "Dendritic Cell-Based Cancer Vaccines." J Immunol **200**(2): 443-449.

Sautes-Fridman, C., F. Petitprez, J. Calderaro and W. H. Fridman (2019). "Tertiary lymphoid structures in the era of cancer immunotherapy." Nat Rev Cancer **19**(6): 307-325.

Savas, P., B. Virassamy, C. Ye, A. Salim, C. P. Mintoff, F. Caramia, R. Salgado, D. J. Byrne, Z. L. Teo, S. Dushyanthen, A. Byrne, L. Wein, S. J. Luen, C. Poliness, S. S. Nightingale, A. S. Skandarajah, D. E. Gyorki, C. M. Thornton, P. A. Beavis, S. B. Fox, C. Kathleen Cuningham Foundation Consortium for Research into Familial Breast, P. K. Darcy, T. P. Speed, L. K. Mackay, P. J. Neeson and S. Loi (2018). "Single-cell profiling of breast cancer T cells reveals a tissue-resident memory subset associated with improved prognosis." Nat Med **24**(7): 986-993.

Scharping, N. E., A. V. Menk, R. S. Moreci, R. D. Whetstone, R. E. Dadey, S. C. Watkins, R. L. Ferris and G. M. Delgoffe (2016). "The Tumor Microenvironment Represses T Cell Mitochondrial Biogenesis to Drive Intratumoral T Cell Metabolic Insufficiency and Dysfunction." Immunity **45**(2): 374-388.

Scharping, N. E., D. B. Rivadeneira, A. V. Menk, P. D. A. Vignali, B. R. Ford, N. L. Rittenhouse, R. Peralta, Y. Wang, Y. Wang, K. DePeaux, A. C. Poholek and G. M. Delgoffe (2021). "Mitochondrial stress induced by continuous stimulation under hypoxia rapidly drives T cell exhaustion." Nat Immunol **22**(2): 205-215.

Scheper, W., S. Kelderman, L. F. Fanchi, C. Linnemann, G. Bendle, M. A. J. de Rooij, C. Hirt, R. Mezzadra, M. Slagter, K. Dijkstra, R. J. C. Kluin, P. Snaebjornsson, K. Milne, B. H. Nelson, H. Zijlmans, G. Kenter, E. E. Voest, J. Haanen and T. N. Schumacher (2019). "Low and variable tumor reactivity of the intratumoral TCR repertoire in human cancers." Nat Med **25**(1): 89-94.

Schietinger, A., M. Philip, V. E. Krisnawan, E. Y. Chiu, J. J. Delrow, R. S. Basom, P. Lauer, D. G. Brockstedt, S. E. Knoblaugh, G. J. Hammerling, T. D. Schell, N. Garbi and P. D. Greenberg (2016). "Tumor-Specific T Cell Dysfunction Is a Dynamic Antigen-Driven Differentiation Program Initiated Early during Tumorigenesis." Immunity **45**(2): 389-401.

Schumacher, K., W. Haensch, C. Roefzaad and P. M. Schlag (2001). "Prognostic significance of activated CD8(+) T cell infiltrations within esophageal carcinomas." Cancer Res **61**(10): 3932-3936.

Schumacher, T. N. and R. D. Schreiber (2015). "Neoantigens in cancer immunotherapy." Science **348**(6230): 69-74.

Scott, E. N., A. M. Gocher, C. J. Workman and D. A. A. Vignali (2021). "Regulatory T Cells: Barriers of Immune Infiltration Into the Tumor Microenvironment." Front Immunol **12**: 702726.

Scrimieri, F., D. Askew, D. J. Corn, S. Eid, I. D. Bobanga, J. A. Bjelac, M. L. Tsao, F. Allen, Y. S. Othman, S. C. Wang and A. Y. Huang (2013). "Murine leukemia virus envelope gp70 is a shared biomarker for the high-sensitivity quantification of murine tumor burden." Oncoimmunology **2**(11): e26889.

Sedger, L. M., M. B. Glaccum, J. C. Schuh, S. T. Kanaly, E. Williamson, N. Kayagaki, T. Yun, P. Smolak, T. Le, R. Goodwin and B. Gliniak (2002). "Characterization of the in vivo function of TNF-alpha-related apoptosis-inducing ligand, TRAIL/Apo2L, using TRAIL/Apo2L gene-deficient mice." Eur J Immunol **32**(8): 2246-2254.

Setiady, Y. Y., J. A. Coccia and P. U. Park (2010). "In vivo depletion of CD4+FOXP3+ Treg cells by the PC61 anti-CD25 monoclonal antibody is mediated by FcgammaRIII+ phagocytes." Eur J Immunol **40**(3): 780-786.

Shang, B., Y. Liu, S. J. Jiang and Y. Liu (2015). "Prognostic value of tumor-infiltrating FoxP3+ regulatory T cells in cancers: a systematic review and meta-analysis." Sci Rep **5**: 15179.

Sharma, P. and J. P. Allison (2015). "Immune checkpoint targeting in cancer therapy: toward combination strategies with curative potential." Cell **161**(2): 205-214.

Shimizu, J., S. Yamazaki and S. Sakaguchi (1999). "Induction of tumor immunity by removing CD25+CD4+ T cells: a common basis between tumor immunity and autoimmunity." J Immunol **163**(10): 5211-5218.

Shimizu, K., D. Sugiura, I. M. Okazaki, T. Maruhashi, T. Takemoto and T. Okazaki (2021). "PD-1 preferentially inhibits the activation of low-affinity T cells." Proc Natl Acad Sci U S A **118**(35).

Shukla, S. A., M. S. Rooney, M. Rajasagi, G. Tiao, P. M. Dixon, M. S. Lawrence, J. Stevens, W. J. Lane, J. L. Dellagatta, S. Steelman, C. Sougnez, K. Cibulskis, A. Kiezun, N. Hacohen, V. Brusic, C. J. Wu and G. Getz (2015). "Comprehensive analysis of cancer-associated somatic mutations in class I HLA genes." Nat Biotechnol **33**(11): 1152-1158.

Sica, A., T. Schioppa, A. Mantovani and P. Allavena (2006). "Tumour-associated macrophages are a distinct M2 polarised population promoting tumour progression: potential targets of anti-cancer therapy." Eur J Cancer **42**(6): 717-727.

Simoni, Y., E. Becht, M. Fehlings, C. Y. Loh, S. L. Koo, K. W. W. Teng, J. P. S. Yeong, R. Nahar, T. Zhang, H. Kared, K. Duan, N. Ang, M. Poidinger, Y. Y. Lee, A. Larbi, A. J. Khng, E. Tan, C. Fu, R. Mathew, M. Teo, W. T. Lim, C. K. Toh, B. H. Ong, T. Koh, A. M. Hillmer, A. Takano, T. K. H. Lim, E. H. Tan, W. Zhai, D. S. W. Tan, I. B. Tan and E. W. Newell (2018). "Bystander CD8(+) T cells are abundant and phenotypically distinct in human tumour infiltrates." Nature **557**(7706): 575-579.

Singhal, S., J. Stadanlick, M. J. Annunziata, A. S. Rao, P. S. Bhojnagarwala, S. O'Brien, E. K. Moon, E. Cantu, G. Danet-Desnoyers, H. J. Ra, L. Litzky, T. Akimova, U. H. Beier, W. W. Hancock, S. M. Albelda and E. B. Eruslanov (2019). "Human tumor-associated monocytes/macrophages and their regulation of T cell responses in early-stage lung cancer." Sci Transl Med **11**(479).

Slansky, J. E., F. M. Rattis, L. F. Boyd, T. Fahmy, E. M. Jaffee, J. P. Schneck, D. H. Margulies and D. M. Pardoll (2000). "Enhanced antigen-specific antitumor immunity with altered peptide ligands that stabilize the MHC-peptide-TCR complex." Immunity **13**(4): 529-538.

Smith, C. C., K. E. Beckermann, D. S. Bortone, A. A. De Cubas, L. M. Bixby, S. J. Lee, A. Panda, S. Ganesan, G. Bhanot, E. M. Wallen, M. I. Milowsky, W. Y. Kim, W. K. Rathmell, R. Swanstrom, J. S. Parker, J. S. Serody, S. R. Selitsky and B. G. Vincent (2018). "Endogenous retroviral signatures predict immunotherapy response in clear cell renal cell carcinoma." J Clin Invest **128**(11): 4804-4820.

Smyth, M. J., S. E. Street and J. A. Trapani (2003). "Cutting edge: granzymes A and B are not essential for perforin-mediated tumor rejection." J Immunol **171**(2): 515-518.

Smyth, M. J., K. Y. Thia, S. E. Street, D. MacGregor, D. I. Godfrey and J. A. Trapani (2000). "Perforin-mediated cytotoxicity is critical for surveillance of spontaneous lymphoma." J Exp Med **192**(5): 755-760.

Solomon, I., M. Amann, A. Goubier, F. A. Vargas, D. Zervas, C. Qing, J. Y. Henry, E. Ghorani, A. U. Akarca, T. Marafioti, A. Sledzinska, M. W. Sunderland, D. F. Demane, J. R. Clancy, A. Georgiou, J. Salimu, P. Merchiers, M. A. Brown, R. Flury, J. Eckmann, C. Murgia, J. Sam, B. Jacobsen, E. Marrer-Berger, C. Boetsch, S. Belli, L. Leibrock, J. Benz, H. Koll, R. Sutmuller, K. S. Peggs and S. A. Quezada (2020). "CD25-Treg-depleting antibodies preserving IL-2 signaling on effector T cells enhance effector activation and antitumor immunity." Nat Cancer **1**(12): 1153-1166.

Speiser, D. E., P. Baumgaertner, C. Barbey, V. Rubio-Godoy, A. Moulin, P. Corthesy, E. Devevre, P. Y. Dietrich, D. Rimoldi, D. Lienard, J. C. Cerottini, P. Romero and N. Rufer (2006). "A novel approach to characterize clonality and differentiation of human melanoma-specific T cell responses: spontaneous priming and efficient boosting by vaccination." J Immunol **177**(2): 1338-1348.

Spranger, S., D. Dai, B. Horton and T. F. Gajewski (2017). "Tumor-Residing Batf3 Dendritic Cells Are Required for Effector T Cell Trafficking and Adoptive T Cell Therapy." Cancer Cell **31**(5): 711-723 e714.

Stadtmauer, E. A., J. A. Fraietta, M. M. Davis, A. D. Cohen, K. L. Weber, E. Lancaster, P. A. Mangan, I. Kulikovskaya, M. Gupta, F. Chen, L. Tian, V. E. Gonzalez, J. Xu, I. Y. Jung, J. J. Melenhorst, G. Plesa, J. Shea, T. Matlawski, A. Cervini, A. L. Gaymon, S. Desjardins, A. Lamontagne, J. Salas-Mckee, A. Fesnak, D. L. Siegel, B. L. Levine, J. K. Jadlowsky, R. M. Young, A. Chew, W. T. Hwang, E. O. Hexner, B. M. Carreno, C. L. Nobles, F. D. Bushman, K. R. Parker, Y. Qi, A. T. Satpathy, H. Y. Chang, Y. Zhao, S. F. Lacey and C. H. June (2020). "CRISPR-engineered T cells in patients with refractory cancer." Science **367**(6481).

Stahl, S., T. Sacher, A. Bechtold, U. Protzer, R. Ganss, G. J. Hammerling, B. Arnold and N. Garbi (2009). "Tumor agonist peptides break tolerance and elicit effective CTL responses in an inducible mouse model of hepatocellular carcinoma." Immunol Lett **123**(1): 31-37.

Stifter, K., I. Dekhtiarenko, J. Krieger, A. C. Tissot, T. Seufferlein, M. Wagner and R. Schirmbeck (2020). "A tumor-specific neoepitope expressed in homologous/self or heterologous/viral antigens induced comparable effector CD8(+) T-cell responses by DNA vaccination." Vaccine **38**(21): 3711-3719.

Stone, J. D., D. T. Harris and D. M. Kranz (2015). "TCR affinity for p/MHC formed by tumor antigens that are self-proteins: impact on efficacy and toxicity." Curr Opin Immunol **33**: 16-22.

Stopforth, R. J. and E. S. Ward (2020). "The Role of Antigen Presentation in Tumor-Associated Macrophages." Crit Rev Immunol **40**(3): 205-224.

Street, S. E., E. Cretney and M. J. Smyth (2001). "Perforin and interferon-gamma activities independently control tumor initiation, growth, and metastasis." Blood **97**(1): 192-197.

Street, S. E., J. A. Trapani, D. MacGregor and M. J. Smyth (2002). "Suppression of lymphoma and epithelial malignancies effected by interferon gamma." J Exp Med **196**(1): 129-134.

Stuart, P. M. (2015). "Major Histocompatibility Complex (MHC): Mouse." eLS, John Wiley & Sons.

Stuge, T. B., S. P. Holmes, S. Saharan, A. Tuettenberg, M. Roederer, J. S. Weber and P. P. Lee (2004). "Diversity and recognition efficiency of T cell responses to cancer." PLoS Med **1**(2): e28.

Sugiyarto, G., D. Prossor, O. Dadas, E. D. Arcia-Anaya, T. Elliott and E. James (2021). "Protective low-avidity anti-tumour CD8+ T cells are selectively attenuated by regulatory T cells." Immunotherapy Advances **1**(1).

Suri, A., J. J. Walters, M. G. Levisetti, M. L. Gross and E. R. Unanue (2006). "Identification of naturally processed peptides bound to the class I MHC molecule H-2Kd of normal and TAP-deficient cells." Eur J Immunol **36**(3): 544-557.

Takahashi, Y., N. Harashima, S. Kajigaya, H. Yokoyama, E. Cherkasova, J. P. McCoy, K. Hanada, O. Mena, R. Kurlander, A. Tawab, R. Srinivasan, A. Lundqvist, E. Malinzak, N. Geller, M. I. Lerman and R. W. Childs (2008). "Regression of human kidney cancer following allogeneic stem cell transplantation is associated with recognition of an HERV-E antigen by T cells." J Clin Invest **118**(3): 1099-1109.

Takeda, J., Y. Sato, H. Kiyosawa, T. Mori, S. Yokoya, A. Irisawa, M. Miyata, K. Obara, T. Fujita, T. Suzuki, R. Kasukawa and A. Wanaka (2000). "Anti-tumor immunity against CT26 colon tumor in mice immunized with plasmid DNA encoding beta-galactosidase fused to an envelope protein of endogenous retrovirus." Cell Immunol **204**(1): 11-18.

Tan, C., V. Reddy, J. Dannull, E. Ding, S. K. Nair, D. S. Tyler, S. K. Pruitt and W. T. Lee (2013). "Impact of anti-CD25 monoclonal antibody on dendritic cell-tumor fusion vaccine efficacy in a murine melanoma model." J Transl Med **11**: 148.

Tang, B., W. Zhou, J. Du, Y. He and Y. Li (2015). "Identification of human leukemia antigen A*0201-restricted epitopes derived from epidermal growth factor pathway substrate number 8." Mol Med Rep **12**(2): 1741-1752.

Tay, N. Q., D. C. P. Lee, Y. L. Chua, N. Prabhu, N. R. J. Gascoigne and D. M. Kemeny (2017). "CD40L Expression Allows CD8(+) T Cells to Promote Their Own Expansion and Differentiation through Dendritic Cells." Front Immunol **8**: 1484.

Tcyganov, E., J. Mastio, E. Chen and D. I. Gabrilovich (2018). "Plasticity of myeloid-derived suppressor cells in cancer." Curr Opin Immunol **51**: 76-82.

Tenzer, S., E. Wee, A. Burgevin, G. Stewart-Jones, L. Friis, K. Lamberth, C. H. Chang, M. Harndahl, M. Weimershaus, J. Gerstoft, N. Akkad, P. Klenerman, L. Fugger, E. Y. Jones, A. J. McMichael, S. Buus, H. Schild, P. van Endert and A. K. Iversen (2009). "Antigen processing influences HIV-specific cytotoxic T lymphocyte immunodominance." Nat Immunol **10**(6): 636-646.

Thaxton, J. E. and Z. Li (2014). "To affinity and beyond: harnessing the T cell receptor for cancer immunotherapy." Hum Vaccin Immunother **10**(11): 3313-3321.

The_Nobel_Prize. (2018). "The Nobel Prize in Physiology or Medicine 2018." Retrieved June 21st, 2021, from https://www.nobelprize.org/prizes/medicine/2018/press-release/.

Thomas, L. (1982). "On immunosurveillance in human cancer." Yale J Biol Med **55**(3-4): 329-333.

Thommen, D. S., V. H. Koelzer, P. Herzig, A. Roller, M. Trefny, S. Dimeloe, A. Kiialainen, J. Hanhart, C. Schill, C. Hess, S. Savic Prince, M. Wiese, D. Lardinois, P. C. Ho, C. Klein, V. Karanikas, K. D. Mertz, T. N. Schumacher and A. Zippelius (2018). "A transcriptionally and functionally distinct PD-1(+) CD8(+) T cell pool with predictive potential in non-small-cell lung cancer treated with PD-1 blockade." Nat Med **24**(7): 994-1004.

Thommen, D. S., J. Schreiner, P. Muller, P. Herzig, A. Roller, A. Belousov, P. Umana, P. Pisa, C. Klein, M. Bacac, O. S. Fischer, W. Moersig, S. Savic Prince, V. Levitsky, V. Karanikas, D. Lardinois and A. Zippelius (2015). "Progression of Lung Cancer Is Associated with Increased Dysfunction of T Cells Defined by Coexpression of Multiple Inhibitory Receptors." Cancer Immunol Res **3**(12): 1344-1355.

Thomsen, A. R. and B. L. Jensen (1980). "Concanavalin A-mediated in vitro activation of a secondary cytotoxic T-cell response in virus-primed splenocytes." Scand J Immunol **12**(2): 109-118.

Thorsson, V., D. L. Gibbs, S. D. Brown, D. Wolf, D. S. Bortone, T. H. Ou Yang, E. Porta-Pardo, G. F. Gao, C. L. Plaisier, J. A. Eddy, E. Ziv, A. C. Culhane, E. O. Paull, I. K. A. Sivakumar, A. J. Gentles, R. Malhotra, F. Farshidfar, A. Colaprico, J. S. Parker, L. E. Mose, N. S. Vo, J. Liu, Y. Liu, J. Rader, V. Dhankani, S. M. Reynolds, R. Bowlby, A. Califano, A. D. Cherniack, D. Anastassiou, D. Bedognetti, Y. Mokrab, A. M. Newman, A. Rao, K. Chen, A. Krasnitz, H. Hu, T. M. Malta, H. Noushmehr, C. S. Pedamallu, S. Bullman, A. I. Ojesina, A. Lamb, W. Zhou, H. Shen, T. K. Choueiri, J. N. Weinstein, J. Guinney, J. Saltz, R. A. Holt, C. S. Rabkin, N. Cancer Genome Atlas Research, A. J. Lazar, J. S. Serody, E. G. Demicco, M. L. Disis, B. G. Vincent and I. Shmulevich (2018). "The Immune Landscape of Cancer." Immunity **48**(4): 812-830 e814.

Topalian, S. L., C. G. Drake and D. M. Pardoll (2015). "Immune checkpoint blockade: a common denominator approach to cancer therapy." Cancer Cell **27**(4): 450-461.

Townsend, A., C. Ohlen, J. Bastin, H. G. Ljunggren, L. Foster and K. Karre (1989). "Association of class I major histocompatibility heavy and light chains induced by viral peptides." Nature **340**(6233): 443-448.

Trapani, J. A., K. Y. Thia, M. Andrews, I. D. Davis, C. Gedye, P. Parente, S. Svobodova, J. Chia, K. Browne, I. G. Campbell, W. A. Phillips, I. Voskoboinik and J. S. Cebon (2013). "Human perforin mutations and susceptibility to multiple primary cancers." Oncoimmunology **2**(4): e24185.

Tumeh, P. C., C. L. Harview, J. H. Yearley, I. P. Shintaku, E. J. Taylor, L. Robert, B. Chmielowski, M. Spasic, G. Henry, V. Ciobanu, A. N. West, M. Carmona, C. Kivork, E. Seja, G. Cherry, A. J. Gutierrez, T. R. Grogan, C. Mateus, G. Tomasic, J. A. Glaspy, R. O. Emerson, H. Robins, R. H. Pierce, D. A. Elashoff, C. Robert and A. Ribas (2014). "PD-1 blockade induces responses by inhibiting adaptive immune resistance." Nature **515**(7528): 568-571.

Tung, C. W. and S. Y. Ho (2007). "POPI: predicting immunogenicity of MHC class I binding peptides by mining informative physicochemical properties." Bioinformatics **23**(8): 942-949.

Tung, C. W., M. Ziehm, A. Kamper, O. Kohlbacher and S. Y. Ho (2011). "POPISK: T-cell reactivity prediction using support vector machines and string kernels." BMC Bioinformatics **12**: 446.

Turnis, M. E., D. V. Sawant, A. L. Szymczak-Workman, L. P. Andrews, G. M. Delgoffe, H. Yano, A. J. Beres, P. Vogel, C. J. Workman and D. A. Vignali (2016). "Interleukin-35 Limits Anti-Tumor Immunity." Immunity **44**(2): 316-329.

van den Broek, M. E., D. Kagi, F. Ossendorp, R. Toes, S. Vamvakas, W. K. Lutz, C. J. Melief, R. M. Zinkernagel and H. Hengartner (1996). "Decreased tumor surveillance in perforin-deficient mice." J Exp Med **184**(5): 1781-1790.

van der Leun, A. M., D. S. Thommen and T. N. Schumacher (2020). "CD8(+) T cell states in human cancer: insights from single-cell analysis." Nat Rev Cancer **20**(4): 218-232.

van Duikeren, S., M. F. Fransen, A. Redeker, B. Wieles, G. Platenburg, W. J. Krebber, F. Ossendorp, C. J. Melief and R. Arens (2012). "Vaccine-induced effector-memory CD8+ T cell responses predict therapeutic efficacy against tumors." J Immunol **189**(7): 3397-3403.

van Hateren, A. and T. Elliott (2021). "The role of MHC I protein dynamics in tapasin and TAPBPR-assisted immunopeptidome editing." Curr Opin Immunol **70**: 138-143.

Vergara Bermejo, A., E. Ragonnaud, J. Daradoumis and P. Holst (2020). "Cancer Associated Endogenous Retroviruses: Ideal Immune Targets for Adenovirus-Based Immunotherapy." Int J Mol Sci **21**(14).

Verneau, J., C. Sautes-Fridman and C. M. Sun (2020). "Dendritic cells in the tumor microenvironment: prognostic and theranostic impact." Semin Immunol **48**: 101410.

Viais, R., M. Farina-Mosquera, M. Villamor-Paya, S. Watanabe, L. Palenzuela, C. Lacasa and J. Luders (2021). "Augmin deficiency in neural stem cells causes p53-dependent apoptosis and aborts brain development." Elife **10**.

Vigneron, N. (2015). "Human Tumor Antigens and Cancer Immunotherapy." Biomed Res Int **2015**: 948501.

Vigneron, N., V. Stroobant, B. J. Van den Eynde and P. van der Bruggen (2013). "Database of T cell-defined human tumor antigens: the 2013 update." Cancer Immun **13**: 15.

Waldman, A. D., J. M. Fritz and M. J. Lenardo (2020). "A guide to cancer immunotherapy: from T cell basic science to clinical practice." Nat Rev Immunol **20**(11): 651-668.

Walker, L. S. and D. M. Sansom (2011). "The emerging role of CTLA4 as a cell-extrinsic regulator of T cell responses." Nat Rev Immunol **11**(12): 852-863.

Wang, B., S. Wu, H. Zeng, Z. Liu, W. Dong, W. He, X. Chen, X. Dong, L. Zheng, T. Lin and J. Huang (2015). "CD103+ Tumor Infiltrating Lymphocytes Predict a Favorable Prognosis in Urothelial Cell Carcinoma of the Bladder." J Urol **194**(2): 556-562.

Wang, J., Y. Tian, G. Zhu, Z. Li, Z. Wu, G. Wei, L. Zhuang, Z. Li, X. Chen, X. Zhang, J. Zheng and G. Cai (2021). "Establishment and validation of immune microenvironmental gene signatures for predicting prognosis in patients with head and neck squamous cell carcinoma." Int Immunopharmacol **97**: 107817.

Wang, P., Y. Chen and C. Wang (2021). "Beyond Tumor Mutation Burden: Tumor Neoantigen Burden as a Biomarker for Immunotherapy and Other Types of Therapy." Front Oncol **11**: 672677.

Wang, Y., Y. Xiang, V. W. Xin, X. W. Wang, X. C. Peng, X. Q. Liu, D. Wang, N. Li, J. T. Cheng, Y. N. Lyv, S. Z. Cui, Z. Ma, Q. Zhang and H. W. Xin (2020). "Dendritic cell biology and its role in tumor immunotherapy." J Hematol Oncol **13**(1): 107.

Wang, Z. Q., K. Milne, H. Derocher, J. R. Webb, B. H. Nelson and P. H. Watson (2016). "CD103 and Intratumoral Immune Response in Breast Cancer." Clin Cancer Res **22**(24): 6290-6297.

Waterhouse, P., J. M. Penninger, E. Timms, A. Wakeham, A. Shahinian, K. P. Lee, C. B. Thompson, H. Griesser and T. W. Mak (1995). "Lymphoproliferative disorders with early lethality in mice deficient in Ctla-4." Science **270**(5238): 985-988.

Wculek, S. K., F. J. Cueto, A. M. Mujal, I. Melero, M. F. Krummel and D. Sancho (2020). "Dendritic cells in cancer immunology and immunotherapy." Nat Rev Immunol **20**(1): 7-24.

Webb, J. R., K. Milne, P. Watson, R. J. Deleeuw and B. H. Nelson (2014). "Tumor-infiltrating lymphocytes expressing the tissue resident memory marker CD103 are associated with increased survival in high-grade serous ovarian cancer." Clin Cancer Res **20**(2): 434-444.

Weber, J. S., S. P. D'Angelo, D. Minor, F. S. Hodi, R. Gutzmer, B. Neyns, C. Hoeller, N. I. Khushalani, W. H. Miller, Jr., C. D. Lao, G. P. Linette, L. Thomas, P. Lorigan, K. F. Grossmann, J. C. Hassel, M. Maio, M. Sznol, P. A. Ascierto, P. Mohr, B. Chmielowski, A. Bryce, I. M. Svane, J. J. Grob, A. M. Krackhardt, C. Horak, A. Lambert, A. S. Yang and J. Larkin (2015). "Nivolumab versus chemotherapy in patients with advanced melanoma who progressed after anti-CTLA-4 treatment (CheckMate 037): a randomised, controlled, open-label, phase 3 trial." Lancet Oncol **16**(4): 375-384.

Wei, S. C., C. R. Duffy and J. P. Allison (2018). "Fundamental Mechanisms of Immune Checkpoint Blockade Therapy." Cancer Discov **8**(9): 1069-1086.

Wei, S. C., J. H. Levine, A. P. Cogdill, Y. Zhao, N. A. S. Anang, M. C. Andrews, P. Sharma, J. Wang, J. A. Wargo, D. Pe'er and J. P. Allison (2017). "Distinct Cellular Mechanisms Underlie Anti-CTLA-4 and Anti-PD-1 Checkpoint Blockade." Cell **170**(6): 1120-1133 e1117.

Wells, D. K., M. M. van Buuren, K. K. Dang, V. M. Hubbard-Lucey, K. C. F. Sheehan, K. M. Campbell, A. Lamb, J. P. Ward, J. Sidney, A. B. Blazquez, A. J. Rech, J. M. Zaretsky, B. Comin-Anduix, A. H. C. Ng, W. Chour, T. V. Yu, H. Rizvi, J. M. Chen, P. Manning, G. M. Steiner, X. C. Doan, A. Tumor Neoantigen Selection, T. Merghoub, J. Guinney, A. Kolom, C. Selinsky, A. Ribas, M. D. Hellmann, N. Hacohen, A. Sette, J. R. Heath, N. Bhardwaj, F. Ramsdell, R. D. Schreiber, T. N. Schumacher, P. Kvistborg and N. A. Defranoux (2020). "Key Parameters of Tumor Epitope Immunogenicity Revealed Through a Consortium Approach Improve Neoantigen Prediction." Cell **183**(3): 818-834 e813.

Welters, M. J., G. G. Kenter, S. J. Piersma, A. P. Vloon, M. J. Lowik, D. M. Berends-van der Meer, J. W. Drijfhout, A. R. Valentijn, A. R. Wafelman, J. Oostendorp, G. J. Fleuren, R. Offringa, C. J. Melief and S. H. van der Burg (2008). "Induction of tumor-specific CD4+ and CD8+ T-cell immunity in cervical cancer patients by a human papillomavirus type 16 E6 and E7 long peptides vaccine." Clin Cancer Res **14**(1): 178-187.

Wendel, M., I. E. Galani, E. Suri-Payer and A. Cerwenka (2008). "Natural killer cell accumulation in tumors is dependent on IFN-gamma and CXCR3 ligands." Cancer Res **68**(20): 8437-8445.

Wert-Carvajal, C., R. Sanchez-Garcia, J. R. Macias, R. Sanz-Pamplona, A. M. Perez, R. Alemany, E. Veiga, C. O. S. Sorzano and A. Munoz-Barrutia (2021). "Predicting MHC I restricted T cell epitopes in mice with NAP-CNB, a novel online tool." Sci Rep **11**(1): 10780.

Wherry, E. J. (2011). "T cell exhaustion." Nat Immunol **12**(6): 492-499.

Williams, E. L., S. N. Dunn, S. James, P. W. Johnson, M. S. Cragg, M. J. Glennie and J. C. Gray (2013). "Immunomodulatory monoclonal antibodies combined with peptide vaccination provide potent immunotherapy in an aggressive murine neuroblastoma model." Clin Cancer Res **19**(13): 3545-3555.

Williams, J. W., M. Y. Tjota, B. S. Clay, B. Vander Lugt, H. S. Bandukwala, C. L. Hrusch, D. C. Decker, K. M. Blaine, B. R. Fixsen, H. Singh, R. Sciammas and A. I. Sperling (2013). "Transcription factor IRF4 drives dendritic cells to promote Th2 differentiation." Nat Commun **4**: 2990.

Wistuba-Hamprecht, K., A. Martens, F. Heubach, E. Romano, M. Geukes Foppen, J. Yuan, M. Postow, P. Wong, D. Mallardo, B. Schilling, A. M. Di Giacomo, A. Khammari, B. Dreno, M. Maio, D. Schadendorf, P. A. Ascierto, J. D. Wolchok, C. U. Blank, C. Garbe, G. Pawelec and B. Weide (2017). "Peripheral CD8 effector-memory type 1 T-cells correlate with outcome in ipilimumab-treated stage IV melanoma patients." Eur J Cancer **73**: 61-70.

Woo, S. R., M. E. Turnis, M. V. Goldberg, J. Bankoti, M. Selby, C. J. Nirschl, M. L. Bettini, D. M. Gravano, P. Vogel, C. L. Liu, S. Tangsombatvisit, J. F. Grosso, G. Netto, M. P. Smeltzer, A. Chaux, P. J. Utz, C. J. Workman, D. M. Pardoll, A. J. Korman, C. G. Drake and D. A. Vignali (2012). "Immune inhibitory molecules LAG-3 and PD-1 synergistically regulate T-cell function to promote tumoral immune escape." Cancer Res **72**(4): 917-927.

Workel, H. H., F. L. Komdeur, M. C. Wouters, A. Plat, H. G. Klip, F. A. Eggink, G. B. Wisman, H. J. Arts, M. H. Oonk, M. J. Mourits, R. Yigit, M. Versluis, E. W. Duiker, H. Hollema, M. de Bruyn and H. W. Nijman (2016). "CD103 defines intraepithelial CD8+ PD1+ tumour-infiltrating lymphocytes of prognostic significance in endometrial adenocarcinoma." Eur J Cancer **60**: 1-11.

Wu, F., W. Zhang, H. Shao, H. Bo, H. Shen, J. Li, Y. Liu, T. Wang, W. Ma and S. Huang (2013). "Human effector T cells derived from central memory cells rather than CD8(+)T cells modified by tumor-specific TCR gene transfer possess superior traits for adoptive immunotherapy." Cancer Lett **339**(2): 195-207.

Wu, S., W. Zhu, Y. Peng, L. Wang, Y. Hong, L. Huang, D. Dong, J. Xie, T. Merchen, E. Kruse, Z. S. Guo, D. Bartlett, N. Fu and Y. He (2017). "The Antitumor Effects of Vaccine-Activated CD8(+) T Cells Associate with Weak TCR Signaling and Induction of Stem-Like Memory T Cells." Cancer Immunol Res **5**(10): 908-919.

Wustemann, T., U. Haberkorn, J. Babich and W. Mier (2019). "Targeting prostate cancer: Prostate-specific membrane antigen based diagnosis and therapy." Med Res Rev **39**(1): 40-69.

Yadav, M., S. Jhunjhunwala, Q. T. Phung, P. Lupardus, J. Tanguay, S. Bumbaca, C. Franci, T. K. Cheung, J. Fritsche, T. Weinschenk, Z. Modrusan, I. Mellman, J. R. Lill and L. Delamarre (2014).

"Predicting immunogenic tumour mutations by combining mass spectrometry and exome sequencing." Nature **515**(7528): 572-576.

Yamamoto, K., A. Venida, J. Yano, D. E. Biancur, M. Kakiuchi, S. Gupta, A. S. W. Sohn, S. Mukhopadhyay, E. Y. Lin, S. J. Parker, R. S. Banh, J. A. Paulo, K. W. Wen, J. Debnath, G. E. Kim, J. D. Mancias, D. T. Fearon, R. M. Perera and A. C. Kimmelman (2020). "Autophagy promotes immune evasion of pancreatic cancer by degrading MHC-I." Nature **581**(7806): 100-105.

Yang, X., L. Zhao, F. Wei and J. Li (2021). "DeepNetBim: deep learning model for predicting HLA-epitope interactions based on network analysis by harnessing binding and immunogenicity information." BMC Bioinformatics **22**(1): 231.

Yarchoan, M., B. A. Johnson, 3rd, E. R. Lutz, D. A. Laheru and E. M. Jaffee (2017). "Targeting neoantigens to augment antitumour immunity." Nat Rev Cancer **17**(9): 569.

Yasuda, T., T. Kamigaki, K. Kawasaki, T. Nakamura, M. Yamamoto, K. Kanemitsu, S. Takase, D. Kuroda, Y. Kim, T. Ajiki and Y. Kuroda (2007). "Superior anti-tumor protection and therapeutic efficacy of vaccination with allogeneic and semiallogeneic dendritic cell/tumor cell fusion hybrids for murine colon adenocarcinoma." Cancer Immunology, Immunotherapy **56**(7): 1025-1036.

Ye, Q., Y. Shen, X. Wang, J. Yang, F. Miao, C. Shen and J. Zhang (2010). "Hypermethylation of HLA class I gene is associated with HLA class I down-regulation in human gastric cancer." Tissue Antigens **75**(1): 30-39.

Yee, N. S., N. Ignatenko, N. Finnberg, N. Lee and D. Stairs (2015). "Animal Models of Cancer Biology." Cancer Growth Metastasis **8**(Suppl 1): 115-118.

Yeh, M.-H. (2005). Identification of CD8+ T cell-stimulating shared antigens that are uncoverd in CT26 vaccinated mice in the abscence of CD25+ regulatory T cells. Doctor of Philosophy, University of Southampton.

Yewdell, J. W. (2006). "Confronting complexity: real-world immunodominance in antiviral CD8+ T cell responses." Immunity **25**(4): 533-543.

Yu, J. W., S. Bhattacharya, N. Yanamandra, D. Kilian, H. Shi, S. Yadavilli, Y. Katlinskaya, H. Kaczynski, M. Conner, W. Benson, A. Hahn, L. Seestaller-Wehr, M. Bi, N. J. Vitali, L. Tsvetkov, W. Halsey, A. Hughes, C. Traini, H. Zhou, J. Jing, T. Lee, D. J. Figueroa, S. Brett, C. B. Hopson, J. F. Smothers, A. Hoos and R. Srinivasan (2018). "Tumor-immune profiling of murine syngeneic tumor models as a framework to guide mechanistic studies and predict therapy response in distinct tumor microenvironments." PLoS One **13**(11): e0206223.

Yuan, J., M. Adamow, B. A. Ginsberg, T. S. Rasalan, E. Ritter, H. F. Gallardo, Y. Xu, E. Pogoriler, S. L. Terzulli, D. Kuk, K. S. Panageas, G. Ritter, M. Sznol, R. Halaban, A. A. Jungbluth, J. P. Allison, L. J. Old, J. D. Wolchok and S. Gnjatic (2011). "Integrated NY-ESO-1 antibody and CD8+ T-cell responses correlate with clinical benefit in advanced melanoma patients treated with ipilimumab." Proc Natl Acad Sci U S A **108**(40): 16723-16728.

Yuan, J., S. Gnjatic, H. Li, S. Powel, H. F. Gallardo, E. Ritter, G. Y. Ku, A. A. Jungbluth, N. H. Segal, T. S. Rasalan, G. Manukian, Y. Xu, R. A. Roman, S. L. Terzulli, M. Heywood, E. Pogoriler, G. Ritter, L. J. Old, J. P. Allison and J. D. Wolchok (2008). "CTLA-4 blockade enhances polyfunctional NY-ESO-1 specific T cell responses in metastatic melanoma patients with clinical benefit." Proc Natl Acad Sci U S A **105**(51): 20410-20415.

Zamora, A. E., J. C. Crawford and P. G. Thomas (2018). "Hitting the Target: How T Cells Detect and Eliminate Tumors." J Immunol **200**(2): 392-399.

Zaretsky, J. M., A. Garcia-Diaz, D. S. Shin, H. Escuin-Ordinas, W. Hugo, S. Hu-Lieskovan, D. Y. Torrejon, G. Abril-Rodriguez, S. Sandoval, L. Barthly, J. Saco, B. Homet Moreno, R. Mezzadra, B. Chmielowski, K. Ruchalski, I. P. Shintaku, P. J. Sanchez, C. Puig-Saus, G. Cherry, E. Seja, X. Kong, J. Pang, B. Berent-Maoz, B. Comin-Anduix, T. G. Graeber, P. C. Tumeh, T. N. Schumacher, R. S. Lo and A. Ribas (2016). "Mutations Associated with Acquired Resistance to PD-1 Blockade in Melanoma." N Engl J Med **375**(9): 819-829.

Zhang, H. H., M. H. Mei, R. Fei, W. J. Liao, X. Y. Wang, L. L. Qin, J. H. Wang, L. Wei and H. S. Chen (2010). "Regulatory T cell depletion enhances tumor specific CD8 T-cell responses, elicited by tumor antigen NY-ESO-1b in hepatocellular carcinoma patients, in vitro." Int J Oncol **36**(4): 841-848.

Zhang, L., Z. Li, K. M. Skrzypczynska, Q. Fang, W. Zhang, S. A. O'Brien, Y. He, L. Wang, Q. Zhang, A. Kim, R. Gao, J. Orf, T. Wang, D. Sawant, J. Kang, D. Bhatt, D. Lu, C. M. Li, A. S. Rapaport, K. Perez, Y. Ye, S. Wang, X. Hu, X. Ren, W. Ouyang, Z. Shen, J. G. Egen, Z. Zhang and X. Yu (2020). "Single-Cell Analyses Inform Mechanisms of Myeloid-Targeted Therapies in Colon Cancer." Cell **181**(2): 442-459 e429.

Zhang, Y., X. Y. Guan and P. Jiang (2020). "Cytokine and Chemokine Signals of T-Cell Exclusion in Tumors." Front Immunol **11**: 594609.

Zhong, W., J. S. Myers, F. Wang, K. Wang, J. Lucas, E. Rosfjord, J. Lucas, A. T. Hooper, S. Yang, L. A. Lemon, M. Guffroy, C. May, J. R. Bienkowska and P. A. Rejto (2020). "Comparison of the molecular and cellular phenotypes of common mouse syngeneic models with human tumors." BMC Genomics **21**(1): 2.

Zhou, F. (2009). "Molecular mechanisms of IFN-gamma to up-regulate MHC class I antigen processing and presentation." Int Rev Immunol **28**(3-4): 239-260.

Zhou, F., J. Krishnamurthy, Y. Wei, M. Li, K. Hunt, G. L. Johanning, L. J. Cooper and F. Wang-Johanning (2015). "Chimeric antigen receptor T cells targeting HERV-K inhibit breast cancer and its metastasis through downregulation of Ras." Oncoimmunology **4**(11): e1047582.

Zhou, J., M. E. Dudley, S. A. Rosenberg and P. F. Robbins (2005). "Persistence of multiple tumor-specific T-cell clones is associated with complete tumor regression in a melanoma patient receiving adoptive cell transfer therapy." J Immunother **28**(1): 53-62.

Zhou, Q., M. E. Munger, R. G. Veenstra, B. J. Weigel, M. Hirashima, D. H. Munn, W. J. Murphy, M. Azuma, A. C. Anderson, V. K. Kuchroo and B. R. Blazar (2011). "Coexpression of Tim-3 and PD-1 identifies a CD8+ T-cell exhaustion phenotype in mice with disseminated acute myelogenous leukemia." Blood **117**(17): 4501-4510.

Zou, W. and L. Chen (2008). "Inhibitory B7-family molecules in the tumour microenvironment." Nat Rev Immunol **8**(6): 467-477.

Zou, W., J. D. Wolchok and L. Chen (2016). "PD-L1 (B7-H1) and PD-1 pathway blockade for cancer therapy: Mechanisms, response biomarkers, and combinations." Sci Transl Med **8**(328): 328rv324.